frontiers | Research Topics

Nitrogen metabolism in crops and model plant species

Edited by
Luisa Bascunan-Godoy, Enrique Ostria-Gallardo and
Néstor Fernández Del-Saz

Published in
Frontiers in Plant Science

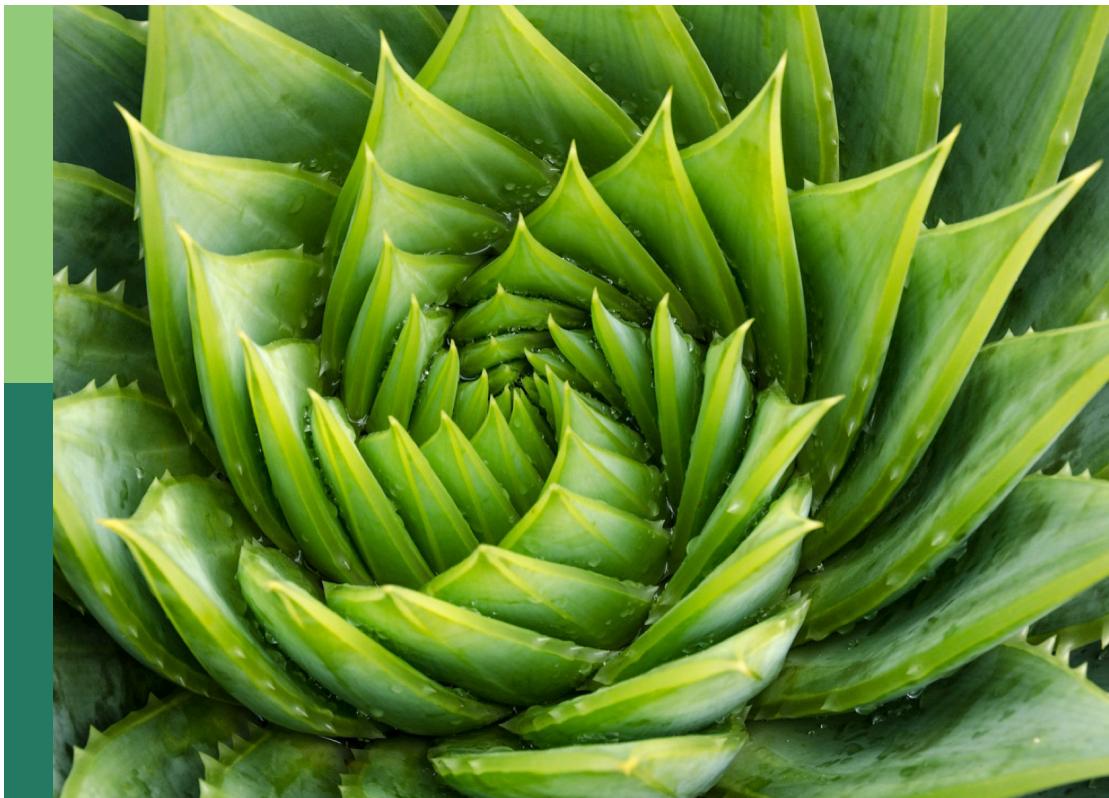

ISSN 1664-8714
ISBN 978-2-8325-5580-4
DOI 10.3389/978-2-8325-5580-4

About Frontiers

Frontiers is more than just an open access publisher of scholarly articles: it is a pioneering approach to the world of academia, radically improving the way scholarly research is managed. The grand vision of Frontiers is a world where all people have an equal opportunity to seek, share and generate knowledge. Frontiers provides immediate and permanent online open access to all its publications, but this alone is not enough to realize our grand goals.

Frontiers journal series

The Frontiers journal series is a multi-tier and interdisciplinary set of open-access, online journals, promising a paradigm shift from the current review, selection and dissemination processes in academic publishing. All Frontiers journals are driven by researchers for researchers; therefore, they constitute a service to the scholarly community. At the same time, the *Frontiers journal series* operates on a revolutionary invention, the tiered publishing system, initially addressing specific communities of scholars, and gradually climbing up to broader public understanding, thus serving the interests of the lay society, too.

Dedication to quality

Each Frontiers article is a landmark of the highest quality, thanks to genuinely collaborative interactions between authors and review editors, who include some of the world's best academicians. Research must be certified by peers before entering a stream of knowledge that may eventually reach the public - and shape society; therefore, Frontiers only applies the most rigorous and unbiased reviews. Frontiers revolutionizes research publishing by freely delivering the most outstanding research, evaluated with no bias from both the academic and social point of view. By applying the most advanced information technologies, Frontiers is catapulting scholarly publishing into a new generation.

What are Frontiers Research Topics?

Frontiers Research Topics are very popular trademarks of the *Frontiers journals series*: they are collections of at least ten articles, all centered on a particular subject. With their unique mix of varied contributions from Original Research to Review Articles, Frontiers Research Topics unify the most influential researchers, the latest key findings and historical advances in a hot research area.

Find out more on how to host your own Frontiers Research Topic or contribute to one as an author by contacting the Frontiers editorial office: frontiersin.org/about/contact

Nitrogen metabolism in crops and model plant species

Topic editors
Luisa Bascunan-Godoy — University of Concepcion, Chile
Enrique Ostria-Gallardo — University of Concepcion, Chile
Néstor Fernández Del-Saz — University of the Balearic Islands, Spain

Citation
Bascunan-Godoy, L., Ostria-Gallardo, E., Fernández Del-Saz, N., eds. (2024).
Nitrogen metabolism in crops and model plant species.
Lausanne: Frontiers Media SA. doi: 10.3389/978-2-8325-5580-4

Table of contents

frontiers | Frontiers in Plant Science

TYPE Editorial
PUBLISHED 08 October 2024
DOI 10.3389/fpls.2024.1502273

OPEN ACCESS

EDITED AND REVIEWED BY
Laigeng Li,
Chinese Academy of Sciences (CAS), China

*CORRESPONDENCE
Luisa Bascuñán-Godoy
lubascun@udec.cl
Néstor Fernández Del-Saz
nestor.fernandez@ugr.es

RECEIVED 26 September 2024
ACCEPTED 30 September 2024
PUBLISHED 08 October 2024

CITATION
Ostria-Gallardo E, Bascuñán-Godoy L and Fernández Del-Saz N (2024) Editorial: Nitrogen metabolism in crops and model plant species.
Front. Plant Sci. 15:1502273.
doi: 10.3389/fpls.2024.1502273

Editorial: Nitrogen metabolism in crops and model plant species

Enrique Ostria-Gallardo[1], Luisa Bascuñán-Godoy[1]* and Néstor Fernández Del-Saz[2]*

[1]Laboratorio de Fisiología Vegetal, Departamento de Botánica, Universidad de Concepción, Concepción, Chile, [2]Department of Plant Physiology, University of Granada, Granada, Spain

KEYWORDS

assimilation, transport, development, nutrition, nitrogen use efficiency, omics, biostimulants, stable isotopes

Editorial on the Research Topic
Nitrogen metabolism in crops and model plant species

Introduction

Nitrogen (N) is a critical macronutrient that influences various physiological, molecular, and metabolic processes in plants, playing a critical role in determining plant growth, crop yield, and environmental sustainability (O'Brien et al., 2016; The et al., 2021). However, excessive or inefficient use of nitrogen fertilizers has raised concerns regarding environmental degradation, including soil acidification and nitrogen leaching (Qasim et al., 2020; Dimkpa et al., 2020). This is especially pertinent as global demand for crop productivity continues to rise in conjunction with increased environmental stressors, both biotic and abiotic, driven by climate change (Coskun et al., 2017). This Research Topic brings together a collection of studies from molecular and physiological responses of either crops or model plants to large-scale agroecological solutions, reflecting the multidimensional efforts to optimize nitrogen use for both crop productivity and environmental sustainability.

Molecular and genetic regulation of nitrogen uptake and signaling

A comprehensive review by Xu et al. examines the NRT2 family of nitrate transporters in *Arabidopsis*, detailing the roles of specific family members, such as NRT2.1, NRT2.4, and NRT2.5, in nitrate uptake under varying nitrogen conditions. By exploring how these transporters function within broader biological processes—including nitrogen remobilization and plant-microbe interactions—the authors provide a roadmap for future research aimed at enhancing NUE through genetic modification and selective breeding.

Similarly, Svietlova et al. investigate how glutamine, a key nitrogen compound, regulates nitrate transporter genes in *Arabidopsis thaliana*, particularly focusing on NRT2.4. Their research reveals that glutamine serves as both a nitrogen source and a

signaling molecule, modulating the expression of nitrate transporters under nitrogen starvation conditions. This study underscores the importance of glutamine in nitrogen signaling and highlights potential pathways for optimizing nitrogen uptake at the molecular level.

Pélissier et al. further expand the discussion of nitrogen uptake by analyzing gene regulatory networks in rice, a staple crop. Their research identifies key transcription factors that govern nitrate and ammonium uptake, providing insights into the genetic control of nitrogen metabolism. This work not only deepens our understanding of nitrogen signaling but also highlights potential targets for improving nitrogen efficiency in crop production.

Metabolic pathways and nitrogen assimilation

The metabolic regulation of nitrogen in plants is another focus of this Research Topic. Hu et al. explore the physiological mechanisms that enhance ammonium tolerance in wheat. Their findings demonstrate that glucose metabolism plays a critical role in supporting ammonium assimilation, ultimately reducing ammonium toxicity and promoting nitrogen uptake. This work offers potential strategies for developing wheat varieties that are more efficient in nitrogen assimilation, particularly under conditions of nitrogen stress.

In maize, Feng et al. investigate the interactions between nitrogen application and carbohydrate metabolism during grain filling. Their study demonstrates that an optimal nitrogen rate significantly enhances enzymatic activity related to both nitrogen and carbohydrate metabolism, improving grain quality and yield. These findings offer practical insights into nitrogen management strategies aimed at optimizing both metabolic efficiency and crop productivity.

The role of symbiotic relationships in nitrogen management is critical to reducing reliance on chemical fertilizers and improving agricultural sustainability. Alquichire-Rojas et al. introduce an exciting avenue of nitrogen management in *Chenopodium quinoa* through plant symbiosis with endophytic insect pathogenic fungi. These fungi promote nitrogen transfer from the soil to the plant, improving carbon storage, photosynthesis, and overall plant growth. Such symbiotic interactions represent promising tools for increasing nitrogen efficiency in agricultural systems, providing a more sustainable alternative to conventional fertilizers.

Nitrogen management in horticultural and field systems

Zhang et al. focus on the role of nitrogen in metabolic shifts within pepper fruits, particularly how nitrogen influences carotenoid biosynthesis and fruit quality. Their research demonstrates that moderate nitrogen application optimizes pigment production, yield, and fruit quality, offering valuable guidance for nitrogen management in horticultural systems where quality is paramount.

The tight relationship between nitrogen and carbon is addressed in Feng et al. who explored the effects of nitrogen on carbohydrate metabolism in waxy maize, emphasizing the importance of nitrogen management during grain filling. Their findings show that appropriate nitrogen application enhances both starch and protein accumulation in grains, improving crop quality and performance. This research emphasizes the critical role of nitrogen management strategies in field crops.

Water management and agroecosystem approaches

Chen et al. present a study on the impact of shallow wet irrigation (SWI) in paddy fields, addressing the persistent issue of nitrogen leaching in rice cultivation. Their work shows that SWI reduces nitrogen leaching by fostering beneficial microbial communities that enhance nitrogen fixation and rice yield. The integration of water management practices with nitrogen use efficiency highlights the potential for holistic agroecological approaches to improve both productivity and sustainability in cropping systems.

Tang et al. take a technological approach to nitrogen management, developing a precision fertilization model for durian cultivation using the IM-RBNNA algorithm. This data-driven tool provides accurate predictions of soil nutrient levels, optimizing nitrogen application and reducing fertilizer waste. The

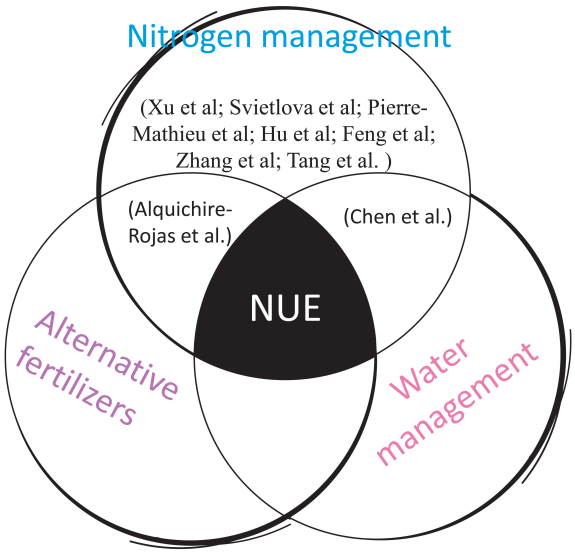

FIGURE 1
A Venn diagram showing the different studies belonging to this Research Topic, and three strategies (nitrogen assimilation, water management and alternative fertilizers), proposed by their authors, to improve NUE. These strategies require the integration of molecular, metabolic, and genetic approaches, as well as the use of soil microorganisms, and precision agriculture techniques.

integration of advanced technology in fertilization strategies underscores the importance of precision agriculture in achieving higher yields while minimizing environmental impact.

Perspective: toward an integrated approach for nitrogen use efficiency

The papers in this Research Topic illustrate the complexity of nitrogen metabolism and management, from molecular signaling mechanisms to agroecosystem applications. As global agricultural systems face increasing pressure to produce more food with fewer resources, the insights from these studies will play a pivotal role in guiding the next generation of sustainable nitrogen management practices.

By integrating molecular biology, metabolic regulation, microbial symbiosis, precision agriculture, and innovative water management (Figure 1), these contributions pave the way for more efficient and sustainable agricultural systems for a world experiencing an accelerated climate change.

Author contributions

EO-G: Writing – original draft, Writing – review & editing. LB-G: Writing – review & editing. ND-S: Writing – review & editing.

Acknowledgments

We would like to express our gratitude to all the authors and reviewers who contributed to this Research Topic. Their collective efforts have made this compilation of cutting-edge research possible. We also thank the editorial team at Frontiers in Plant Science for their support throughout this process.

Conflict of interest

The authors declare that the research was conducted in the absence of any commercial or financial relationships that could be construed as a potential conflict of interest.

Publisher's note

References

Coskun, D., Britto, D., Shi, W., and Kronzucker, H. (2017). Nitrogen transformations in modern agriculture and the role of biological nitrification inhibition. *Nat. Plants* 3. doi: 10.1038/nplants.2017.74

Dimkpa, C., Fugice, J., Singh, U., and Lewis, T. (2020). Development of fertilizers for enhanced nitrogen use efficiency - Trends and perspectives. *Sci. total Environ.* 731, 139113. doi: 10.1016/j.scitotenv.2020.139113

O'Brien, J., Vega, A., Bouguyon, E., Krouk, G., Gojon, A., Coruzzi, G., et al. (2016). Nitrate transport, sensing, and responses in plants. *Mol. Plant* 9, 837–856. doi: 10.1016/j.molp.2016.05.004

Qasim, W., Xia, L., Lin, S., Wan, L., Zhao, Y., and Butterbach-Bahl, K. (2020). Global greenhouse vegetable production systems are hotspots of soil N2O emissions and nitrogen leaching: A meta-analysis. *Environ. pollut.* 272, 116372. doi: 10.1016/j.envpol.2020.116372

The, S., Snyder, R., and Tegeder, M. (2021). Targeting nitrogen metabolism and transport processes to improve plant nitrogen use efficiency. *Front. Plant Sci.* 11. doi: 10.3389/fpls.2020.628366

frontiers | Frontiers in Plant Science

TYPE Original Research
PUBLISHED 22 January 2024
DOI 10.3389/fpls.2024.1339105

OPEN ACCESS

EDITED BY
Enrique Ostria-Gallardo,
University of Concepcion, Chile

REVIEWED BY
Catalina Castro,
Universidad de Concepción, Chile
Asif Iqbal,
Hazara University, Pakistan

*CORRESPONDENCE
Tingbo Dai
tingbod@njau.edu.cn

RECEIVED 15 November 2023
ACCEPTED 05 January 2024
PUBLISHED 22 January 2024

CITATION
Hu J, Zheng Q, Neuhäuser B, Dong C, Tian Z and Dai T (2024) Superior glucose metabolism supports NH_4^+ assimilation in wheat to improve ammonium tolerance. *Front. Plant Sci.* 15:1339105. doi: 10.3389/fpls.2024.1339105

Superior glucose metabolism supports NH_4^+ assimilation in wheat to improve ammonium tolerance

Jinling Hu[1], Qiaomei Zheng[1], Benjamin Neuhäuser[2], Chaofeng Dong[1], Zhongwei Tian[1] and Tingbo Dai[1*]

[1]Key Laboratory of Crop Physiology Ecology and Production Management of Ministry of Agriculture, Nanjing Agricultural University, Nanjing, Jiangsu, China, [2]Institute of Crop Science, Nutritional Crop Physiology, University of Hohenheim, Stuttgart, Germany

The use of slow-release fertilizers and seed-fertilizers cause localized high-ammonium (NH_4^+) environments in agricultural fields, adversely affecting wheat growth and development and delaying its yield. Thus, it is important to investigate the physiological responses of wheat and its tolerance to NH_4^+ stress to improve the adaptation of wheat to high NH_4^+ environments. In this study, the physiological mechanisms of ammonium tolerance in wheat (*Triticum aestivum*) were investigated in depth by comparative analysis of two cultivars: NH_4^+-tolerant Xumai25 and NH_4^+-sensitive Yangmai20. Cultivation under hydroponic conditions with high NH_4^+ (5 mM NH_4^+, AN) and nitrate (5 mM NO_3^-, NN), as control, provided insights into the nuanced responses of both cultivars. Compared to Yangmai20, Xumai25 displayed a comparatively lesser sensitivity to NH_4^+ stress, as evident by a less pronounced reduction in dry plant biomass and a milder adverse impact on root morphology. Despite similarities in NH_4^+ efflux and the expression levels of *TaAMT1.1* and *TaAMT1.2* between the two cultivars, Xumai25 exhibited higher NH_4^+ influx, while maintaining a lower free NH_4^+ concentration in the roots. Furthermore, Xumai25 showed a more pronounced increase in the levels of free amino acids, including asparagine, glutamine, and aspartate, suggesting a superior NH_4^+ assimilation capacity under NH_4^+ stress compared to Yangmai20. Additionally, the enhanced transcriptional regulation of vacuolar glucose transporter and glucose metabolism under NH_4^+ stress in Xumai25 contributed to an enhanced carbon skeleton supply, particularly of 2-oxoglutarate and pyruvate. Taken together, our results demonstrate that the NH_4^+ tolerance of Xumai25 is intricately linked to enhanced glucose metabolism and optimized glucose transport, which contributes to the robust NH_4^+ assimilation capacity.

KEYWORDS

ammonium stress, ammonium tolerance, ammonium assimilation, glucose metabolism, wheat

1 Introduction

Ammonium (NH_4^+) stress is a global challenge that severely affects crop production (Esteban et al., 2016). Accumulation of NH_4^+ in soils can be attributed to natural events and human activities, including atmospheric NH_4^+ deposition (Liu et al., 2013), soil NH_4^+ adsorption (Liu et al., 2008), and localized application of NH_4^+-based fertilizers (Pan et al., 2016; Marino and Moran, 2019). Plants subjected to high NH_4^+ conditions display distinct characteristics from those grown in NO_3^- conditions, including external acidification, reduced cationic absorption, imbalances in carbon and nitrogen metabolisms, and oxidative damage (Bittsánszky et al., 2015; Esteban et al., 2016). Over the past two decades, several factors contributing to NH_4^+ tolerance have been identified, primarily via studies on NH_4^+-tolerant rice (*Oryza sativa*) and *Arabidopsis thaliana*. However, the specific plant traits that are responsible for NH_4^+ tolerance, especially in NH_4^+-sensitive species such as wheat (*Triticum aestivum*), remain unclear.

To mitigate NH_4^+ toxicity, plants must delicately balance NH_4^+ uptake, assimilation, and release (Bittsánszky et al., 2015). This balance can be achieved by either regulating transporters to reduce NH_4^+ uptake or developing effective detoxification mechanisms to counteract excess NH_4^+ accumulation (Ijato et al., 2021). In plants, the high-affinity uptake of NH_4^+ is primarily mediated by ammonium transporters (AMTs). Studies showed that *AMT1* gene knockout significantly inhibits NH_4^+ uptake, while *AMT1* overexpression enhances NH_4^+ permeability in the roots (Ranathunge et al., 2014; Li et al., 2016). In *Arabidopsis*, the three AMT1 proteins (AMT1;1, AMT1;2, and AMT1;3) contribute to approximately 90% of NH_4^+ uptake (Yuan et al., 2007). In addition, some studies have pointed to the existence of multiple NH_4^+ uptake channels in plants aside from AMT (Esteban et al., 2016), and the simultaneous presence of NH_4^+ influx and efflux has been observed in barley (*Hordeum vulgare*) and rice root cells under high external NH_4^+ conditions (Britto et al., 2001). Collectively, NH_4^+ uptake and efflux by plant roots is complex and needs to be assessed from multiple perspectives. The status of NH_4^+ uptake and efflux and the relationship of this NH_4^+ movement with NH_4^+ tolerance under NH_4^+ stress is still unknown.

After NH_4^+ is absorbed by plant cells, it is converted into glutamine (Gln) by combining with glutamate. The synthesis of glutamate from 2-oxoglutarate (2-OG) is a critical step in NH_4^+ assimilation and cellular defense against NH_4^+ stress (Bittsánszky et al., 2015). Under NH_4^+ stress, many plant species exhibit an increase in the activities of NH_4^+ assimilation enzymes, such as glutamine synthetase (GS, EC 6.3.1.2) and glutamate synthase (GOGAT, EC 1.4.7.1) (Britto and Kronzucker, 2002; Vega-Mas et al., 2019a; González-Moro et al., 2021). Notably, *A. thaliana* mutants lacking the GLN1;2 isoform exhibit excessive NH_4^+ accumulation and a high sensitivity to NH_4^+ stress (Hachiya et al., 2021), underscoring the significance of this pathway in the protection of plants against NH_4^+ toxicity. However, there remains some debate regarding the activity of GS under NH_4^+ stress (Jian et al., 2018). Consequently, the variability in the activities of NH_4^+ assimilation-related enzymes among NH_4^+-tolerant species/cultivars needs to be further investigated.

The principal products of NH_4^+ assimilation in plants are nitrogen-rich compounds, primarily amino acids, and proteins. The accumulation of these compounds reflects the capacity of plants to assimilate NH_4^+ and adapt to NH_4^+ stress (Vega-Mas et al., 2019b). Among the free amino acids, glutamate (Glu), glutamine (Gln), aspartic acid (Asp), and asparagine (Asn) consistently accumulated under NH_4^+ stress across various plant species (Jian et al., 2018; de la Peña et al., 2019; Vega-Mas et al., 2019a). Studies suggested that Asn and Gln, as crucial forms of nitrogen storage and transportation, reflect the nitrogen status and regulate NH_4^+ uptake and assimilation (Xu et al., 2012; Konishi et al., 2016). Distinctly, a previous study observed that Gln and Asn concentrations in the *Arabidopsis chl1-1* mutant were lower than those in the wild type, indicating that the decline in Gln and Asn may be related to ammonium tolerance in the mutant (Jian et al., 2018). Therefore, different NH_4^+-tolerant cultivars might exhibit varied accumulations of NH_4^+ assimilates, which might be attributed to varying NH_4^+ assimilation capacities, however, it still needs to be validated.

Adequate carbon (C) skeleton supply is also essential to address excess NH_4^+ under NH_4^+ stress (Britto and Kronzuker, 2005). A classic hypothesis on NH_4^+ toxicity suggests that insufficient carbon skeletons in the root lead to NH_4^+ poisoning in the plant (Esteban et al., 2016). Numerous studies have reported that excess NH_4^+ in the root leads to a reduction in soluble sugar content and enhances the TCA cycle, to produce 2-oxoglutarate and oxaloacetate (OAA) for NH_4^+ assimilation (Viktor and Cramer, 2005; Ariz et al., 2013; Vega-Mas et al., 2019a). Conversely, some studies indicated that NH_4^+ stress increases soluble sugar content and uncouples carbon and nitrogen metabolism (Jian et al., 2018; Li et al., 2020). The complex relationship between sugar metabolism and carbon skeleton supply under NH_4^+ stress is responsible for varying response mechanisms and severities of NH_4^+ stress in plants. Improving sugar metabolism and carbon skeleton availability under NH_4^+ stress may enhance NH_4^+ tolerance in plants.

As a major global crop, wheat is essential to ensure food security for the world's population. Notably, wheat plants exhibit high sensitivity to NH_4^+ stress, especially during the seedling and reproductive stages (Wang et al., 2016; Liu et al., 2021). In recent years, there has been growing evidence that NH_4^+ stress adversely impacts wheat seedling growth (Ijato et al., 2021; Liu et al., 2021). However, studies on the precise underlying response mechanisms in different NH_4^+-tolerant wheat cultivars are still scarce. In this research, we aimed to investigate the physiological and molecular processes underlying NH_4^+ tolerance in wheat plants. We conducted a comparative analysis of NH_4^+-tolerant and NH_4^+-sensitive cultivars under NH_4^+ stress, including growth responses,

Abbreviations: AMTs, ammonium transporters; Asn, asparagine; Asp, aspartate; DAT, days after treatment; ERDL, tonoplast H^+/glucose symporter; GDH, glutamate dehydrogenase; GS, glutamine synthetase; GOGAT, glutamate synthase; Gln, glutamine; Glu, glutamate; HXK, hexokinase; LR, lateral root; OAA, oxaloacetate; PEPc, phosphoenolpyruvate carboxylase; PFK, phosphofructokinase; PK, pyruvate kinase; PR, primary root; TST, tonoplast sugar transporter; 2-OG, 2-oxoglutarate.

NH_4^+ uptake and assimilation, glucose metabolism, and carbon skeleton supply. The study seeks to test two hypotheses: (i) the NH_4^+-tolerant cultivar may have a weaker NH_4^+ uptake capacity than the NH_4^+-sensitive cultivar, and (ii) the NH_4^+-tolerant cultivar may have a stronger sugar metabolism, thus providing more carbon skeletons for NH_4^+ assimilation under NH_4^+ stress.

2 Materials and methods

2.1 Plant materials and experimental design

We selected two wheat cultivars (as illustrated in Supplementary Figure S1), Xumai25 (NH_4^+-tolerant) and Yangmai20 (NH_4^+-sensitive), based on the observed tolerance and sensitivity to NH_4^+ during pre-experiments (data not shown). The seeds of both cultivars were surface sterilized using a 10% (v/v) H_2O_2 solution for 15 min, followed by thorough rinsing with sterile distilled water. Subsequently, the seeds were germinated under dark conditions in Petri dishes until the seed bud was ~1 cm long. Then, the seedlings were transplanted into opaque plastic containers (45 cm × 32 cm × 25 cm, volume: 36 L) filled with water. The seedlings at the two-leaf stage were grown in a modified 50% Hoagland nutrient solution until they reached the four-leaf stage. Following this pre-treatment, the seedlings were divided into two groups. One group was treated with nitrate nitrogen (NN, 5 mM NO_3^--N) nutrient solutions and the other with ammonium nitrogen (AN, 5 mM NH_4^+-N) nutrient solution. The concentrations and composition of macronutrients in both treatments are listed in Supplementary Table S1. The micronutrient composition in both treatments remained consistent, as previously described by Liu et al. (2021). To ensure a consistent nitrogen supply in each solution, the solutions were refreshed every three days and were continuously aerated to prevent anoxic conditions. The pH of each treatment was adjusted daily to 5.8 using 0.1 mM H_2SO_4 or 0.1 mM NaOH. The entire experiment was conducted in a controlled greenhouse environment with a 16 h/8 h light/dark cycle and temperature maintained at 18°C during the day and 8.5°C at night. The light intensity and relative air humidity in the greenhouse were set at 400 μmol m^{-2} s^{-1} and 60%, respectively. We adopted a completely randomized block design, and each experiment was replicated three times. Each replication consisted of three containers, and each container housed 60 plants.

The entire ammonium stress treatment was sustained for 20 days. Seedlings were collected at 0, 1, 3, 5,10, and 20 days after treatment (DAT) to assess biochemical and physiological changes. The leaves, stems, and roots of the seedlings were separated and divided into two segments. One segment was subjected to oven drying at 105°C for 20 min, followed by drying at 85°C, for dry weight and nitrogen concentration measurements. The other segment was promptly frozen in liquid nitrogen and stored at −80°C for subsequent analyses.

2.2 Root morphology analysis

After 20 days of treatment, the entire root of each wheat seedling was scanned using a V700 scanner system (Epson, Indonesia). Briefly, eight seedlings per treatment group were randomly selected and labeled before the start of the treatment. The plant roots were rinsed with water, placed in a scanning disk with a small amount of water, laid flat and evenly, and scanned. The obtained root images were analyzed using the WinRhizo Pro V700 1.0 software (Regent Instruments, Canada). The data on the length, volume, surface area, and average diameter of the roots were obtained from the software directly. Additionally, the number of lateral roots was determined by counting directly.

2.3 Measurement of root NH_4^+ flux

The net NH_4^+ influx and efflux at the root surface of two cultivars were determined using Non-invasive Micro-test Technology (NMT Physiolyzer®, Younger USA LLC, MA, USA), Xuyue (Beijing) Sci. &Tech. Co., Ltd., Beijing, China, provided the measure services. Wheat seedlings of uniform growth were selected before treatment. The measurement of root NH_4^+ influx according to Sun et al. (2022). The seedlings were treated with 5.0 mM NH_4^+ solution (mentioned above), and tested directly after 0.17, 2, 6, 24, 72, and 120 hours treatment with the high concentration NH_4^+ measuring solution (2.5 mM $(NH_4)_2SO_4$, 0.1 mM $CaCl_2$, pH 5.8), respectively. The measurement of root NH_4^+ efflux according to Di et al. (2021), wheat seedlings were treated for 0.5, 6, 24, 72, and 120 hours with the 5.0 mM NH_4^+ solution in advance, respectively, and then moved to a low concentration NH_4^+ measuring solution (0.1 mM $(NH_4)_2SO_4$, 0.1 mM $CaCl_2$, pH 5.8) for testing. Briefly, two roots were randomly selected from each plant, rinsed with distilled water, and immersed at the bottom of the Petri dish containing fresh measure solution (for the NH_4^+ efflux measurement, the roots were equilibrated in measure solution for 20 min). The NH_4^+ flux microsensor was positioned at an apex of 1600 μm on the root surface (the position with the maximum net fluxes of NH_4^+ selected from our preliminary experiment). Stable data was recorded for 3 min, with 8 replicates for each set of assays.

2.4 NH_4^+ concentration

The determination of NH_4^+ concentration followed the procedure outlined by Balkos et al. (2009). Root samples were collected and subsequently desorbed in a 10 mM $CaSO_4$ solution for 5 min to remove extracellular NH_4^+. Then the roots were ground to powder in liquid nitrogen, and 0.2 g of the powder was homogenized in 2 ml of pre-cooled 10 mM formic acid. The resulting mixture was subjected to centrifugation at 53,000 × g for 5 min at 2°C. The supernatant was then filtered through a 0.45 μm filter into a 2 mL polypropylene tube and assayed for NH_4^+ concentration using the o-phthalaldehyde (OPA) method.

2.5 Nitrogen accumulation and amino acid concentration

Fresh root, stem, and leaf samples were freeze-dried and then ground into powder for the following measurements.

For N concentration analyses, approximately 0.1g of the powder was accurately weighed and mixed with 5 ml of H_2SO_4. The resulting mixture was heated to 200°C until achieving a clear solution. Subsequently, the reaction was terminated by adding H_2O_2. The resulting solutions were then analyzed using ICP-OES (Optima 8000, Perkin Elmer). Plant nitrogen accumulation = (plant dry weight - plant dry weight before treatment) × N concentration.

The total free amino acid was determined using the ninhydrin method, following a previously described protocol with slight modifications (Yokoyama and Hiramatsu, 2003). Briefly, 0.1 g root sample powder was weighed and mixed with the extraction buffer, which consisted of acetic acid/sodium acetate (pH 5.4). Then, centrifuging the mixture and collecting the supernatant. The OD value of the supernatant was measured at 580 nm and recorded using a Pharmacia Ultra Spec Pro UV/VIS spectrophotometer (Pharmacia, Cambridge, England). The final concentration of free amino acid was calculated according to the measured simultaneously with leucine as substrate.

To determine glutamate, glutamine, aspartic acid, and asparagine concentrations, 0.1 g of the root sample powder was weighed and extracted with 3% sulfosalicylic acid (w/v) for 12 hours. Afterward, the mixture was centrifuged at 10,000 g for 10 min, and the resulting supernatant was collected. This extraction process was repeated twice, and all the supernatants were combined and then filtered through a 0.22-μm aqueous film filter. The amino acids in the filtrate were quantified using the Hitachi L-8900 automatic amino acid analyzer (L-8900; Hitachi Corp., Tokyo, Japan), following the method described by Ma et al. (2017).

2.6 Soluble sugars and carbon skeleton concentration

The sucrose and fructose concentrations were determined using the resorcinol method described by Zeng et al. (2014). Briefly, 0.1g of the root sample powder (fresh samples were freeze-dried and ground) was weighed and extracted with a sugar extraction solution. For sucrose determination, the supernatant was mixed with 2 M NaOH and incubated at 95°C for 10 min. Subsequently, 0.1 M resorcinol and 10 M HCl were added to the mixture, further incubating at 80°C for 60 min. The concentration of fructose was determined similarly to that of sucrose but without NaOH treatment before the color reaction. Both absorbances were measured at 500 nm using a Pharmacia Ultra Spec Pro UV/VIS spectrophotometer (Pharmacia, Cambridge, England). The concentration of fructose derived from hydrolyzed sucrose was subtracted to determine the free fructose concentration. The concentrations of sucrose and fructose were determined based on the corresponding standard curves.

For the quantification of glucose, pyruvate, 2-oxoglutarate (2-OG), and oxaloacetate (OAA) concentrations of roots, the HPLC method described by Georgelis et al. (2018) was used with some modifications. Approximately 0.2 g of fresh root samples were ground into a powder using liquid nitrogen and then mixed with 4 ml of the extraction solution (preheated 80% ethanol) for 5 min at 80 °C. Subsequently, the mixtures were centrifuged at 12000 g for 10 min, and the resulting supernatants were collected. After the first collection of supernatants, the pellets were resuspended in 2 ml of 50% ethanol, and the extraction procedure was repeated as described above. The supernatants were collected again, and the pellets were resuspended with 2 ml of dd-water and repeated the extraction procedure. All supernatants were collected and vigorously shaken after mixing with an equal volume of chloroform. After the extraction procedure, the aqueous phase was collected, dried under vacuum, and re-dissolved in 1 ml of 50% acetonitrile (acetonitrile: water =50: 50). Before analysis using the anion-exchange HPLC system, the samples were filtered through a 0.45 μm filter membrane. Sugar compounds were separated on a Sugar-D column (4.6×250 mm, Nacalai Tesque Inc., Japan) using a mobile phase of acetonitrile/water (75: 25, v/v) at a 1.0 ml/min flow rate. The column temperature was 40 °C, and the injection volume was 30 μl. The quantification of each sugar was performed by comparing the peak areas of the samples with those of the standard solutions.

2.7 Enzyme activity

The root GS activity was determined using a previously described method (Jiang et al., 2017). Briefly, 0.5 g of frozen root samples were weighed and extracted with 1.2 mL of extraction buffer (1 mmol L^{-1} EDTA, 100 mmol L^{-1} pH 7.6 Tris-HCl, 1 mmol L^{-1} $MgCl_2$, and 10 mmol L^{-1} β-mercaptoethanol). This reaction mixture was then incubated at 25°C for 5 min and then transferred to a hydroxylamine hydrochloride bath at 25°C for 15 min. Subsequently, the mixture was subjected to chromatography utilizing $FeCl_3$ solution. Then, the mixture was centrifuged at 4000 rpm for 10 min at 25°C. Finally, the optical density of the supernatant at 540 nm was measured using the Pharmacia Ultra Spec Pro UV/VIS spectrophotometer (Pharmacia, Cambridge, England).

The activity of glutamate dehydrogenase (GDH, EC 1.5.1) was determined according to the procedure outlined by Skopelitis et al. (2007). Briefly, for the assay of NADH-GDH activity, 2.6 ml of the reservoir solution (115.4 mmol L^{-1} pH 8.0 Tris-HCl, 23.1 mmol L^{-1} 2-oxoglutarate, 231 mmol L^{-1} NH_4Cl), 0.1 ml 30 mmol L^{-1} $CaCl_2$, 0.1 ml 0.2 mmol L^{-1} NAD(P)H, and 0.1 ml deionized water were pre-added to the test tubes. The reaction was then initiated by adding 0.1 ml of root extract (same as that of GS), and the absorbance value was measured at 340 nm using a Pharmacia Ultra Spec Pro UV/VIS spectrophotometer (Pharmacia, Cambridge, England), and again after 3 min to calculate the difference. Test tubes with distilled water instead of NADH and root extracts were used as blank controls. For the analysis of NAD^+-GDH activity, 2.6 ml of the reservoir solution (115.4 mmol L^{-1} pH 9.3 Tris-HCl, 115.4 mmol L^{-1} L-glutamate, 30 mmol L^{-1} $CaCl_2$), 0.05 ml 30 mmol L^{-1} $CaCl_2$, 0.1 ml 30 mmol L^{-1} NAD^+, and 0.15 ml deionized water were pre-added to the test tubes. Other measurement steps were the same as for NADH-GDH. The activity of GDH was expressed as one unit of enzyme activity in terms of the amount of enzyme required to oxidize or reduce 1 μmol of NADH or NAD^+ min^{-1} at 30 °C.

The activities of GOGAT, hexokinase (HXK, EC 2.7.1.1), phosphofructokinase activity (PFK, EC 2.7.1.11), pyruvate kinase (PK, EC 2.7.1.40), and phosphoenolpyruvate carboxylase (PEPc, 4.1.1.31) were measured using respective kits (catalog numbers: BC0070, BC1465, BC0745, BC0530, BC0540, and BC2190, respectively) purchased from Beijing Solarbio Science & Technology Co., Ltd. (Beijing, China). All enzyme activities were measured using the spectrophotometer as described previously (Chen et al., 2023). Briefly, 0.05 g of each fresh root sample was weighed and ground into powder using a freezer-mill. The powder was then treated with the respective kit reagents as per the manufacturer's instructions. Finally, the rate of decrease in the absorbance of each reaction solution was obtained using the spectrophotometer.

2.8 RT-PCR

Total RNA from root samples was extracted using TRIzol reagent (Vazyme Bio, China). For cDNA synthesis, the HiScript III Q RT SuperMix (Vazyme Bio, China) was employed following the manufacturer's instruction, and the cDNA samples were diluted 5× before being subjected to qPCR analysis. Real-time quantitative RT-PCR was carried out using the CFX Connect Real-Time PCR Detection System (Bio-Rad, USA) with ChamQ SYBR qPCR Master Mix (Vazyme Bio, China).

The primer sequences for *TaPFK*, *TaHXK*, and *TaPK* were sourced from Li et al. (2019). The primers for *AMT1s* (*TaAMT1.1* and *TaAMT1.2*) were referred to by Ijato et al. (2021). The primer for *TaAmt2.1* was referred to by Porras Murillo et al. (2023). The primers for tonoplast sugar transporter *TaTST*, tonoplast H^+/glucose symporter *TaERDL*, and the internal reference genes *ACT* and *ADP* were listed in Supplementary Table S2. Relative expression levels were determined using the Livak and Schmittgen (2001) method.

2.9 Statistical analysis

The experiment was repeated three times during two years. Statistical analyses were performed using SPSS software version 19 (IBM Corp., Armonk, NY, USA). Analysis of variance (ANOVA) was subsequently carried out, and *post hoc* comparisons of means were performed using Duncan's test. Graphs and tables were generated using Excel and Origin 2018 software (OriginLab, Northampton, MA, USA).

3 Results

3.1 Dry weight and root morphology

We first examined the growth responses of the two wheat cultivars to NH_4^+ stress. The AN-treated plants exhibited significantly reduced shoot, root, and total plant dry weight than the NN-treated plants, with the impact being more pronounced in Yangmai20 than in Xumai25 (Figure 1). Notably, the decrease in the root dry weight for Yangmai20 commenced at 3 DAT, while that for Xumai25 began at 5 DAT (Figure 1C).

Next, we assessed the root morphology of the cultivars to analyze the differential root responses under NH_4^+ stress. At 20 DAT, for both cultivars, we observed significantly reduced length, surface area, and volume of both primary and lateral roots for AN-treated plants than NN-treated plants (Table 1). After AN treatment, Yangmai20 exhibited more prominent reductions in the length, surface area, and volume of the primary root than Xumai25 (64%, 60%, and 64% vs. 50%, 49%, and 47%, respectively). Similarly, Yangmai20 exhibited more prominent reductions in the length, surface area, and volume of the lateral roots than Xumai25 post-AN treatment (36%, 43%, and 48% vs. 22%, 27%, and 29%, respectively). Moreover, the average diameter of the primary roots of AN-treated plants was comparable to that of NN-treated plants. However, the AN-treated Yangmai20 and Xumai25 exhibited a 23% and 25% increase in the average diameter of the lateral roots and a 33% and 23% reduction in the number of lateral roots, respectively, than their NN-treated counterparts (Table 1).

3.2 Free NH_4^+ concentration

Accumulation of free NH_4^+ in the root contributes to NH_4^+ toxicity in plants. Hence, we next compared free NH_4^+ accumulation in the roots of the two wheat cultivars. The free NH_4^+ concentration in the roots of both cultivars did not differ significantly after NN treatment. However, AN treatment led to an increase in the free NH_4^+ concentration of the roots of both cultivars, with a more prominent increase in Yangmai20 than Xumai25 (Figure 2).

3.3 NH_4^+ influx and efflux

Changes in influx and efflux of NH_4^+ are closely related to NH_4^+ concentration in the plant and the severity of NH_4^+ toxicity. Here, we employed non-invasive micro-test technology (NMT) to dynamically measure changes in net NH_4^+ influx and efflux, thus revealing the differences in root NH_4^+ uptake between the two cultivars under NH_4^+ stress. The results revealed that treatment with 5 mM NH_4^+ stimulated NH_4^+ influx in the root of both cultivars, peaking at 6 h after treatment. Notably, NH_4^+-tolerant Xumai25 exhibited a more pronounced NH_4^+ influx (Figure 3A) despite a lower free NH_4^+ concentration in the root than NH_4^+-sensitive Yangmai20 (Figure 2).

NH_4^+ efflux was observed in the roots of both cultivars at 0.5 h after treatment, gradually increasing with time and peaking at 72 h after treatment. While Yangmai20 tended to exhibit higher NH_4^+ efflux, the efflux did not differ significantly between the two cultivars (Figure 3B).

10.3389/fpls.2024.1339105

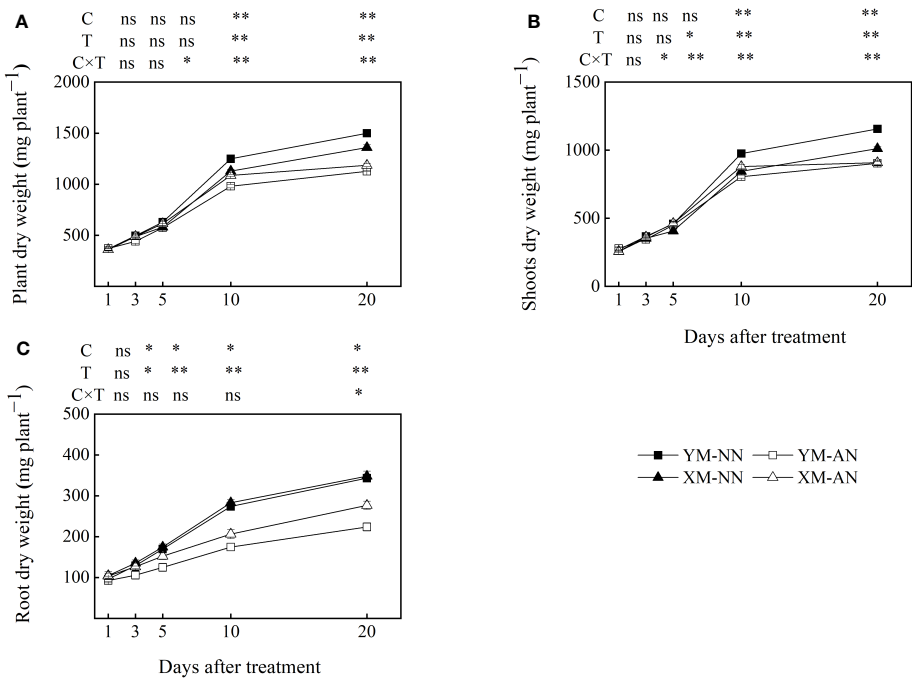

FIGURE 1
Effect of ammonium stress on biomass accumulation of two different ammonium-sensitive cultivars. **(A)** plant dry weight; **(B)** shoot dry weight; **(C)** root dry weight. Data are given as means of three biological replicates, and error bars indicate SD. NN, nitrate conditions; AN, ammonium stress conditions. YM, NH_4^+-sensitive cultivar Yangmai20; XM, NH_4^+-tolerant cultivar Xumai25. C, T, and C×T represent the F-value of cultivar, treatment, and the interaction between cultivar and treatment, respectively. The symbols * and ** indicate significant differences at the 0.05 and 0.01 levels, respectively, while ns refers to no significant difference.

3.4 Nitrogen status

Nitrogen accumulation intuitively reflects the plant's ability to assimilate NH_4^+. Hence, we measured and compared the nitrogen status of the two wheat cultivars. Compared to the NN-treated plants, the AN-treated plants exhibited significantly enhanced nitrogen accumulation in the leaves, with more prominent accumulation in Xumai25 than in Yangmai20 (Figure 4). Differently, the stem nitrogen accumulation decreased in Yangmai20, while no significant difference was observed in Xumai25. Furthermore, compared to the NN-treated plants, the AN-treated plants exhibited significantly reduced nitrogen accumulation in the roots, with a more prominent reduction in Yangmai20 than Xumai25 (Figure 4A).

TABLE 1 Effects of ammonium stress on the root morphology of wheat seedlings after 20 days of treatment.

Cultivar	Treatment	Root length (cm)		Root surface area (cm^2)		Average diameter (mm)		Root volume (cm^3)		LR numbers
		PR	LR	PR	LR	PR	LR	PR	LR	
Yangmai20	NN	3405 ± 58a	484 ± 12a	332 ± 6.2a	86 ± 2.1a	0.32 ± 0.009a	0.42 ± 0.014c	2.55 ± 0.053a	0.93 ± 0.014b	20 ± 1.0a
	AN	1218 ± 25d	312 ± 10c	132 ± 11.3d	50 ± 1.8c	0.30 ± 0.008a	0.52 ± 0.01a	0.93 ± 0.005c	0.56 ± 0.006d	13.3 ± 0.33c
Xumai25	NN	3037 ± 50b	527 ± 16a	307 ± 6.4b	95 ± 4.6a	0.32 ± 0.011a	0.40 ± 0.019c	2.41 ± 0.109a	1.08 ± 0.015a	23 ± 1.5a
	AN	1528 ± 31c	413 ± 19b	154 ± 6.5c	74 ± 2.2b	0.31 ± 0.014a	0.49 ± 0.009b	1.22 ± 0.033b	0.77 ± 0.023c	17.7 ± 0.23b
F-value	$F_{Cultivar}$	0.74	23.61**	0.05	25.68**	7.81*	10.8*	1.04	95.07**	48.86**
	$F_{Treatment}$	2947.57**	94.23**	902.67**	74**	27.71**	94.54**	362.21**	340.9**	132.25**
	$F_{C\times T}$	99.43**	3.73	16.04**	5.84	9.62*	0.11	7.99*	2.68	0.46

NN, nitrate conditions; AN, ammonium stress conditions. Yangmai20, NH_4^+-sensitive cultivar; Xumai25, NH_4^+-tolerant cultivar. PR, primary root; LR, lateral root. Data are means ± standard deviation (SD) of eight wheat seedlings, and different letters indicate significant differences ($P<0.05$) according to ANOVA. $F_{Cultivar}$, $F_{Treatment}$, and $F_{C\times T}$ refer to the F-value of cultivar, treatment, and interaction of cultivar by treatment, respectively. * and ** indicate significant differences at the 0.05 and 0.01 levels.

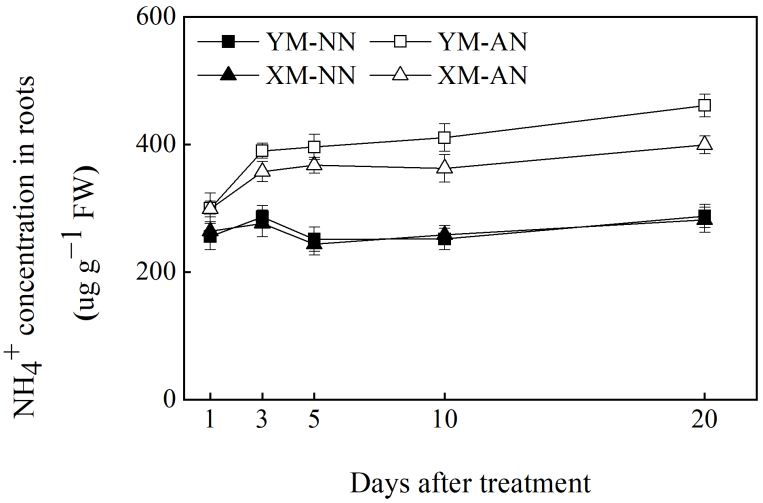

FIGURE 2
Effects of ammonium stress on root free NH_4^+ concentration of wheat seedlings after 1, 3, 5, 10, and 20 days. Data are given as means of three biological replicates, and error bars indicate SD. NN, nitrate conditions; AN, ammonium stress conditions. YM, NH_4^+-sensitive cultivar Yangmai20; XM, NH_4^+-tolerant cultivar Xumai25.

To elucidate the reasons underlying the varying nitrogen accumulation patterns in the two cultivars, we further measured the concentration of NH_4^+ assimilates in the plants. Compared to the NN-treated plants, the AN-treated plants exhibited significantly increased total free amino acid levels in the roots at 3 and 20 DAT, with substantially higher levels in Xumai25 roots than in Yangmai20 roots at 20 DAT (Figure 4B). Furthermore, the AN-treated plants exhibited significantly higher Asn, Gln, Asp, and Glu levels than the NN-treated plants (Figures 4C–F). Among the AN-treated plants, Xumai25 exhibited a higher increase in Asp, Asn, and Gln levels, but a lower increase in Glu levels than Yangmai20 (Figures 4C–F).

3.5 Root carbon skeleton supply

To investigate the effects of NH_4^+ stress on the carbon distribution and supply, we measured the concentrations of sucrose, fructose, glucose, pyruvate, 2-OG acid, and OAA acid in the roots of both wheat cultivars. We observed substantially decreased sucrose levels in the AN-treated plants than the NN-treated plants at 3 and 20 DAT, with higher sucrose levels in Xumai25 than Yangmai20 at 20 DAT (Figure 5A). Furthermore, we observed lower fructose concentrations in AN-treated plants than the NN-treated plants at 20 DAT; however, the fructose levels did not differ significantly between the two cultivars at any point in time (Figure 5B). Conversely, the glucose concentration steadily increased in both cultivars at 3 and 20 DAT after AN treatment (Figure 5C), with 87% and 81% increases in Yangmai20 and 58% and 43% increases in Xumai25, respectively.

Furthermore, the AN-treated plants exhibited significantly reduced pyruvate and 2-OG concentrations than the NN-treated plants (Figures 5D, E), with more prominent reductions in Yangmai20 than Xumai25 (Figures 5D, E). Similarly, the AN-treated plants exhibited reduced OAA concentrations in the roots than the NN-treated plants at 20 DAT, with more prominent reductions in Yangmai20 than Xumai25 (Figure 5F).

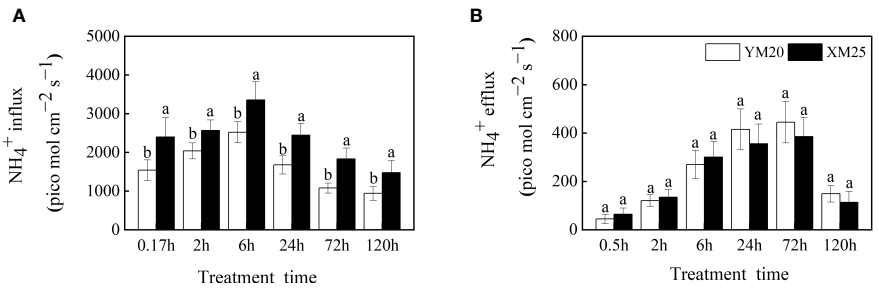

FIGURE 3
Effects of ammonium stress on root NH_4^+ influx and efflux of wheat seedlings. **(A)** NH_4^+ influx; **(B)** NH_4^+ efflux. Data are given as means of 8 replicates. Error bar labels with different letters indicate significant differences ($P < 0.05$) between cultivars. YM20, NH_4^+-sensitive cultivar Yangmai20; XM25, NH_4^+-tolerant cultivar Xumai25.

10.3389/fpls.2024.1339105

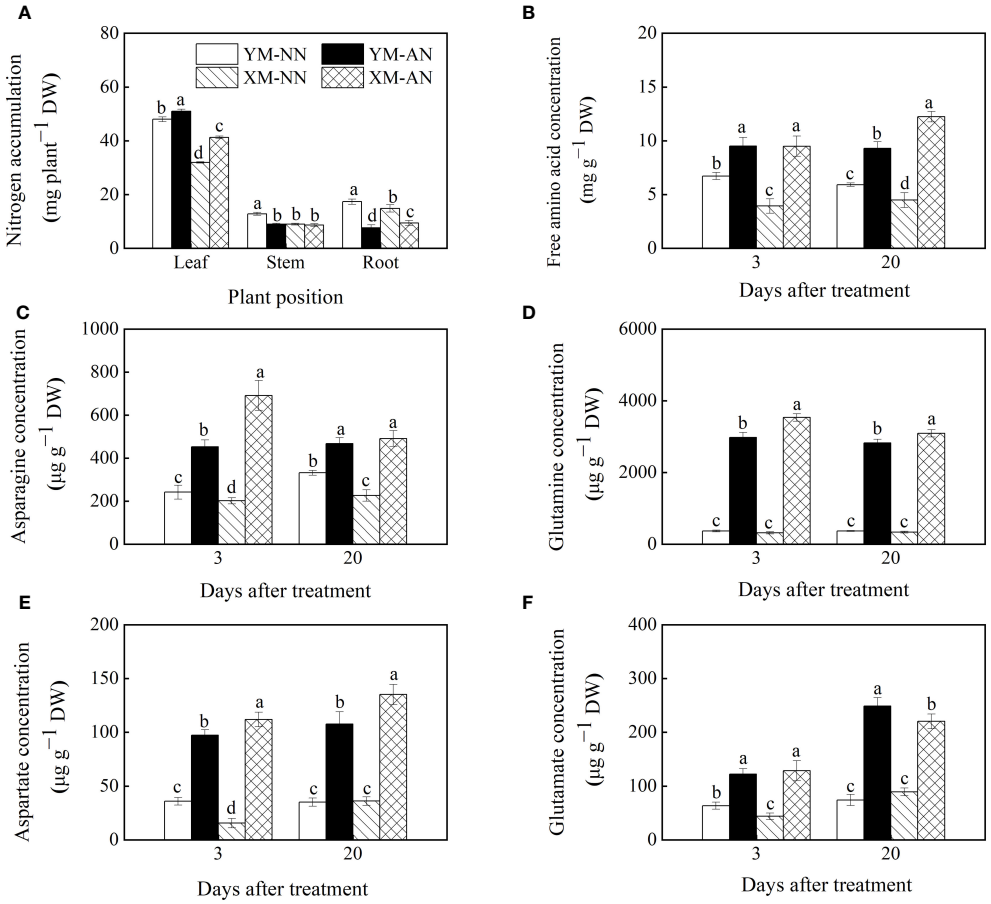

FIGURE 4
Effects of ammonium stress on nitrogen status of wheat seedlings at 3 and 20 days after treatment. **(A)** Plant nitrogen accumulation; **(B)** Root free amino acid concentration; **(C)** Root asparagine concentration; **(D)** Root glutamine concentration; **(E)** Root aspartate concentration; **(F)** Root glutamate concentration. Data are provided as means of three biological replicates and error bar labels with different letters indicate significant differences ($P < 0.05$) between cultivars and treatment. NN, nitrate conditions; AN, ammonium stress conditions. YM, NH_4^+-sensitive cultivar Yangmai20; XM, NH_4^+-tolerant cultivar Xumai25.

3.6 Activities of NH_4^+-assimilating and sugar-metabolizing enzymes

To explore the mechanisms underlying lower glucose accumulation in Xumai25, we measured the activities of enzymes related to glucose metabolism. We observed significantly increased activities of HXK, PEPc, PFK, and PK in the AN-treated plants than the NN-treated plants (Figures 6A–D). Notably, Xumai25 exhibited a more substantial increase in HXK and PFK activities (294% and 169%, respectively) than Yangmai20 (154% and 64%, respectively) at 20 DAT (Figures 6A, B).

The activities of NH_4^+ assimilation–related enzymes are closely related to the NH_4^+ assimilation capacity and NH_4^+ tolerance of plants. In this study, the AN-treated plants exhibited higher activities of GS, ferredoxin-dependent glutamate synthase (Fe-GOGAT), NADH-GDH, and NAD^+-GDH than the NN-treated plants (Figures 7A–D). The activities of these enzymes were mildly higher in Xumai25 than in Yangmai20.

3.7 Relative gene expression correlates to NH_4^+ uptake and carbon supply in roots

Unlike the NN-treated plants, the AN-treated plants exhibited a rapid upregulation of *TaAMT1.1* and *TaAMT1.2* at 6 and 120 h post-treatment (Figures 8A–C), with no significant differences between the two cultivars. Furthermore, the AN-treated plants also exhibited *TaAMT2.1* upregulation in the roots. Moreover, the NN-treated Xumai25 exhibited higher *TaAMT2.1* expression than NN-treated Yangmai20 (Figure 8C).

Similarly, we observed upregulation of *TaPK*, *TaHXK*, and *TaPFK* in AN-treated plants at 6 h and 120 h after treatment (Figures 8D–F), with more prominent upregulation in Xumai25 than Yangmai25 at 120 h (Figures 8D–F).

Tonoplast sugar transporter (TST) and H^+/glucose symporter (ERDL) mediate glucose transport across the vacuolar membrane. In this study, the AN-treated Yangmai20 exhibited a lower *TaERDL* expression than its NN-treated counterpart at 6 h; however, no significant differences were observed between AN- and NN-treated Xumai25. Moreover, at 120 h, all AN-treated plants exhibited

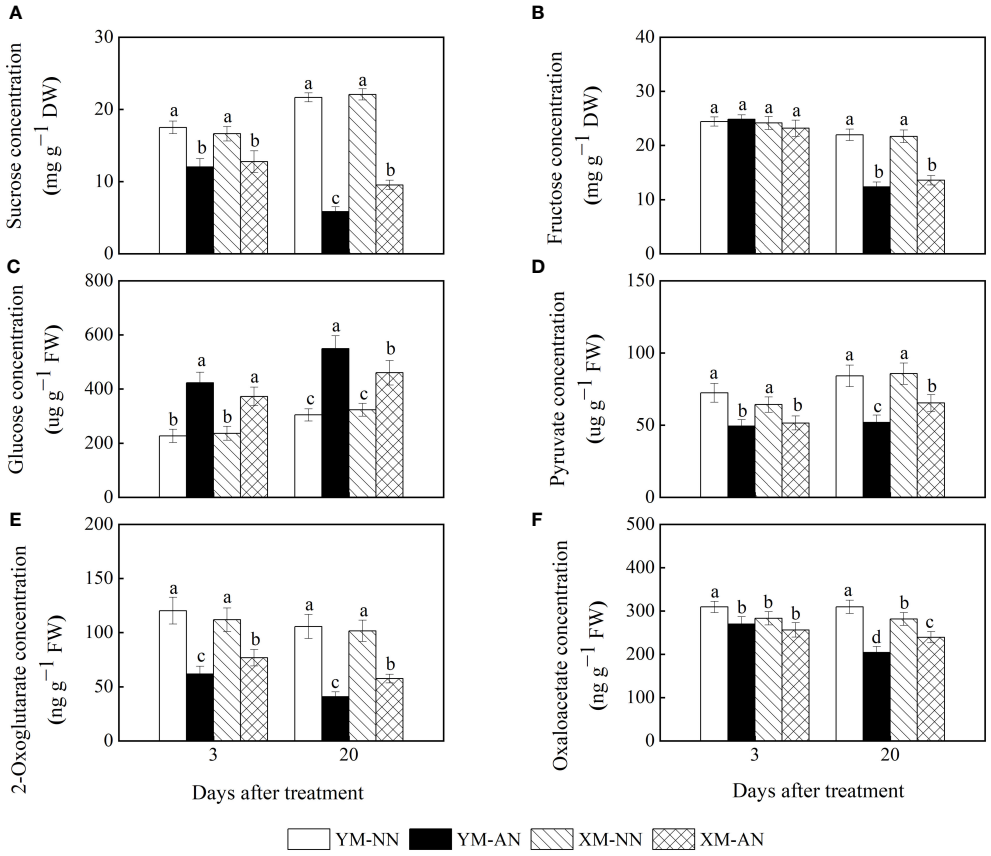

FIGURE 5
Effects of ammonium stress on root carbon skeleton supply of wheat seedlings at 3 and 20 days after treatment (DAT). **(A)** Sucrose concentration; **(B)** Fructose concentration; **(C)** Glucose concentration; **(D)** Pyruvate concentration; **(E)** 2-Oxoglutarate concentration; **(F)** Oxaloacetate concentration. Data are supplied as means of six biological replicates. Error bar labels with different letters indicate significant differences ($P < 0.05$) between cultivars and treatment. NN, nitrate conditions; AN, ammonium stress conditions. YM, NH_4^+-sensitive cultivar Yangmai20; XM, NH_4^+-tolerant cultivar Xumai25.

significantly more *TaERDL* downregulation than the NN-treated plants (Figure 8G). In addition, the *TaTST* expression did not differ significantly between AN- and NN-treated plants at 6 h; however, this gene was significantly inhibited in the AN-treated plants than the NN-treated plants at 120 h (Figure 8H).

4 Discussion

It is well known that wheat is sensitive to NH_4^+ (Liu and von Wirén, 2017). In the present study, we assessed the responses of two wheat cultivars, NH_4^+-sensitive Yangmai20 and NH_4^+-tolerant Xumai25, to NH_4^+ stress to elucidate the mechanism of NH_4^+tolerance in wheat. Our results showed that NH_4^+ stress had a significant adverse impact on the growth of wheat seedlings (Table 1, Figure 1), which is consistent with similar observations in other plant species (Chen et al., 2020; Guo et al., 2021; Tian et al., 2021). Notably, the NH_4^+-tolerant cultivar, Xumai25, exhibited a less reduction in root growth and an enhanced NH_4^+ accumulation capacity than the NH_4^+-sensitive cultivar, Yangmai20, resulting in a superior overall growth of Xumai25 under NH_4^+ stress.

4.1 Superior root development and stronger NH_4^+ uptake enhances NH_4^+ tolerance in Xumai25

The phytotoxicity of NH_4^+ on root growth, even at moderate concentrations, is a well-known phenomenon across several plant species (Li et al., 2014; Di et al., 2021). The present study showed that NH_4^+ stress markedly impacted wheat root morphology and root dry matter accumulation, with a more pronounced effect on the primary root (Figure 1C, Table 1). This effect was manifested as suppression of root length, surface area, and volume of both cultivars (Table 1), aligning with previous observations in *Arabidopsis* (Liu and von Wirén, 2017). The primary root of the NH_4^+-sensitive cultivar, Yangmai20, was more substantially affected by NH_4^+ stress. Furthermore, lateral roots are known to be highly responsive to nutrient availability (Giehl and von Wiren, 2014). In this study, we observed that the plasticity of lateral roots was adversely affected by NH_4^+ stress as evidenced by an increase in root average diameter and a decrease in length, surface area, and volume in both cultivars, with more pronounced effects in Yangmai20 (Table 1). Concurrently, NH_4^+ stress led to a reduction in the number of lateral roots in

10.3389/fpls.2024.1339105

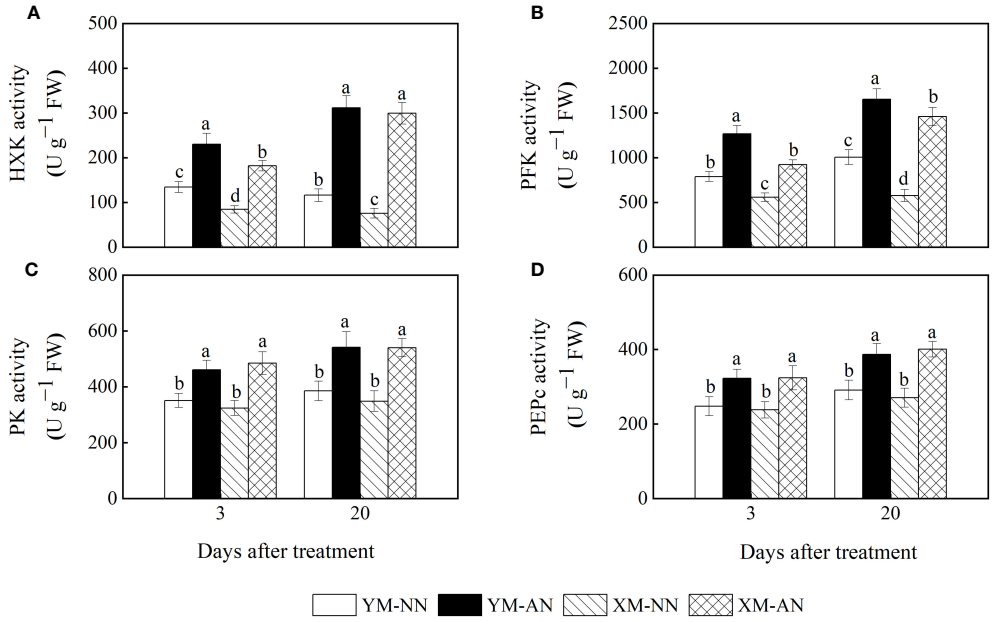

FIGURE 6
Effects of ammonium stress on the activity of sugar metabolizing enzyme in wheat seedlings at 3 and 20 days after treatment (DAT). **(A)** Hexokinase (HXK) activity; **(B)** Phosphofructokinase (PFK) activity; **(C)** Pyruvate kinase (PK) activity; **(D)** Phosphoenolpyruvate carboxylase (PEPc) activity. Data are expressed as means of three biological replicates. Error bar labels with different letters indicate significant differences ($P < 0.05$) between cultivars and treatment. NN, nitrate conditions; AN, ammonium stress conditions. YM, NH_4^+-sensitive cultivar Yangmai20; XM, NH_4^+-tolerant cultivar Xumai25.

both cultivars (Table 1), consistent with prior observations in *Arabidopsis* (Li et al., 2013), implying that NH_4^+ stress inhibits the germination of lateral roots in wheat (Liu and von Wirén, 2017). Taken together, our findings suggest that 5 mM NH_4^+ stress inhibits the growth of primary and lateral roots in the wheat seedlings, resulting in a decrease in root dry matter. The better NH_4^+ stress acclimatization capacity of Xumai25, compared with Yangmai20, might contribute to the superior root development in the former.

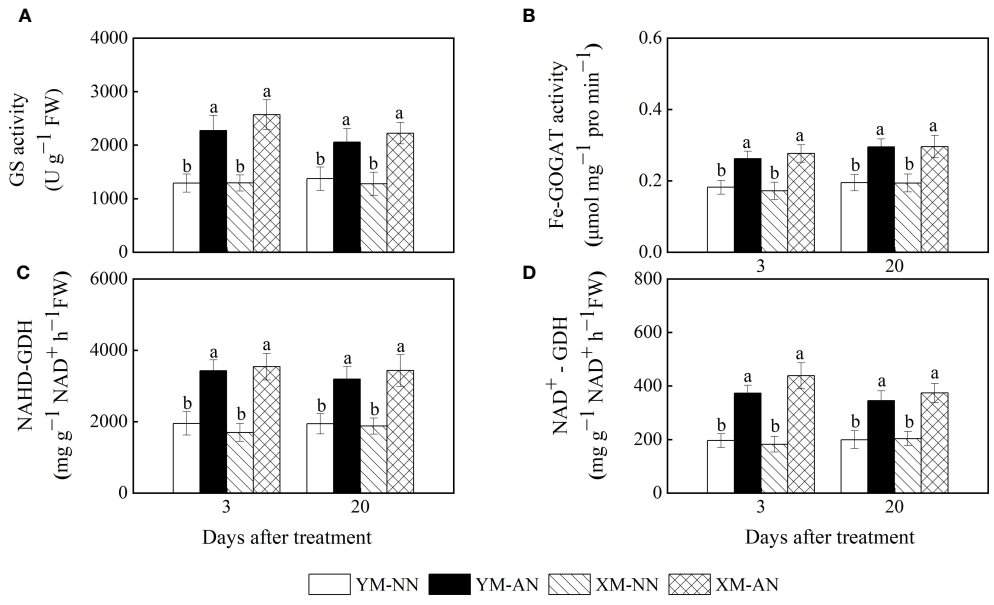

FIGURE 7
Effects of ammonium stress on the activity of ammonium metalizing in wheat seedlings at 3 and 20 days after treatment (DAT). **(A)** Glutamine synthetase activity; **(B)** Glutamate synthase activity; **(C)** NADH-GDH activity; **(D)** NAD^+-GDH activity. Data are expressed as means of three biological replicates. Error bar labels with different letters indicate significant differences ($P < 0.05$) between cultivars and treatment. NN, nitrate conditions; AN, ammonium stress conditions. YM, NH_4^+-sensitive cultivar Yangmai20; XM, NH_4^+-tolerant cultivar Xumai25.

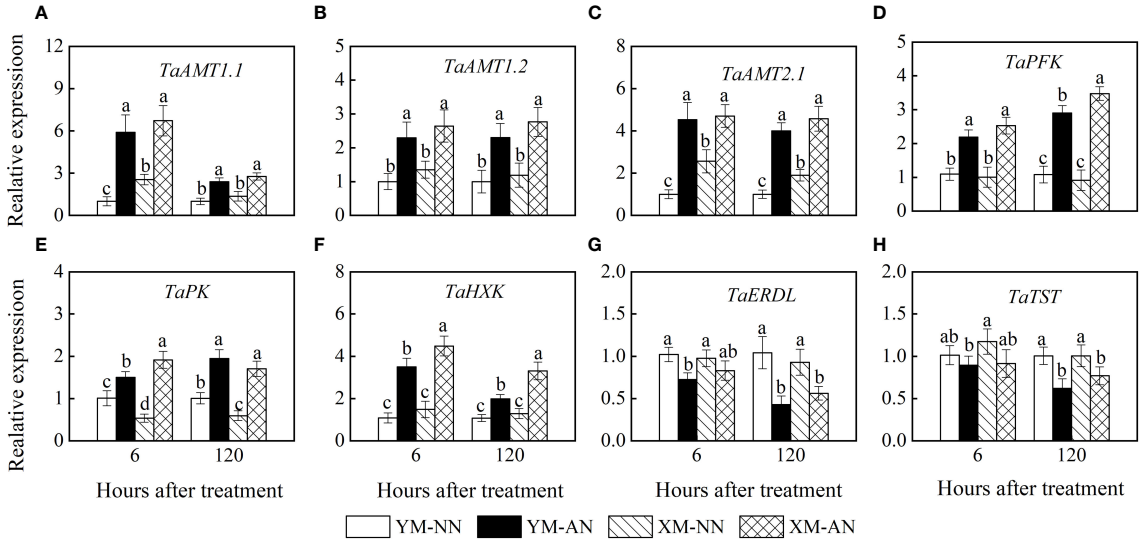

FIGURE 8
Effects of ammonium stress on relative gene expression in the root of wheat seedlings at 6 and 120 hours after treatment. **(A)** *TaAMT1.1*; **(B)** *TaAMT1.2*; **(C)** *TaAMT2.1*; **(D)** *TaPFK*; **(E)** *TaPK*; **(F)** *TaHXK*; **(G)** *TaERDL*; **(H)** *TaTST*. Data are expressed as means of three biological replicates. Error bar labels with different letters indicate significant differences ($P < 0.05$) between cultivars. NN, nitrate conditions; AN, ammonium stress conditions. YM, NH_4^+-sensitive cultivar Yangmai20; XM, NH_4^+-tolerant cultivar Xumai25.

NH_4^+ uptake and transport in plant tissues are predominantly mediated by AMTs. The expression of *AMTs* is influenced by plant species as well as NH_4^+ concentration (Li et al., 2017). Previous studies have identified persistent NH_4^+ absorption via AMTs as a major contributor to the excessive free NH_4^+ accumulation in *Arabidopsis* (Li et al., 2020). Furthermore, exposure to high NH_4^+ concentrations tends to suppress the expressions of *AMTs* (Loqué et al., 2006). In the present study, both wheat cultivars exhibited an upregulation of *TaAMT1.1*, *TaAMT1.2*, and *TaAMT2.1* under NH_4^+ stress (Figures 8A–C), which promoted NH_4^+ entry into the root. These findings align with the previous studies on wheat (Li et al., 2017; Ijato et al., 2021), demonstrating that, unlike *Arabidopsis*, wheat did not suppress the expression of *AMTs* under NH_4^+ stress to reduce NH_4^+ uptake. In addition, the enhanced expression of *TaAMT2.1* in Xumai25 correlated with its superior NH_4^+ influx capacity (Figures 3A, 8C).

In addition, previous studies have shown the existence of other NH_4^+ uptake pathways in plant roots (Bittsánszky et al., 2015; Esteban et al., 2016). Therefore, to precisely measure NH_4^+ influx and efflux from wheat root epidermis, we employed the non-invasive micro-test technology (NMT) (Kühtreiber and Jaffe, 1990), which helps to exclude the influence of other NH_4^+ uptake channels on the results. In this study, we observed a higher NH_4^+ influx in Xumai25 than in Yangmai20 (Figure 3A), consistent with trends observed in $^{15}NH_4^+$ uptake (Supplementary Figure S2). Such NH_4^+ influx patterns have also been reported among different bamboo species (Zou et al., 2020). In addition, several studies have reported that despite the high net influx of NH_4^+ via plant roots, there might be a substantial NH_4^+ efflux from the roots to the outside (Britto et al., 2001; Di et al., 2021). Indeed, in the present study, both wheat cultivars exhibited NH_4^+ efflux from the root, but there was no significant difference in the amount of NH_4^+ efflux between them (Figure 3B). Taken together, the higher NH_4^+ influx and lower root free NH_4^+ concentration in Xumai25 (Figure 2), compared with that of Yangmai20, indicates its stronger NH_4^+ assimilation capacity, which is related to its higher ammonium tolerance. In addition, these data suggest that the NH_4^+-tolerant cultivar has a stronger NH_4^+ uptake capacity than the sensitive cultivar, disproving our first research hypothesis.

4.2 Superior NH_4^+ assimilation capacity positively impacts NH_4^+ tolerance in Xumai25

After entering plant cells, NH_4^+ is rapidly converted to glutamine and glutamate via the GS-GOGAT-GDH cycle (Xiao et al., 2023). Our study observed a significant increase in the activities of GS/Fe-GOGAT, NADH-GDH, and NAD^+-GDH in the roots of both wheat cultivars under NH_4^+ stress (Figures 7A–D), further evidencing the activation of NH_4^+ assimilation-associated enzymes in wheat seedlings by NH_4^+ stress (Setién et al., 2013; González-Moro et al., 2021). In addition, some studies have suggested that GDH activity is linked to NH_4^+ tolerance (Cruz et al., 2006). Indeed, the current study observed a higher NADH-GDH and NAD^+-GDH activities in Xumai25 than in Yangmai20, indicating a stronger NH_4^+ assimilation capacity of Xumai25.

A well-documented strategy for maintaining intracellular NH_4^+ levels in various plant species, including wheat, is to enhance NH_4^+ assimilation into organic molecules (Setién et al., 2013). In the present study, both cultivars exhibited a significant increase in total free amino acid levels under NH_4^+ stress, with Xumai25 having higher free amino acid levels than Yangmai20 (Figures 2, 4B),

further evidencing the superior NH_4^+ assimilation capacity of Xumai25. A previous study suggested that the metabolic adaptation to NH_4^+ in different species is associated with their preference for synthesizing amino acid (González-Moro et al., 2021). In line with a prior study on wheat (Vega-Mas et al., 2019b), the current study observed a substantial accumulation of Asn and Gln in the root under NH_4^+ stress (Figures 4B, C), highlighting Asn and Gln as major storage amino acids in wheat plants. Additionally, the higher concentration of Asn in the roots of Xumai 25, compared to Yangmai 20, indicates the potential role of Asn in reducing NH_4^+ accumulation as well as the better adaptation of Xumai25 to NH_4^+ stress (Figure 4C).

Contrary to the findings in tomatoes, where NH_4^+ stress did not significantly alter Glu concentration (Xun et al., 2020), our study revealed a significant increase in Glu concentration in both wheat cultivars under NH_4^+ stress (Figure 4F), aligning with other studies on wheat (Setién et al., 2013; Vega-Mas et al., 2019a). Notably, in this present study, the Glu accumulation was lower in Xumai25 than in Yangmai20 (Figure 4F), indicating that Xumai25 was able to convert Glu to other amino acids or nitrogenous compounds more efficiently. This efficiency might also contribute to the higher tolerance of Xumai25 to NH_4^+ stress (Wang et al., 2020).

4.3 More efficient glucose metabolism and transport contribute to the stronger NH_4^+ assimilation in Xumai25

NH_4^+ assimilation is closely dependent on large amounts of pyruvate entering the tricarboxylic acid cycle to meet the high demand for carbon skeletons for ammonium detoxification (Vega-Mas et al., 2019b). In plants, sucrose is transported from photosynthetic leaves to the roots via the phloem and then hydrolyzed to hexoses (Glc and Fru) (Zhu et al., 2021), followed by further catabolism to provide a carbon skeleton for NH_4^+ assimilation. Under NH_4^+ stress, the sucrose and fructose levels substantially declined in the roots of both cultivars (Figures 5A, B), with a more prominent decline in Yangmai20 roots. According to Cruz et al. (2006), this decline is associated with the depletion of the carbon skeleton by root NH_4^+ assimilation. On the other hand, we speculate that it is also related to the inhibition of photosynthesis, which was reported to vary between the two cultivars in our previous study (Hu et al., 2024). In addition, we observed a remarkable increase in glucose concentration under NH_4^+ stress (Figure 5C), aligning with similar observations in *Arabidopsis* (Jian et al., 2018; Li et al., 2020). This result implies that NH_4^+ stress induces glucose accumulation in the root, and the sugar supply status from the shoot is independent of NH_4^+ toxicity, in agreement with Jian et al. (2018). Moreover, we observed that Xumai25 exhibited lower glucose accumulation (Figure 5C) but higher levels of pyruvate, 2-OG, and OAA at 20 DAT (Figures 5C–F) compared to Yangmai20, indicating a superior glucose metabolism in Xumai25.

In plants, glucose is metabolized to pyruvate via glycolysis (Li et al., 2019), and hexokinase, pyruvate kinase, and phosphofructokinase are key enzymes that regulate the process. A study on the transcriptome of duckweed indicated that genes associated with glycolysis are upregulated under NH_4^+ stress, thereby regulating carbon metabolism for ammonium detoxification (Tian et al., 2021). Consistently, our results showed that the activities of key glycolysis-related enzymes, such as HXK, PK, and PFK, were significantly increased under NH_4^+ stress in both cultivars (Figures 6A, B). Moreover, we observed an upregulation of the genes encoding these enzymes (Figures 8D, F), further suggesting that glycolysis is enhanced under NH_4^+ stress. Importantly, Xumai25 exhibited higher HXK and PFK activities and expression of genes encoding these enzymes than Yangmai20, demonstrating the former has a superior glycolytic capacity. This higher glycolytic capacity of Xumai25 can generate more pyruvate compared to Yangmai20, which explains its lower glucose accumulation and superior NH_4^+ assimilation.

Additionally, sugar transport into vacuoles, a crucial aspect of sugar homeostasis, is predominantly facilitated by various classes of sugar transporters in the tonoplast (Zhu et al., 2021). This phenomenon includes H^+/sugar antiporters (TST) and H^+/sugar symporters (ERDL), responsible for sugar influx into and efflux from vacuoles, respectively (Klemens et al., 2014). Notably, our study observed that both *TaTST* and *TaERDL* were down-regulated under NH_4^+ stress, with the down-regulation being more pronounced in Yangmai20 (Figures 8G, H). These results imply that NH_4^+ stress inhibits glucose transport, which is associated with glucose accumulation, and Xumai25 had a stronger glucose transport capacity than Yangmai20. Given that NH_4^+ stress encompasses osmotic stress (Bittsánszky et al., 2015; Esteban et al., 2016), it is reasonable to hypothesize that the inhibition of glucose transport under NH_4^+ stress might be a plant response mechanism aimed at maintaining cellular osmotic potential and mitigating oxidative stress (Xu et al., 2012). Further research is needed to decipher the molecular mechanisms underlying the role of glucose transport under NH_4^+ stress.

5 Conclusion

In conclusion, our investigation highlights the substantial impact of NH_4^+ stress on root growth, NH_4^+ uptake and assimilation, and glucose metabolism in different NH_4^+ tolerant wheat cultivars. The growth of both wheat cultivars was significantly inhibited under NH_4^+ stress. The NH_4^+-tolerant cultivar, Xumai25, showed a more robust glucose metabolism and enhanced glucose transport, which provided more carbon skeleton for NH_4^+ assimilation and reduced the accumulation of free NH_4^+

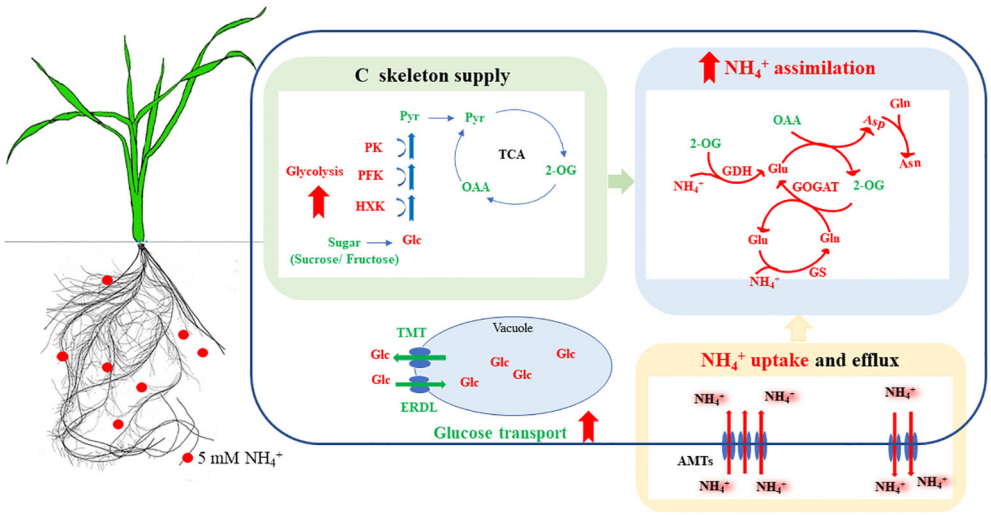

FIGURE 9
Physiological mechanisms of the enhanced NH_4^+ assimilation in NH_4^+-tolerant wheat cultivar under NH_4^+ stress. Under NH_4^+ stress, the NH_4^+-tolerant cultivar has an increased NH_4^+ uptake, its superior glucose metabolism and transport capacity contributed to the acquisition of more C skeletons, which improved NH_4^+ assimilation and reduced the accumulation of free NH_4^+ in the root, thus effectively alleviating the inhibitory effects of NH_4^+ stress. Red and green, respectively, indicate inhibition/reduction, and activation/increase under NH_4^+ stress. Solid red arrows indicate enhanced metabolism of the NH_4^+-tolerant cultivar, compared to the NH_4^+-sensitive cultivar. AMTs, ammonium transporters; Asn, asparagine; Asp, aspartate; ERDL, tonoplast H+/glucose symporter; GDH, glutamate dehydrogenase; GS, glutamine synthetase; GOGAT, glutamate synthase; Gln, glutamine; Glu, glutamate; HXK, hexokinase; OAA, oxaloacetate; PEPc, phosphoenolpyruvate carboxylase; PFK, phosphofructokinase; PK, pyruvate kinase; TST, tonoplast sugar transporter; 2-OG, 2-oxoglutarate.

in the root, thereby exhibiting a stronger NH_4^+ assimilation capacity and a better root growth performance (Figure 9). This study uncovers the relationship between glucose metabolism, carbon skeleton supply induced by NH_4^+ stress, and NH_4^+ tolerance of wheat, and will provide a basis for the cultivation and breeding of new NH_4^+-tolerant cultivar.

Data availability statement

The raw data supporting the conclusions of this article will be made available by the authors, without undue reservation.

Author contributions

JH: Data curation, Formal analysis, Methodology, Writing – original draft. QZ: Writing – review & editing. BN: Writing – review & editing. CD: Writing – review & editing. ZT: Writing – review & editing. TD: Supervision, Writing – review & editing.

Funding

The author(s) declare financial support was received for the research, authorship, and/or publication of this article. We gratefully acknowledge the financial support received from the National Natural Science Foundation of China (Grant No. 32272215) and Jiangsu Provincial Key Research and Development Program (BE2021361-1) for conducting this study.

Acknowledgments

We are sincerely grateful to the other researchers and staff members involved in this project for their valuable contributions, expertise, and assistance in project management.

Conflict of interest

The authors declare that the research was conducted in the absence of any commercial or financial relationships that could be construed as a potential conflict of interest.

Publisher's note

Supplementary material

The Supplementary Material for this article can be found online at: https://www.frontiersin.org/articles/10.3389/fpls.2024.1339105/full#supplementary-material

References

Ariz, I., Asensio, A. C., Zamarreño, A. M., García-Mina, J. M., Aparicio-Tejo, P. M., and Moran, J. F. (2013). Changes in the C/N balance caused by increasing external ammonium concentrations are driven by carbon and energy availabilities during ammonium nutrition in pea plants: the key roles of asparagine synthetase and anaplerotic enzymes. *Physiologia Planta.* 4, 522–537. doi: 10.1111/j.1399-3054.2012.01712.x

Balkos, K. D., Britto, D. T., and Kronzuceker, H. J. (2009). Optimization of ammonium acquisition and metabolism by potassium in rice (Oryza sativa L. cv. IR-72). *Plant Cell Environ.* 33, 23–32. doi: 10.1111/j.1365-3040.2009.02046.x

Bittsánszky, A., Pilinszky, K., Gyulai, G., and Komives, T. (2015). Overcoming ammonium toxicity. *Plant Sci.* 231, 184–190. doi: 10.1016/j.plantsci.2014.12.005

Britto, D. T., and Kronzucker, H. J. (2002). NH_4^+ toxicity in higher plants: a critical review. *J. Plant Physiol.* 6, 567–584. doi: 10.1078/0176-1617-0774

Britto, D. T., and Kronzuker, H. J. (2005). Nitrogen acquisition, PEP carboxylase, and cellular pH homeostasis: new views on old paradigms. *Plant Cell Environ.* 11, 1396–1409. doi: 10.1111/j.1365-3040.2005.01372.x

Britto, D. T., Siddiqi, M. Y., Anthony, D. M. G., and Kronzucker, H. J. (2001). Futile transmembrane NH_4^+ Cycling: A cellular hypothesis to explain ammonium toxicity in plants. *Proc. Natl. Acad. Sci.* 7, 4255–4258. doi: 10.1073/pnas.061034698

Chen, H., Jia, Y., Xu, H., Wang, Y., Zhou, Y., Huang, Z., et al. (2020). Ammonium nutrition inhibits plant growth and nitrogen uptake in citrus seedlings. *Scientia Hortic.* 272, 109526. doi: 10.1016/j.scienta.2020.109526

Chen, T., Zhao, M., Tang, X., Wei, W, Wen, X, Zhou, S, et al. (2023). The tigecycline resistance gene tetX has an expensive fitness cost based on increased outer membrane permeability and metabolic burden in Escherichia coli. *J. Hazard. Mater.* 458, 131889. doi: 10.1016/j.jhazmat.2023.131889

Cruz, C., Bio, A. F. M., Domínguez-Valdivia, M. D., Aparicio-Tejo, P. M., Lamsfus, C., and Martins-Loução, M. A. (2006). How does glutamine synthetase activity determine plant tolerance to ammonium? *Planta.* 5, 1068–1080. doi: 10.1007/s00425-005-0155-2

de la Peña, M., González-Moro, M. B., and Marino, D. (2019). Providing carbon skeletons to sustain amide synthesis in roots underlines the suitability of Brachypodium distachyon for the study of ammonium stress in cereals. *AoB Plants* 3. doi: 10.1093/aobpla/plz029

Di, D. W., Sun, L., Wang, M., Wu, J., Kronzucker, H. J., Fang, S., et al. (2021). WRKY46 promotes ammonium tolerance in Arabidopsis by repressing NUDX9 and indole-3-acetic acid-conjugating genes and by inhibiting ammonium efflux in the root elongation zone. *New Phytologist.* 1, 190–207. doi: 10.1111/nph.17554

Esteban, R., Ariz, I., Cruz, C., and Moran, J. F. (2016). Review: Mechanisms of ammonium toxicity and the quest for tolerance. *Plant Sci.* 248, 92–101. doi: 10.1016/j.plantsci.2016.04.008

Georgelis, N., Fencil, K., and Richael, C. M. (2018). Validation of a rapid and sensitive HPLC/MS method for measuring sucrose, fructose and glucose in plant tissues. *Food Chem.* 262, 191–198. doi: 10.1016/j.foodchem.2018.04.051

Giehl, R. F. H., and von Wiren, N. (2014). Root nutrient foraging. *Plant Physiol.* 2, 509–517. doi: 10.1104/pp.114.245225

González-Moro, M. B., González-Moro, I., de la Peña, M., Estavillo, J. M., Aparicio-Tejo, P. M., Marino, D., et al. (2021). A multi-species analysis defines anaplerotic enzymes and amides as metabolic markers for ammonium nutrition. *Front. Plant Sci.* 11. doi: 10.3389/fpls.2020.632285

Guo, K., An, G., Wang, N., Pang, B., Shi, Z., Bai, H., et al. (2021). Thymol ameliorates ammonium toxicity via repressing polyamine oxidase-derived hydrogen peroxide and modulating ammonium transporters in rice root. *Food Prod. Process. Nutr.* 1. doi: 10.1186/s43014-021-00053-1

Hachiya, T., Inaba, J., Wakazaki, M., Sato, M., Toyooka, K., Miyagi, A., et al. (2021). Excessive ammonium assimilation by plastidic glutamine synthetase causes ammonium toxicity in Arabidopsis thaliana. *Nat. Commun.* 1. doi: 10.1038/s41467-021-25238-7

Hu, J., Zheng, Q., Dong, C., Liang, Z., Tian, Z., and Dai, T. (2024). Enhanced stomatal conductance supports photosynthesis in wheat to improved NH_4^+ Tolerance. *Plants* 13, (1). doi: 10.3390/plants13010086

Ijato, T., Porras Murillo, R., Ganz, P., Ludewig, U., and Neuhäuser, B. (2021). Concentration - dependent physiological and transcriptional adaptations of wheat seedlings to ammonium. *Physiologia Planta.* 3, 328–342. doi: 10.1111/ppl.13113

Jian, S., Liao, Q., Song, H., Liu, Q., Lepo, J. E., Guan, C., et al. (2018). NRT1.1-related NH_4^+ Toxicity is associated with a disturbed balance between NH_4^+ Uptake and assimilation. *Plant Physiol.* 4, 1473–1488. doi: 10.1104/pp.18.00410

Jiang, S., Sun, J., Tian, Z., Hu, H., Michel, E. J. S., Gao, J., et al. (2017). Root extension and nitrate transporter up-regulation induced by nitrogen deficiency improves nitrogen status and plant growth at the seedling stage of winter wheat (Triticum aestivum L.). *Environ. Exp. Bot.* 141, 28–40. doi: 10.1016/j.envexpbot.2017.06.006

Klemens, P. A. W., Patzke, K., Trentmann, O., Poschet, G., Büttner, M., Schulz, A., et al. (2014). Overexpression of a proton-coupled vacuolar glucose exporter impairs freezing tolerance and seed germination. *New Phytologist.* 1, 188–197. doi: 10.1111/nph.12642

Konishi, N., Ishiyama, K., Beier, M. P., Inoue, E., Kanno, K., Yamaya, T., et al. (2016). Contributions of two cytosolic glutamine synthetase isozymes to ammonium assimilation in Arabidopsis roots. *J. Exp. Bot.*, w454. doi: 10.1093/jxb/erw454

Kühtreiber, W. M., and Jaffe, L. F. (1990). Detection of extracellular calcium gradients with a calcium-specific vibrating electrode. *J. Cell Biol.* 5, 1565–1573. doi: 10.1083/jcb.110.5.1565

Li, G., Li, B., Dong, G., Feng, X., Kronzucker, H. J., and Shi, W. (2013). Ammonium-induced shoot ethylene production is associated with the inhibition of lateral root formation in Arabidopsis. *J. Exp. Botany.* 5, 1413–1425. doi: 10.1093/jxb/ert019

Li, B., Li, G., Kronzucker, H. J., Baluška, F., and Shi, W. (2014). Ammonium stress in Arabidopsis: signaling, genetic loci, and physiological targets. *Trends Plant Sci.* 2, 107–114. doi: 10.1016/j.tplants.2013.09.004

Li, T., Liao, K., Xu, X., Gao, Y., Wang, Z., Zhu, X., et al. (2017). Wheat ammonium transporter (AMT) gene family: diversity and possible role in host–pathogen interaction with stem rust. *Front. Plant Sci.* 8. doi: 10.3389/fpls.2017.01637

Li, W., Liu, Y., Liu, M., Zheng, Q, Li, B, Li, Z, et al. (2019). Sugar accumulation is associated with leaf senescence induced by long-term high light in wheat. *Plant Sci.* 287, 110169. doi: 10.1016/j.plantsci.2019.110169

Li, C., Tang, Z., Wei, J., Qu, H., Xie, Y., and Xu, G. (2016). The OsAMT1.1 gene function in ammonium uptake and ammonium–potassium homeostasis over low and high ammonium concentration ranges. *J. Genet. Genomics* 11, 639–649. doi: 10.1016/j.jgg.2016.11.001

Li, Y., Zhou, J., Hao, D., Yang, S., and Su, Y. (2020). Arabidopsis under ammonium over-supply: Characteristics of ammonium toxicity in relation to the activity of ammonium transporters. *Pedosphere* 3, 314–325. doi: 10.1016/S1002-0160(20)60011-X

Liu, Y., Li, Y., Tian, Z., Hu, J., Adkins, S., and Dai, T. (2021). Changes of oxidative metabolism in the roots of wheat (Triticum aestivum L.) seedlings in response to elevated ammonium concentrations. *J. Integr. Agric.* 5, 1216–1228. doi: 10.1016/S2095-3119(20)63216-6

Liu, Y., and von Wirén, N. (2017). Ammonium as a signal for physiological and morphological responses in plants. *J. Exp. Botany.* 10, 2581–2592. doi: 10.1093/jxb/erx086

Liu, X., Zhang, Y., Han, W., Tang, A., Shen, J., Cui, Z., et al. (2013). Enhanced nitrogen deposition over China. *Nature* 7438, 459–462. doi: 10.1038/nature11917

Liu, Y., Zhang, B., Li, C., Hu, F., and Velde, B. (2008). Long-term fertilization influences on clay mineral composition and ammonium adsorption in a rice paddy soil. *Soil Sci. Soc. America J.* 6, 1580–1590. doi: 10.2136/sssaj2007.0040

Livak, K. J., and Schmittgen, T. D. (2001). Analysis of relative gene expression data using real-time quantitative PCR and the $2^{-\Delta\Delta CT}$ method. *Methods* 4, 402–408. doi: 10.1006/meth.2001.1262

Loqué, D., Yuan, L., Kojima, S., Gojon, A., Wirth, J., Gazzarrini, S., et al. (2006). Additive contribution of AMT1;1 and AMT1;3 to high-affinity ammonium uptake across the plasma membrane of nitrogen-deficient Arabidopsis roots. *Plant J.* 4, 522–534. doi: 10.1111/j.1365-313X.2006.02887.x

Ma, Q., Cao, X., Xie, Y., Gu, Y., Feng, Y., Mi, W., et al. (2017). Effect of pH on the uptake and metabolism of glycine in pak choi (Brassica chinensis L.). *Environ. Exp. Bot.* 133, 139–150. doi: 10.1016/j.envexpbot.2016.10.013

Marino, D., and Moran, J. F. (2019). Can ammonium stress be positive for plant performance? *Front. Plant Sci.* 10. doi: 10.3389/fpls.2019.01103

Pan, W. L., Madsen, I. J., Bolton, R. P., Graves, L., and Pan, T. (2016). A sistrunkmmonia/ammonium toxicity root symptoms induced by inorganic and organic fertilizers and placement. *Agron. J.* 6, 2485–2492. doi: 10.2134/agronj2016.02.0122

Porras Murillo, R., Zhao, Y., Hu, J., Ijato, T., Retamal, J. P., Ludewig, U., et al. (2023). The wheat AMT2 (AMmonium Transporter) family, possible functions in ammonium uptake and pathogenic/symbiotic interactions. *J. Plant Nutr. Soil Sci.* 186, 164–168. doi: 10.1002/jpln.202200362

Ranathunge, K., El-kereamy, A., Gidda, S., Bi, Y., and Rothstein, S. J. (2014). AMT1;1 transgenic rice plants with enhanced NH_4^+ permeability show superior growth and higher yield under optimal and suboptimal NH_4^+ conditions. *J. Exp. Botany.* 4, 965–979. doi: 10.1093/jxb/ert458

Setién, I., Fuertes-Mendizabal, T., González, A., Aparicio-Tejo, P. M., González-Murua, C., González-Moro, M. B., et al. (2013). High irradiance improves ammonium tolerance in wheat plants by increasing N assimilation. *J. Plant Physiol.* 8, 758–771. doi: 10.1016/j.jplph.2012.12.015

Skopelitis, D. S., Paranychianakis, N. V., Kouvarakis, A., Spyros, A., Stephanou, E. G., and Roubelakis-Angelakis, K. A. (2007). The isoenzyme 7 of tobacco NAD(H)-dependent glutamate dehydrogenase exhibits high deaminating and low aminating activities in vivo. *Plant Physiol.* 145, 1726–1734. doi: 10.1104/pp.107.107813

Sun, K., Lu, F., Huang, P. W., Tang, M. J., Xu, F. J., Zhang, W., et al. (2022). Root endophyte differentially regulates plant response to NO_3^- and NH_4^+ nutrition by modulating N fluxes at the plant-fungal interface. *Plant Cell Environ.* 6, 1813–1828. doi: 10.1111/pce.14304

Tian, X., Fang, Y., Jin, Y., Yi, Z., Li, J., Du, A., et al. (2021). Ammonium detoxification mechanism of ammonium-tolerant duckweed (Landoltia punctata) revealed by carbon and nitrogen metabolism under ammonium stress. *Environ. Pollut.* 277, 116834. doi: 10.1016/j.envpol.2021.116834

Vega-Mas, I., Cukier, C., Coleto, I., Gonzalez-Murua, C., Limami, A. M., Gonzalez-Moro, M. B., et al. (2019a). Isotopic labelling reveals the efficient adaptation of wheat root TCA cycle flux modes to match carbon demand under ammonium nutrition. *Sci. Rep.* 9, 8925. doi: 10.1038/s41598-019-45393-8

Vega-Mas, I., Rossi, M. T., Gupta, K. J., González-Murua, C., Ratcliffe, R. G., Estavillo, J. M., et al. (2019b). Tomato roots exhibit in *vivo* glutamate dehydrogenase aminating capacity in response to excess ammonium supply. *J. Plant Physiol.*, 83–91. doi: 10.1016/j.jplph.2019.03.009

Viktor, A., and Cramer, M. D. (2005). The influence of root assimilated inorganic carbon on nitrogen acquisition/assimilation and carbon partitioning. *New Phytologist.* 1, 157–169. doi: 10.1111/j.1469-8137.2004.01204.x

Wang, F., Gao, J., Tian, Z., Liu, Y., Abid, M., Jiang, D., et al. (2016). Adaptation to rhizosphere acidification is a necessary prerequisite for wheat (Triticum aestivum L.) seedling resistance to ammonium stress. *Plant Physiol. Biochem.* 108, 447–455. doi: 10.1016/j.plaphy.2016.08.011

Wang, F., Gao, J., Yong, J. W.H., Liu, Y., Cao, D., and He, X. (2020). Glutamate over-accumulation may serve as an endogenous indicator of tricarboxylic acid (TCA) cycle suppression under NH_4^+ nutrition in wheat (Triticum aestivum L.) seedlings. *Environ. Exp. Botany.* 177, 104130. doi: 10.1016/j.envexpbot.2020.104130

Xiao, C., Fang, Y., Wang, S., and He, K. (2023). The alleviation of ammonium toxicity in plants. *J. Integr. Plant Biol.* 65, 1362–1368. doi: 10.1111/jipb.13467

Xu, G., Fan, X., and Miller, A. J. (2012). Plant nitrogen assimilation and use efficiency. *Annu. Rev. Plant Biol.* 1, 153–182. doi: 10.1146/annurev-arplant-042811-105532

Xun, Z., Guo, X., Li, Y., Wen, X, Wang, C, and Wang, Y (2020). Quantitative proteomics analysis of tomato growth inhibition by ammonium nitrogen. *Plant Physiol. Biochem.* 154, 129–141. doi: 10.1016/j.plaphy.2020.05.036

Yokoyama, S., and Hiramatsu, J. (2003). A modified ninhydrin reagent using ascorbic acid instead of potassium cyanide. *J. Biosci. Bioeng.* 2, 204–205. doi: 10.1016/S1389-1723(03)80131-7

Yuan, L., Loqué, D., Kojima, S., Rauch, S., Ishiyama, K., Inoue, E, et al. (2007). The organization of high-affinity ammonium uptake in arabidopsis roots depends on the spatial arrangement and biochemical properties of AMT1-type transporters. *Plant Cell.* 8, 2636–2652. doi: 10.1105/tpc.107.052134

Zeng, Y., Yu, J., Cang, J., Liu, L., Mu, Y., Wang, J., et al. (2014). Detection of Sugar Accumulation and Expression Levels of Correlative Key Enzymes in Winter Wheat (Triticum aestivum) at Low Temperatures. *Biosci. Biotechnol. Biochem.* 4, 681–687. doi: 10.1271/bbb.100813

Zhu, L., Li, B., Wu, L., Li, H, Wang, Z, W, X, et al. (2021). MdERDL6-mediated glucose efflux to the cytosol promotes sugar accumulation in the vacuole through up-regulating TSTs in apple and tomato. *Proc. Natl. Acad. Sci.* 118 (1). doi: 10.1073/pnas.2022788118

Zou, N., Shi, W., Hou, L., Kronzucker, H. J., Huang, L., Gu, H., et al. (2020). Superior growth, N uptake and NH_4^+ tolerance in the giant bamboo Phyllostachys edulis over the broad-leaved tree Castanopsis fargesii at elevated NH_4^+ may underlie community succession and favor the expansion of bamboo. *Tree Physiol.* 11, 1606–1622. doi: 10.1093/treephys/tpaa086

frontiers | Frontiers in Plant Science

TYPE Original Research
PUBLISHED 20 February 2024
DOI 10.3389/fpls.2024.1319680

OPEN ACCESS

EDITED BY
Luisa Bascunan-Godoy,
University of Concepcion, Chile

REVIEWED BY
Teodoro Coba De La Peña,
Catholic University of the North, Chile
Alexander Vergara,
UmeåUniversity, Sweden

*CORRESPONDENCE
Xinping Chen
chenxp2017@swu.edu.cn
Yan Deng
dyan0907@swu.edu.cn

RECEIVED 11 October 2023
ACCEPTED 06 February 2024
PUBLISHED 20 February 2024

CITATION
Zhang L, Zhang F, He X, Dong Y, Sun K, Liu S, Wang X, Yang H, Zhang W, Lakshmanan P, Chen X and Deng Y (2024) Comparative metabolomics reveals complex metabolic shifts associated with nitrogen-induced color development in mature pepper fruit. *Front. Plant Sci.* 15:1319680. doi: 10.3389/fpls.2024.1319680

Comparative metabolomics reveals complex metabolic shifts associated with nitrogen-induced color development in mature pepper fruit

Lu Zhang[1,2], Fen Zhang[1,2], Xuanyi He[1,2], Yuehua Dong[1,2], Kai Sun[1,2], Shunli Liu[1,2], Xiaozhong Wang[1,2], Huaiyu Yang[1,3], Wei Zhang[1,3], Prakash Lakshmanan[1,4,5], Xinping Chen[1,2]* and Yan Deng[1,2]*

[1]Interdisciplinary Research Center for Agriculture Green Development in Yangtze River Basin, College of Resources and Environment, Southwest University, Chongqing, China, [2]Key Laboratory of Low-carbon Green Agriculture in Southwestern China, Ministry of Agriculture and Rural Affairs, Southwest University, Chongqing, China, [3]Key Laboratory of Efficient Utilization of Soil and Fertilizer Resources, Southwest University, Chongqing, China, [4]Key Laboratory of Sugarcane Biotechnology and Genetic Improvement (Guangxi), Ministry of Agriculture and Rural Affairs; Guangxi Key Laboratory of Sugarcane Genetic Improvement, Sugarcane Research Institute, Guangxi Academy of Agricultural Sciences, Nanning, China, [5]Queensland Alliance for Agriculture and Food Innovation, The University of Queensland, Brisbane, QLD, Australia

Pigments derived from red pepper fruits are widely used in food and cosmetics as natural colorants. Nitrogen (N) is a key nutrient affecting plant growth and metabolism; however, its regulation of color-related metabolites in pepper fruit has not been fully elucidated. This study analyzed the effects of N supply (0, 250, and 400 kg N ha^{-1}) on the growth, fruit skin color, and targeted and non-target secondary metabolites of field-grown pepper fruits at the mature red stage. Overall, 16 carotenoids were detected, of which capsanthin, zeaxanthin, and capsorubin were the dominant ones. N application at 250 kg ha^{-1} dramatically increased contents of red pigment capsanthin, yellow-orange zeaxanthin and β-carotene, with optimum fruit yield. A total of 290 secondary metabolites were detected and identified. The relative content of most flavonoids and phenolic acids was decreased with increasing N supply. Correlation analysis showed that color parameters were highly correlated with N application rates, carotenoids, flavonoids, phenolic acids, lignans, and coumarins. Collectively, N promoted carotenoid biosynthesis but downregulated phenylpropanoid and flavonoid biosynthesis, which together determined the spectrum of red color expression in pepper fruit. Our results provide a better understanding of the impact of N nutrition on pepper fruit color formation and related physiology, and identification of target metabolites for enhancement of nutritional quality and consumer appeal.

KEYWORDS

pepper, fruit color, nitrogen, carotenoids, flavonoids, metabolome

1 Introduction

Chili peppers (*Capsicum annuum* L.) are cultivated and consumed worldwide. Approximately 38.03 million tons of fresh peppers and 4.25 million tons of dry peppers were produced globally in 2019 (Barik et al., 2022). Pepper fruit is a rich source of phytochemicals with antioxidant properties, such as carotenoids and flavonoids, and it is also used as natural colorant (del Rocío Gomez-Garcia and Ochoa-Alejo, 2013; Baenas et al., 2019). As such, the global demand for pepper fruit pigments for food and cosmetics is steadily increasing (Leong et al., 2018; Saini et al., 2022).

Carotenoids are tetraterpenoid pigments, and their chromogenic characteristics are usually what give the fruits their yellow, orange, red, or purple coloring (Maoka, 2020). Capsanthin and capsorubin (very pepper-specific pigments), which represent 40%–60% of the total carotenoids, confer pepper fruits their red color, while α-carotene, β-carotene, and zeaxanthin make yellow-orange-colored peppers (Baenas et al., 2019; Villa-Rivera and Ochoa-Alejo, 2020). Owing to their strong antioxidant properties, carotenoids are now widely used in food and cosmetics (Baenas et al., 2019). The global market for carotenoids was estimated to be $2.0 billion in 2022, with consumption reaching 6222.6 metric tons (Bogacz-Radomska et al., 2020), and capsanthin having the largest market share.

Flavonoids, together with phenolic acid derivatives, represent the major groups of phenolic compounds in pepper fruit, providing taste, color, and flavor to fruits (Shen et al., 2018). As carotenoids, flavonoids are among the most common and important sources of color pigments in plants, which can produce a spectrum of color from bright yellow to red or from faint yellow to orange (Scarano et al., 2018; Peng et al., 2022). Importantly, flavonol glycosides (such as quercetin-O-glycosides) are abundant in peppers and demonstrate higher levels of antioxidant and anti-inflammatory activity than other phenolic compounds (Barik et al., 2022).

Most of the previous studies on pepper fruit color have focused on individual or a select group of carotenoids or flavonoids (Dubey et al., 2015; Liu et al., 2020). Most studies report the characterization, quantitation, or genotypic distribution of carotenoids, total phenols, and flavonoids, and their antioxidant properties (Giuffrida et al., 2013; Wahyuni et al., 2013; Mi et al., 2020; Zoccali et al., 2021; Mi et al., 2022). Non-saponification is the common method used to differentiate carotenoids in these studies. For example, Giuffrida et al. (2013) identified 52 carotenoids by non-saponification and found considerable compositional variation among them in 12 different *Capsicum* cultivars. However, saponification employed to hydrolyze esters can simplify the chromatographic analysis of carotenoids, making it useful for the detection of minor carotenoids (Feng et al., 2022). Therefore, targeted carotenoid metabolomics using saponification has the potential to expand our knowledge of specific classes of carotenoid metabolites contributing to color expression. Additionally, non-targeted metabolomics can help to identify a broader spectrum of metabolic products and understand their metabolism in relation to fruit color development (Luo et al., 2022; Marinov et al., 2023). Until now, such comprehensive saponification-assisted targeted carotenoid metabolomics and non-targeted secondary metabolomics studies on pepper fruit color development have not been reported.

Besides the genotype, the diversity and content of carotenoids and flavonoids are influenced by crop environmental conditions, including nutrition. Nitrogen (N), amongst the main environmental factors, is one of the most important nutrients for crop growth, product quality, and yield formation (Farneselli et al., 2018; Zhao et al., 2021). It provides functional groups for carbon skeletons and modulates the biosynthesis of secondary metabolites, such as flavonoids, phenolic acids, and carotenoids (Narvekar and Tharayil, 2021). Generally, N supply has a negative effect on flavonoids and phenolic acids, whereas it increases the content of chlorophyll and carotenoids across different plant species (Ibrahim et al., 2012; Narvekar and Tharayil, 2021). However, the production of other phenolic compounds may be stimulated, or not affected with the increase in N supply (Bustamante et al., 2020; Saloner and Bernstein, 2021). Although N fertilization is a common practice used to increase yield in pepper production, research on the influence of N supply on pigment-related metabolites in pepper is rare, and much less is known about N-mediated metabolic regulation of pepper color development.

In the present study, we integrated targeted carotenoid metabolomics, non-targeted secondary metabolomics, and different color parameters for a comprehensive investigation of pepper fruit color formation as influenced by different N supply at the mature red stage. The results we report here will provide new insights into the N regulation of pigment production, and help specify potential targets for controlling pepper fruit color formation through molecular genetics and/or agronomic practices.

2 Materials and methods

2.1 Experimental site and treatments

This study was conducted in 2021 at the Hechuan Experiment Station of Southwest University in Weituo Town, Chongqing City, China (30°01′N, 106°13′E). This region has a typical subtropical monsoon climate. During the pepper season in 2021, the average air temperature and total precipitation were 26.5°C and 699 mm, respectively. A long-term field experiment on Chinese cabbage-pepper rotation was started in 2018, and the present work was carried out during the fourth pepper cropping season. The soil type was alluvium, and the chemical properties of the top 20-cm layer at the beginning of the long-term experiment were as follows: pH, 5.65 (soil-water ratio 1:2.5); organic matter, 9.21 g kg^{-1}; total N, 0.50 g kg^{-1}; available phosphorus (Olsen-P), 19.51 mg kg^{-1}; and ammonium acetate extractable potassium (K), 56.0 mg kg^{-1}.

The red chili pepper variety "Xinxiang 8" was planted under three N rate treatments: (1) control without N fertilizer (N0; 0 kg N ha^{-1}, 140 kg P_2O_5 ha^{-1}, 300 kg K_2O ha^{-1}); (2) recommended N rate based on root zone N management (N250; 250 kg N ha^{-1}, 140 kg P_2O_5 ha^{-1}, 300 kg K_2O ha^{-1}); and (3) N rate routinely used by farmers (N400; 400 kg N ha^{-1}, 290 kg P_2O_5 ha^{-1}, 230 kg K_2O ha^{-1}). The N400 treatment was set based on the fertilization practice

found in a survey of 314 farmers conducted as part of our preliminary work, which found that inputs of N and P were too high but input of K was relatively low. Therefore, the N0 and N250 treatments were set based on optimizing P and K input to meet the needs of pepper growth. The three treatments were arranged in a randomized complete block design with four replicates, totaling 12 plots. Each plot (replicate) measured 46.6 m^2 (8.25 m × 5.65 m), and they were spaced 1.5 m apart. A total of 160 plants were grown in rows (0.6-m row spacing) with 0.4-m inter-plant distance in each plot. Chemical fertilizers urea (46% N), superphosphate (12% P_2O_5), and potassium sulphate (50% K_2O) were used to supply the N, P, and K nutrients. The amount of fertilizer and application date for different growth periods are presented in Supplementary Table S1. The experiment was conducted from 20 May to 1 September, 2021, and the crop management followed the local conventional agronomy practices for pepper production.

2.2 Plant and soil sampling

Pepper fruits were sampled at the mature red stage (16 August, 2021) (Supplementary Figure S1). In each plot, 10 plants of similar growth were randomly selected, and fruits, two per plant, were collected from the same plant part of the chosen plants. From each plot (replicate), half of the sample (10 fruits) was used for measuring single fruit fresh weight and surface color parameters, and the remaining half (10 fruits) was quickly cleaned and dissected. Pericarps were then collected and combined into one replicate sample. This sampling procedure was followed to produce four independent replicate samples for each treatment. Homogenized pericarp samples were frozen immediately in liquid nitrogen, transported to the laboratory and stored at -80°C for metabolite analysis. Simultaneously, soil samples from the top 20-cm layer were taken from each plot for measurement of soil mineral N (NH_4^+-N and NO_3^-N) level.

2.3 Soil mineral N level analysis

In the laboratory, fresh soil samples from the top 20-cm layer were quickly sieved (2-mm sieve size), then sub-samples were taken and extracted by 0.01 mol L^{-1} $CaCl_2$ solution. Meanwhile, sub-samples were oven-dried to measure soil water content. The NH_4^+-N and NO_3^-N content in the extraction solution was determined using an Auto Analyzer 3 Continuous-flow Analysis-CFA (SEAL Analytical GmbH, Norderstedt, Germany). Soil NH_4^+-N and NO_3^-N level was calculated based on soil dry weight.

2.4 Determination of pepper fruit growth and nutrient content

For measurement of single fruit fresh weight, 10 pepper fruits per replicate sample were weighed individually, and the average weight was calculated for each treatment replicate. To determine fruit yield and biomass, 24 (six plants × four rows) plants were selected from the middle of each plot, and all the fruits from the chosen plants were picked. Their fresh weight was measured and then dried at 75°C to measure dry weight. More specially, after drying, pericarp and the other parts were separated and weighed individually. Fruit yield and fruit biomass per hectare were calculated based on sampling area and fruit fresh weight (yield) or dry weight (biomass). Dried fruit samples were finely powdered and used for N, P, and K measurement. Fruit N content was determined using the Kjeldahl method (Yang et al., 2008), while P and K were assayed using inductively-coupled plasma-optical emission spectrometry (ICP-OES, 5110 SVDV; Agilent, Santa Clara, CA, United States) (Lu et al., 2021).

2.5 Measurement of fruit surface color

Surface color of harvested pepper fruits was determined using a colorimeter (CR-10Plus; Konica Minolta, Tokyo, Japan). After measuring the single fruit fresh weight, the same 10 fruits were used for fruit color measurement for each treatment replicate, with each fruit sample measured at three different positions. The CIE (International Commission on Illumination) color parameters, i.e., L* value (brightness), a* (green-red index), and b* (yellow-blue index) coordinates were used to describe the color. The hue angle [$h^* = \tan^{-1}(b^*/a^*)$] (when $h^* < 50$, the smaller, the redder) and chroma [$C^* = (a^{*2} + b^{*2})/2$)] parameters were calculated as reported previously (Guo et al., 2021; Feng et al., 2022).

2.6 Determination of total phenol content

The total phenol content in pericarp samples was determined by the Folin–Denis method using assay kits (Suzhou Grace Biotechnology Co., Ltd., Suzhou, China) according to the manufacturer's instructions. Briefly, 0.2 g of ground sample was mixed with 1.5 mL of 60% ethanol, then the mixture was stirred for 1 h at 60°C, and centrifuged at 12,000 rpm under 25°C for 10 min. The supernatant was collected and its volume was adjusted to 1.5 mL with 60% ethanol. This ethanolic extract was assayed for phenols using the assay kit. The total phenol content was determined at 760 nm with a UV-5200 spectrophotometer (Shanghai Metash Instruments Co., Ltd., Shanghai, China), and the content was expressed on sample fresh weight basis (mg g^{-1} FW).

2.7 Carotenoid identification and quantification

The extraction of carotenoids by saponification and the analysis of targeted carotenoids were performed by Metware Biotechnology Co., Ltd., Wuhan, China (http://www.metware.cn), according to the procedure described by Feng et al. (2022) with some modifications. More specifically, 50 mg freeze-dried pericarp powder was vortexed with 0.5 mL n-hexane/acetone/ethanol (1:1:1, v/v/v) solution for 20 min at room temperature, then the mixture was centrifuged at

12,000 rpm for 5 min at 4°C and the supernatant was collected. This extraction step was repeated once. The combined supernatant was mixed with 0.5 mL of saturated NaCl solution and vortexed until the solution was stratified, and the supernatant was collected. This step was repeated twice. Afterwards, the supernatant was evaporated to dryness and the dry residue was dissolved in 0.5 mL of methyl tert-butyl ether (MTBE), and saponified with 0.5 mL of 10% KOH-MeOH for 18 h in the dark at room temperature. The saponified extract was thoroughly mixed with 1 mL of saturated NaCl solution and 0.5 mL of MTBE and the upper layer was collected. This step was repeated twice. The combined supernatant was evaporated to dryness and reconstituted with 100 µL of MeOH/MTBE (1:1, v/v) solution. The solution was filtered through a 0.22-µm membrane filter and used for identification and quantification of carotenoids using an LC-APCI-MS/MS system (UPLC: ExionLC™ AD, Sciex Framingham, MA, USA; MS: 6500 Triple Quadrupole, Applied Biosystems, Foster City, CA, USA). The working conditions and procedures of this analysis system are described in Supplementary Method S1.

2.7 Non-targeted secondary metabolite analysis

Non-targeted metabolome analysis was also performed by MetWare Biotechnology Co., Ltd., Wuhan, China. The pericarp samples were freeze-dried in a vacuum freeze-dryer (Scientz-100F; Scientz, Ningbo, China) and then crushed using a mixer mill (MM 400; Retsch, Haan, Germany) with zirconia beads for 1.5 min at 30 Hz. The lyophilized powder (100 mg) was dissolved in 1.2 mL of 70% methanol solution, vortexed for 30 s every 30 min for six times, and stored in a refrigerator at 4°C overnight. The next day, the mixed solution was centrifugated at 12,000 rpm for 10 min and the supernatant was filtrated (SCAA-104, 0.22-µm pore size; ANPEL, Shanghai, China, http://www.anpel.com.cn/). All extracts were analyzed using an UPLC-ESI-MS/MS system (UPLC: Nexera X2, SHIMADZU, Kanagawa, Japan; MS: 4500 Q TRAP, Applied Biosystems). The working conditions and procedures of this analysis system are described in Supplementary Method S2.

Metabolites in the extracts were identified by comparing their spectral information to the standard reference materials in the MWDB database (MetWare Biological Science and Technology Co., Ltd.). They were quantified by triple quadrupole mass spectrometry using multi-reaction monitoring (MRM) mode. To produce maximal signal, collision energy and de-clustering potential were optimized for each precursor-product ion (Q1–Q3) transition (Zhu et al., 2018). The chromatographic peak area integral was used to represent the metabolite content. The potential differentially-accumulated metabolites (DAMs) between pairs of N treatments were identified using VIP (variable importance in projection) ≥ 1 criterion in the orthogonal partial least squares-discriminant analysis (OPLS-DA) results. A permutation test with 200 iterations was performed. Next, the DAMs between N treatments were identified based on VIP ≥ 1 and $P < 0.05$ (t-test). Identified metabolites were further annotated using the Kyoto Encyclopedia of Genes and Genomes (KEGG) compound database (http://www.kegg.jp/kegg/compound/) and mapped using the KEGG pathway database (http://www.kegg.jp/kegg/pathway.html). Pathways with corrected P-values ≤ 0.05 (hypergeometric test) were considered significantly altered. The carotenoid, phenylpropanoid, and flavonoid biosynthesis pathways were constructed based on the KEGG pathway and published literature (Tohge et al., 2017; Berry et al., 2019; Villa-Rivera and Ochoa-Alejo, 2020).

2.8 Data analysis

Statistical analyses were performed using SPSS 25.0 (SPSS, Inc., Chicago, IL, USA). Data were subjected to one-way ANOVA and significant differences were analyzed by the Duncan's multiple range test at $P < 0.05$. The cluster heat map (normalized by Z-score) was performed using Origin 2021 (OriginLab Corp., Northampton, MA, United States). Correlation coefficients were determined by the Pearson test. Correlations with a coefficient (r) value > 0.7 (positive) or < −0.7 (negative) were considered to be crucial relationships. The relationship visualization was performed using Cytoscape software (version 3.9.1; https://apps.cytoscape.org/).

3 Results

3.1 Soil mineral N level, pepper fruit growth, and nutrient content

At harvest, with increasing N supply, soil NH_4^+-N levels did not differ much between treatments while soil NO_3^-N levels were greatly increased under N250 and N400 conditions (Supplementary Table S2). Correspondingly, single fruit fresh weight, fruit yield, fruit biomass (dry weight), and fruit N content were all significantly increased under N250 treatment compared to the control condition (N0) (Figure 1; Supplementary Table S2). No further change in any of these parameters occurred with increased N supply (N400). On the other hand, N treatments did not change fruit P and K content significantly (Supplementary Table S2).

3.2 Color characteristics of pepper fruit

The L* (brightness) and a* (green-red index) values of fruit skin were not affected by N application rate. However, compared to N0 treatment, the b* (yellow-blue index), C* (chroma), and h* (hue angle) values were decreased with N application (N250 and N400 conditions), with no significant difference detected between the two N treatments (Figure 2A).

3.3 Carotenoids and total phenols in pepper fruit

For carotenoid identification, a typical total ion chromatogram (TIC) of a quality control (QC) sample is shown

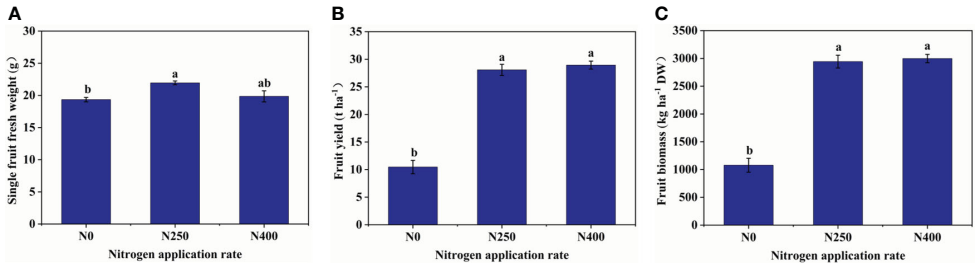

FIGURE 1
Single fruit fresh weight **(A)**, fruit yield **(B)**, and fruit biomass **(C)** of mature red peppers produced under different N application rates. Values are presented as means ± SE (n = 4). Different lowercase letters above the bars indicate a significant difference between N application rates at a $P < 0.05$ level (Duncan's test).

in Supplementary Figure S2A, with each differently-colored peak representing a detected metabolite. A multi-peak detection plot of metabolites acquired in multiple reaction monitoring (MRM) mode is shown in Supplementary Figure S2B. Following such measuring standards, a total of 20 carotenoids were detected in pepper fruit pericarp, but only 16 were identified, with the other four detected at a concentration too low to be identified (Supplementary Table S3).

The 16 identified carotenoids in pericarp included six carotenes and 10 xanthophylls (Table 1). With increasing N supply, no consistent trend in the content of different carotenoids was observed. The content of total carotenes in fruits produced under

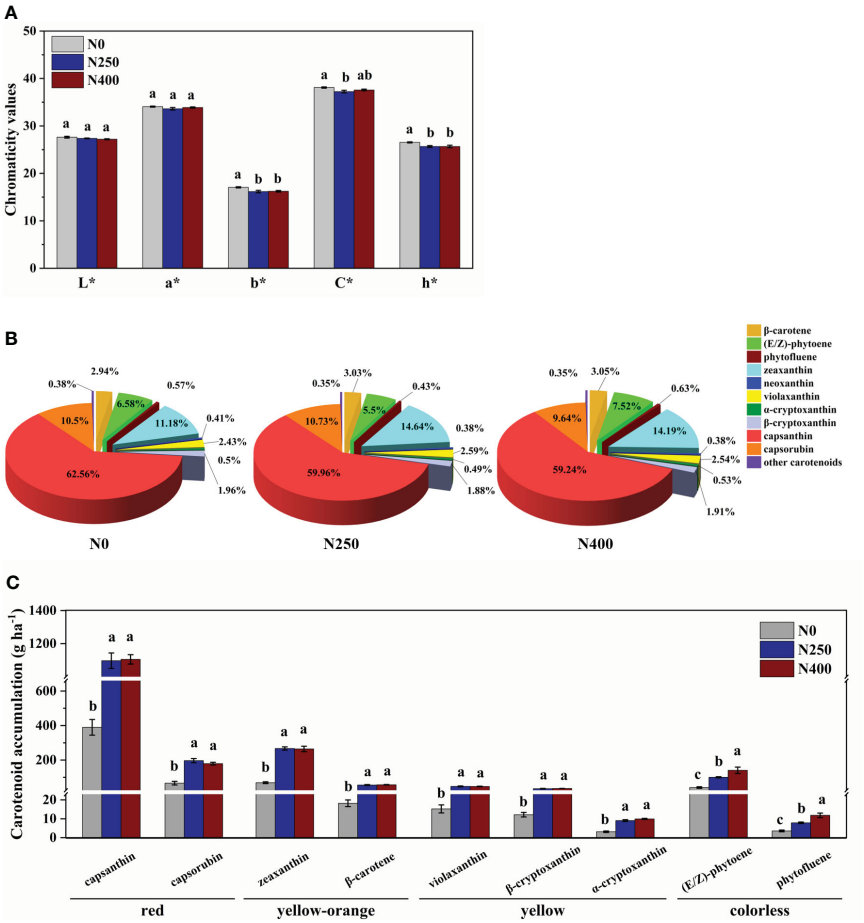

FIGURE 2
Color parameters **(A)**, proportion of different carotenoids in total carotenoid content **(B)**, and accumulation per hectare of main carotenoids **(C)** for mature red pepper fruits produced under different N application rates. L*, brightness index; a*, green-red index; b*, yellow-blue index; h*, hue angle, $h^* = \tan^{-1}(b^*/a^*)$; C*, chroma index, $C^* = (a^{*2} + b^{*2})/2$. In plot **(A, C)**, values are presented as means ± SE (n = 4), and different lowercase letters above the bars indicate a significant difference between N application rates at a $P < 0.05$ level (Duncan's test).

10.3389/fpls.2024.1319680

N0 and N250 treatments was similar, but was significantly higher in those produced under N400. The total xanthophyll content increased remarkably with N application (N250 and N400). As a result, the response of total carotenoid content to N supply was similar to that of total xanthophyll. In contrast to carotenoids, the total phenol content was significantly reduced with N application (N250 and N400), but with no N rate effect.

Capsanthin, zeaxanthin, capsorubin and (E/Z)-phytoene were the main carotenoids detected in pepper pericarp (Table 1). Together, they accounted for approximately 90% of the total carotenoid content, with capsanthin being the most dominant carotenoid (approximately 60%) (Figure 2B). N application significantly decreased the proportion of capsanthin in total carotenoid content, while an opposite trend was evident for zeaxanthin (Figure 2B). Based on the tissue content and pericarp biomass (dry weight), the accumulation of main carotenoids per hectare was calculated and the results are presented in Figure 2C. The accumulation of red (capsanthin and capsorubin), yellow-orange (zeaxanthin and β-carotene), and yellow (violaxanthin, β-cryptoxanthin and α-cryptoxanthin) pigments were increased significantly with N application (N250 and N400), but with no significant N rate effect. However, the accumulation of colorless pigments, (E/Z)-phytoene and phytofluene, kept increasing with the increase in N application rate.

3.4 Carotenoid biosynthesis pathway analysis

The carotenoid biosynthesis pathway in pepper was constructed based on the KEGG pathway and literature references (Figure 3). Thirteen of the 16 identified carotenoids were mapped in the pathway. As the primary carotenoid metabolites, colorless pigments (E/Z)-phytoene and phytofluene were reduced under N250 treatment but were increased greatly under N400 treatment compared with the control condition (N0). A similar increasing trend in response to N supply was found for carotenoid pigments in the δ-carotene pathway. Nitrogen application decreased the content of γ-carotene and increased the level of its derivatives in the γ-carotene pathway. Capsanthin and capsorubin, the most abundant xanthophyll derivatives, were increased remarkably in fruits produced under N250 compared with those grown under the control (N0) and high N (N400) conditions.

TABLE 1 Content of carotenoids and total phenols in the pericarp of mature red pepper fruit produced under different N application rates.

Compounds		Coloration	N application rate		
			N0	N250	N400
Carotenes (μg g^{-1} DW)	α-carotene	yellow-orange	2.01 ± 0.06^{a}	2.04 ± 0.08^{a}	2.04 ± 0.08^{a}
	β-carotene	yellow-orange	23.27 ± 0.42^{b}	25.84 ± 0.56^{a}	26.03 ± 0.90^{a}
	phytofluene	colorlesss	4.51 ± 0.18^{ab}	3.68 ± 0.2^{b}	5.4 ± 0.52^{a}
	(E/Z)-phytoene	colorlesss	52.1 ± 0.68^{ab}	46.85 ± 1.45^{b}	64.12 ± 7.80^{a}
	γ-carotene	yellow	0.29 ± 0.01^{a}	0.26 ± 0.005^{b}	0.25 ± 0.01^{b}
	ϵ-carotene		0.13 ± 0.002^{b}	0.14 ± 0.006^{ab}	0.16 ± 0.015^{a}
	Total carotenes		82.31 ± 1.14^{b}	78.8 ± 1.95^{b}	98.01 ± 7.74^{a}
Xanthophylls (μg g^{-1} DW)	capsanthin	intense red	495.55 ± 2.51^{b}	510.45 ± 2.65^{a}	505.11 ± 5.88^{ab}
	capsorubin	red-brown	83.17 ± 3.35^{a}	91.42 ± 3.3^{a}	82.23 ± 4.84^{a}
	zeaxanthin	yellow-orange	88.55 ± 3.64^{b}	124.7 ± 4.73^{a}	120.99 ± 6.81^{a}
	violaxanthin	yellow	19.24 ± 0.48^{b}	22.07 ± 0.50^{a}	21.65 ± 0.62^{a}
	neoxanthin	yellow	3.21 ± 0.06^{a}	3.22 ± 0.18^{a}	3.23 ± 0.40^{a}
	β-cryptoxanthin	yellow	15.54 ± 0.43^{a}	16.05 ± 0.68^{a}	16.27 ± 0.52^{a}
	α-cryptoxanthin	yellow	3.98 ± 0.09^{b}	4.21 ± 0.09^{b}	4.54 ± 0.13^{a}
	echinenone		0.02 ± 0.0005^{a}	0.02 ± 0.0006^{a}	0.02 ± 0.001^{a}
	β-citraurin		0.48 ± 0.01^{a}	0.42 ± 0.01^{a}	0.45 ± 0.03^{a}
	8'-apo-beta-carotenal		0.07 ± 0.002^{b}	0.10 ± 0.004^{a}	0.10 ± 0.003^{a}
	Total xanthophylls		709.81 ± 1.88^{b}	772.66 ± 5.18^{a}	754.59 ± 8.82^{a}
Total carotenoids (μg g^{-1} DW)			792.12 ± 1.03^{b}	851.46 ± 6.93^{a}	852.6 ± 4.04^{a}
Total phenols (mg g^{-1} FW)			1.24 ± 0.03^{a}	1.00 ± 0.03^{b}	1.05 ± 0.06^{b}

In the same row values (mean ± SE, n = 4) followed by different superscript letters indicate a significant difference between N application rates at a $P < 0.05$ level (Duncan's test).

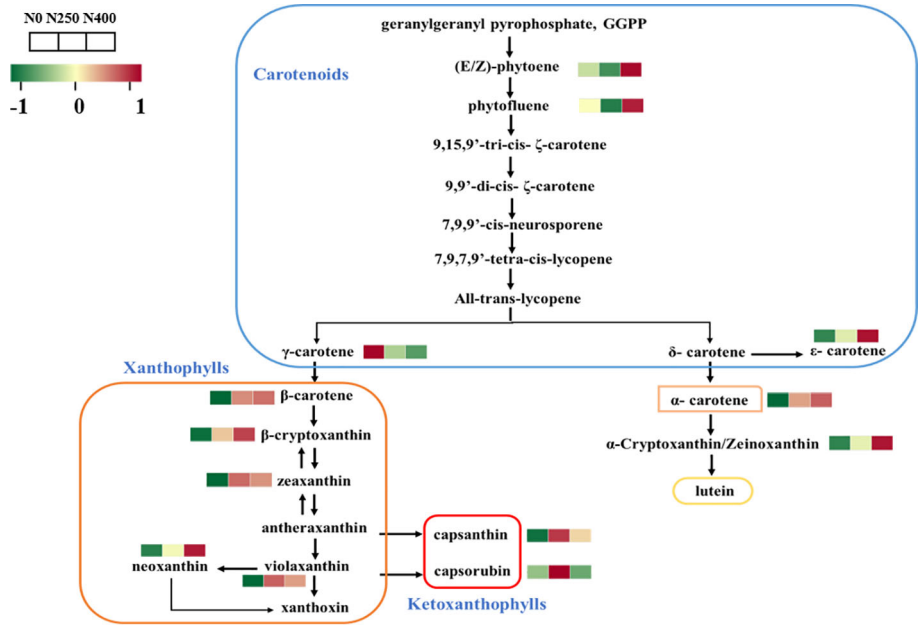

FIGURE 3
Heat map of metabolites involved in carotenoid biosynthesis following different N application rates. Each colored cell represents the normalized content of each compound by standardized Z-score (mean of four replicates for each N rate). The Z score is shown on a green (low) to red (high) color scale. As relative content of metabolites increases, the color of the cell changes from green to red.

3.5 Identification and analysis of secondary metabolites

A total of 290 secondary metabolites, including 133 flavonoids, 135 phenolic acids, 12 lignans and 10 coumarins were identified. OPLS-DA analysis helped maximize the identification of metabolites with little quantitative difference between them, which aided screening for metabolites with differential accumulation (Supplementary Figure S3). R^2Y scores and Q^2 values represent the interpretation rate of the OPLS-DA model to the Y matrix and the prediction ability of the model, respectively. Results showed that R^2Y scores were all higher than 0.99, and Q^2 values were all larger than 0.68, confirming the differential accumulation response of metabolites to N treatment (Supplementary Figure S4).

Potential DAMs were identified using the VIP ≥ 1 criterion. A total of 152, 144, and 93 potential DAMs were identified from N0 vs. N250, N0 vs. N400, and N250 vs. N400 comparisons, respectively (Figure 4; Supplementary Table S4). From this analysis, N0 vs. N250 (Figure 4A; Supplementary Table S4A) and N0 vs. N400 (Figure 4B; Supplementary Table S4B) comparisons had the greatest number of flavonoids (especially flavonols, flavanones, and flavones) and phenolic acids. In the N250 vs. N400 comparison, most potential DAMs were phenolic acids (Figure 4C; Supplementary Table S4C).

To further screen for the DAMs occurring in different pairwise comparisons of N treatments, the DAMs were screened according to the combination of VIP ≥ 1 and $P < 0.05$ (t-test). The relationships between VIP value and *P*-value for different group comparisons were analyzed to confirm the validity of DAM identification (Supplementary Figure S5). The number of DAMs was 88 between N0 and N250 (23 up, 65 down) (Figure 5A; Supplementary Table S5A), 92 between N0 and N400 (21 up, 71 down) (Figure 5C; Supplementary Table S5B), and 29 between N250 and N400 (12 up, 17 down) (Figure 5E; Supplementary Table S5C). Notably, lignans (epipinoresinol and pinoresinol) were upregulated > 4-fold, while the flavonoids (luteolin-7-O-neohesperidoside, kaempferol-3-O-glucorhamnoside, kaempferol-3-O-neohesperidoside, kaempferol-3-O-rutinoside, 6-C-glucosyl-2-hydroxynaringenin, eriodictyol-8-C-glucoside, choerospondin, aromadendrin-7-O-glucoside, and dihydrocharcone-4′-O-glucoside) and phenolic acids (6-O-caffeoylarbutin and 3-O-p-Coumaroylquinic acid-O-glucoside) were decreased < 0.3-fold under N250 and N400 conditions compared with the control (N0) condition (Supplementary Table S5).

Additionally, eriodictyol-7-O-glucoside (a flavanone), decursinol and acoumarin were only detected in N250 and N400, and apigenin-6-C-(2″-xylosyl) glucoside, a flavonoid carbonoside, was found only in N0 and N400. The flavanones 5,4′-dihydroxy-7-methoxyflavanone (sakuranetin) and persicoside, and the chalcones 2′,3,4,4′,6′-pentahydroxychalcone-4′-O-glucoside were detected only in N250, while dihydromyricetin, aflavanonol, and the phenolic acids 2-hydroxybenzaldehyde, anthranilic acid, and trihydroxycinnamoylquinic acid were identified in the N400 condition only (Supplementary Tables S4, S5).

To identify the trends between DAM content and N application rate, K-means analysis was performed (Supplementary Figure S6). The 129 DAMs were further divided into six sub-classes (1 to 6), containing 60, 20, 11, 18, 12, and 6 metabolites, respectively (Supplementary Figure S6; Supplementary Table S6). The DAMs

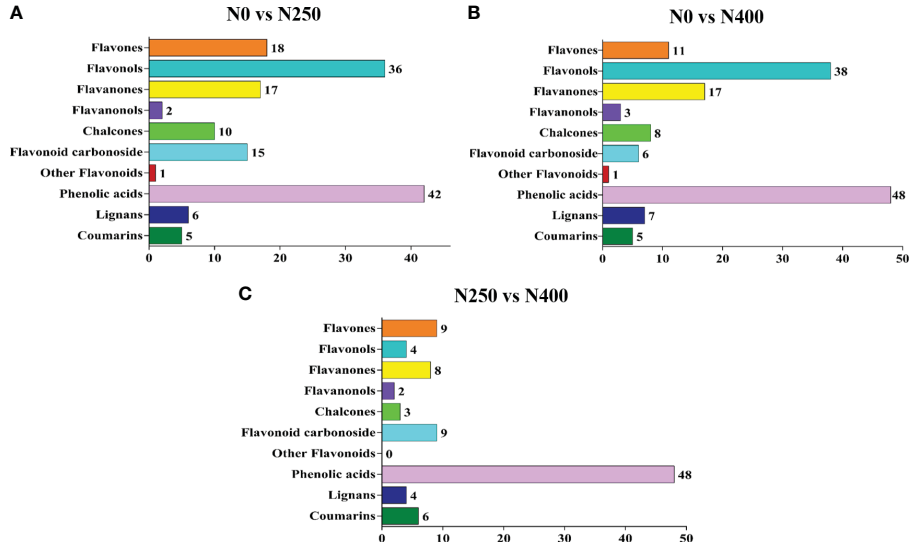

FIGURE 4
The number of potential differentially-accumulated metabolites in the pericarp of mature red pepper fruits in the following comparisons: N0 vs. N250 **(A)**, N0 vs. N400 **(B)**, and N250 vs. N400 **(C)**. The metabolites are screened according to variable importance in projection (VIP) ≥ 1 in the orthogonal partial least squares-discriminant analysis (OPLS-DA).

in sub-class 1, 2, and 6 were mainly flavonoids and phenolic acids, while those in sub-class 3, 4, and 5 were mostly lignans and coumarins, with some flavonoids and phenolic acids (Supplementary Table S6). The DAM content in sub-class 1, 2, and 6 were decreased with N supply (N250) (Supplementary Figures S6A, B, F), while those in sub-class 3, 4, and 5 were increased with the same N treatment (N250) (Supplementary Figures S6C-E). When N supply was further increased to N400, changes in metabolite content displayed a downward trend for DAMs in sub-class 2, 3, and 5, whereas it was increased for those in sub-class 4 and 6, and remained stable for DAMs in sub-class 1.

3.6 Metabolic pathway enrichment analysis

The pathways associated with pigment metabolites were identified using the KEGG database. The number of DAMs annotated by KEGG with significant difference from the N0 vs. N250, N0 vs. N400, N250 vs. N400 comparisons was 19, 20, and 7, respectively (Figures 5B, D, F). The most enriched KEGG terms among the DAMs were flavonoid biosynthesis, flavone and flavonol biosynthesis, and phenylpropanoid biosynthesis. The DAMs involved in the flavonoid biosynthesis pathway were highly enriched in the N0 vs. N250 and N0 vs. N400 comparisons.

More specifically, the main metabolites of flavonoid biosynthesis (naringenin, eriodictyol, hesperetin-7-O-glucoside, pinobanksin, naringenin chalcone, phloretin, and phlorizin), flavone and flavonol biosynthesis (luteolin-7-O-neohesperidoside, kaempferol-3-O-rutinoside [nicotiflorin], quercetin-3-O-[2″-O-xylosyl] rutinoside), and phenylpropanoid biosynthesis (caffeic aldehyde) were downregulated with N application (N250 and N400) (Figure 6). The flavanonol dihydromyricetin involved in flavonoid biosynthesis was only detected under N400 treatment, while flavanone metabolite sakuranetin (5,4′-dihydroxy-7-methoxyflavanone) and chalcone metabolite 2′,3,4,4′,6′-pentahydroxychalcone-4′-O-glucoside were found only under N250.

3.7 Relationship between color parameters and metabolites

To investigate the correlations between metabolites and color parameters in pepper fruit, a correlation network analysis of color parameters, carotenoids, flavonoids, phenolic acids, lignans, and coumarins was conducted (Figure 7; Supplementary Table S7). Most carotenoids were negatively correlated with flavonoids and phenolic acids (Figure 7B). Most flavonoids were positively correlated with phenolic acids (Figure 7A) and negatively correlated with coumarin and lignans (Figure 7B). Total phenol content was negatively correlated with β-carotene, zeaxanthin, violaxanthin, fruit fresh weight and fruit yield (Supplementary Table S7). The N application rate showed a negative correlation with L*, b*, and h* values, total phenols, and most flavonoids and phenolic acids, but a positive correlation with most carotenoids, total carotenoids, lignans, coumarins, and yield (Supplementary Table S7).

The hue angle h* value showed a significant positive correlation with most flavonoids and phenolic acids, but was negatively correlated with capsanthin, capsorubin, β-carotene, zeaxanthin, violaxanthin, 8′-apo-beta-carotenal, total phenol, some ligans (liriodendrin, epipinoresinol, syringaresinol-4′-O-[6″-acetyl] glucoside) and coumarins (decursinol and esculin [6,7-dihydroxycoumarin-6-glucoside]) (Supplementary Table S7).

Capsanthin and capsorubin are unique pigments in pepper fruit. Capsanthin was negatively correlated with flavones (chrysoeriol-5,7-di-O-glucoside, luteolin-7-O-(6″-malonyl) glucoside-5-O-arabinoside, rhamnetin-3-O-rutinoside, quercetin-

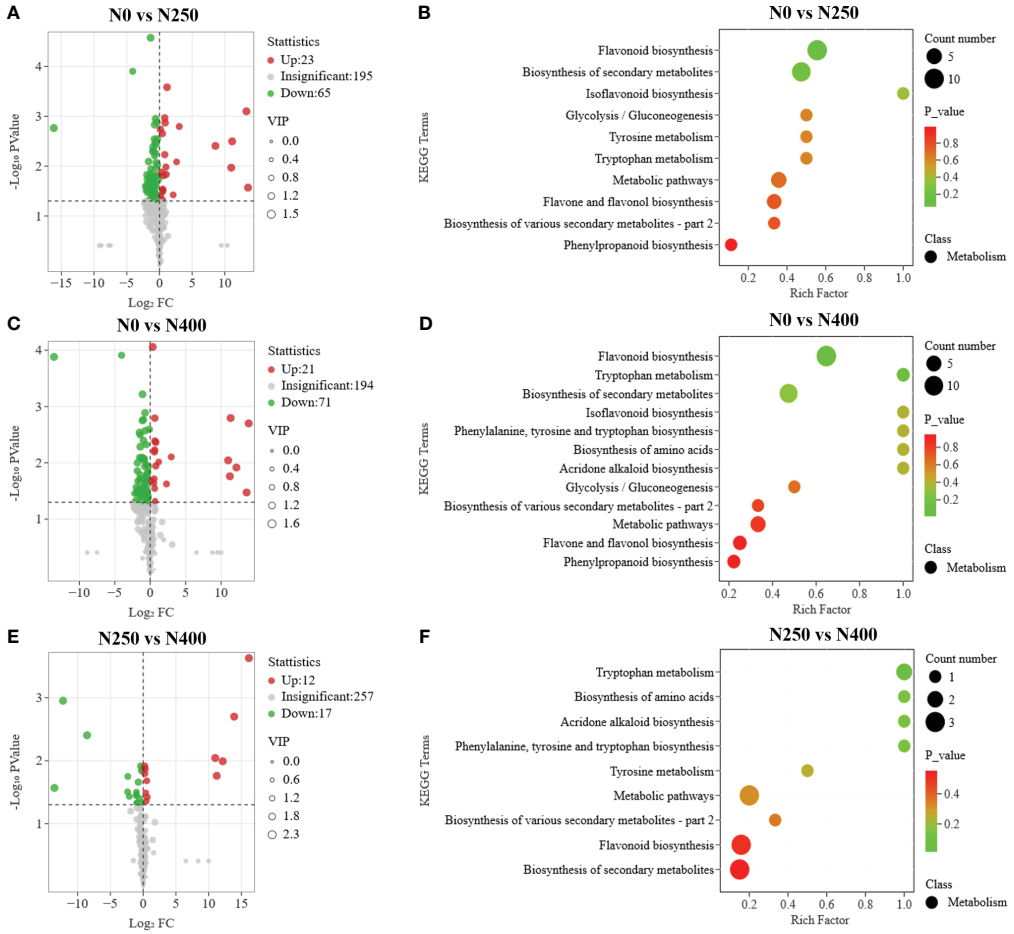

FIGURE 5
Differential metabolite analysis and Kyoto Encyclopedia of Genes and Genomes (KEGG) enrichment analysis for comparisons of N0 vs. N250 **(A, B)**, N0 vs. N400 **(C, D)**, and N250 vs. N400 **(E, F)**. In the volcano plot **(A, C, E)**, the red dots represent upregulated metabolites, blue dots represent downregulated metabolites and gray dots represent metabolites with no significant difference. In the KEGG enrichment plot **(B, D, F)**, each circle represents the number of associated metabolites and is positioned according to its enrichment factor. The *P*-values represent the hypergeometric test result of the degree of differential metabolite enrichment, which are indicated by color scale from green (low) to red (high).

3-O-xylosyl(1→2) glucosyl (1→2)glucoside) and phenolic acid (3-O-p-Coumaroylquinic acid-O-glucoside), and positively correlated with flavonoid carbonoside (chrysoeriol-6-C-glucoside-4′-O-glucoside), lignan (pinoresinol), and coumarin (decursinol) (Supplementary Table S7).On the other hand, capsorubin was positively correlated with flavanones (persicoside), and negatively correlated with flavonoid carbonoside (apigenin-6-C-(2″-xylosyl) glucoside) and phenolic acid (protocatechuic acid-4-O-glucoside) (Supplementary Table S7).

4 Discussion

4.1 Reduced N supply is optimal for maximum pepper fruit yield and superior fruit quality

N is a vital nutrient required for plant growth and development. In this study, the three N rate treatments influenced pepper fruit N content but not P and K content (Supplementary Table S2), indicating that plant N nutrition is an important determinant of differential responses of pepper fruits grown under these N treatments. A highly positive correlation ($P \leq 0.01$) between N application rate and fruit yield was observed (Supplementary Table S7). However, N supply beyond 250 kg ha^{-1} had little impact on fruit yield (Figure 1) and fruit N content (Supplementary Table S2). Thus, N supply at 250 kg ha^{-1} is considered optimal for maximum pepper yield. Moreover, a much lower level of soil NO_3^-N was found under N250 treatment than that under N400 treatment (Supplementary Table S2), indicating a lesser risk of NO_3^-N leaching and denitrification loss.

Fruit color is one of the criteria determining the commercial value of peppers (Korkmaz et al., 2021). Red pepper is generally evaluated by L*, a *, and b * color parameters (Baenas et al., 2019). Discolored red pepper skins have lower L* (brightness), a* (redness) and b* (yellowness) values than normal red pepper fruits (Feng et al., 2022). In this study, the L* and a* values were not affected by N application rate, whereas the b* value showed a significant reduction with N application (N250 and N400) compared with N0 supply (Figure 2A). As a result, the h* value (h* = tan^{-1}(b*/a*)

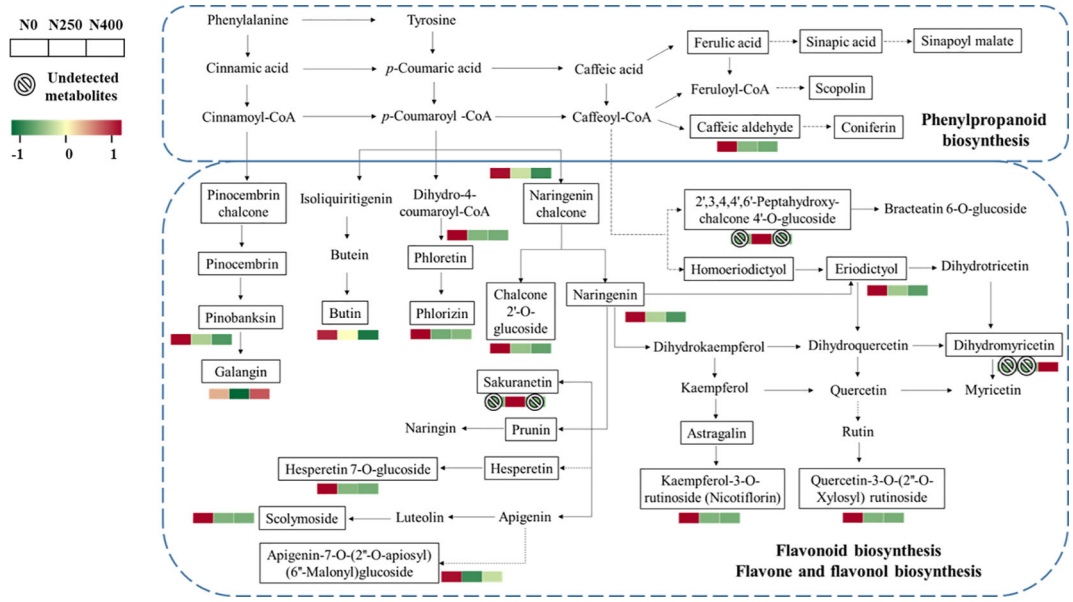

FIGURE 6
Heat map of metabolites involved in phenylpropanoid and flavonoid biosynthesis pathways as affected by different N application rates. Each colored cell represents the normalized accumulation of each compound by standardized Z-score (mean of four replicates for each N rate). The Z score is shown on a green (low) to red (high) color scale. As relative accumulation of metabolites increases, the color of the cell changes from green to red. The metabolites in the box and not shown in red or green scale represent those that are detected but do not change significantly in response to N supply.

was substantially decreased with N supply (N250 and N400), making pepper fruits more reddish. Because there was no significant difference for these color parameters between N250 and N400, N application at 250 kg ha^{-1} is also sufficient to produce commercially-appealing red-colored pepper fruits. Thus, a much lower N input (250 kg N ha^{-1}) than the current farmer practice (400 kg N ha^{-1}) will produce more nutritious pepper without compromising yield and reduce fertilizer cost with potential environmental benefits.

4.2 Level of N supply regulates pepper fruit carotenoids content and composition

As a large class of natural lipid-soluble pigments, carotenoids may respond differently to N supply in different plants. Previous studies have reported positive effects of increased N application on β-carotene content in grapes and lutein in kiwiberry fruits (Gutierrez-Gamboa et al., 2018; Stefaniak et al., 2020). More than 50 carotenoids have been identified in different red pepper varieties (Arimboor et al., 2015), and the type and content of carotenoids are known to change with pepper fruit development (Liu et al., 2020). In this study, a total of 16 carotenoids were identified in the pericarp of red chili pepper at full maturity (Table 1). Of these, capsanthin, zeaxanthin, capsorubin, and (E/Z)-phytoene were the main compounds. The content of colored carotenoids capsanthin (intense red), zeaxanthin (yellow-orange), and capsorubin (red-brown) peaked with N application at 250 kg ha^{-1}, while the colorless carotenoid, (E/Z)-phytoene, demonstrated its lowest level under this treatment. Capsanthin was the most dominant (approximately 60%) carotenoid in pepper fruit and its proportion was reduced with increased N supply, while the proportion of zeaxanthin, the second most abundant pigment, increased initially (N250) and remained unchanged with increased N supply (N400) (Figure 2B). The proportion of capsorubin and (E/Z)-phytoene in the total carotenoid content responded differently with changing N application rate. However, when calculated on a hectare basis using tissue (pericarp) content and tissue dry weight, the amount of all main carotenoids was increased significantly with N supply, with no difference detected between the N250 and N400 conditions except for the N rate-dependent rise in (E/Z)-phytoene accumulation (Figure 2C). Thus, the variation in response of tissue carotenoid content and carotenoid production in pepper per unit cropped area was due to the differential response of carotenoid levels in the tissue and fruit yield to the N application rate (Table 1; Figures 1B, C).

The content and composition of the carotenoids in pepper fruits during ripening are determined by two metabolic processes, i.e., transformation of existing photosynthetic pigments and *de novo* carotenoid biosynthesis (del Rocío Gomez-Garcia and Ochoa-Alejo, 2013; Berry et al., 2019; Zheng et al., 2019). The first committed step for carotenoid biosynthesis involves the condensation of two geranylgeranyl diphosphate molecules into colorless phytoene catalyzed by phytoene synthase (PSY) (Meng et al., 2019). Then, the synthesis of carotenoid is divided into two branches mediated by two key enzymes, lycopene β-cyclase (LCYB) and lycopene ϵ-cyclase (LCYE) (Liu et al., 2020). Finally, capsanthin-capsorubin synthase (CCS) transforms zeaxanthin and violaxanthin into capsanthin and capsorubin respectively, and the final products of the carotenoid biosynthetic pathway produce the red color of pepper fruits (Guo et al., 2021). In this study, 13 out of the 16

10.3389/fpls.2024.1319680

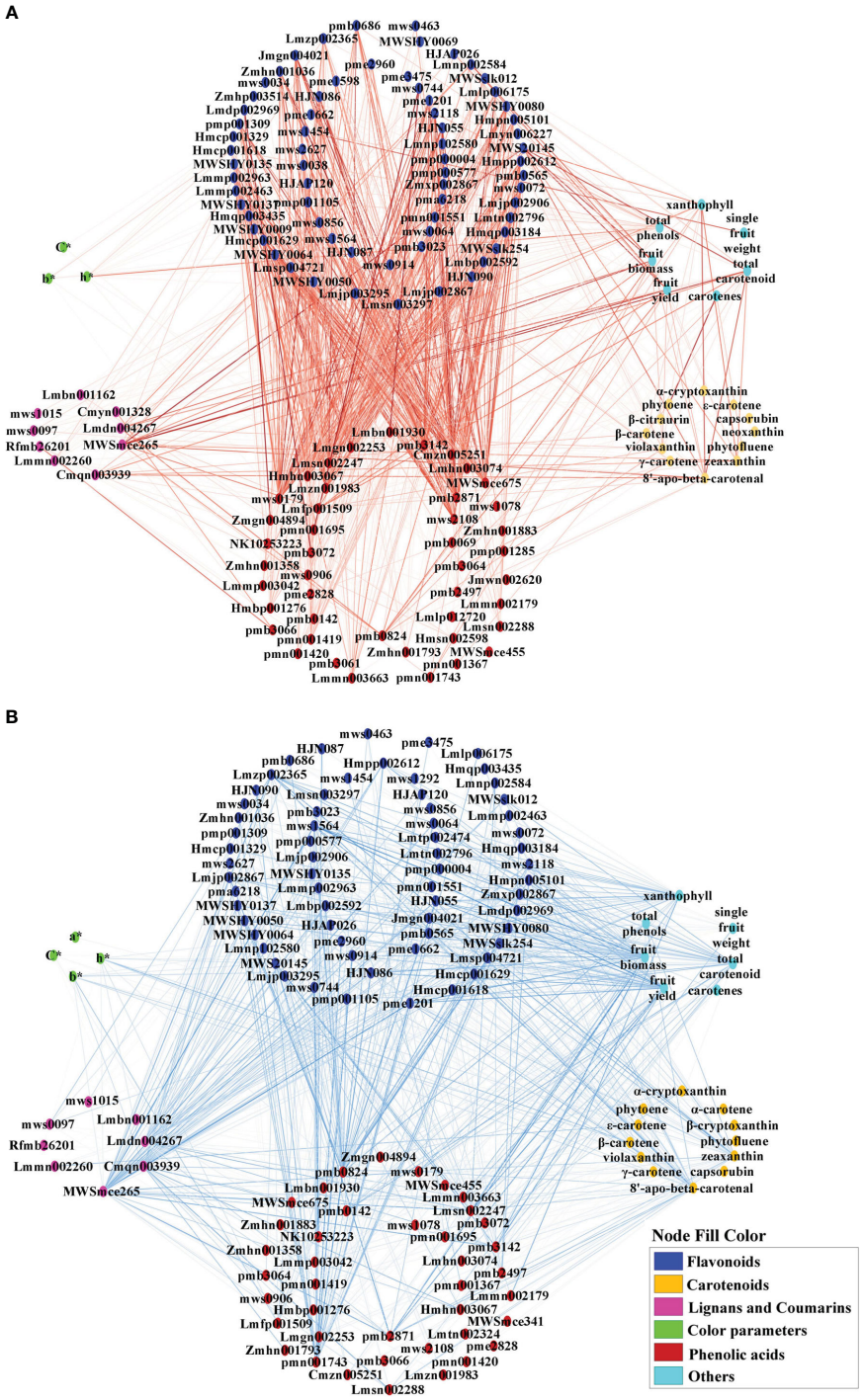

FIGURE 7
Positive **(A)** and negative **(B)** correlation network analysis of color parameters, growth indicators, pigments, and associated metabolites for mature red pepper fruit based on Pearson correlation. a*, green-red index; b*, yellow-blue index; h*, hue angle, h* = $\tan^{-1}$(b*/a*); C*, chroma index, C* = $(a^{*2} + b^{*2})/2$. Edges colored in red and blue represent positive and negative correlations, as determined by a Pearson correlation coefficient > 0.7 or < −0.7 ($P < 0.05$), respectively. The width of the edges indicates the strength of the correlation.

identified carotenoids were related to the *de novo* carotenoid biosynthesis (Figure 3). The KEGG pathway mapping showed that the effects of different N supply on the accumulation of primary precursors, (E/Z)-phytoene and phytofluene, differed from that on the downstream carotenes and xanthophylls in the two branched pathways. It seems that the optimal N application of 250 kg ha^{-1} would favor the fast transformation of (E/Z)-phytoene and phytofluene into capsanthin and capsorubin via a large increase in the accumulation of zeaxanthin and violaxanthin but limiting the production of neoxanthin in the γ-carotene pathway, with reduced

carbon influx into the δ-carotene pathway. However, the higher N application rate of 400 kg N ha^{-1} tends to maintain greater accumulation of precursors, (E/Z)-phytoene and phytofluene, and increases downstream production of ϵ-carotene, α-carotene, and α-cryptoxanthin in the δ-carotene pathway and neoxanthin in the γ-carotene pathway, but with relatively reduced capsanthin and capsorubin production. Thus, although the total carotenoid content was similar under N250 and N400 conditions, it can be speculated that the optimal N supply (250 kg N ha^{-1}) is more beneficial for *de novo* carotenoid biosynthesis into capsanthin and capsorubin.

As mentioned above, four catalytic enzymes (PSY, LCYB, LCYE, and CCS) play important roles in carotenoid synthesis. A previous study has reported positive correlations between total carotenoid content and *PSY1*, *LCYB*, and *CCS* expression in pepper fruit pulp, and *CCS* expression in the fruit peel (Filyushin et al., 2020). Furthermore, another combined metabolome and transcriptome analysis of pepper fruits with different colors has found that the *PSY1* gene regulates the accumulation of phytoene, the *LCYB* and *LCYE* genes synergistically regulate the accumulation of α-carotene, γ-carotene, and β-carotene, while the accumulation of capsanthin was not determined solely by the *CCS* gene (Liu et al., 2020). Moreover, a recent work reported an R-R-type MYB transcription factor promoting carotenoid biosynthetic gene transcript levels and capsanthin content (Song et al., 2023). These studies provide additional insights into the potential genetic regulation of carotenoid biosynthesis, but the role of N nutrition on the expression of these genes in pepper fruits requires further study.

4.3 Phenolic compound accumulation and their relationships with carotenoids as influenced by N supply

Phenolic acids and flavonoids are the major groups of phenolic compounds present in pepper fruits (Suseela and Tharayil, 2018). Previous studies have shown that p-coumaric, caffeic, sinapic, and ferulic glycosides are the characteristic phenolic acid derivatives in pepper fruits (Materska and Perucka, 2005; Baenas et al., 2019). Research suggests that N fertilization decreases the amount of polyphenols in some plants (Larbat et al., 2012; Radusiene et al., 2019; Narvekar and Tharayil, 2021). In this study, N supply (N250 and N400) dramatically decreased the total phenol content (Table 1), in accordance with former reports. Most of the phenolic compounds are biosynthesized through the phenylpropanoid pathway which starts with phenylalanine (Jakovljevic et al., 2019). The restriction of N will decrease protein synthesis and thus reduce competition for phenylalanine (Bustamante et al., 2020). In the present study, caffeic aldehyde was upregulated under N deficiency (N0) (Figure 6). However, the metabolites in the other branches of phenylpropane metabolism (scopolin and sinapoyl malate) were not affected, which may be due to the reorientation of metabolic fluxes between branches of the phenylpropane pathway to cope with low N stress and maintain the homeostasis of metabolism (Dong and Lin, 2021).

Flavonoids are synthesized from phenylalanine via phenylpropanoid and flavonoid pathways (Tohge et al., 2017; Liu et al., 2020). Previous studies have found that expression of flavonoid biosynthesis pathway genes is affected by nutrient depletion (Liu et al., 2021). N deficiency could decrease chlorophyll content and photosynthesis (Li et al., 2021). A malfunctioning photosystem renders the plants more exposed to oxidative damage and the increased flavanoid production in such conditions is thought to protect plants from photo-oxidative damage (Gill and Tuteja, 2010). In this study, significant enrichment was observed for metabolites in flavonoid biosynthesis and flavone-flavonol biosynthesis under the control (N0) condition (Figure 6). Moreover, N application rate was negatively correlated with most flavonoid compounds, especially luteolin, kaempferol, eriodictyol, hesperetin, and quercetin derivatives, which were present either at the C-3 or C-7 position in the form of O-glycosides, as well as naringenin and naringenin chalcone (Supplementary Table S7). Under the influence of flavonol synthase, dihydroflavonol can be synthesized into flavonols such as kaempferol, quercetin, and myricetin (Shen et al., 2022). Therefore, the downregulation of kaempferol-3-O-rutinoside (nicotiflorin) and quercetin-3-O-(2″-O-Xylosyl) rutinoside observed in this study might have caused higher dihydromyricetin accumulation under the N250 and N400 conditions compared with the N0 condition (Figure 6). These results indicate that sufficient N supply may reduce flavonoid accumulation and their contribution to the red pigmentation of pepper fruit.

The synthesis and accumulation of carotenoids usually accompany the degradation of chlorophyll and flavonoids when pepper fruits mature (Liu et al., 2020). Both carotenoids and flavonoids are carbon-based compounds that do not contain N, but they may demonstrate contrasting responses to N deficiency (Becker et al., 2015). In the present study, correlation network analysis showed that most carotenoids were negatively correlated with flavonoids and phenolic acids (Figure 7). N application rates showed a negative correlation with most flavonoids and phenolic acids, but a positive correlation with most carotenoids, lignans, and coumarins (Supplementary Table S7). These results partially confirmed the common viewpoint that high N supply could decrease secondary metabolite accumulation in plants (Deng et al., 2019). Although there was a general decrease in the relative amount of most flavonoids and phenolic acids with increased N supply, the production of other compounds were stimulated, or not affected (Supplementary Figure S6; Supplementary Table S6), as shown in other studies (Ormeno and Fernandez, 2012; Saloner and Bernstein, 2021). It is worth noting that content of some flavonoids and phenolic acids in sub-class 3 and 5 peaked under N250 compared with N0 and N400, indicating the optimized N supply was beneficial for these compounds. Thus, our results highlight the differential response of secondary metabolites to N supply in pepper fruits, and the consequent variation in pigments content, composition, and accumulation. Understanding the mechanistic basis of this biochemical response of pepper fruit will help develop molecular and crop management tools and technologies for producing nutritionally-superior peppers.

5 Conclusions

In this study, growth and color parameters together with targeted and non-targeted metabolomics of secondary products were used to understand and explain the color formation in mature pepper fruits produced under different N supply. N fertilization promoted carotenoid biosynthesis but downregulated phenylpropanoid and flavonoid biosynthesis in peppers. The red color deepened with increased N supply, which is attributed to the accumulation of carotenoids (mainly capsanthin, zeaxanthin, and capsorubin), as well as the decrease in flavonoids (especially luteolin, kaempferol, eriodictyol, hesperetin, and quercetin derivatives) and phenolic acids (caffeic aldehyde). Compared with the current practice of farmers (400 kg N ha^{-1}), a much-reduced N input (250 kg N ha^{-1}) than is sufficient to achieve high yield and high pepper fruit nutritional quality for human health, in addition to promoting the red color formation that increases consumer appeal. Furthermore, the reduced N input reduces production cost and facilitates positive environmental outcomes, i.e., reducing N leaching loss. Future work can be combined with transcriptomics, proteomics, and other molecular methods to further reveal the regulatory mechanism of N nutrition on pigment formation in peppers.

Data availability statement

The original contributions presented in the study are included in the article/Supplementary Material. Further inquiries can be directed to the corresponding authors.

Author contributions

LZ: Conceptualization, Data curation, Methodology, Writing – original draft. FZ: Methodology, Writing – review & editing. XH: Methodology, Writing – review & editing. YD: Methodology, Writing – review & editing. KS: Methodology, Writing – review & editing. SL: Methodology, Writing – review & editing. XW: Writing – review & editing. HY: Writing – review & editing. WZ: Writing – review & editing. PL: Writing – review & editing. XC: Conceptualization, Funding acquisition, Supervision, Writing – review & editing. YD: Conceptualization, Supervision, Writing – original draft.

Funding

The author(s) declare financial support was received for the research, authorship, and/or publication of this article. This study was supported by the Innovation Research 2035 Pilot Plan of Southwest University (SWU-XDZD22001) and National Natural Science Foundation of China (U20A2047).

Conflict of interest

The authors declare that the research was conducted in the absence of any commercial or financial relationships that could be construed as a potential conflict of interest.

Publisher's note

Supplementary material

The Supplementary Material for this article can be found online at: https://www.frontiersin.org/articles/10.3389/fpls.2024.1319680/full#supplementary-material

References

Arimboor, R., Natarajan, R. B., Menon, K. R., Chandrasekhar, L. P., and Moorkoth, V. (2015). Red pepper (*Capsicum annuum*) carotenoids as a source of natural food colors: analysis and stability-a review. *J. Food Sci. Technol.-Mysore* 52, 1258–1271. doi: 10.1007/s13197-014-1260-7

Baenas, N., Belovic, M., Ilic, N., Moreno, D. A., and Garcia-Viguera, C. (2019). Industrial use of pepper (*Capsicum annum* L.) derived products: Technological benefits and biological advantages. *Food Chem.* 274, 872–885. doi: 10.1016/j.foodchem.2018.09.047

Barik, S., Ponnam, N., Reddy, A. C., Reddy, D. C. L., Saha, K., Acharya, G. C., et al. (2022). Breeding peppers for industrial uses: Progress and prospects. *Ind. Crops Prod.* 178, 114626. doi: 10.1016/j.indcrop.2022.114626

Becker, C., Urlic, B., Spika, M. J., Klaering, H.-P., Krumbein, A., Baldermann, S., et al. (2015). Nitrogen limited red and green leaf lettuce accumulate flavonoid glycosides, caffeic acid derivatives, and sucrose while losing chlorophylls, β-carotene and xanthophylls. *PloS One* 10, e0142867. doi: 10.1371/journal.pone.0142867

Berry, H. M., Rickett, D. V., Baxter, C. J., Enfissi, E. M. A., and Fraser, P. D. (2019). Carotenoid biosynthesis and sequestration in red chilli pepper fruit and its impact on colour intensity traits. *J. Exp. Bot.* 70, 2637–2650. doi: 10.1093/jxb/erz086

Bogacz-Radomska, L., Harasym, J., and Piwowar, A. (2020). ""Commercialization Aspects of Carotenoids," in *Carotenoids: Properties, Processing and Applications*. Ed. C. M. Galanakis (Academic Press, Cambridge, MA), 327–357. doi: 10.1016/B978-0-12-817067-0.00010-5

Bustamante, M. A., Michelozzi, M., Caracciolo, A. B., Grenni, P., Verbokkem, J., Geerdink, P., et al. (2020). Effects of soil fertilization on terpenoids and other carbon-based secondary metabolites in Rosmarinus officinalis plants: A comparative study. *Plants-Basel* 9, 830. doi: 10.3390/plants9070830

del Rocío Gomez-Garcia, M., and Ochoa-Alejo, N. (2013). Biochemistry and molecular biology of carotenoid biosynthesis in chili peppers (*Capsicum* spp.). *Int. J. Mol. Sci.* 14, 19025–19053. doi: 10.3390/ijms140919025

Deng, B., Li, Y., Lei, G., and Liu, G. (2019). Effects of nitrogen availability on mineral nutrient balance and flavonoid accumulation in Cyclocarya paliurus. *Plant Physiol. Biochem.* 135, 111–118. doi: 10.1016/j.plaphy.2018.12.001

Dong, N.-Q., and Lin, H.-X. (2021). Contribution of phenylpropanoid metabolism to plant development and plant-environment interactions. *J. Integr. Plant Biol.* 63, 180–209. doi: 10.1111/jipb.13054

Dubey, R. K., Singh, V., Upadhyay, G., Pandey, A. K., and Prakash, D. (2015). Assessment of phytochemical composition and antioxidant potential in some indigenous chilli genotypes from North East India. *Food Chem.* 188, 119–125. doi: 10.1016/j.foodchem.2015.04.088

Farneselli, M., Tosti, G., Onofri, A., Benincasa, P., Guiducci, M., Pannacci, E., et al. (2018). Effects of N sources and management strategies on crop growth, yield and potential N leaching in processing tomato. *Eur. J. Agron.* 98, 46–54. doi: 10.1016/j.eja.2018.04.006

Feng, X., Yu, Q., Li, B., and Kan, J. (2022). Comparative analysis of carotenoids and metabolite characteristics in discolored red pepper and normal red pepper based on non-targeted metabolomics. *Lwt-Food Sci. Technol.* 153, 112398. doi: 10.1016/j.lwt.2021.112398

Filyushin, M. A., Dzhos, E. A., Shchennikova, A., and Kochieva, E. Z. (2020). Dependence of pepper fruit colour on basic pigments ratio and expression pattern of carotenoid and anthocyanin biosynthesis genes. *Russ. J. Plant Physiol.* 67, 1054–1062. doi: 10.1134/S1021443720050040

Gill, S. S., and Tuteja, N. (2010). Reactive oxygen species and antioxidant machinery in abiotic stress tolerance in crop plants. *Plant Physiol. Biochem.* 48, 909–930. doi: 10.1016/j.plaphy.2010.08.016

Giuffrida, D., Dugo, P., Torre, G., Bignardi, C., Cavazza, A., Corradini, C., et al. (2013). Characterization of 12 Capsicum varieties by evaluation of their carotenoid profile and pungency determination. *Food Chem.* 140, 794–802. doi: 10.1016/j.foodchem.2012.09.060

Guo, Y., Bai, J., Duan, X., and Wang, J. (2021). Accumulation characteristics of carotenoids and adaptive fruit color variation in ornamental pepper. *Sci. Hortic.* 275, 109699. doi: 10.1016/j.scienta.2020.109699

Gutierrez-Gamboa, G., Marin-San Roman, S., Jofre, V., Rubio-Breton, P., Perez-Alvarez, E. P., and Garde-Cerdan, T. (2018). Effects on chlorophyll and carotenoid contents in different grape varieties (*Vitis vinifera* L.) after nitrogen and elicitor foliar applications to the vineyard. *Food Chem.* 269, 380–386. doi: 10.1016/j.foodchem.2018.07.019

Ibrahim, M. H., Jaafar, H. Z. E., Rahmat, A., and Rahman, Z. A. (2012). Involvement of nitrogen on flavonoids, glutathione, anthocyanin, ascorbic acid and antioxidant activities of Malaysian medicinal plant *Labisia pumila Blume* (Kacip Fatimah). *Int. J. Mol. Sci.* 13, 393–408. doi: 10.3390/ijms13010393

Jakovljevic, D., Topuzovic, M., and Stankovic, M. (2019). Nutrient limitation as a tool for the induction of secondary metabolites with antioxidant activity in basil cultivars. *Ind. Crops Prod.* 138, 111462. doi: 10.1016/j.indcrop.2019.06.025

Korkmaz, A., Atasoy, A. F., and Hayaloglu, A. A. (2021). The effects of production methods on the color characteristics, capsaicinoid content and antioxidant capacity of pepper spices (*C. annuum* L.). *Food Chem.* 341, 128184. doi: 10.1016/j.foodchem.2020.128184

Larbat, R., Olsen, K. M., Slimestad, R., Lovdal, T., Benard, C., Verheul, M., et al. (2012). Influence of repeated short-term nitrogen limitations on leaf phenolics metabolism in tomato. *Phytochemistry* 77, 119–128. doi: 10.1016/j.phytochem.2012.02.004

Leong, H. Y., Show, P. L., Lim, M. H., Ooi, C. W., and Ling, T. C. (2018). Natural red pigments from plants and their health benefits: A review. *Food Rev. Int.* 34, 463–482. doi: 10.1080/87559129.2017.1326935

Li, Z., Jiang, H., Yan, H., Jiang, X., Ma, Y., and Qin, Y. (2021). Carbon and nitrogen metabolism under nitrogen variation affects flavonoid accumulation in the leaves of Coreopsis tinctoria. *Peerj* 9, e12152. doi: 10.7717/peerj.12152

Liu, J., Liu, M., Fang, H., Zhang, Q., and Ruan, J. (2021). Accumulation of amino acids and flavonoids in young tea shoots Is highly correlated with carbon and nitrogen metabolism in roots and mature leaves. *Front. Plant Sci.* 12. doi: 10.3389/fpls.2021.756433

Liu, Y., Lv, J., Liu, Z., Wang, J., Yang, B., Chen, W., et al. (2020). Integrative analysis of metabolome and transcriptome reveals the mechanism of color formation in pepper fruit (*Capsicum annuum* L.). *Food Chem.* 306, 125629. doi: 10.1016/j.foodchem.2019.125629

Lu, M., Liu, D., Shi, Z., Gao, X., Liang, Y., Yao, Z., et al. (2021). Nutritional quality and health risk of pepper fruit as affected by magnesium fertilization. *J. Sci. Food. Agric.* 101, 582–592. doi: 10.1002/jsfa.10670

Luo, M., Li, A., Wang, F., Jiang, J., Wang, Z., and You, J. (2022). Integrative analysis of multiple metabolomes and transcriptome revealed color expression mechanism in red skin root syndrome of Panax ginseng. *Ind. Crops Prod.* 177, 114491. doi: 10.1016/j.indcrop.2021.114491

Maoka, T. (2020). Carotenoids as natural functional pigments. *J. Nat. Med.* 74, 1–16. doi: 10.1007/s11418-019-01364-x

Marinov, O., Nomberg, G., Sarkar, S., Arya, G. C., Karavani, E., Zelinger, E., et al. (2023). Microscopic and metabolic investigations disclose the factors that lead to skin cracking in chili-type pepper fruit varieties. *Hortic. Res.* 10, uhad036. doi: 10.1093/hr/uhad036

Materska, M., and Perucka, I. (2005). Antioxidant activity of the main phenolic compounds isolated from hot pepper fruit (*Capsicum annuum* L.). *J. Agric. Food Chem.* 53, 1750–1756. doi: 10.1021/jf035331k

Meng, Y., Wang, Z., Wang, Y., Wang, C., Zhu, B., Liu, H., et al. (2019). The MYB activator WHITE PETAL1 associates with MtTT8 and MtWD40-1 to regulate carotenoid-derived flower pigmentation in *Medicago truncatula*. *Plant Cell* 31, 2751–2767. doi: 10.1105/tpc.19.00480

Mi, S., Yu, W., Li, J., Liu, M., Sang, Y., and Wang, X. (2020). Characterization and discrimination of chilli peppers based on multi-element and non-targeted metabolomics analysis. *Lwt-Food Sci. Technol.* 131, 109742. doi: 10.1016/j.lwt.2020.109742

Mi, S., Zhang, X., Wang, Y., Zheng, M., Zhao, J., Gong, H., et al. (2022). Effect of different genotypes on the fruit volatile profiles, flavonoid composition and antioxidant activities of chilli peppers. *Food Chem.* 374, 131751. doi: 10.1016/j.foodchem.2021.131751

Narvekar, A. S., and Tharayil, N. (2021). Nitrogen fertilization influences the quantity, composition, and tissue association of foliar phenolics in strawberries. *Front. Plant Sci.* 12. doi: 10.3389/fpls.2021.613839

Ormeno, E., and Fernandez, C. (2012). Effect of soil nutrient on production and diversity of volatile terpenoids from plants. *Curr. Bioact Compd* 8, 71–79. doi: 10.2174/157340712799828188

Peng, L., Gao, W., Song, M., Li, M., He, D., and Wang, Z. (2022). Integrated metabolome and transcriptome analysis of fruit flavor and carotenoids biosynthesis differences between mature-green and tree-ripe of cv. "Golden Phoenix" Mangoes (*Mangifera indica* L.). *Front. Plant Sci.* 13. doi: 10.3389/fpls.2022.816492

Radusiene, J., Marksa, M., Ivanauskas, L., Jakstas, V., Caliskan, O., Kurt, D., et al. (2019). Effect of nitrogen on herb production, secondary metabolites and antioxidant activities of Hypericum pruinatum under nitrogen application. *Ind. Crops Prod.* 139, 111519. doi: 10.1016/j.indcrop.2019.111519

Saini, R. K., Prasad, P., Lokesh, V., Shang, X., Shin, J., Keum, Y.-S., et al. (2022). Carotenoids: dietary sources, extraction, encapsulation, bioavailability, and health benefits-A review of recent advancements. *Antioxidants* 11, 794. doi: 10.3390/antiox11040795

Saloner, A., and Bernstein, N. (2021). Nitrogen supply affects cannabinoid and terpenoid profile in medical cannabis (*Cannabis sativa* L.). *Ind. Crops Prod.* 167, 113516. doi: 10.1016/j.indcrop.2021.113516

Scarano, A., Chieppa, M., and Santino, A. (2018). Looking at flavonoid biodiversity in horticultural crops: A colored mine with nutritional benefits. *Plants-Basel* 7, 98. doi: 10.3390/plants7040098

Shen, N., Wang, T., Gan, Q., Liu, S., Wang, L., and Jin, B. (2022). Plant flavonoids: Classification, distribution, biosynthesis, and antioxidant activity. *Food Chem.* 383, 132531. doi: 10.1016/j.foodchem.2022.132531

Shen, J., Zou, Z., Zhang, X., Zhou, L., Wang, Y., Fang, W., et al. (2018). Metabolic analyses reveal different mechanisms of leaf color change in two purple-leaf tea plant (*Camellia sinensis* L.) cultivars. *Hortic. Res.* 5, 7. doi: 10.1038/s41438-017-0010-1

Song, J., Sun, B., Chen, C., Ning, Z., Zhang, S., Cai, Y., et al. (2023). An R-R -type MYB transcription factor promotes non-climacteric pepper fruit carotenoid pigment biosynthesis. *Plant J.* 115, 724–741. doi: 10.1111/tpj.16257

Stefaniak, J., Przybyl, J. L., Latocha, P., and Lata, B. (2020). Bioactive compounds, total antioxidant capacity and yield of kiwiberry fruit under different nitrogen regimes in field conditions. *J. Sci. Food Agric.* 100, 3832–3840. doi: 10.1002/jsfa.10420

Suseela, V., and Tharayil, N. (2018). Decoupling the direct and indirect effects of climate on plant litter decomposition: Accounting for stress-induced modifications in plant chemistry. *Glob. Change Biol.* 24, 1428–1451. doi: 10.1111/gcb.13923

Tohge, T., de Souza, L. P., and Fernie, A. R. (2017). Current understanding of the pathways of flavonoid biosynthesis in model and crop plants. *J. Exp. Bot.* 68, 4013–4028. doi: 10.1093/jxb/erx177

Villa-Rivera, M. G., and Ochoa-Alejo, N. (2020). Chili pepper carotenoids: nutraceutical properties and mechanisms of action. *Molecules* 25, 5573. doi: 10.3390/molecules25235573

Wahyuni, Y., Ballester, A.-R., Tikunov, Y., de Vos, R. C. H., Pelgrom, K. T. B., Maharijaya, A., et al. (2013). Metabolomics and molecular marker analysis to explore pepper (*Capsicum* sp.) biodiversity. *Metabolomics* 9, 130–144. doi: 10.1007/s11306-012-0432-6

Yang, J., Wang, C., and Dai, H. (2008). *Soil agrochemical Analysis and Environmental Monitoring Techniques* (Beijing: Chinese Dadi Press), 18–64.

Zhao, C., Wang, Z., Cui, R., Su, L., Sun, X., Borras-Hidalgo, O., et al. (2021). Effects of nitrogen application on phytochemical component levels and anticancer and antioxidant activities of Allium fistulosum. *Peerj* 9, e11706. doi: 10.7717/peerj.11706

Zheng, X., Zhu, K., Sun, Q., Zhang, W., Wang, X., Cao, H., et al. (2019). Natural variation in CCD4 promoter underpins species-specific evolution of red coloration in citrus peel. *Mol. Plant* 12, 1294–1307. doi: 10.1016/j.molp.2019.04.014

Zhu, G., Wang, S., Huang, Z., Zhang, S., Liao, Q., Zhang, C., et al. (2018). Rewiring of the fruit metabolome in tomato breeding. *Cell* 172, 249–261. doi: 10.1016/j.cell.2017.12.019

Zoccali, M., Giuffrida, D., Salafia, F., Rigano, F., Dugo, P., Casale, M., et al. (2021). Apocarotenoids profiling in different Capsicum species. *Food Chem.* 334, 127595. doi: 10.1016/j.foodchem.2020.127595

frontiers | Frontiers in Plant Science

TYPE Review
PUBLISHED 04 March 2024
DOI 10.3389/fpls.2024.1351998

OPEN ACCESS

EDITED BY
Néstor Fernández Del-Saz,
University of the Balearic Islands, Spain

REVIEWED BY
Maurizio Chiurazzi,
National Research Council (CNR), Italy
Meng Xu,
Chinese Academy of Agricultural Sciences, China

*CORRESPONDENCE
Fei Liu
liufei280429@163.com

RECEIVED 07 December 2023
ACCEPTED 06 February 2024
PUBLISHED 04 March 2024

CITATION
Xu N, Cheng L, Kong Y, Chen G, Zhao L and Liu F (2024) Functional analyses of the NRT2 family of nitrate transporters in *Arabidopsis*. *Front. Plant Sci.* 15:1351998. doi: 10.3389/fpls.2024.1351998

Functional analyses of the NRT2 family of nitrate transporters in *Arabidopsis*

Na Xu[1], Li Cheng[1], Yuan Kong[1], Guiling Chen[1], Lufei Zhao[2] and Fei Liu[1]*

[1]School of Biological Science, Jining Medical University, Rizhao, Shandong, China, [2]Agricultural Science and Engineering School, Liaocheng University, Liaocheng, Shandong, China

Nitrogen is an essential macronutrient for plant growth and development. Nitrate is the major form of nitrogen acquired by most crops and also serves as a vital signaling molecule. Nitrate is absorbed from the soil into root cells usually by the low-affinity NRT1 NO_3^- transporters and high-affinity NRT2 NO_3^- transporters, with NRT2s serving to absorb NO_3^- under NO_3^-limiting conditions. Seven NRT2 members have been identified in *Arabidopsis*, and they have been shown to be involved in various biological processes. In this review, we summarize the spatiotemporal expression patterns, localization, and biotic and abiotic responses of these transporters with a focus on recent advances in the current understanding of the functions of the seven *AtNRT2* genes. This review offers beneficial insight into the mechanisms by which plants adapt to changing environmental conditions and provides a theoretical basis for crop research in the near future.

KEYWORDS

***Arabidopsis*, high-affinity nitrate transport system (HATS), NRT2s, C-N homeostasis, plant-microbe interactions, systemic nitrate signaling**

1 Introduction

Plants rely on nitrogen (N) as an essential macronutrient that is vital for their growth and productivity. Nitrate (NO_3^-) is the most abundant source of inorganic nitrogen taken up by most terrestrial plant species (Crawford and Forde, 2002). Kinetic criteria have been used to characterize such nitrate uptake as being mediated by three distinct systems, including a low-affinity transport system (LATS) as well as inducible and constitutive high-affinity transport systems (iHATS and cHATS) (Glass et al., 1995; Crawford and Glass, 1998; Forde, 2000). The cHATS and iHATS systems are generally active at NO_3^- concentrations in the 10-250 μM range, whereas LATS activity is only apparent when these concentrations exceed 250 μM. The NO_3^- affinity of the iHATS (Km: 13-79 μM) is lower than that of the cHATS (Km: 6-20 μM) (Forde and Clarkson, 1999), iHATS capacity

for the uptake of NO_3^- greatly exceeds that of cHATS. For example, analyses of iHATS activity in response to induction with a NO_3^- concentration of 100 μM yielded a V_{max} that was roughly 25-fold higher than that for the cHATS (Siddiqi et al., 1990). Members of the NRT1 protein family serve as low-affinity NO_3^- transporters with Km values in the mM range, while members of the NRT2 protein family function as high-affinity transporters with Km values in the μM range (Wang et al., 2012; O'Brien et al., 2016).The *Aspergillus nidulans crnA* gene was the first high-affinity NO_3^- transporter cloned from a eukaryotic species, and mutations in this gene can confer chlorate (ClO_3^-) resistance while resulting in the partial impairment of NO_3^- uptake (Brownlee and Arst, 1983; Unkles et al., 1991). The uptake of NO_2^- and NO_3^- in *Chlamydomonas reinhardtii* was subsequently determined to be under the control of three genes related to *crnA*, including *CrNRT2.1*, *CrNRT2.2*, and *CrNRT2.3* (Quesada et al., 1994; Galván et al., 1996; Quesada et al., 1998). More recently, researchers have identified high-affinity nitrate transporters from a wide range of plants including *Arabidopsis thaliana*, *Hordeum vulgare*, and *Nicotiana plumbaginifolia* (Quesada et al., 1997; Filleur and Daniel-Vedele, 1999; Zhuo et al., 1999; Vidmar et al., 2000). In the case of *Arabidopsis*, RT-PCR analyses performed using degenerate primers led to the initial cloning of the two related *AtNRT2.1* and *AtNRT2.2* transporter genes (Zhuo et al., 1999). With the completion of the *Arabidopsis* genome project, a total of seven *Arabidopsis* NRT2 family members were identified in this model species. The roots are the predominant site of expression for all *AtNRT2* genes other than *AtNRT2.7*, which is expressed at the highest levels in seeds (Orsel et al., 2002; Okamoto et al., 2003; Chopin et al., 2007a). The responsivity of different *NRT2* genes to changes in nitrate availability following N starvation varies markedly. For example, NO_3^- exposure strongly induced the expression of *NRT2.1* and *NRT2.2*, while *NRT2.4* was modestly upregulated, *NRT2.5* expression was repressed, and the expression of *NRT2.3*, *NRT2.6*, and *NRT2.7* was unaffected by the available nitrate supply (Okamoto et al., 2003). In addition to their roles as mediators of high-affinity NO_3^- influx, these NRT2 family members have been reported to play key roles in an array of biological processes involved in regulating processes such as N starvation, root architecture, seed development, cadmium uptake, plant-microbe interactions, systemic nitrate signaling, and the maintenance of appropriate nitrogen and carbon homeostasis (Table 1). This review offers an overview of information that is currently known regarding the molecular mechanisms and functions associated with plant members of the *NRT2* gene family.

2 High-affinity nitrate absorption

To date, seven NRT2 proteins have been identified in *Arabidopsis thaliana* (Glass et al., 2001). Of these, high-affinity root NO_3^- influx is only mediated by NRT2.1, NRT2.2, NRT2.4, and NRT2.5, each of which exhibits distinct context-dependent contributions to this absorptive process (Filleur et al., 2001; Kiba et al., 2012; Lezhneva et al., 2014).

TABLE 1 Summary of *Arabidopsis NRT2* nitrate transporter genes.

Name	Locus	Spatial Expression Pattern	Protein Localization	Nitrate Response	Other Regulations	Interaction With NRT3.1	Functions in *Arabidopsis*
NRT2.1	At1G08090	Mainly expressed in the roots, especially in the epidermal, cortical, and endodermal cell layers of the mature root parts	Plasma membrane	Induction	N starvation induction, ammonium and glutamine repression, light and sugar induction, cadmium repression	Yes	High-affinity nitrate uptake, cadmium uptake, plant-microbe interactions, systemic N signal, carbon and nitrogen metabolism
NRT2.2	At1G08100	Expressed in roots at low levels	Plasma membrane	Induction	Cadmium repression	Yes	High-affinity nitrate uptake
NRT2.3	At5G60780	Expressed in roots and shoots	Plasma membrane	Constitutive	Not known	Yes	Not known
NRT2.4	At5G60770	Expressed in the lateral root epidermis and the shoot vascular tissue	Plasma membrane	Induction	N starvation induction, cadmium repression	Yes	High-affinity nitrate uptake, N starvation, N remobilization
NRT2.5	At1G12940	Expressed in the root hair zone of the primary and the lateral roots and in the higher-order veins of leaves	Plasma membrane	Repression	N starvation induction, PGPR strain STM196 induction	Yes	High-affinity nitrate uptake, N starvation, N remobilization, plant-microbe interactions
NRT2.6	At3G45060	Strong preferential expression in roots	Plasma membrane	Constitutive	PGPR strain STM196 induction, bacterium *Erwinia amylovora* induction	Yes	Plant-microbe interactions
NRT2.7	At5G14570	Highly expressed in seeds	Tonoplast	Constitutive	Not known	No	Seed nitrate storage, seed germination, seed color

2.1 AtNRT2.1 and AtNRT2.2

The ability of *AtNRT2.1* and *AtNRT2.2* to function in an iHATS is supported by the fact that the *Atnrt2* T-DNA mutant, in which both of these genes are disrupted, exhibited a reduction in high-affinity nitrate uptake (Cerezo et al., 2001; Filleur et al., 2001). Notably, *AtNRT2.1* transcript levels are strictly correlated with high-affinity uptake of nitrogen when nitrate is supplied to plants that were initially nitrate-deprived (Okamoto et al., 2003). Further studies have explored the iHATS, cHATS, and LATS systems in *Atnrt2.1* mutant plants that were cultivated for 4 weeks in a 1 mM NH_4NO_3 solution followed by a 7-day nitrogen deprivation period in order to deplete nitrogen reserves (Li et al., 2007). Upon initial exposure of these plants to 100 µM $^{13}NO_3^-$, cHATS flux is first observed. Moreover, after the 1-week nitrogen deprivation period, plants were treated for 6 h with 1 mM KNO_3 followed by exposure to 100 µM $^{13}NO_3^-$, with the resultant flux representing the combination of iHATS and cHATS flux. These two flux measurements can be used to estimate iHATS activity based on the difference between the two. These sample plants were also utilized to assess LATS influx after a 6-hour induction period with 1 mM KNO_3 and subsequent exposure to 10 mM $^{13}NO_3^-$. These analyses revealed a ~72% reduction in iHATS activity in *Atnrt2.1* mutants without any corresponding change in cHATS or LATS flux (Li et al., 2007). Similarly, a 19% drop in iHATS flux was observed in *Atnrt2.2* mutants, whereas cHATS and LATS fluxes remained intact (Li et al., 2007). *AtNRT2.2* expression levels are significantly lower than *AtNRT2.1* levels (Zhuo et al., 1999; Orsel et al., 2002; Okamoto et al., 2003), but these levels were ~3-fold higher in *Atnrt2.1* mutant plants, indicating that *AtNRT2.2* overexpression may partially compensate for the loss of *Atnrt2.1*. Consistent with such a mechanism, *nrt2.1 nrt2.2* double mutants exhibit more dramatic iHATS and cHATS fluxes by ~80% and 30%, respectively, relative to *nrt2.1* and *nrt2.2* single mutants. These data emphasize the importance of *NRT2.1* as the key driver of iHATS activity, whereas *NRT2.2* exhibits a smaller compensatory role in this context (Li et al., 2007).

AtNRT2.1 expression is primarily evident in roots (Orsel et al., 2002), and it primarily localizes to the plasma membrane of root epidermal and cortical cells, consistent with this being the primary site of nitrate uptake (Wirth et al., 2007; Chopin et al., 2007b). NRT2.1 protein level changes reportedly differ from corresponding shifts in the mRNA expression of *NRT2.1* (Wirth et al., 2007), and *35S::NRT2.1* transformants constitutively overexpressing *NRT2.1* still exhibited reductions in HATS activity (Laugier et al., 2012), consistent with mechanisms responsible for post-translationally regulating *NRT2.1*. Phosphoproteomic analyses indicated that NRT2.1 is subject to phosphorylation, with the degree of its phosphorylation shifting as a function of the availability of nitrate (Engelsberger and Schulze, 2012; Menz et al., 2016). NRT2.1 reportedly harbors four phosphorylation sites as confirmed through high-accuracy mass spectrometry-based efforts to detect phosphopeptides (Engelsberger and Schulze, 2012; Menz et al., 2016; Jacquot et al., 2020). The Ser28 phosphorylation of NRT2.1 is evident in plants subject to N starvation, but dephosphorylation occurs rapidly when nitrate becomes available (Engelsberger and Schulze, 2012). Consistent with this observation, other studies have confirmed the stabilization and enhanced Ser28 phosphorylation of NRT2.1 under conditions of nitrate limitation. To explore the role of Ser28 phosphorylation, researchers established transgenic $NRT2.1^{S28E}$ and $NRT2.1^{S28A}$ plants that respectively mimic the phosphorylates and dephosphorylated forms of this protein (Zou et al., 2020). The Ser28 alanine substitution was associated with NRT2.1 destabilization, and $NRT2.1^{S28A}$ overexpression under conditions of limited nitrate availability failed to rescue defective *nrt2* mutant plant phonotypes. In contrast, greater levels of the $NRT2.1^{S28E}$ isoform enhanced protein stability and were sufficient to restore *nrt2* mutant phonotypes when cultivated in the presence of low nitrate levels (Zou et al., 2020). NRT2.1 Ser28 phosphorylation thus plays a key role in regulating NRT2.1 stability. Jacquot et al. further determined that the C-terminal portion of NRT2.1 (aa 494-513) is essential for the appropriate function of this protein, as demonstrated using transgenic *nrt2.1-2* mutant plants expressing truncated NRT2.1 isoforms (*NRT2.1*$\Delta C_{494\text{-}530}$ and *NRT2.1*$\Delta C_{514\text{-}530}$) (Jacquot et al., 2020). While the *pNRT2.1*::*NRT2.1*$\Delta C_{494\text{-}530}$ transgene was unable to restore HAST activity and growth to wild-type levels, the *pNRT2.1*::*NRT2.1*$\Delta C_{514\text{-}530}$ transgene was able to do so. Through mass spectrometry-based phosphopeptide detection efforts, the authors were able to identify the Ser501 phosphorylation site within this region of the protein, and the phonotypes of phosphomimetic S501D transgenic plants were comparable to those of *nrt2* mutants. Higher levels of Ser501 phosphorylation were observed under cultivation on 1 mM NO_3^- followed by transfer for 4 h onto 10 mM NH_4NO_3, consistent with a reduction in the influx of nitrate evident in wild-type plants (Jacquot et al., 2020). Ser501 phosphorylation is thus capable of inactivating the activity of NRT2.1. Notably, this Ser501 phosphorylation site is highly conserved across plant species, emphasizing the key role that it plays as a regulator of NRT2.1 functionality (Jacquot et al., 2020). This protein has also been shown to harbor N-terminal Ser11 and C-terminal Thr521 phosphorylation sites (Menz et al., 2016), although additional research will be necessary to clarify their functions.

2.2 AtNRT2.4 and AtNRT2.5

AtNRT2.4 is a high-affinity nitrate transporter as demonstrated by its expression in plants and heterologous expression in *Xenopus laevis* oocytes. When *nrt2.1 nrt2.2* double mutant plants exhibiting impaired high-affinity uptake of nitrate were transformed with *NRT2.4* cDNA under the control of the root-specific RolD promoter (Fraisier et al., 2000), *NRT2.4* overexpression was associated with a pronounced increase in $^{15}NO_3^-$ uptake relative to non-transformed *nrt2.1 ntr2.2* double mutant plants under conditions of low nitrate availability (0.2 mM NO_3^-), supporting the ability of *NRT2.4* to regulate the high-affinity uptake of NO_3 (Kiba et al., 2012). To further confirm its ability to function in this regulatory context, Xenopus oocytes were injected for 3 days with *NRT2.4* mRNA or with water as a vehicle control, followed by exposure for 16 h to 0.2 mM $Na^{15}NO_3$. Subsequent analyses of the

accumulation of ^{15}N within oocytes revealed that those oocytes injected with the *NRT2.4* mRNA-injected oocytes took up significantly more NO_3^- than water-injected controls (Kiba et al., 2012).

AtNRT2.4 levels in plant roots were lower than those of *AtNRT2.1* at baseline, but it is strongly upregulated in response to N deprivation. When growing plants on complete N medium for 7 days followed by N starvation for 5 days, wild-type plants exhibited maximal *NRT2.4* expression. Significantly decreased $^{15}NO_3^-$ uptake relative to wild-type was detected in *nrt2.4* null mutants supplied with extremely low concentrations of $^{15}NO_3^-$ (0.025 or 0.01 mM), whereas no differences between the two were apparent when the available concentration of $^{15}NO_3^-$ was higher (0.2, 0.5, or 6 mM). This highlights a role for NRT2.4 as a mediator of very-high-affinity NO_3^- uptake. Much like *NRT2.4*, the transformation of *nrt2.1 ntr2.2* double mutants with *NRT2.5* under the control of the RolD promoter resulted in a pronounced increase in the influx of $^{15}NO_3^-$ in roots as compared to non-transformed double mutants in the presence of 0.2 mM NO_3^- conditions, consistent with the ability of NRT2.5 to serve as a NO_3^- transporter (Lezhneva et al., 2014). In contrast to *nrt2.4* mutants for which no alterations in $^{15}NO_3^-$ influx were evident relative to wild-type plants, *nrt2.5* mutants exhibited significantly reduced high-affinity $^{15}NO_3^-$ influx in the presence of 0.2 mM NO_3^- (Lezhneva et al., 2014). NRT2.5 therefore functions as a high-affinity transporter of nitrate.

2.3 Two-component high-affinity nitrate transporters

Besides transcriptional regulation, posttranscriptional events also can influence NRT2 protein activity and/or abundance, strongly influencing HATS functionality. Early studies demonstrated that the functionality of the *C. reinhardtii* was dependent on two gene products. The genes that encode these two proteins, *CrNRT2* and *CrNAR2*, are present within a single cluster of nitrate-regulated genes, and mutant plants with deletions in this region of the genome exhibit dramatically lower levels of high-affinity nitrate uptake that were only restored by the transformation of these plants with constructs encoding *CrNAR2* and either *CrNRT2.1* or *CrNRT2.2*, whereas none of these constructs alone were sufficient (Quesada et al., 1994). Studies of Xenopus oocytes provided further confirmation of the existence of this two-component high-affinity nitrate transport system, as the injection of mRNAs *CrNAR2* or *CrNRT2.1* alone failed to induce nitrate currents, whereas high levels of nitrate uptake were evident when both were co-injected with one another (Zhou et al., 2000a). Similar findings were also detected in barley such that only the co-injection of Xenopus oocytes with the *HvNRT2.1* and *HvNAR2.3* mRNAs encoding homologous barley proteins was sufficient to enhance nitrate transport (Tong et al., 2005; Ishikawa et al., 2009).

Through subsequent research efforts, researchers determined that *Arabidopsis* also encodes a two-component high-affinity nitrate transport system. Okamoto et al. (2006) searched for genes homologous to the *NAR2* sequences from *C. reinhardtii*, ultimately leading to the identification of the *AtNRT3.1* and *AtNRT3.2* genes (Okamoto et al., 2006; Feng et al., 2011a), the former of which was expressed at much higher levels than the latter. Strong *AtNRT3.1* upregulation was evident when the roots of plants that had been N starved were treated for 3 or 6 h with 1 mM KNO_3, whereas only limited upregulation of *AtNRT3.2* was evident at the 6 h time point (Okamoto et al., 2006). Relative to wild-type plants, *Atnrt3.1* mutants exhibited a significant reduction in root nitrate influx under conditions of low $^{13}NO_3^-$ availability (10 - 150 μM), consistent with a role for this gene product as a regulator of NO_3^- HATS activity. A ~70% reduction in iHATS activity was reported for *Atntr2.1* mutants (Filleur et al., 2001; Li et al., 2007), whereas this reduction was upwards of 95% when *AtNRT3.1* was mutated (Okamoto et al., 2006; Orsel et al., 2006). Oocyte injection experiments in which the *NRT2.1* or *NRT3.1* mRNAs were individually injected or co-injected revealed that significant uptake of $^{15}NO_3^-$ was only apparent following the co-injection of both genes (Orsel et al., 2006). *Arabidopsis* HATS activity is thus dependent on both the *AtNRT2.1* and *AtNRT3.1* genes, in line with the phenotypes observed in *C. reinhardtii* (Quesada et al., 1994; Zhou et al., 2000a). These data suggest that while *NRT3.1* is dispensable for the regulation of *NRT2.1* transcription, it can serve as a facilitator of the transport activity of the NRT2.1 protein, potentially through a mechanism mediated by direct interactions. Additional yeast split-ubiquitin system assays indicated that the NRT2.1 and NRT3.1 proteins are capable of interacting with one another (Orsel et al., 2006), and this interaction localizes to the plasma membrane (Yong et al., 2010). Consistently, an absence of NRT2.1 plasma membrane localization was evident in *nrt3.1* mutants (Wirth et al., 2007). Further confirming this result, Yong et al. conducted western blotting experiments in which they used anti-NRT2.1 to detect a 150-kDa oligomeric polypeptide extracted from the root membrane fraction, and this fraction was further resolved, revealing it to be composed of NRT2.1 (48 kDa) and myc-tagged NRT3.1 (26 kDa). This, coupled with the absence of this 150-kDa complex in *nrt2.1* or *nrt3.1* mutants, suggests that a tetrameric complex composed of two NRT2.1 subunits and two NRT3.1 subunits may be responsible for high-affinity nitrate uptake activity (Yong et al., 2010). With the exception of AtNRT2.7, which was identified as a tonoplast transporter (Chopin et al., 2007a), all NRT2 family members were shown to be capable of engaging in strong interactions with NRT3.1 in bimolecular fluorescence complementation and yeast two-hybrid experiments (Kotur et al., 2012). In Xenopus oocytes, different *NRT2* mRNAs were injected alone or in combination with *NRT3.1* to evaluate the effects on nitrate uptake. These experiments revealed that *NRT3.1* and *NRT2* co-injections were associated with greater $^{15}NO_3^-$ uptake, with this effect being particularly pronounced for *NRT3.1* coinjection with *NRT2.1*/*NRT2.5*, which yielded respective increases in nitrate uptake of 532% and 334%, as compared to only slight increases when co-injected with *NRT2.3*/*NRT2.4* (Kotur et al., 2012). Much like NRT2.1, NRT2.5 was also capable of forming a 150-kDa tetrameric complex with NRT3.1 at the plasma membrane to facilitate the high-affinity uptake of nitrate (Yong et al., 2010; Kotur and Glass, 2015). The existence of two-component NRT2/NAR2 nitrate uptake machinery has also been confirmed in plants including barley (Tong et al., 2005; Ishikawa et al., 2009), rice (Yan

et al., 2011), wheat (Taulemesse et al., 2015), maize (Pii et al., 2016; Liu et al., 2020), and chrysanthemum (Gu et al., 2016). This system is not universal, however, as the *NRT2.1* homolog in *A. nidulans*, *crnA*, did not require any corresponding *NAR2* activity in Xenopus oocytes to facilitate nitrate current generation (Zhou et al., 2000b). These differences may be related to the longer *crnA* central loop and the lack of any homolog of *NAR2* in *A. nidulans* (Yong et al., 2010). Strikingly, all NRT2 proteins other than AtNRT2.1 were capable of mediating small levels of nitrate flux following the injection of the individual encoding mRNA sequences into Xenopus oocytes, with this being most apparent for *NRT2.4* and *NRT2.7* (Chopin et al., 2007a; Kiba et al., 2012; Kotur et al., 2012). Additional research focused on the specific mechanisms whereby NRT2 family proteins mediate high-affinity nitrate transport is thus warranted.

3 N starvation and remobilization

Under conditions of N deficiency, the NO_3^- that is stored in plants can undergo remobilization and phloem-mediated transport (Wang et al., 2012). Marked increases in *NRT2.4* and *NRT2.5* expression are evident in response to N deprivation, with *NRT2.5* being induced at much higher levels than *NART2.4* in shoots and roots. Both of these genes are expressed in shoot vascular tissue in N-starved plants (Kiba et al., 2012; Lezhneva et al., 2014). In experiment in which plants were growth with access to normal N levels for 6 weeks followed by a 4-week period of N starvation, a 45% reduction in leaf phloem exudate NO_3^- concentrations was observed in *nrt2.4* mutants relative to wild-type plants, without any corresponding change in *nrt2.5* mutants, and an even stronger reduction in *nrt2.4 nrt2.5* double mutants such that these exudate levels were just 20% of those observed in wild-type plants. This phenotype was restricted to phloem exudate NO_3^- levels, as none of these mutants exhibited changes in whole leaf NO_3^- concentrations or phloem exudate amino acid content, demonstrating specific roes for *NRT2.4* and *NRT2.5* in the remobilization of nitrate within shoots in response to N starvation (Kiba et al., 2012; Lezhneva et al., 2014).

A summary of the various contributions of different NRT2 family members to specific phases of the processes of nitrate uptake and allocation is presented in Figure 1 and Table 1. In *Arabidopsis*, NRT2.1, NRT2.2, NRT2.4, and NRT2.5 all serve as mediators of high-affinity nitrate uptake, although the functions of the latter two of these proteins are only evident in the context of N starvation. After an extended starvation interval, NRT2.5 expression levels are increased such that it serves as the primary high-affinity uptake transporter protein. *NRT2.1*, *NRT2.4*, and *NRT2.5* also exhibit differences in their spatial expression profiles, with *NRT2.1* expression primarily being evident in older portions of primary roots (Nazoa et al., 2003), whereas *NRT2.4* is most prominently expressed in younger portions of the primary roots and distal areas of lateral roots (Kiba et al., 2012), and *NRT2.5* is expressed in the root hair regions of both primary and lateral roots (Figure 1). Future research is warranted to clarify the degree to which nitrate affinity differs among these transporters, given that higher-affinity transporters may be important to allow plants to better deal with the stress associated with extended N starvation in soil with poor fertility. NRT2.4 and NRT2.5 expression are also evident in the phloem of the major and minor shoot veins, influencing shoot phloem nitrate levels under certain conditions or in the context of specific mutations. NRT2.7 expression is primarily evident during seed development in the tonoplast, wherein it serves to regulate seed nitrate levels.

4 Plant growth and development

4.1 Shoot growth

Members of the NRT2 family are vital to the activity of the NO_3^- HATS (Cerezo et al., 2001; Filleur et al., 2001; Li et al., 2007), and

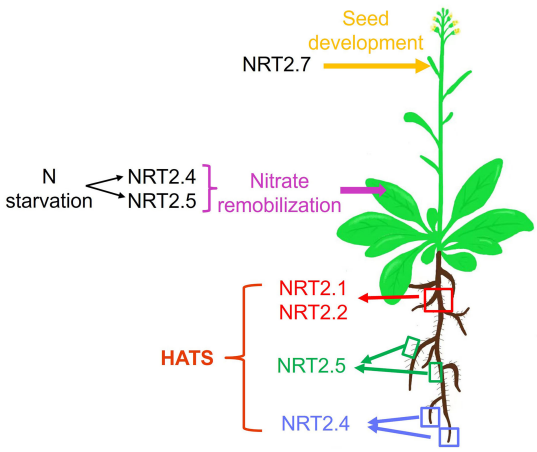

FIGURE 1
The physiological roles played by *Arabidopsis* NRT2 nitrate transporters, from the uptake of soil nitrate to its remobilization among leaves and the function of these transporters during seed development. HATS: high-affinity transport system; red square indicates the older parts of both primary roots and lateral roots; green squares indicate root hair of both primary roots and lateral roots; blue squares indicate the younger parts of both primary roots and lateral roots.

they thereby strongly influence plant growth when cultivating plants in the context of NO_3^-poor solution (Orsel et al., 2004; Li et al., 2007; Kiba et al., 2012; Lezhneva et al., 2014). Indeed, *nrt2.1 nrt2.2* double mutant plants exhibit markedly reduced shoot growth as compared to wild-type plants, with their leaves turning a pink color (Li et al., 2007). The growth of *Arabidopsis* plants for 4 weeks in hydroponic tanks in a 1 mM NH_4NO_3 solution with subsequent nitrogen starvation for 1 week resulted in significantly lower shoot-to-root ratios and shoot weight for *nrt2.1* mutants as compared with wild-type plants, while no corresponding changes were evident for *nrt2.2* single mutants, and even greater reductions in both parameters were evident for *nrt2.1 nrt2.2* double mutants relative to plants in which only *nrt2.1* was mutated (Li et al., 2007). This supports a model wherein both of these genes serve as important regulators of growth, albeit with *NRT2.1* playing the most important role in this context. While no significant differences in *nrt2.4* single mutant plant fresh weight were detected when compared to wild-type controls cultivated in the presence of low (0.05 or 0.5 mM) KNO_3 levels, the triple *nrt2.1 nrt2.2 nrt2.4* mutation was associated with even greater reductions in biomass productivity relative to *nrt2.1 nrt2.2* mutants, particularly at the lower tested KNO_3 level. This may be attributable to the ability of NRT2.4 to mediate the high-affinity transport of nitrate only when its concentrations are very low (Kiba et al., 2012). In a similar vein, *nrt2.5* mutants and wild-type *Arabidopsis* exhibited comparable shoot biomass, while a 10% drop in shoot fresh weight was detected for triple *nrt2.1 nrt2.2 nrt2.5* mutant plants, and this decline was even more marked if *nrt2.4* was also mutated (Lezhneva et al., 2014). Together, these data provide clear evidence for the essential roles that NRT2.1, NRT2.2, NRT2.4, and NRT2.5 play in supporting plant growth when N levels are limited. This is consistent with the fact that the expression of these four genes is largely restricted to the roots, wherein they facilitate root NO_3^- influx (Filleur and Daniel-Vedele, 1999; Orsel et al., 2002; Okamoto et al., 2003; Vidal et al., 2020). Rightfully so, mutation of the partner protein NRT3.1 resulted in the poor shoot growth when plant grown on plates containing 250 mM NO_3^- as the sole nitrogen source (Okamoto et al., 2006). Shoot growth deficiencies in these mutants may thus be attributable to the long-distance effects of NO_3^-, indicative of the shifts in whole-plant N distributions.

4.2 Root system architecture

In order to contend with shifting soil N source availability under changing environmental conditions, plants have evolved a range of adaptive strategies that include root system architecture plasticity (Robinson, 1994; Zhang and Forde, 2000). Both nitrate and sugar can induce the expression of *NRT2.1* (Lejay et al., 1999; Cerezo et al., 2001). Relative to the use of standard growth medium, cultivating seedlings on media with a high C/N ratio results in the significant repression of lateral root initiation compared to a standard growth medium (Malamy and Ryan, 2001), whereas this repression was not evident in *nrt2.1* mutant plants (Little et al., 2005), supporting a role for *NRT2.1* in this repressive mechanism. Under nitrate-free conditions, such repression of lateral root initiation was still evident, simulating defective transport activity and thus revealing that this impairment of lateral root initiation was not nitrogen uptake-dependent (Remans et al., 2006b). NRT2.1 may thus serve as a sensor or signal transducer for nitrate involved in a signaling pathway that ultimately represses lateral root initiation. Relative to wild-type plants, those harboring *nrt2.1* mutations also presented with lower levels of lateral root growth following transfer from nitrate-rich to nitrate-poor medium (10 to 0.5 mM) (Remans et al., 2006b; Li et al., 2007), with this reduction being even more pronounced in *nrt2.1 nrt2.2* double mutants consistent with both of these genes serving as important factors involved in the regulation of lateral root growth (Li et al., 2007). NRT2.1 thus appears to help coordinate the development of lateral roots when NO_3^- availability is limited.

Nitrate treatment can reportedly enhance the initiation and emergence of lateral roots (Vidal et al., 2010, 2013), with both of these processes being impaired for *nrt2.1 nrt2.2* mutant plants relative to wild-type controls cultivated in the presence of 1 mM ammonium for 2 weeks in a hydroponic system followed by a 3-day treatment with 5 mM KNO_3. Strikingly, *tga1 tga4* and *nrt2.1 nrt2.2* plants presented with similar lateral root initiation phenotypes (Alvarez et al., 2014). In subsequent analyses, the TGA1/TGA4 transcription factors were identified as direct regulators of *NRT2.1*/*NRT2.2* (Alvarez et al., 2014), supporting their ability to regulate the development of lateral roots at least in part through the control of *NRT2.1* and *NRT2.2* expression.

A recent forward genetic screening effort additionally established NRT2.1 as a key regulator of primary root elongation under limited NO_3^- stress conditions, as evidenced by the significant increase in primary root length for *nrt2.1* mutant seedlings cultivated in the presence of 0.05 mM NO_3^- relative to wild-type controls. The root tips of these *nrt2.1* seedlings also exhibited higher levels of the key root growth regulator auxin as compared to wild-type root tips in the presence of low nitrate concentrations. However, *nrt2.1 pin7* double mutants exhibited root tips comparable to those of wild-type plants and shorter than those of *nrt2.1* plants, consistent with the ability of PIN7, which is an auxin efflux carrier, to function downstream of NRT2.1 as a regulator of the growth of roots in the presence of limited NO_3^- availability. A series of assays confirmed the ability of PIN7 and NRT2.1 to physically interact with one another when NO_3^- levels are low, thereby suppressing the PIN7-mediated acropetal efflux of auxin, thus slowing the elongation of primary roots. Together these results support a model in which NRT2.1 is capable of influencing root growth activity through interactions with the PIN7-mediated auxin transport machinery when levels of available NO_3^- are low (Wang et al., 2023).

4.3 Seed development and germination

There are three primary stages to the process of *Arabidopsis* seed development. After initial morphogenesis, a maturation phase occurs that entails the production of N and C storage compounds in the form of seed storage proteins (Heath et al., 1986; Baud et al., 2002). NPF2.12/NRT1.6 localizes to the plasma membrane and is

vital for early embryonic development (Almagro et al., 2008), with mutations in this gene reducing rates of nitrate accumulation within mature seeds while enhancing seed abortion rates. *NPF2.12* expression was only detectable in funiculus and silique vascular tissues, with upregulation immediately following pollination. This suggests a role for *NPF2.12* in the delivery of nitrate from maternal tissues to nascent embryos (Almagro et al., 2008). In contrast, NRT2.7 is primarily active within mature seeds. The homology of NRT2.7 is markedly lower relative to other NRT2 family members, sharing just 55% similarity with NRT2.1, for example (Orsel et al., 2002; Chopin et al., 2007a). Unlike most other members of this gene family, it is also primarily expressed in developing seeds rather than in roots, with its upregulation being particularly pronounced as seeds undergo dessication (Orsel et al., 2002; Okamoto et al., 2003; Chopin et al., 2007a). While oocyte-based experiments have confirmed that NRT2.7 can function as a nitrate transporter, it has no role in the direct uptake of soil nitrate via the roots, nor does it impact the distribution of nitrate in plant vegetative organs (Chopin et al., 2007a). Subcellular localization analyses have demonstrated that NRT2.7 primarily localizes to the tonoplast surrounding the vacuoles. Studies of the effects of *nrt2.7* mutations on seeds have been conducted with the mutant *nrt2.7-1* (Col-8 background) and *nrt2.7-2* (Ws background) plant lines. Both exhibit similar seed weights to those of wild-type plants, but reduced seed nitrate levels under nonlimiting N conditions. Nitrate has also been posited to serve as a signal that can trigger seeds to break dormancy and begin germination (Alboresi et al., 2005; Chopin et al., 2007a). In line with such a model, when the same batches of freshly harvested seeds were sown on water-containing medium, both *nrt2.7* mutants exhibited germination delays relative to wild-type controls within 2 days. While *nrt2.7-2* mutants exhibited lower rates of germination throughout a 7-day analytical period relative to the control Ws line, no apparent difference in germination was evident between the Col-8 and *nrt2.7-1* mutant lines from days 3-7 post-sowing (Chopin et al., 2007a). Col seeds and foliar tissues exhibited higher nitrate storage capabilities relative to those of Ws plants, suggesting that Col plants are better able to tolerate N deprivation (Chopin et al., 2007a; North et al., 2009). Differences in such tolerance among plant ecotypes may thus account for varying seed germination phenotypes. Overall, these data highlight a key role for NRT2.7 in seed nitrate concentration and germination.

David et al. performed further characterization of *nrt2.7-2* mutants exhibiting a distinctive phenotype consisting of a seed coat that was a plane-brown color in contrast to that of wild-type Ws (David et al., 2014). Seed coloration is generally related to flavonoid oxidation levels (Pourcel et al., 2005; Lepiniec et al., 2006; Routaboul et al., 2012), and additional analysis indicated that these *nrt2.7-2* mutant seeds accumulated higher levels of soluble proanthocyanidins (PAs) that could undergo oxidation in the testa with seed dessication (David et al., 2014). This seed PA accumulation was apparently unrelated to fluctuations in seed NO_3^- content, in line with the observation that *npf2.12* and *clca* mutant seeds did not exhibit any change in color or PA content despite the reduction in NO_3^- levels therein (Almagro et al., 2008; Monachello et al., 2009). These data support a specific link between the accumulation of PA in seeds and the function of NRT2.7, rather than linking it to NO_3^- accumulation. Lower NO_3^- levels and higher concentrations of soluble PAs were also apparent in *nrt2.7-2* mutant seeds relative to Ws, resembling *tt10* mutant phenotypes (David et al., 2014). The TRANSPARENT TESTA 10 (TT10) protein serves as a laccase candidate enzyme that facilitates the oxidative polymerization of PAs and other flavonoids (Pourcel et al., 2005). No studies to date, however, have revealed any ability of NRT2.7 to influence the enzymatic activity of TT10, and additional research aimed at clarifying the activity of TT10 will be vital to understanding the mechanisms that ultimately result in the higher levels of soluble Pas within *nrt2.7-2* seeds. These findings thus reveal a central role for NRT2.7 as a regulator of the accumulation and oxidation of PAs within seeds. While NRT1 family proteins have been shown to serve as transporters for non-nitrate molecules (Léran et al., 2014), whether NRT2 proteins can function in a similar manner remains poorly understood, and additional research will be vital to test this hypothesis.

5 *AtNRT2.1, AtNRT2.5*, and *AtNRT2.6* are influence plant-microbe interactions

Plant nutritional status can strongly shape the ability of these plants to defend against pathogens such as *Pseudomonas syringae* (Long et al., 2000; Modolo et al., 2005, 2006). Relative to wild-type controls, *nrt2.1* and *nrt2.1 nrt2.2* mutant plants exhibit a reduction in susceptibility to *P. syringae pv tomato DC3000* (*Pst*) (Camañes et al., 2012). Under infection conditions, *nrt2.1* exhibited more robust and more rapid SA-dependent defense priming, which was a key mechanism responsible for enhanced *Pst* resistance (Zimmerli et al., 2000; Conrath et al., 2006; Jung et al., 2009). These *nrt2.1* mutants were also partially deficient in their ability to detect coronatine, a bacterial effector important in the context of infection (Brooks et al., 2004; Melotto et al., 2008; Camañes et al., 2012). These decreases in *nrt2.1* susceptibility to *Pst* may thus stem from both coronatine insensitivity and improved SA priming. The inoculation of plants with the phytopathogen *Erwinia amylovora* also resulted in an increase in the expression of *NRT2.6*, with plants expressing lower *NRT2.6* levels exhibiting greater pathogen susceptibility as a consequence of impaired reactive oxygen species production, although these *nrt2.6* mutants did not exhibit any apparent nitrate-associated phenotypes (Dechorgnat et al., 2012). Together, these data suggest that members of the NRT2 family can serve as sensors for a range of environmental stimuli, thereby coordinating abiotic and biotic stress responses in addition to shaping the ability of plants to respond to nutritional cues.

The plant growth-promoting rhizobacterium (PGPR) strain *Phyllobacterium brassicacearum* STM196 has been reported to promote the growth of *Arabidopsis* and to overcome lateral root developmental inhibition under conditions of high nitrate availability (Mantelin et al., 2006). Notable increases in *NRT2.5* and *NRT2.6* expression have been observed in plants exposed to STM196, but *nrt2.5* and *nrt2.6* mutants failed to exhibit such

STM196-induced growth (Kechid et al., 2013), indicating that these two genes encode proteins that can influence the outcomes of beneficial biotic interactions.

6 Biological processes by *AtNRT2.1*

6.1 AtNRT2.1 controls cadmium uptake

Supplying plants with NO_3^- has been shown to result in higher concentrations of Cd and more pronounced Cd toxicity in exposed plants (Mao et al., 2014; Yang et al., 2015; Cheng et al., 2020). Moreover, nitrate transporters NPF6.3/NRT1.1, NPF7.3/NRT1.5, and NPF7.2/NRT1.8 are responsive to Cd stress conditions in *Arabidopsis*, regulating the accumulation of Cd under conditions of both high and normal NO_3^- availability (Li et al., 2010; Chen et al., 2012; Mao et al., 2014; Wang et al., 2018). Further studies have indicated that Cd can suppress the expression of key HATS-related genes including *NRT2.1*, *NRT2.2*, and *NRT2.4*, thereby suppressing the uptake and accumulation of nitrate in roots when nitrate levels are low, which results in a corresponding reduction in root Cd uptake (Guan et al., 2021). This suggests that efforts to control nitrate transporter activity may provide a means of abrogating Cd accumulation when growing crops in soil contaminated with this heavy metal.

6.2 AtNRT2.1 influences light-responsive carbon and nitrogen metabolism

As reported previously, root transport systems are generally regulated by shoot photosynthetic activity, especially in the context of the uptake of NO_3^- (Delhon et al., 1995; Forde, 2002). NO_3^- uptake is under the control of downwardly transported sugars, CO_2, carboxylic acids, and other photosynthates (Delhon et al., 1996). Root *NRT2.1* expression has been demonstrated to be both sugar- and light-inducible (Lejay et al., 1999). However, sugar analog treatment or analyses of sugar-sensing mutant plants revealed no changes in sugar-induced *NRT2.1* induction, suggesting that this process occurs through a mechanism distinct from the primary mechanisms that have been documented to facilitate plant sugar sensing (Lejay et al., 2003). Mutants lacking the expression of hexokinase (HXK), in contrast, exhibited an absence of sugar-induced *NRT2.1* expression, consistent with the metabolic activity downstream of HXK being key to this regulatory process, rather than sugar itself (Lejay et al., 2003). *HXK* catalyzes a reaction that produces glucose-6-P (G6P), and treating roots with glycerol to reduce G6P concentrations can strongly impair normal *NRT2.1* upregulation following the dark/light transition (Lejay et al., 2008). However, the treatment of plants with 6-aminonicotinamide (6-AN), which can potently inhibit phosphor-gluconate dehydrogenase activity and impair OPPP, the near total absence of sugar-induced *NRT2.1* expression was evident despite no corresponding change in G6P levels relative to sucrose treatment. This suggests that *NRT2.1* upregulation in response to C signals is associated with OPPP activity rather than being directly induced by G6P (Lejay et al., 2008). Relative to wild-type plants, *gin2-1* mutant plants with defective sugar responses exhibited impaired *NRT2.1* upregulation in response to Glc, while treatment with the OPPP intermediates shikimate and pyruvate was sufficient to restore this defect (de Jong et al., 2014). Sugar-induced *NRT2.1* expression is thus dependent on the OPPP pathway.

C and N acquisition rates are regulated in a tightly coupled manner (Matt et al., 2010; Nunes-Nesi et al., 2010), and light serves an important regulatory role for both of these processes (Lillo, 2008). Wild-type *Arabidopsis* seedlings with shoots and roots respectively exposed to light and dark conditions [S(L)/R(D)] exhibited significant increases in both primary root length and NO_3^- uptake as compared to wild-type seedlings placed under the opposite conditions [S(D)/R(L)], supporting a model wherein light-induced shoot-to-root signaling activity can favor nitrate uptake and the growth of roots (Chen X. et al., 2016). Strikingly, mutations in the *HY5* gene encoding a photomorphogenic bZIP transcription factor were capable of eliminating this nitrate uptake and root growth induced by shoot illumination, and further hypocotyl graft chimera-based studies codified HY5 as a shoot-root phloem-mobile signal (Chen X. et al., 2016). The *nrt2.1* mutant plants also exhibited reduced levels of NO_3^- uptake in response to shoot illumination, with HY5 derived from shoot tissue promoting the autoactivation of HY5 in the roots, thereby promoting NO_3^- uptake in the roots via *NRT2.1* activation (Chen X. et al., 2016). *NRT2.1* promoter binding by HY5 can be enhanced when sucrose availability, with HY5 regulating its fixation and translocation (Chen X. et al., 2016). Mobile HY5 thus serves as an important regulator of *NRT2.1* in the context of illumination-responsive N and C metabolism.

6.3 AtNRT2.1 involves in systemic nitrate signaling mechanisms

Soil nitrate distributions are generally heterogeneous. To adapt to this inconsistent availability, plants have evolved intricate systemic responses whereby stimuli that are perceived at the local level can be communicated to distant organs. For example, in plants grown in split-root plates for which half of their root system was nitrate-deprived while the other half was in a nitrate-rich environment, more pronounced proliferation of roots on the nitrate-rich side was evident relative to plants cultivated under homogenously nitrate-rich conditions, with this response being dependent on shoot nitrate accumulation (Remans et al., 2006a; Ruffel et al., 2011; Vidal et al., 2020). The transcription factor gene *TEOSINTE BRANCHED1/CYCLOIDEA/PROLIFERATING CELL FACTOR1-20 (TCP20)* mutations in these split-root experiments were sufficient to impair the preferential growth of lateral roots on the nitrate-rich site (Guan et al., 2014). Additional analyses demonstrated the ability of TCP20 to interact directly with HOMOLOG OF BRASSINOSTEROID ENHANCED EXPRESSION2 INTERACTING WITH IBH1 (HBI1), a bHLH transcription factor, with nitrate starvation enhancing this interaction. The resultant HBI1-TCP20 complex was then capable of directly binding the C-terminally encoded peptide (CEP) promoters, inducing their expression in a cooperative fashion

(Chu et al., 2021). The resultant CEPs were secreted from roots and functioned as ascending signals of N starvation that were detected by the LRR-RK receptor (CEPR) in shoots, thereby triggering shoot-derived descending CEPD1 (CEP downstream 1) and CEPD2 peptide production. These peptides, in turn, triggered the upregulation of *NRT2.1*, *NRT3.1*, and other nitrate-related genes in the roots, thereby inducing higher levels of nitrate uptake and root proliferation in areas rich in nitrates (Tabata et al., 2014; Ohkubo et al., 2017). The CEPD-like 2 (CEPDL2) peptide was also induced by low nitrate concentrations and shoot N deprivation in a CEPR-independent fashion, whereupon it functions as a leaf-derived systemic signal that controls the root-mediated uptake of nitrate by regulating the expression of key genes including *NRT2.1*, *NRT3.1*, and *NRT2.4* (Ota et al., 2020). The RNAPII complex component IWS1 is also capable of suppressing the expression of *NRT2.1* under high levels of nitrate availability by enhancing the H3K27me3 of the chromatin region encoding this gene (Girin et al., 2010; Widiez et al., 2011). A range of post-translational mechanisms also shape the activity of NRT2.1 in response to systemic N-related signaling activity. For example, the CEPD1/2- and CEPDL2-mediated signals are capable of promoting the upregulation of CEPH, a root-specific PP2C phosphatase that can dephosphorylate NRT2.1 Ser501 to activate the high-affinity uptake of nitrate in *Arabidopsis* (Ohkubo et al., 2021). At the systemic level, both transcriptional and post-translational switches govern the activity of NRT2.1 to maintain N homeostasis, particularly under conditions of limited soil N availability and/or increased shoot N demands (Figure 2).

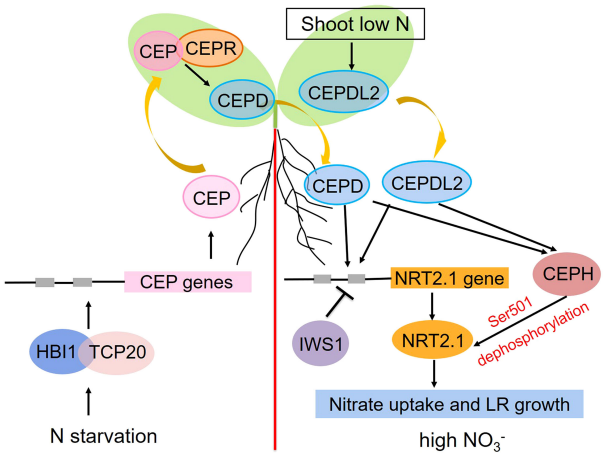

FIGURE 2
Schematic overview of the roles that *AtNRT2.1* plays in the systemic nitrate signaling pathway under heterogeneous conditions. Positive and negative regulation are respectively represented with arrows and blunted lines.

7 Conclusions

Since the first identification of *crnA* as the founding member of the *NRT2* gene family, countless studies have sought to clarify the characteristics and functions of different NRT2 proteins in specific plant species. This review offers an overview of the spatiotemporal expression patterns, localization, biotic and abiotic responses, and functional roles of the seven *AtNRT2* genes (Table 1). While some progress has been made on this front to date, much remains to be done. For example, how *AtNRT2.3* and *AtNRT2.6* contribute to nitrate-related regulatory processes remains uncertain, and it remains uncertain as to whether NRT2 proteins can serve as transporters for molecules other than nitrate. Similarly, the status of NRT2.1 as a potential nitrate sensor warrants further investigation. As such, additional studies will be vital to fully clarify how plants are able to sense and respond to changing environmental conditions in order to provide a sound basis for crop-focused research.

Arabidopsis-based findings can be extended to other economically important plant species, highlighting valuable targets for efforts to enhance crop yields in harsh or otherwise unfavorable environments. In recent years, significant progress has been made in the research of *NRT2* genes in crops. In rice, overexpression of *OsNRT2.1* increased the transcription level of auxin transporter genes *OsPIN1a/b/c* and *OsPIN2* and which in turn promoted total root length under 0.5 mM NO_3^- conditions (Naz et al., 2019). Knockout of *OsNRT2.4* inhibited lateral root length and number under 0.25 Mm and 2.5 mM NO_3^- conditions (Wei et al., 2018). In addition, knockdown of *OsNAR2.1* suppressed lateral root formation under low NO_3^- conditions (Song et al., 2020). These results suggest that *OsNRT2.1/NRT2.4/NAR2.1* play a critical role in controlling root development. Moreover, transgenic lines overexpressing *OsNRT2.1/2.2* could improve nitrogen use efficiency (NUE) and grain yield in rice (Chen J. et al., 2016; Hu et al., 2023). Transgenic lines co-overexpressing *OsNAR2.1* and *OsNRT2.3a* increased agronomic nitrogen use efficiency (Chen et al., 2020). Meanwhile, Fan's group reported that overexpression of *OsNRT2.3b* could also enhance NUE and rice grain yield in the field (Fan et al., 2016). In wheat, transcription factor TaNAC2-5A could directly bind to the promoters of *TaNRT2.1-6B*, *TaNRT2.5-3B*, *TaNPF7.1-6D*, and *TaGS2-2A* and activate their expression to affect NO_3^- transport and assimilation, and ultimately increased grain yield and NUE (Li et al., 2020; Gao et al., 2022). Furthermore, new information have been obtained about unexpected peculiar roles played by some *NRT2* genes. The NRT2 transporter family has at least 4 members in *Lotus japonicus* (Criscuolo et al., 2012), 5 in *Oryza sativa* (Feng et al., 2011b) and 49 in the *Wheat* genome (Deng et al., 2023). In *Lotus japonicus*, high NO_3^- treatment attenuated nodulation, but the effect of nitrate was suppressed by the *LjNRT2.1* mutation (Misawa et al., 2022). Of note, the nodulation phenotypes of the *Ljnlp1* and the *Ljnlp4* mutants are similar to those of the *Ljnrt2.1* mutants under high NO_3^- conditions (Nishida et al., 2021). Further investigation suggested that NODULE INCEPTION (NIN)-LIKE PROTEIN1 (*LjNLP1*) could directly bind to the *LjNRT2.1* promoter and activate its transcript and subsequently promote nitrate uptake/transport process, which ultimately affected nuclear localization of LjNLP4 and subsequent regulation of the expression of nodulation-related genes (Misawa et al., 2022). Phylogenic analysis revealed *LjNRT2.4* to be a close relative of *AtNRT2.7* which was the most diverged of all the NRT2 sequence (Valkov et al., 2020). Unlike *AtNRT2.7* which expressed

mainly in seeds and the protein localized to vacuolar membrane (Chopin et al., 2007a), *LjNRT2.4* was expressed in root and nitrogen-fixing nodule vascular tissues and localized at the plasma membrane. Mutation of *LjNRT2.4* caused much more severe N_2-fixation related phenotypes in nodulated plants grown under hydroponic conditions (Valkov et al., 2020). In rice, all OsNRT2 members except OsNRT2.4 which shares the highest value of amino acid identity with AtNRT2.7 need OsNAR2.1 for root NO_3^- acquisition in response to both low- and high- nitrate supply (Wei et al., 2018). Interestingly, unlike other NRT2s which function as the high-affinity NO_3^- transporter, OsNRT2.4 is a dual-affinity NO_3^- transporter (Wei et al., 2018). These findings are just the tip of the iceberg, more endeavors are needed to decipher the mechanism of NRT2 family, improve NUE in crops, eliminate the pollution from N as field fertilizer, and maintain nutrient homeostasis.

Author contributions

NX: Writing – original draft. LC: Writing – original draft. YK: Writing – original draft. GC: Writing – review & editing. LZ: Writing – review & editing. FL: Writing – review & editing.

Funding

The author(s) declare financial support was received for the research, authorship, and/or publication of this article. This research was funded by the National Natural Science Foundation of China (No. 32000194), the Shandong Provincial University Youth Innovation Team, China (No. 2022KJ102), the Shandong Provincial Natural Science Foundation (No. ZR201702210017), the Open Project Program of State Key Laboratory of Crop Biology (No. 2021KF04), the Education Science Planning Project for the Subject of Innovation Capability of Shandong Province (No. 2022CYB210).

Acknowledgments

The authors acknowledge the support of many fundings.

Conflict of interest

The authors declare that the research was conducted in the absence of any commercial or financial relationships that could be construed as a potential conflict of interest.

Publisher's note

References

Alboresi, A., Gestin, C., Leydecker, M. T., Bedu, M., Meyer, C., and Truong, H. N. (2005). Nitrate, a signal relieving seed dormancy in *Arabidopsis*. *Plant Cell Environ.* 28, 500–512. doi: 10.1111/j.1365-3040.2005.01292.x

Almagro, A., Lin, S. H., and Tsay, Y. F. (2008). Characterization of the *Arabidopsis* nitrate transporter NRT1.6 reveals a role of nitrate in early embryo development. *Plant Cell* 20, 3289–3299. doi: 10.1105/tpc.107.056788

Alvarez, J. M., Riveras, E., Vidal, E. A., Gras, D. E., Contreras-López, O., Tamayo, K. P., et al. (2014). Systems approach identifies TGA1 and TGA4 transcription factors as important regulatory components of the nitrate response of *Arabidopsis thaliana* roots. *Plant J.* 80, 1–13. doi: 10.1111/tpj.12618

Baud, S., Boutin, J. P., Miquel, M., Lepiniec, L. C., and Rochat, C. (2002). An integrated overview of seed development in *Arabidopsis thaliana* ecotype WS. *Plant Physiol. Biochem.* 40, 151–160. doi: 10.1016/S0981-9428(01)01350-X

Brooks, D. M., Hernández-Guzmán, G., Kloek, A. P., Alarcón-Chaidez, F., Sreedharan, A., Rangaswamy, V., et al. (2004). Identification and characterization of a well-defined series of coronatine biosynthetic mutants of *Pseudomonas syringae* pv. *tomato* DC3000. *Mol. Plant Microbe Interact.* 17, 162–174. doi: 10.1094/MPMI.2004.17.2.162

Brownlee, A. G., and Arst, H. N. (1983). Nitrate uptake in Aspergillus nidulans and involvement of the third gene of the nitrate assimilation gene cluster. *J. Bacteriol.* 155, 1138–1146. doi: 10.1128/jb.155.3.1138-1146.1983

Camañes, G., Pastor, V., Cerezo, M., García-Andrade, J., Vicedo, B., García-Agustín, P., et al. (2012). A deletion in *NRT2.1* attenuates *Pseudomonas syringae*-induced hormonal perturbation, resulting in primed plant defenses. *Plant Physiol.* 158, 1054–1066. doi: 10.1104/pp.111.184424

Cerezo, M., Tillard, P., Filleur, S., Munos, S., Daniel-Vedele, F., and Gojon, A. (2001). Major alterations of the regulation of root NO_3- uptake are associated with the mutation of *Nrt2.1* and *Nrt2.2* genes in *Arabidopsis*. *Plant Physiol.* 127, 262–271. doi: 10.1104/pp.127.1.262

Chen, J., Liu, X., Liu, S., Fan, X., Zhao, L., Song, M., et al. (2020). Co-overexpression of OsNAR2.1 and OsNRT2.3a increased agronomic nitrogen use efficiency in transgenic rice plants. *Front. Plant Sci.* 11. doi: 10.3389/fpls.2020.01245

Chen, C. Z., Lv, X. F., Li, J. Y., Yi, H. Y., and Gong, J. M. (2012). *Arabidopsis* NRT1.5 is another essential component in the regulation of nitrate reallocation and stress tolerance. *Plant Physiol.* 159, 1582–1590. doi: 10.1104/pp.112.199257

Chen, J., Yong, Z., Tan, Y., Min, Z., and Fan, X. (2016). Agronomic nitrogen-use efficiency of rice can be increased by driving OsNRT2.1 expression with the OsNAR2.1 promoter. *Plant Biotechnol. J.* 14, 1705–1715. doi: 10.1111/pbi.12531

Chen, X., Yao, Q., Gao, X., Jiang, C., Harberd, N. P., and Fu, X. (2016). Shoot-to-root mobile transcription factor HY5 coordinates plant carbon and nitrogen acquisition. *Curr. Biol.* 26, 640–646. doi: 10.1016/j.cub.2015.12.066

Cheng, Y., Bao, Y., Chen, X., Yao, Q., Wang, C., Chai, S., et al. (2020). Different nitrogen forms differentially affect Cd uptake and accumulation in dwarf Polish wheat (*Triticum polonicum* L.) seedlings. *J. Hazard. Mater.* 400, 123209. doi: 10.1016/j.jhazmat.2020.123209

Chopin, F., Orsel, M., Dorbe, M. F., Chardon, F., Truong, H. N., Miller, A. J., et al. (2007a). The *Arabidopsis* ATNRT2.7 nitrate transporter controls nitrate content in seeds. *Plant Cell* 19, 1590–1602. doi: 10.1105/tpc.107.050542

Chopin, F., Wirth, J., Dorbe, M. F., Lejay, L., Krapp, A., Gojon, A., et al. (2007b). The *Arabidopsis* nitrate transporter AtNRT2.1 is targeted to the root plasma membrane. *Plant Physiol. Biochem.* 45, 630–635. doi: 10.1016/j.plaphy.2007.04.007

Chu, X., Li, M., Zhang, S., Fan, M., Han, C., Xiang, F., et al. (2021). HBI1-TCP20 interaction positively regulates the CEPs-mediated systemic nitrate acquisition. *J. Integr. Plant Biol.* 63, 902–912. doi: 10.1111/jipb.13035

Conrath, U., Beckers, G. J., Flors, V., García-Agustín, P., Jakab, G., Mauch, F., et al. (2006). Priming: Getting ready for battle. *Mol. Plant Microbe Interact.* 19, 1062–1071. doi: 10.1094/MPMI-19-1062

Crawford, N. M., and Forde, B. G. (2002). Molecular and developmental biology of inorganic nitrogen nutrition. *Arabidopsis Book* 1, e0011. doi: 10.1199/tab.0011

Crawford, N. M., and Glass, A. D. M. (1998). Molecular and physiological aspects of nitrate uptake in plants. *Trends Plant Sci.* 3, 389–395. doi: 10.1016/S1360-1385(98)01311-9

Criscuolo, G., Valkov, V. T., Parlati, A., Alves, L. M., and Chiurazzi, M. (2012). Molecular characterization of the *Lotus japonicus* NRT1(PTR) and NRT2 families. *Plant Cell Environ.* 35, 1567–1581. doi: 10.1111/j.1365-3040.2012.02510.x

David, L. C., Dechorgnat, J., Berquin, P., Routaboul, J. M., Debeaujon, I., Daniel-Vedele, F., et al. (2014). Proanthocyanidin oxidation of *Arabidopsis* seeds is altered in mutant of the high-affinity nitrate transporter NRT2.7. *J. Exp. Bot.* 65, 885–893. doi: 10.1093/jxb/ert481

Dechorgnat, J., Patrit, O., Krapp, A., Fagard, M., and Daniel-Vedele, F. (2012). Characterization of the Nrt2.6 gene in *Arabidopsis* thaliana: A link with plant response to biotic and abiotic stress. *PloS One* 7, e42491. doi: 10.1371/journal.pone.0042491

de Jong, F., Thodey, K., Lejay, L. V., and Bevan, M. W. (2014). Glucose elevates NITRATE TRANSPORTER2.1 protein levels and nitrate transport activity independently of its HEXOKINASE1-mediated stimulation of NITRATE TRANSPORTER2.1 expression. *Plant Physiol.* 164, 308–320. doi: 10.1104/pp.113.230599

Delhon, P., Gojon, A., Tilard, P., and Passama, L. (1995). Diurnal regulation of NO_3^- uptake in soybean plants I. Changes in NO_3^- influx, efflux, and N utilization in the plant during the day/night cycle. *J. Exp. Bot.* 46, 1585–1594. doi: 10.1093/jxb/46.10.1585

Delhon, P., Gojon, A., Tilard, P., and Passama, L. (1996). Diurnal regulation of NO_3^- uptake in soybean plants. III. Implication of the Dijkshoorn-Ben Zioni model in relation with the diurnal changes in NO_3^- assimilation. *J. Exp. Bot.* 47, 885–892. doi: 10.1093/jxb/47.7.885

Deng, Q. Y., Luo, J. T., Zheng., J. M., Tan, W. F., Pu, Z. J., and Wang, F. (2023). Genome-wide systematic characterization of the *NRT2* gene family and its expression profile in wheat (*Triticum aestivum L.*) during plant growth and in response to nitrate deficiency. *BMC. Plant Biol.* 23, 353. doi: 10.1186/s12870-023-04333-5

Engelsberger, W. R., and Schulze, W. X. (2012). Nitrate and ammonium lead to distinct global dynamic phosphorylation patterns when resupplied to nitrogen-starved *Arabidopsis* seedlings. *Plant J.* 69, 978–995. doi: 10.1111/j.1365-313X.2011.04848.x

Fan, X., Tang, Z., Tan, Y., Zhang, Y., Luo, B., Yang, M., et al. (2016). Overexpression of a pH-sensitive nitrate transporter in rice increases crop yields. *Proc. Natl. Acad. Sci. U. S. A.* 114, 7118–7123. doi: 10.1073/pnas.1525184113

Feng, H., Fan, X., Fan, X., Liu, X., Miller, A. J., and Xu, G. (2011a). Multiple roles of nitrate transport accessory protein NAR2 in plants. *Plant Signal. Behav.* 6, 1286–1289. doi: 10.4161/psb.6.9.16377

Feng, H., Yan, M., Fan, X., Li, B., Shen, Q., Miller, A. J., et al. (2011b). Spatial expression and regulation of rice high-affinity nitrate transporters bynitrogen and carbon status. *J. Exp. Bot.* 62, 2319–2332. doi: 10.1093/jxb/erq403

Filleur, S., and Daniel-Vedele, F. (1999). Expression analysis of a high-affinity nitrate transporter isolated from *Arabidopsis* thaliana by differential display. *Planta* 207, 461–469. doi: 10.1007/s004250050505

Filleur, S., Dorbe, M. F., Cerezo, M., Orsel, M., Granier, F., Gojon, A., et al. (2001). An *arabidopsis* T-DNA mutant affected in Nrt2 genes is impaired in nitrate uptake. *FEBS Lett.* 489, 220–224. doi: 10.1016/S0014-5793(01)02096-8

Forde, B. G. (2000). Nitrate transporters in plants: Structure, function and regulation. *Biochim. Biophys. Acta* 1465, 219–235. doi: 10.1016/S0005-2736(00)00140-1

Forde, B. G. (2002). Local and long-range signaling pathways regulating plant responses to nitrate. *Annu. Rev. Plant Biol.* 53, 203–224. doi: 10.1146/annurev.arplant.53.100301.135256

Forde, B. G., and Clarkson, D. T. (1999). Nitrate and ammonium nutrition of plants: Physiological and molecular perspectives. *Adv. Bot. Res.* 30, 1–90. doi: 10.1016/S0065-2296(08)60226-8

Fraisier, V., Gojon, A., Tillard, P., and Daniel-Vedele, F. (2000). Constitutive expression of a putative high-affinity nitrate transporter in Nicotiana plumbaginifolia: Evidence for post-transcriptional regulation by a reduced nitrogen source. *Plant J.* 23, 489–496. doi: 10.1046/j.1365-313x.2000.00813.x

Galván, A., Quesada, A., and Fernández, E. (1996). Nitrate and nitrate are transported by different specific transport systems and by a bispecific transporter in *Chlamydomonas reinhardtii*. *J. Biol. Chem.* 271, 2088–2092. doi: 10.1074/jbc.271.4.2088

Gao, Y., Qi, S., and Wang, Y. (2022). Nitrate signaling and use efficiency in crops. *Plant Commun.* 3, 100353. doi: 10.1016/j.xplc.2022.100353

Girin, T., El-Kafafi, E. S., Widiez, T., Erban, A., Hubberten, H. M., Kopka, J., et al. (2010). Identification of *Arabidopsis* mutants impaired in the systemic regulation of root nitrate uptake by the nitrogen status of the plant. *Plant Physiol.* 153, 1250–1260. doi: 10.1104/pp.110.157354

Glass, A. D. M., Brito, D. T., Kaiser, B. N., Kronzucker, H. J., Kumar, A., Okamoto, M., et al. (2001). Nitrogen transport in plants, with an emphasis on the regulation of fluxes to match plant demand. *J. Plant Nutr. Soil Sci.* 164, 199–207. doi: 10.1002/1522-2624(200104)164:2<199::AID-JPLN199>3.0.CO;2-K

Glass, A. D. M., and Siddiqi, M. Y. (1995). "Nitrogen absorption by plant roots," in *Nitrogen Nutrition in Higher Plants*. Ed. H. S. Srivastava and R. P. Singh (New Delhi, India: Associated Publishing Co.), pp. 21–56.

Gu, C., Song, A., Zhang, X., Wang, H., Li, T., Chen, Y., et al. (2016). Cloning of chrysanthemum high-affinity nitrate transporter family (CmNRT2) and characterization of CmNRT2.1. *Sci. Rep.* 6, 23462. doi: 10.1038/srep23462

Guan, M., Chen, M., and Cao, Z. (2021). NRT2.1, a major contributor to cadmium uptake controlled by high-affinity nitrate transporters. *Ecotoxicol. Environ. Saf.* 218, 112269. doi: 10.1016/j.ecoenv.2021.112269

Guan, P., Wang, R., Nacry, P., Breton, G., Kay, S. A., Pruneda-Paz, J. L., et al. (2014). Nitrate foraging by *Arabidopsis* roots is mediated by the transcription factor TCP20 through the systemic signaling pathway. *Proc. Natl. Acad. Sci. U. S. A.* 111, 15267–15272. doi: 10.1073/pnas.1411375111

Heath, J. D., Weldon, R., Monnot, C., and Meinke, D. W. (1986). Analysis of storage proteins in normal and aborted seeds from embryo-lethal mutants of *Arabidopsis thaliana*. *Planta* 169, 304–312. doi: 10.1007/BF00392124

Hu, Z., Guo, Y., Ying, S., Tang, Y., Niu, J., Wang, T., et al. (2023). OsCBL1 modulates rice nitrogen use efficiency *via* negative regulation of OsNRT2.2 by OsCCA1. *BMC Plant Biol.* 23, 502. doi: 10.1186/s12870-023-04520-4

Ishikawa, S., Ito, Y., Sato, Y., Fukaya, Y., Takahashi, M., Morikawa, H., et al. (2009). Two-component high-affinity nitrate transport system in barley: Membrane localization, protein expression in roots and a direct protein-protein interaction. *Plant Biotechnol.* 26, 197–205. doi: 10.5511/plantbiotechnology.26.197

Jacquot, A., Chaput, V., Mauries, A., Li, Z., Tillard, P., Fizames, C., et al. (2020). NRT2.1 C-terminus phosphorylation prevents root high affinity nitrate uptake activity in *Arabidopsis thaliana*. *New Phytol.* 228, 1038–1054. doi: 10.1111/nph.16710

Jung, H. W., Tschaplinski, T. J., Wang, L., Glazebrook, J., and Greenberg, J. T. (2009). Priming in systemic plant immunity. *Science* 324, 89–91. doi: 10.1126/science.1170025

Kechid, M., Desbrosses, G., Rokhsi, W., Varoquaux, F., Djekoun, A., and Touraine, B. (2013). The NRT2.5 and NRT2.6 genes are involved in growth promotion of *Arabidopsis* by the plant growth-promoting rhizobacterium (PGPR) strain Phyllobacterium brassicacearum STM196. *New Phytol.* 198, 514–524. doi: 10.1111/nph.12158

Kiba, T., Feria-Bourrellier, A. B., Lafouge, F., Lezhneva, L., Boutet-Mercey, S., Orsel, M., et al. (2012). The *Arabidopsis* nitrate transporter NRT2.4 plays a double role in roots and shoots of nitrogen-starved plants. *Plant Cell* 24, 245–258. doi: 10.1105/tpc.111.092221

Kotur, Z., and Glass, A. D. (2015). A 150 kDa plasma membrane complex of AtNRT2.5 and AtNAR2.1 is the major contributor to constitutive high-affinity nitrate influx in *Arabidopsis thaliana*. *Plant Cell Environ.* 38, 1490–1502. doi: 10.1111/pce.12496

Kotur, Z., Mackenzie, N., Ramesh, S., Tyerman, S., Kaiser, B., and Glass, A. (2012). Nitrate transport capacity of the *Arabidopsis thaliana* NRT2 family members and their interactions with AtNAR2.1. *New Phytol.* 194, 724–731. doi: 10.1111/j.1469-8137.2012.04094.x

Laugier, E., Bouguyon, E., Mauriès, A., Tillard, P., Gojon, A., and Lejay, L. (2012). Regulation of high-affinity nitrate uptake in roots of *Arabidopsis* depends predominantly on posttranscriptional control of the NRT2.1/NAR2.1 transport system. *Plant Physiol.* 158, 1067–1078. doi: 10.1104/pp.111.188532

Lejay, L., Gansel, X., Cerezo, M., Tillard, P., Müller, C., Krapp, A., et al. (2003). Regulation of root ion transporters by photosynthesis: Functional importance and relation with hexokinase. *Plant Cell* 15, 2218–2232. doi: 10.1105/tpc.013516

Lejay, L., Tillard, P., Lepetit, M., Olive, D. F., Filleur, S., Daniel-Vedele, F., et al. (1999). Molecular and functional regulation of two NO_3^- uptake systems by N- and C-status of *Arabidopsis* plants. *Plant J.* 18, 509–519. doi: 10.1046/j.1365-313X.1999.00480.x

Lejay, L., Wirth, J., Pervent, M., Cross, J. M., Tillard, P., and Gojon, A. (2008). Oxidative pentose phosphate pathway-dependent sugar sensing as a mechanism for regulation of root ion transporters by photosynthesis. *Plant Physiol.* 146, 2036–2053. doi: 10.1104/pp.107.114710

Lepiniec, L., Debeaujon, I., Routaboul, J. M., Baudry, A., Pourcel, L., Nesi, N., et al. (2006). Genetics and biochemistry of seed flavonoids. *Annu. Rev. Plant Biol.* 57, 405–430. doi: 10.1146/annurev.arplant.57.032905.105252

Léran, S., Varala, K., Boyer, J. C., Chiurazzi, M., Crawford, N., Daniel-Vedele, F., et al. (2014). A unified nomenclature of NITRATE TRANSPORTER 1/PEPTIDE TRANSPORTER family members in plants. *Trends Plant Sci.* 19, 5–9. doi: 10.1016/j.tplants.2013.08.008

Lezhneva, L., Kiba, T., Feria-Bourrellier, A. B., Lafouge, F., Boutet-Mercey, S., Zoufan, P., et al. (2014). The *Arabidopsis* nitrate transporter NRT2.5 plays a role in nitrate acquisition and remobilization in nitrogen-starved plants. *Plant J.* 80, 230–241. doi: 10.1111/tpj.12626

Li, J. Y., Fu, Y. L., Pike, S. M., Bao, J., Tian, W., Zhang, Y., et al. (2010). The *Arabidopsis* nitrate transporter NRT1.8 functions in nitrate removal from the xylem sap and mediates cadmium tolerance. *Plant Cell* 22, 1633–1646. doi: 10.1105/tpc.110.075242

Li, W., He, X., Chen, Y., Jing, Y., Shen, C., Yang, J., et al. (2020). A wheat transcription factor positively sets seed vigor by regulating the grain nitrate signal. *New Phytol.* 225, 1667–1680. doi: 10.1111/nph.16234

Li, W., Wang, Y., Okamoto, M., Crawford, N. M., Siddiqi, M. Y., and Glass, A. D. (2007). Dissection of the AtNRT2.1:AtNRT2.2 inducible high-affinity nitrate transporter gene cluster. *Plant Physiol.* 143, 425–433. doi: 10.1104/pp.106.091223

Lillo, C. (2008). Signaling cascades integrating light-enhanced nitrate metabolism. *Biochem. J.* 415, 11–19. doi: 10.1042/BJ20081115

Little, D. Y., Rao, H., Oliva, S., Daniel-Vedele, F., Krapp, A., and Malamy, J. E. (2005). The putative high-affinity nitrate transporter NRT2.1 represses lateral root initiation in response to nutritional cues. *Proc. Natl. Acad. Sci. U. S. A.* 102, 13693–13698. doi: 10.1073/pnas.0504219102

Liu, R., Jia, T., Cui, B., and Song, J. (2020). The expression patterns and putative function of nitrate transporter 2.5 in plants. *Plant Signal. Behav.* 15, 1815980. doi: 10.1080/15592324.2020.1815980

Long, D. H., Lee, F. N., and TeBeest, D. O. (2000). Effect of nitrogen fertilization on disease progress of rice blast on susceptible and resistant cultivars. *Plant Dis.* 84, 403–409. doi: 10.1094/PDIS.2000.84.4.403

Malamy, J. E., and Ryan, K. S. (2001). Environmental regulation of lateral root initiation in *Arabidopsis*. *Plant Physiol.* 127, 899–909. doi: 10.1104/pp.010406

Mantelin, S., Desbrosses, G., Larcher, M., Tranbarger, T. J., Cleyet-Marel, J. C., and Touraine, B. (2006). Nitrate-dependent control of root architecture and N nutrition are altered by a plant growth-promoting Phyllobacterium sp. *Planta* 223, 591–603. doi: 10.1007/s00425-005-0106-y

Mao, Q. Q., Guan, M. Y., Lu, K. X., Du, S. T., Fan, S. K., Ye, Y. Q., et al. (2014). Inhibition of nitrate transporter 1.1-controlled nitrate uptake reduces cadmium uptake in *Arabidopsis*. *Plant Physiol.* 166, 934–944. doi: 10.1104/pp.114.243766

Matt, P., Geiger, M., Walch-Liu, P., Engels, C., Krapp, A., and Stitt, M. (2010). Elevated carbon dioxide increases nitrate uptake and nitrate reductase activity when tobacco is growing on nitrate, but increases ammonium uptake and inhibits nitrate reductase activity when tobacco is growing on ammonium nitrate. *Plant Cell Environ.* 24, 1119–1137. doi: 10.1046/j.1365-3040.2001.00771.x

Melotto, M., Underwood, W., and He, S. Y. (2008). Role of stomata in plant innate immunity and foliar bacterial diseases. *Annu. Rev. Phytopathol.* 46, 101–122. doi: 10.1146/annurev.phyto.121107.104959

Menz, J., Li, Z., Schulze, W. X., and Ludewig, U. (2016). Early nitrogen-deprivation responses in *Arabidopsis* roots reveal distinct differences on transcriptome and (phospho-) proteome levels between nitrate and ammonium nutrition. *Plant J.* 88, 717–734. doi: 10.1111/tpj.13272

Misawa, F., Ito, M., Nosaki, S., Nishida, H., Watanabe, H., Suzuki, T., et al. (2022). Nitrate transport *via* NRT2.1 mediates NIN-LIKE PROTEIN-dependent suppression of root nodulation in *Lotus japonicus*. *Plant Cell* 34, 1844–1862. doi: 10.1093/plcell/koac046

Modolo, L. V., Augusto, O., Almeida, I. M., Magalhaes, J. R., and Salgado, I. (2005). Nitrite as the major source of nitric oxide production by *Arabidopsis thaliana* in response to *Pseudomonas syringae*. *FEBS Lett.* 579, 3814–3820. doi: 10.1016/j.febslet.2005.05.078

Modolo, L. V., Augusto, O., Almeida, I. M. G., Pinto-Maglio, C. A. F., Oliveira, H. C., Seligman, K., et al. (2006). Decreased arginine and nitrite levels in nitrate reductase-deficient *Arabidopsis thaliana* plants impair nitric oxide synthesis and the hypersensitive response to *Pseudomonas syringae*. *Plant Sci.* 171, 34–40. doi: 10.1016/j.plantsci.2006.02.010

Monachello, D., Allot, M., Oliva, S., Krapp, A., Daniel-Vedele, F., Barbier-Brygoo, H., et al. (2009). Two anion transporters AtClCa and AtClCe fulfil interconnecting but not redundant roles in nitrate assimilation pathways. *New Phytol.* 183, 88–94. doi: 10.1111/j.1469-8137.2009.02837.x

Naz, M., Luo, B., Guo, X., Li, B., Chen, J., and Fan, X. (2019). Overexpression of nitrate transporter OsNRT2.1 enhances nitrate-dependent root elongation. *Genes* 10, 290. doi: 10.3390/genes10040290

Nazoa, P., Vidmar, J. J., Tranbarger, T. J., Mouline, K., Damiani, I., Tillard, P., et al. (2003). Regulation of the nitrate transporter gene AtNRT2.1 in *Arabidopsis thaliana*: Responses to nitrate, amino acids and developmental stage. *Plant Mol. Biol.* 52, 689–703. doi: 10.1023/A:1024899808018

Nishida, H., Nosaki, S., Suzuki, T., Ito, M., Miyakawa, T., Nomoto, M., et al. (2021). Different DNA-binding specificities of NLP and NIN transcription factors underlie nitrate-induced control of root nodulation. *Plant Cell* 33, 2340–2359. doi: 10.1093/plcell/koab103

North, K. A., Ehlting, B., Koprivova, A., Rennenberg, H., and Kopriva, S. (2009). Natural variation in *Arabidopsis* adaptation to growth at low nitrogen conditions. *Plant Physiol. Biochem.* 47, 912–918. doi: 10.1016/j.plaphy.2009.06.009

Nunes-Nesi, A., Fernie, A. R., and Stitt, M. (2010). Metabolic and signaling aspects underpinning the regulation of plant carbon nitrogen interactions. *Mol. Plant* 3, 973–996. doi: 10.1093/mp/ssq049

O'Brien, J. A., Vega, A., Bouguyon, E., Krouk, G., Gojon, A., Coruzzi, G., et al. (2016). Nitrate transport, sensing, and responses in plants. *Mol. Plant* 9, 837–856. doi: 10.1016/j.molp.2016.05.004

Ohkubo, Y., Kuwata, K., and Matsubayashi, Y. (2021). A type 2C protein phosphatase activates high-affinity nitrate uptake by dephosphorylating NRT2.1. *Nat. Plants* 7, 310–316. doi: 10.1038/s41477-021-00870-9

Ohkubo, Y., Tanaka, M., Tabata, R., Ogawa-Ohnishi, M., and Matsubayashi, Y. (2017). Shoot-to-root mobile polypeptides involved in systemic regulation of nitrogen acquisition. *Nat. Plants* 3, 17029. doi: 10.1038/nplants.2017.29

Okamoto, M., Kumar, A., Li, W., Wang, Y., Siddiqi, M. Y., Crawford, N. M., et al. (2006). High-affinity nitrate transport in roots of *Arabidopsis* depends on expression of the NAR2-like gene AtNRT3.1. *Plant Physiol.* 140, 1036–1046. doi: 10.1104/pp.105.074385

Okamoto, M., Vidmar, J. J., and Glass, A. D. M. (2003). Regulation of *NRT1* and *NRT2* gene families of *Arabidopsis thaliana*: Responses to nitrate provision. *Plant Cell Physiol.* 44, 304–317. doi: 10.1093/pcp/pcg036

Orsel, M., Chopin, F., Leleu, O., Smith, S., Krapp, A., Daniel-Vedele, F., et al. (2006). Characterization of a two-component high-affinity nitrate uptake system in *Arabidopsis*. Physiology and protein-protein interaction. *Plant Physiol.* 142, 1304–1317. doi: 10.1104/pp.106.085209

Orsel, M., Eulenburg, K., Krapp, A., and Daniel-Vedele, F. (2004). Disruption of the nitrate transporter genes AtNRT2.1 and AtNRT2.2 restricts growth at low external nitrate concentration. *Planta* 219, 714–721. doi: 10.1007/s00425-004-1266-x

Orsel, M., Krapp, A., and Daniel-Vedele, F. (2002). Analysis of the NRT2 nitrate transporter family in *Arabidopsis*. Structure and gene expression. *Plant Physiol.* 129, 886–896. doi: 10.1104/pp.005280

Ota, R., Ohkubo, Y., Yamashita, Y., Ogawa-Ohnishi, M., and Matsubayashi, Y. (2020). Shoot-to-root mobile CEPD-like 2 integrates shoot nitrogen status to systemically regulate nitrate uptake in *Arabidopsis*. *Nat. Commun.* 11, 641. doi: 10.1038/s41467-020-14440-8

Pii, Y., Alessandrini, M., Dall'Osto, L., Guardini, K., Prinsi, B., Espen, L., et al. (2016). Time-resolved investigation of molecular components involved in the induction of [Formula: see text] high affinity transport system in maize roots. *Front. Plant Sci.* 7. doi: 10.3389/fpls.2016.01657

Pourcel, L., Routaboul, J. M., Kerhoas, L., Caboche, M., Lepiniec, L., and Debeaujon, I. (2005). TRANSPARENT TESTA10 encodes a laccase-like enzyme involved in oxidative polymerization of flavonoids in *Arabidopsis* seed coat. *Plant Cell* 17, 2966–2980. doi: 10.1105/tpc.105.035154

Quesada, A., Galván, A., and Fernández, E. (1994). Identification of nitrate transporter genes in *Chlamydomonas reinhardtii*. *Plant J.* 5, 407–419. doi: 10.1111/j.1365-313X.1994.00407.x

Quesada, A., Hidalgo, J., and Fernández, E. (1998). Three Nrt2 genes are differentially regulated in *Chlamydomonas reinhardtii*. *Mol. Gen. Genet.* 258, 373–377. doi: 10.1007/s004380050743

Quesada, A., Krapp, A., Trueman, L. J., Daniel-Vedele, F., Fernández, E., Forde, B. G., et al. (1997). PCR-identification of a Nicotiana plumbaginifolia cDNA homologous to the high-affinity nitrate transporters of the crnA family. *Plant Mol. Biol.* 34, 265–274. doi: 10.1023/A:1005872816881

Remans, T., Nacry, P., Pervent, M., Filleur, S., Diatloff, E., Mounier, E., et al. (2006a). The *Arabidopsis* NRT1.1 transporter participates in the signaling pathway triggering root colonization of nitrate-rich patches. *Proc. Natl. Acad. Sci. U. S. A.* 103, 19206–19211. doi: 10.1073/pnas.0605275103

Remans, T., Nacry, P., Pervent, M., Girin, T., Tillard, P., Lepetit, M., et al. (2006b). A central role for the nitrate transporter NRT2.1 in the integrated morphological and physiological responses of the root system to nitrogen limitation in *Arabidopsis*. *Plant Physiol.* 140, 909–921. doi: 10.1104/pp.105.075721

Robinson, D. (1994). The responses of plants to non-uniform supplies of nutrients. *New Phytol.* 127, 635–674. doi: 10.1111/j.1469-8137.1994.tb02969.x

Routaboul, J. M., Dubos, C., Beck, G., Marquis, C., Bidzinski, P., Loudet, O., et al. (2012). Metabolite profiling and quantitative genetics of natural variation for flavonoids in *Arabidopsis*. *J. Exp. Bot.* 63, 3749–3764. doi: 10.1093/jxb/ers067

Ruffel, S., Krouk, G., Ristova, D., Shasha, D., Birnbaum, K. D., and Coruzzi, G. M. (2011). Nitrogen economics of root foraging: transitive closure of the nitrate-cytokinin relay and distinct systemic signaling for N supply vs. demand. *Proc. Natl. Acad. Sci. U. S. A.* 108, 18524–18529. doi: 10.1073/pnas.1108684108

Siddiqi, M. Y., Glass, A. D., Ruth, T. J., and Rufty, T. W. (1990). Studies of the uptake of nitrate in barley: I. kinetics of $^{13}NO_3^-$ influx. *Plant Physiol.* 93, 1426–1432. doi: 10.1104/pp.93.4.1426

Song, M., Fan, X., Chen, J., Qu, H., Luo, L., and Xu, G. (2020). OsNAR2.1 interaction with OsNIT1 and OsNIT2 functions in root-growth responses to nitrate and ammonium. *Plant Physiol.* 183, 289–303. doi: 10.1104/pp.19.01364

Tabata, R., Sumida, K., Yoshii, T., Ohyama, K., Shinohara, H., and Matsubayashi, Y. (2014). Perception of root-derived peptides by shoot LRR-RKs mediates systemic N-demand signaling. *Science* 346, 343–346. doi: 10.1126/science.1257800

Taulemesse, F., Le Gouis, J., Gouache, D., Gibon, Y., and Allard, V. (2015). Post-flowering nitrate uptake in wheat is controlled by N status at flowering, with a putative major role of root nitrate transporter NRT2.1. *PloS One* 10, e0120291. doi: 10.1371/journal.pone.0120291

Tong, Y., Zhou, J. J., Li, Z., and Miller, A. J. (2005). A two-component high-affinity nitrate uptake system in barley. *Plant J.* 41, 442–450. doi: 10.1111/j.1365-313X.2004.02310.x

Unkles, S. E., Hawker, K. L., Grieve, C., Campbell, E. I., Montague, P., and Kinghorn, J. R. (1991). crnA encodes a nitrate transporter in Aspergillus nidulans. *Proc. Natl. Acad. Sci. U. S. A.* 88, 204–208. doi: 10.1073/pnas.88.1.204

Valkov, V. T., Sol, S., Rogato, A., and Chiurazzi, M. (2020). The functional characterization of LjNRT2.4 indicates a novel, positive role of nitrate for an efficient nodule N2-fixation activity. *New Phytol.* 228, 682–696. doi: 10.1111/nph.16728

Vidal, E. A., Alvarez, J. M., Araus, V., Riveras, E., Brooks, M. D., Krouk, G., et al. (2020). Nitrate in 2020: Thirty years from transport to signaling networks. *Plant Cell* 32, 2094–2119. doi: 10.1105/tpc.19.00748

Vidal, E. A., Araus, V., Lu, C., Parry, G., Green, P. J., Coruzzi, G. M., et al. (2010). Nitrate-responsive miR393/*AFB3* regulatory module controls root system architecture in *Arabidopsis thaliana*. *Proc. Natl. Acad. Sci. U. S. A.* 107, 4477–4482. doi: 10.1073/pnas.0909571107

Vidal, E. A., Moyano, T. C., Riveras, E., Contreras-López, O., and Gutiérrez, R. A. (2013). Systems approaches map regulatory networks downstream of the auxin receptor AFB3 in the nitrate response of *Arabidopsis thaliana* roots. *Proc. Natl. Acad. Sci. U. S. A.* 110, 12840–12845. doi: 10.1073/pnas.1310937110

Vidmar, J. J., Zhuo, D., Siddiqi, M. Y., and Glass, A. D. (2000). Isolation and characterization of HvNRT2.3 and HvNRT2.4, cDNAs encoding high-affinity nitrate transporters from roots of barley. *Plant Physiol.* 122, 783–792. doi: 10.1104/pp.122.3.783

Wang, Y. Y., Hsu, P. K., and Tsay, Y. F. (2012). Uptake, allocation and signaling of nitrate. *Trends Plant Sci.* 17, 458–467. doi: 10.1016/j.tplants.2012.04.006

Wang, T., Hua, Y., Chen, M., Zhang, J., Guan, C., and Zhang, Z. (2018). Mechanism enhancing *arabidopsis* resistance to cadmium: The role of *NRT1.5* and proton pump. *Front. Plant Sci.* 9. doi: 10.3389/fpls.2018.01892

Wang, Y., Yuan, Z., Wang, J., Xiao, H., Wan, L., Li, L., et al. (2023). The nitrate transporter NRT2.1 directly antagonizes PIN7-mediated auxin transport for root growth adaptation. *Proc. Natl. Acad. Sci. U. S. A.* 120, e2221313120. doi: 10.1073/pnas.2221313120

Wei, J., Zheng, Y., Feng, H., Qu, H., Fan, X., Yamaji, N., et al. (2018). OsNRT2.4 encodes a dual-affinity nitrate transporter and functions in nitrate-regulated root growth and nitrate distribution in rice. *J. Exp. Bot.* 69, 1095–1107. doi: 10.1093/jxb/erx486

Widiez, T., El Kafafi, E. S., Girin, T., Berr, A., Ruffel, S., Krouk, G., et al. (2011). High nitrogen insensitive 9 (HNI9)-mediated systemic repression of root NO3- uptake is associated with changes in histone methylation. *Proc. Natl. Acad. Sci. U. S. A.* 108, 13329–13334. doi: 10.1073/pnas.1017863108

Wirth, J., Chopin, F., Santoni, V., Viennois, G., Tillard, P., Krapp, A., et al. (2007). Regulation of root nitrate uptake at the NRT2.1 protein level in *Arabidopsis* thaliana. *J. Biol. Chem.* 282, 23541–23552. doi: 10.1074/jbc.M700901200

Yan, M., Fan, X., Feng, H., Miller, A. J., Shen, Q., and Xu, G. (2011). Rice OsNAR2.1 interacts with OsNRT2.1, OsNRT2.2 and OsNRT2.3a nitrate transporters to provide uptake over high and low concentration ranges. *Plant Cell Environ.* 34, 1360–1372. doi: 10.1111/j.1365-3040.2011.02335.x

Yang, Y., Xiong, J., Chen, R., Fu, G., Chen, T. T., and Tao, L. (2015). Excessive Nitrate Enhances Cadmium (Cd) Uptake by Up-regulating the expression of *OsIRT1* in rice (*Oryza sativa*). *Environ. Exp. Bot.* 122, 141–149. doi: 10.1016/j.envexpbot.2015.10.001

Yong, Z., Kotur, Z., and Glass, A. D. (2010). Characterization of an intact two-component high-affinity nitrate transporter from *Arabidopsis* roots. *Plant J.* 63, 739–748. doi: 10.1111/tpj.2010.63.issue-5

Zhang, H., and Forde, B. G. (2000). Regulation of *Arabidopsis* root development by nitrate availability. *J. Exp. Bot.* 51, 51–59. doi: 10.1093/jxb/51.342.51

Zhou, J. J., Fernández, E., Galván, A., and Miller, A. J. (2000a). A high affinity nitrate transport system from Chlamydomonas requires two gene products. *FEBS Lett.* 466, 225–227. doi: 10.1016/S0014-5793(00)01085-1

Zhou, J. J., Trueman, L. J., Boorer, K. J., Theodoulou, F. L., Forde, B. G., and Miller, A. J. (2000b). A high affinity fungal nitrate carrier with two transport mechanisms. *J. Biol. Chem.* 275, 39894–39899. doi: 10.1074/jbc.M004610200

Zhuo, D., Okamoto, M., Vidmar, J. J., and Glass, A. D. (1999). Regulation of a putative high-affinity nitrate transporter (*Nrt2;1At*) in roots of *Arabidopsis thaliana*. *Plant J.* 17, 563–568. doi: 10.1046/j.1365-313X.1999.00396.x

Zimmerli, L., Jakab, G., Metraux, J. P., and Mauch-Mani, B. (2000). Potentiation of pathogen-specific defense mechanisms in *Arabidopsis* by beta -aminobutyric acid. *Proc. Natl. Acad. Sci. U. S. A.* 97, 12920–12925. doi: 10.1073/pnas.230416897

Zou, X., Liu, M. Y., Wu, W. H., and Wang, Y. (2020). Phosphorylation at Ser28 stabilizes the *Arabidopsis* nitrate transporter NRT2.1 in response to nitrate limitation. *J. Integr. Plant Biol.* 62, 865–876. doi: 10.1111/jipb.12858

frontiers | Frontiers in Plant Science

TYPE Brief Research Report
PUBLISHED 25 March 2024
DOI 10.3389/fpls.2024.1369543

OPEN ACCESS

EDITED BY
Enrique Ostria-Gallardo,
University of Concepcion, Chile

REVIEWED BY
Guillaume Pilot,
Virginia Tech, United States
Noelia Foresi,
CONICET Mar del Plata, Argentina

*CORRESPONDENCE
Axel Mithöfer
amithoefer@ice.mpg.de

RECEIVED 12 January 2024
ACCEPTED 14 March 2024
PUBLISHED 25 March 2024

CITATION
Svietlova N, Zhyr L, Reichelt M, Grabe V and Mithöfer A (2024) Glutamine as sole nitrogen source prevents induction of nitrate transporter gene *NRT2.4* and affects amino acid metabolism in Arabidopsis. *Front. Plant Sci.* 15:1369543. doi: 10.3389/fpls.2024.1369543

Glutamine as sole nitrogen source prevents induction of nitrate transporter gene *NRT2.4* and affects amino acid metabolism in Arabidopsis

Nataliia Svietlova[1], Liza Zhyr[1], Michael Reichelt[2], Veit Grabe[3] and Axel Mithöfer[1]*

[1]Research Group Plant Defense Physiology, Max Planck Institute for Chemical Ecology, Jena, Germany, [2]Department of Biochemistry, Max Planck Institute for Chemical Ecology, Jena, Germany, [3]Microscopic Imaging Service Group, Max Planck Institute for Chemical Ecology, Jena, Germany

Plants assimilate inorganic nitrogen (N) to glutamine. Glutamine is the most abundant amino acid in most plant species, the N-supplying precursor of all N-containing compounds in the cell and the first organic nitrogen molecule formed from inorganic nitrogen taken up by the roots. In addition to its role in plant nutrition, glutamine most likely also has a function as a signaling molecule in the regulation of nitrogen metabolism. We investigated whether glutamine influences the high-affinity transporter system for nitrate uptake. Therefore, we analyzed the expression of the nitrate transporter *NRT2.4*, which is inducible by N deficiency, in *Arabidopsis thaliana* grown under different nitrogen starvation scenarios, comparing nitrate or glutamine as the sole nitrogen source. Using the reporter line *ProNRT2.4:GFP* and two independent knockout lines, *nrt2.4-1* and *nrt2.4-2*, we analyzed gene expression and amino acid profiles. We showed that the regulation of *NRT2.4* expression depends on available nitrogen in general, for example on glutamine as a nitrogen source, and not specifically on nitrate. In contrast to high nitrate concentrations, amino acid profiles changed to an accumulation of amino acids containing more than one nitrogen during growth in high glutamine concentrations, indicating a switch to nitrogen storage metabolism. Furthermore, we demonstrated that the *nrt2.4-2* line shows unexpected effects on *NRT2.5* gene expression and the amino acids profile in shoots under high glutamine supply conditions compared to Arabidopsis wild type and *nrt2.4-1*, suggesting non-*NRT2.4*-related metabolic consequences in this knockout line.

KEYWORDS

Arabidopsis, nitrogen-deficiency, nitrate, glutamine, amino acids, high-affinity nitrate transporters (NRTs), *NRT2.4*, *NRT2.5*

1 Introduction

Nitrogen (N) is an essential macronutrient for plant growth and productivity. Plants absorb N from the soil mainly in the inorganic form of nitrate (NO_3^-) and ammonium (NH_4^+). While the root can assimilate ammonium directly, nitrate is mostly first transported to the shoot. There nitrate is reduced to ammonium in various enzymatic steps, transferred to the amino acid glutamine by glutamine synthetase and further introduced into the metabolism by aminotransferases. In addition, plants also have the ability to absorb organic nitrogen from soil such as amino acids (AA), peptides, urea, and other nitrogen-containing compounds (Ortiz-Lopez et al., 2000; Yao et al., 2020). Andrews et al. (2013) concluded in a comprehensive review that the form of N, which is available to and taken up by plants can influence timing and rate of seed germination, leaf expansion and function, shoot-to-root dry matter partitioning, and root architecture. Amino acids, which ubiquitously occur in soils due to hydrolysis of soil proteins, are a well-available form of organic N (Näsholm et al., 2009). They can be an important source of N for plants and account for 10% but can go up to 40% of the total soluble N in the soil (Gioseffi et al., 2012). Especially in cropping systems that rely on the recycling and decomposition of organic N sources, AA can have a significant contribution to N-input and represent an available N-pool (El-Naggar et al., 2009). Therefore, this source of nitrogen for plant nutrition should not be underestimated.

In higher plants, inorganic (NH_4^+, NO_3^-) N uptake and distribution is mediated by transporters with high (HATS) and low (LATS) affinities (Wang et al., 2012; Hao et al., 2020). NO_3^- transporters are proteins encoded by four gene families: *Nitrate Transporters 1 (NRT1s), nitrate Transporters 2 (NRT2s)*, *chloride channels* (*CLCs*) and *slow anion channel* associated homologues (*SLAC/SLAHs*) (Wang et al., 2012). The *NRT* gene families of nitrate transporters in Arabidopsis contain 53 *NRT1* and 7 *NRT2* members (Orsel et al., 2002; Okamoto et al., 2003; Vidal et al., 2020), six of which are involved in nitrate uptake by roots (NRT1.1, NRT1.2 and NRT2.1, NRT2.2, NRT2.4, NRT2.5) (Vidal et al., 2020). NRT1s and NRT2s nitrate transporter gene homologues were classified as nitrate-inducible, nitrate-repressible, or nitrate-constitutive (Vidal et al., 2020). *AtNRT1.1*, *2.1*, and *2.2* were strongly and transiently induced by NO_3^-. Influx studies indicated that *AtNRT1.1* and *AtNRT2.1* belong to the LATS and HATS, respectively (Okamoto et al., 2003). By contrast, *AtNRT2.4* showed only modest induction both in shoots and roots, while expression of *AtNRT2.5* was strongly suppressed by nitrate uptake in both roots and shoots. Actually, that means both genes were induced by NO_3^- deficiency (Kiba et al., 2012; Lezhneva et al., 2014). Finally, *AtNRT1.2*, *1.4*, *2.3*, *2.6*, and *2.7*, are characterized by a constitutive expression pattern (Vidal et al., 2020).

In addition, plants express a variety of different amino acid transporters with overlapping specificities and affinities, many of which expressed in roots (Fischer et al., 1998). There are multiple families of amino acid transporters belonging to three major families: ATF (amino acid transporter family, also called AAP, amino acid permease family), APC (amino acid-polyamine-choline transporter family) and UMAMIT (usually multiple acids move in and out transporter family). Some of these transporters take part in uptake of amino acids from the soil, for example AAP1, APP3, AAP5, UMAMIT1, Proline Transporter 2 (ProT2), and Lysine Histidine Transporter 1 (LHT1) (Ortiz-Lopez et al., 2000; Tegeder, 2012; Dinkeloo et al., 2018; Yao et al., 2020). Noteworthy, there is a particular role for LHT1 in the uptake from soil and intracellular distribution of Gln (Svennerstam et al., 2007; Liu et al., 2010). An Arabidopsis *lht1* knock out mutant showed broad pathogen resistance due to Gln-deficiency in chloroplasts and salicylic acid accumulation demonstrating the importance of at least the amino acid Gln and its homeostasis for the plant in plant pathogen interactions (Liu et al., 2010).

The fundamental demand of AA in any organism needs tight AA metabolism to sustain physiological homeostasis. In plants, there are a number of indications that AA metabolism undergoes dynamic changes to control particular growth and development events (Kawade et al., 2023). A large number of studies have shown that also exogenous amino acids present in the underground environment or leaf surface can be taken up by plants, and can have strong impacts on plant growth and/or defense response (Han et al., 2022; and references therein). When added at high concentrations (≥ 1mM) to tobacco (*Nicotiana sylvestris*) cell cultures, amino acids have an inhibitory effect on plant growth, very likely due to feedback inhibition of specific biosynthetic pathways (Bonner et al., 1996; Bonner and Jensen, 1997). Every amino acid causes amino acid-mediated growth inhibition called general amino acid inhibition, with the exception of L-Glutamine (Gln). In fact, Gln completely overcomes general amino acid inhibition (Bonner et al., 1996; Bonner and Jensen, 1997). Aspartate (Asp) and some branched chain amino acids inhibited root growth in barley (*Hordeum vulgare*) (Rognes et al. 1986) and Glutamate (Glu) inhibited cell elongation in *Arabidopsis thaliana* (ecotype Columbia) roots (Sivaguru et al., 2003). However, out of all 20 proteinogenic amino acids, only Glu affects root growth in Arabidopsis (most in ecotype C24), when added singly (Walch-Liu et al., 2006). Related amino acids such as Asp, GABA or Gln did not induce growth inhibitory effects at the low concentrations (50 µM) that Glu was effective; even millimolar concentrations of Gln had no effect on root growth in Arabidopsis (Walch-Liu et al., 2006). At these high concentrations, foliar spray of Glycine (Gly) and Gln stimulate lettuce (*Lactuca sativa*) growth (Noroozlo et al., 2019). In a poplar (*Populus deltoides* × *P. euramericana*) hybrid (Nanlin895), it was demonstrated that Gln concentrations < 0.5 mM as the sole N source had positive effects on various physiological and growth parameters, while concentrations > 0.5 mM showed adverse effects (Han et al., 2022). A very recent study showed growth promoting effects of Asparagine (Asn) and Gln on *A. thaliana* leaves in the mM range (Lardos et al., 2024).

The ability to monitor the cellular N status is essential for maintaining metabolic homeostasis, growth, and development in plants (Xuan et al., 2017). Different N-sensory systems are discussed to fulfill this role and further signaling, eventually leading to appropriate physiological responses. These systems include the TOR (target of rapamycin) signaling pathway, the family of GLRs (glutamate-like receptors), the GCN2 (general control non-derepressible 2) pathway, and the plastidic PII-dependent

pathway (Gent and Forde, 2017). All of those have in common that they are supposed to bind amino acids for their monitoring. Considering that Gln is the most abundant free amino acid in plants, the first organic acceptor of inorganic N, and the key N-providing compound for the synthesis of all N-containing compounds in the plant cell, Gln is a very likely candidate (Lee et al., 2023). Thus, the existence of a common Gln-sensing mechanism (P_{II}) that is widely distributed in the plant kingdom, is not surprising (Chellamuthu et al., 2014; Lee et al., 2023). Strikingly, P_{II} is non-functional in Brassicaceae, including Arabidopsis (Chellamuthu et al., 2014). Therefore, it was reasonable and of major interest, to examine the role of exogenous Gln in Arabidopsis plants.

In combination with a submillimolar nitrate content to break dormancy and enable germination, Gln at mM concentrations was identified as by far the most efficient biostimulatory AA in Arabidopsis (Lardos et al., 2024). This study confirmed previous results that also showed that Gln promotes Arabidopsis growth (Forsum et al., 2008). Here, we investigated the effects of low and high levels of exogenous Gln as the sole N source without additional nitrate. Since the main nitrogen source for the plant is inorganic nitrate, we investigated whether the high-affinity nitrate transporters (*NRT2.4* and *NRT2.5*) are induced even when Gln is available as nitrogen source. Under these nutritional conditions, amino acid metabolism, i.e. their different levels, was also analyzed in comparison to nitrate as N source. We could show that the expression of *NRTs* depends more on available nitrogen in general than on nitrate in particular. In contrast to high nitrate concentrations, the amino acid profile in shoots and roots changed significantly at high Gln supply. Furthermore, we demonstrate that the Arabidopsis line *nrt2.4-2* has side effects on *NRT2.5* gene expression and shoot amino acid profiles.

2 Materials and methods

2.1 Plant materials and growth conditions

Different lines of *Arabidopsis thaliana* seeds were used: wild type (WT, ecotype Columbia-0) and transgenic lines. The reporter line *ProNRT2.4:GFP* was in the Col-0 background (Kiba et al., 2012). The knockout (ko) mutant line *nrt2.4-1* corresponds to a T-DNA insertion in the last exon of the *NRT2.4* gene (MDL-ArBrAr-125) (Forsbach et al., 2003; Kiba et al., 2012). The knockout *nrt2.4-2* line was obtained from the Syngenta Arabidopsis Insertion Library (SAIL) T-DNA insertion line collection (SAIL_205_F02, stock CS872100). T-DNA insertion occurred in the third exon (Alonso et al., 2003; Kiba et al., 2012). No expression of *NRT2.4* could be detected by RT-PCR for either mutant line (Kiba et al., 2012). Genotyping using primers shown in Supplementary Table S2, confirmed T-DNA insertions in NRT2.4 gene in *nrt2.4-2* line, while the NRT2.5 gene was not disrupted.

A. thaliana seeds were surface sterilized using 25% (v/v) sodium hypochloride (ACROS Organics™, Germany) and 0.1% of Triton X-100 (Sigma-Aldrich, Germany) for 8 min, rinsed seven times with sterile water and grown on square plates (120×120×16mm) (Thermo Fisher Scientific, Germany) (12-15 seedlings per plate) containing N-complete (7 mM NO_3^-) MGRL medium (Supplementary Table S1). Seeds were stratified for 48 h at 4°C. According to Svietlova et al. (2023), plants are incubated for 14 days in a growth chamber in vertical position under long-day conditions (16 h light/8 h dark) and light intensity 100 µmol photos m^{-2} s^{-1}, at 22°C. For the different N-source treatments (NO_3^- or Gln), *A. thaliana* seedlings (6 per plate) were transferred for 10 d to MGRL medium (including 1% Sucrose, 0.5% Gelrite, pH 5.8) plates. Plates were either N-free (0 mM NO_3^-/0 mM Gln), N-low (0.25 mM NO_3^-/0.125 mM Gln) or N-complete (7 mM NO_3^-/3.5 mM Gln) supplemented with KCl and $CaCl_2{\cdot}2H_2O$ in appropriate quantity for supporting ion balance (Supplementary Table S1). Plants were harvested by 3 in each vial (roots and shoots separately) and weighed. At least 18 seedlings from each treatment were taken. The samples were frozen immediately in liquid N, and stored at −80°C for RNA preparation and amino acids analysis.

2.2 RNA preparation and expression analysis

Total RNA (2.5 µg) was extracted using TRIzol, according to the manufacturer's method, followed by additional chloroform isolation and isopropanol precipitation steps; it was further digested from DNA contamination by TURBO *DNA-free™ KIT* (Life Technologies, USA) and cleaned by *RNA Clean and Concentrator™* KIT (™Trademarks of Zymo Research Corporation). The cDNA (20 µL) was synthesized using *Thermo Scientific RevertAid First Strand cDNA Synthesis KIT* (Thermo Fisher Scientific, Germany), according to the manufacturers' instructions. The qPCR analysis was performed using Bio-Rad CFX96™ Real-Time System (Bio-Rad Laboratories Inc., USA) using the appropriate pairs for *A. thaliana* specific primers (Supplementary Table S2). The reaction components per 20 µL were as follows: 6.5 µL H_2O, 12.5 µL Brilliant II SYBR Green qPCR Master Mix (Agilent Technologies, USA), 1 µL 10 µM of each primer and 1 µL cDNA. Thermal cycling program was as follows: initial denaturation at 95°C for 180 s, and 44 cycles at 95°C for 30 s, 60°C for 30 s, and 72°C for 30 s. *At*Actin II (AT3G18780) was used as an internal reference gene. The relative quantification of gene expression was evaluated using the delta-delta-Ct method according to Pfaffl (2001). Three biological replicates and three technical replicates were performed for each analysis.

2.3 Extraction and quantification of amino acids and abscisic acid by LC-MS/MS

The plant material was homogenized in a Geno/Grinder® 2010 (Spex Sample Prep, Stanmore, UK) equipped with aluminum racks. Racks were cooled in liquid nitrogen before used to prevent thawing of the plant material throughout the homogenization process. The amino acids were extracted twice with a total of 2 mL of methanol on ice. Supernatants were combined and dried using a Concentrator plus (Eppendorf, Hamburg, Germany) and re-suspended in 500 µL

of methanol. The extract was diluted 1:10 (v/v) with water containing the ^{13}C, ^{15}N-labeled amino acid mix (Isotec, Miamisburg, OH, USA) as the internal standard. Amino acids in the diluted extracts were directly analyzed by LC-MS/MS according to (Crocoll et al., 2016) with a QTRAP6500 mass spectrometer (Sciex, Darmstadt, Germany) coupled to an Agilent 1260 series HPLC system. The mass spectrometer was operated in positive ionization mode in multiple reaction monitoring mode (Supplementary Table S3). All amino acids were quantified relative to the peak area of the corresponding labeled compound, except for asparagine (using aspartate and a response factor of 1.0). Abscisic acid determination was carried out as described (Svietlova et al., 2023).

2.4 Analysis of gene expression in GFP reporter lines

Fluorescence microscopy of GFP signals was optimized for live cell and detected in roots during 10 days every 24 h after transfer the plants on N-depleted medium (Svietlova et al., 2023). Images were acquired using Zeiss AXIO Zoom.V16 (ZEISS, Germany, Oberkochen) equipped with 0.5× PlanApoZ Objective (ZEISS, Germany, Oberkochen), an HXP 120 mercury vapor lamp and a filter set 38 HE (excitation filter BP 450-490nm, FT 495nm, emission filter BP 500-550nm) for the visualization of GFP. Signal intensities after treatment were measured using Fiji ImageJ-2.9.0 Analysis Software. Images were converted to 8-bit and processed using Fiji's "analyze particles" plugin. The average fluorescence intensity was measured in the cells of the apical lateral roots. For the measurement, ten randomly selected fluorescent points in the form of a square of four pixels for each plant were used. Fluorescence images were captured using a TOMOCUBE HT-X1 (Tomocube Inc., Republic of Korea) on 6th day of N starvation. HT-X1 model includes a 470 nm LED source, which was used to acquire 3D fluorescence images of GFP.

2.5 Statistical analysis

Independent experiments were treated as a completely randomized design. Figures were plotted using *GraphPad Prism* Software, version 9.0. Datasets of amino acids analysis was subjected using R studio version 1.1.463 with R version 3.4.4. (R Core Team, 2018). Statistically significant differences were calculated using One- and Two-Way-Analysis of Variance, with Dunnett's multiple comparisons test with $P<0.05$ as the threshold for significance. Data were transformed if assumptions for statistical tests were not met.

3 Results

In order to study if NRT2.4 as part of the high affinity nitrate uptake system is affected by different N sources (NO_3^- or Gln), the well described *ProNRT2.4:GFP* reporter line (Kiba et al., 2012) was employed (Figure 1). While fluorescence was detectable immediately and reached a maximum 2 d after transfer to no N conditions, at low N the fluorescence enhancement was also detectable although slightly slower and reached maxima after 4 d, independent on the N source, NO_3^- or Gln. No induction occurred on both full N media, neither with 7 mM NO_3^- nor with 3.5 mM Gln (Figure 1A). TOMOCUBE HT-X1 microscopy of lateral Arabidopsis roots, which were treated with different N-sources, supported these results (Figure 1B). Moreover, a corresponding qPCR analysis confirmed the rapid *NRT2.4* gene induction over time under N-deficiency in Arabidopsis WT roots (Figure 2A). At day 2, the increase in NRT2.4 transcripts was 12.2-fold under N-free

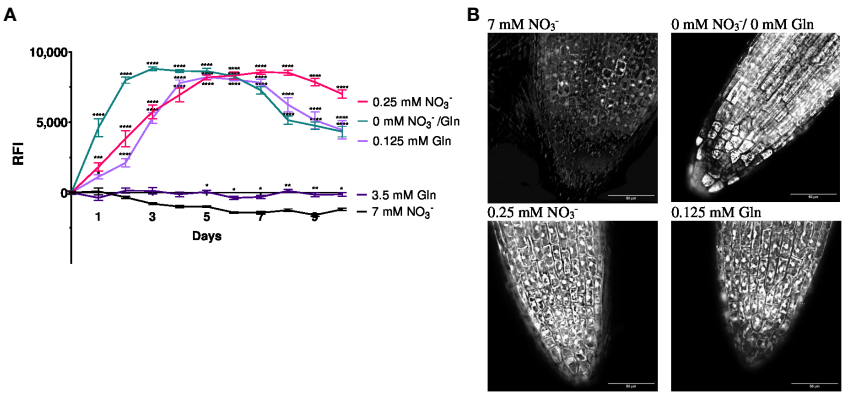

FIGURE 1
Relative fluorescence intensity (RFI) **(A)** and fluorescence microscopy **(B)** of *Arabidopsis thaliana* roots expressing the GFP reporter gene under control of *NRT2.4* promotor *(ProNRT2.4:GFP)*. **(A)** Seedlings were pre-grown on full NO_3^- (7 mM NO_3^-) medium. After two weeks, they grew for additional 10 d on different N-media: N-free (0 mM NO_3^-/0 mM Gln), N-low (0.25 mM NO_3^-/0.125 mM Gln) and N-complete (7mM NO_3^-/3.5 mM Gln) for the indicated time. Shown are the mean (n = 6–8); error bars indicate standard error (SEM). Statistical analysis was performed using repeated measures two-way ANOVA (F_{Days} = 156.7, F_{Media} = 674.0, $P<0.0001$) with Dunnett's multiple comparisons test (each value compared to the respective 7 mM NO_3^- value); *$P<0.05$; **$P<0.01$; *** $P<0.001$; **** $P<0.0001$; ns: not significant. **(B)** Fluorescence intensity of lateral roots treated with different N-sources. Results obtained after 6 d of N starvation using TOMOCUBE HT-X1 microscope.

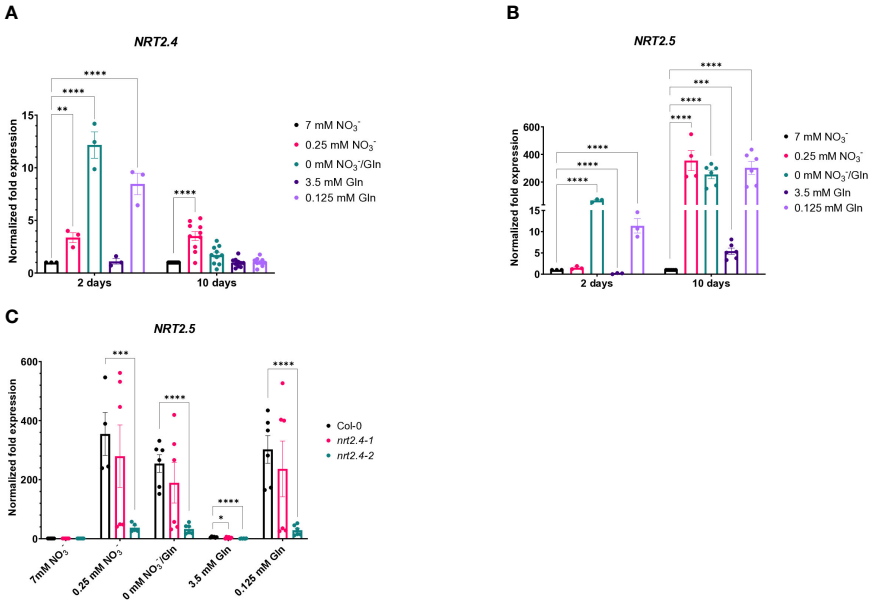

FIGURE 2
Quantitative PCR-based analysis of *NRT2.4* and *NRT2.5* expression in roots of *Arabidopsis thaliana* WT. Seedlings were pre-grown on full NO_3^- (7 mM NO_3^-) medium. After two weeks, they grew for additional 10 d on different N-media: N-free (0 mM NO_3^-/0 mM Gln), N-low (0.25 mM NO_3^-/0.125 mM Gln) and N-complete (7mM NO_3^-/3.5 mM Gln). Expression of **(A)** *NRT2.4* and **(B)** *NRT2.5* on day 2 and 10 after transfer in Col-0 WT. **(C)** Expression of *NRT2.5* in WT and *nrt2.4* ko mutants 10 d after transfer. Shown are the mean (n = 3–10); error bars indicate standard error (SEM). Statistical analysis was performed using Two-way ANOVA (A: F_{Days} = 47.35, F_{Media} = 22.76, P<0.0001; B: F_{Days} =219.0, F_{Media} = 128.7, P<0.0001; C: F_{Media} = 158.0, F_{Lines} = 37.1, P<0.0001) with Dunnett's multiple comparisons test (each value compared to the respective control value); **P<0.01; *** P<0.001; **** P<0.0001.

conditions, 8.5-fold at 0.125 mM Gln, and 3.4-fold at 0.25 mM NO_3^-, all compared to controls grown with 7 mM nitrate. At day 10, almost no *NRT2.4* gene induction was detectable at the different N-concentrations, only a remaining 3.5-fold increase was found on 0.25 mM NO_3^-, suggesting an early but transient induction of this transporter (Figure 2A).

Given that the high affinity nitrate transporter NRT2.5 is induced the most among the seven NRT2 family members in Arabidopsis under long-term nitrogen starvation, and *NRT2.5* becomes the most abundant transcript (Lezhneva et al., 2014), we also investigated the expression of *NRT2.5* upon N-depletion compared to controls grown with 7 mM nitrate (Figure 2B). In contrast to *NRT2.4*, *NRT2.5* expression was relatively lower at day 2 in comparison to day 10. While at day 2 only under no N or 0.125 mM Gln *NRT2.5* expression was detectable, at day 10 its expression was obvious, raising from only 5.4-fold on 3.5 mM Gln up to 355-fold on low NO_3^-, respectively (Figure 2B). No or very low expression of these two genes (*NRT2.4* and *NRT2.5*) belonging to the HATS family was found upon full Gln treatment.

Since Kiba et al. (2012) found a decreased NO_3^- uptake in *nrt2.4* ko mutants under N-starvation conditions (up to 30% less uptake was observed at both 0.025 and 0.01 mM external NO_3^-), we also included the two Arabidopsis ko mutant lines (*nrt2.4-1* and *nrt2.4-2)* in the analysis. An unexpected finding was that *NRT2.5* expression in *nrt2.4-2* ko plants was drastically reduced in comparison to WT or *nrt2.4-1* ko plants under all N-depletion conditions (Figure 2C). This result was reflected in growth of *nrt2.4-2* ko plants (Figure 3). The fresh weight of both shoots (Figure 3A) and roots (Figure 3B) was slightly but significantly reduced in *nrt2.4-2* plants under low N-conditions compared to WT or *nrt2.4-1* plants.

Considering that Gln is the first organic nitrogenous molecule formed from inorganic nitrogen and the precursor of all other amino acids (AA), the free AA content upon growth on the different Gln concentrations was studied in detail. Compositions and changes in the AA pools in the different Arabidopsis lines were analyzed individually in both shoots and roots, depending on the given N-level in the medium. Not surprisingly, we found significant differences in AA profiles of plants at different N-sources (Figure 4). The specificity of these changes is evident. While no obvious differences were found when nitrate or Gln were applied as N-source at low concentrations, a striking change in AAs was found when external Gln was applied at a concentration of 3.5 mM. This applies to both WT and ko mutant plants. Looking deeper in the AA results, it is interesting to note that in WT in both shoots and roots high exogenous Gln had a particular strong effect on the accumulation of AA containing two (Asn, Gln, Lys), three (His) or four (Arg) nitrogen atoms. These changes were more pronounced in shoots than roots. The same trend also occurred in shoots and roots of *nrt2.4-1* and *nrt2.4-2* ko mutant plants (Figure 4). A statistical analysis between the three different lines showed that in the root almost no differences were detected in contrast to shoots (Supplementary Table S4). Here, in *nrt2.4-2*, the content of six AAs (Val, Ile, Leu, Phe, Tyr, Trp) was statistically different to both the Col-0 WT and *nrt2.4-1* plants.

For Arabidopsis, Huang and Jander (2017) have shown that nutrient deficiency can lead to ABA-regulated protein degradation.

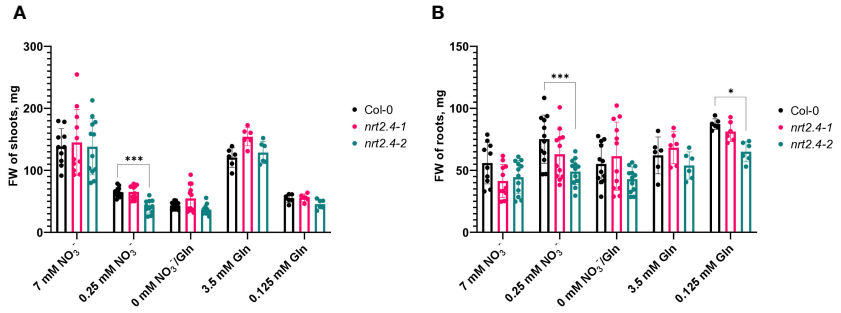

FIGURE 3
Fresh weight of *Arabidopsis thaliana* WT and *nrt2.4* ko mutant plants during N starvation. Shoots **(A)** and roots **(B)**. Seedlings were pre-grown on full NO_3^- (7 mM NO_3^-) medium. After two weeks, they grew for additional 10 d on different N-media: N-free (0 mM NO_3^-/0 mM Gln), N-low (0.25 mM NO_3^-/0.125 mM Gln) and N-complete (7mM NO_3^-/3.5 mM Gln). Shown are the mean (n = 6–12); error bars indicate standard deviation (SD). Statistical analysis was performed using Two-way ANOVA (A: F_{media} = 152.6, F_{Lines} = 12.6, P<0.0001; B: F_{Media} = 12.6, F_{Lines} = 11.9, P<0.0001) with Dunnett's multiple comparisons test (each value compared to the respective Col-0 value); *P<0.05; *** P<0.001.

To get an idea of the origin of the AAs that increased under our experimental conditions, we analyzed the ABA contents in the different lines. Almost no changes in ABA content were observed in roots (Supplementary Figure S1A). In contrast, a clear increase in ABA content was observed in shoots growing on media with lower nitrogen concentrations compared to the 7 mM nitrate control (Figure S1B). While this can be described as a clear trend for the Col-0 and *nrt2.4-1* line, the differences in *nrt2.4-2* were all significant. For further and deeper statistical analysis, we performed a principle component analysis (PCA, Figure 5) of AA compositions. This revealed clear separation of three clusters; i.e. between both full media (7 mM NO_3^-, 3.5 Gln), and all low and no nitrate media (0.25 mM NO_3^-, 0.125 mM Gln and 0 mM NO_3^-/0 mM Gln) in shoots (Figure 5A1) and in roots (Figure 5B1) of WT plants. The same cluster separation was obtained in an analysis where WT and the two mutant lines were included (Figures 5A2, B2). In any case, confidence areas of no and low N overlap sufficiently in shoots and roots. The two principal components, PC1 and PC2, explain in both shoots and roots about 80% or more of all observed variances.

4 Discussion

The decrease in NO_3^- uptake by the roots in plants with sufficient nitrogen levels is caused by feedback regulation from the end-products of NO_3^- assimilation such as amino acids. For example, Thornton (2004) reported that the maximal influx rate associated with HATS was reduced by 66% in the presence of Gln in *Lolium perenne* plants, while LATS-associated influx remained unaffected. Other studies with different nitrogen supply systems showed both the induction of HATS - such as NRT2 activities - by NO_3^- deprivation and the suppression or reduction of HATS induction by the simultaneous or alternative supply of AAs (Zhuo et al., 1999; Nazoa et al., 2003; Thornton, 2004; Miller et al., 2008; Zoufan and Shariati, 2009). Amino acid analysis showed that this repression was specifically related to enhanced internal level of Gln, suggesting a particular role for this amino acid in nitrogen signaling in general, including nitrate uptake regulation (Miller et al., 2008; Lee et al., 2023). These results were obtained with exogenous application of Gln in combination with different concentrations of NO_3^- as background, representing a combination of the two N-sources, whereby additional Gln always alleviated plant nitrogen deficiency. Stimulated by these data, we aimed here to investigate the effects of exogenous Gln as the sole source of nitrogen on HATS, in particular on *NRT2.4* and *NRT2.5*, in Arabidopsis.

Nitrogen starvation-induced *NRT2.4* expression is known to decrease steadily with increasing NO_3^- concentration in the medium (98% decrease between 0 and 10 mM NO_3^-). In addition, low expression of the *NRT2.4* gene can also occur when NH_4^+ is present in the media (Kiba et al., 2012) and Gln has been described as a signaling molecule to regulate gene expression in plants (Kan et al., 2015). Therefore, we investigated whether or not *NRT2.4* expression was affected by an organic N-source, Gln, in comparison with NO_3^-. Using an Arabidopsis reporter line expressing GFP under the control of the *NRT2.4* promotor (*ProNRT2.4:GFP*; Kiba et al., 2012), the GFP expression was faster under no nitrate and no expression was detectable under full N-supply, independent of the form (3.5 mM Gln or 7 mM NO_3^-) (Figure 1A). This finding supports results from Kiba et al. (2012) who showed no induction of *NRT2.4* expression upon transfer of Arabidopsis plants from a NO_3^--containing medium to a medium with NH_4^+ as nitrogen source. Surprisingly, in a recent study Chaput et al. (2023) found NRT2.4 induction after such a transfer on NH_4^+-medium. Strikingly, the GFP expression was very similar when the plants were supplied with 0.25 mM NO_3^- or 0.125 mM Gln, respectively, providing the same amount of N-atoms (Figure 1). These results provide further evidence that the N-sensor responsible for HATS induction is neither their substrate, NO_3^-, nor any other inorganic N-containing compound. More likely, the internal pools of amino acids might indicate the nitrogen status by providing a signal that can regulate NO_3^- uptake by the plant. The regulation of HATS expression thus shows a certain non-specificity and dependence on the general content or organic nitrogen and not on the NO_3^- content.

Our data in addition showed a low level of *NRT2.4* transcript expression, which varied between a 12.2-fold increase in N-free

10.3389/fpls.2024.1369543

Color Code, %	0				100					1000
Amino acids	Shoots					Roots				
	7 NO_3^-	0.25 NO_3^-	0 NO_3^-	0.125 Gln	3.5 Gln	7 NO_3^-	0.25 NO_3^-	0 NO_3^-	0.125 Gln	3.5 Gln
Col-0	% of 7 NO_3^-					% of 7 NO_3^-				
Ala	100	49	52	60	68	100	55	34	47	188
Ser	100	62	71	96	236	100	103	92	85	271
Pro	100	175	169	315	213	100	161	129	110	372
Val	100	176	201	282	278	100	142	103	100	213
Thr	100	59	79	89	236	100	99	93	73	123
Ile	100	379	416	472	280	100	222	168	128	222
Leu	100	234	265	334	291	100	230	171	165	226
Asp	100	146	174	194	874	100	47	46	54	198
Glu	100	171	194	213	489	100	55	46	48	125
Met	100	92	76	50	195	100	203	163	131	153
His	100	566	936	696	1137	100	226	198	113	335
Phe	100	130	162	215	174	100	76	64	50	66
Arg	100	15	19	19	12883	100	108	81	101	492
Tyr	100	257	310	352	277	100	191	177	162	193
Trp	100	588	595	540	204	100	257	256	197	173
Asn	100	35	44	58	1211	100	37	35	40	593
Gln	100	41	51	77	1806	100	40	34	46	1157
Lys	100	49	41	72	525	100	159	108	142	573
GABA	100	101	102	127	291	100	90	71	72	205
SUMM	100	89	102	128	922	100	70	59	61	471
nrt2.4-1										
Ala	100	57	61	56	101	100	37	40	47	168
Ser	100	86	92	88	168	100	71	83	88	245
Pro	100	234	247	218	225	100	55	64	101	621
Val	100	181	197	166	220	100	82	95	94	203
Thr	100	71	80	62	187	100	64	74	67	109
Ile	100	398	440	285	260	100	134	155	136	264
Leu	100	283	281	235	319	100	140	159	174	303
Asp	100	78	89	65	206	100	42	52	51	172
Glu	100	103	113	86	167	100	36	41	44	99
Met	100	62	69	1	160	100	174	188	198	275
His	100	509	608	368	424	100	102	108	102	293
Phe	100	151	156	130	163	100	61	72	70	111
Arg	100	29	36	33	9523	100	79	103	122	359
Tyr	100	280	277	316	360	100	171	197	237	274
Trp	100	524	482	301	174	100	188	222	228	151
Asn	100	57	57	41	533	100	34	37	46	445
Gln	100	53	64	47	869	100	26	34	47	675
Lys	100	40	56	45	242	100	132	190	193	622
GABA	100	79	80	82	240	100	60	76	89	222
SUMM	100	85	94	74	436	100	46	55	63	340
nrt2.4-2										
Ala	100	67	43	54	81	100	50	50	40	172
Ser	100	76	55	59	137	100	65	52	48	147
Pro	100	116	95	99	133	100	95	57	97	244
Val	100	158	117	156	351	100	94	93	74	171
Thr	100	61	51	62	193	100	94	97	56	77
Ile	100	264	216	235	408	100	152	164	82	165
Leu	100	124	113	177	416	100	110	101	88	145
Asp	100	168	130	112	407	100	56	59	41	158
Glu	100	101	96	114	276	100	42	38	39	93
Met	100	1	0	2	167	100	131	93	86	110
His	100	784	711	491	763	100	212	245	74	224
Phe	100	117	106	130	337	100	59	44	46	61
Arg	100	24	22	27	11209	100	106	95	118	449
Tyr	100	175	183	274	613	100	125	121	95	121
Trp	100	380	329	328	320	100	280	216	155	142
Asn	100	53	44	51	1405	100	41	43	33	431
Gln	100	50	49	63	1620	100	39	39	51	1183
Lys	100	45	25	52	548	100	141	120	191	370
GABA	100	121	86	87	364	100	72	83	69	210
SUMM	100	85	73	85	698	100	61	60	53	390

FIGURE 4
Heat map of free amino acids levels in shoots and roots in *Arabidopsis thaliana* WT and *nrt2.4* ko mutants during N starvation. Seedlings were pre-grown on full NO_3^- (7 mM NO_3^-) medium. After two weeks, they grew for additional 10 d on different N-media: N-free (0 mM NO_3^-/0 mM Gln), N-low (0.25 mM NO_3^-/0.125 mM Gln) and N-complete (7mM NO_3^-/3.5 mM Gln). Amino acid profiles were identified 10 d after transfer. Data are given as the percentage of full NO_3^- (7 mM NO_3^-) medium; n = 3.

medium after 2 days and a 3.5-fold increase in 0.25 mM NO_3^- after 10 days (Figure 2A). While under no nitrate conditions, *NRT2.4* gene was transiently but already highly expressed after 2 d (Figure 2A), *NRT2.5* was induced as well but with a different kinetics, i.e. much higher after 10 d than after 2 d of nitrate deficiency (Figure 2B). Moreover, in contrast to *NRT2.4, NRT2.5* transcript expression was *per se* higher, showing a 5.5-fold increase on full Gln source and 355-fold increase on 0.25 mM NO_3^- after 10 days, compared with 7 mM NO_3^- (Figure 2B), supporting results by Lezhneva et al. (2014). Such expression of *NRT2.5* may explain why *nrt2.4* ko mutant plant can survive even under strong N-deficiency, suggesting that the missing *NRT2.4* could be compensated by other nitrate uptake systems and the mutant lines show similar growth performance (Figure 3). Analysis of *NRT2.5* gene expression in the *nrt2.4* ko-mutants supported this hypothesis, at least for *nrt2.4-1* (Figure 2C). However, we found a difference in *NRT2.5* transcript expression in the two *nrt2.4* ko-mutants: high *NRT2.5* expression in *nrt2.4-1* and a strongly reduced expression in *nrt2.4-2* (Figure 2C). It is tempting to speculate that the even further impaired N-supply in the *nrt2.4-2* mutant line could explain the particular difference in

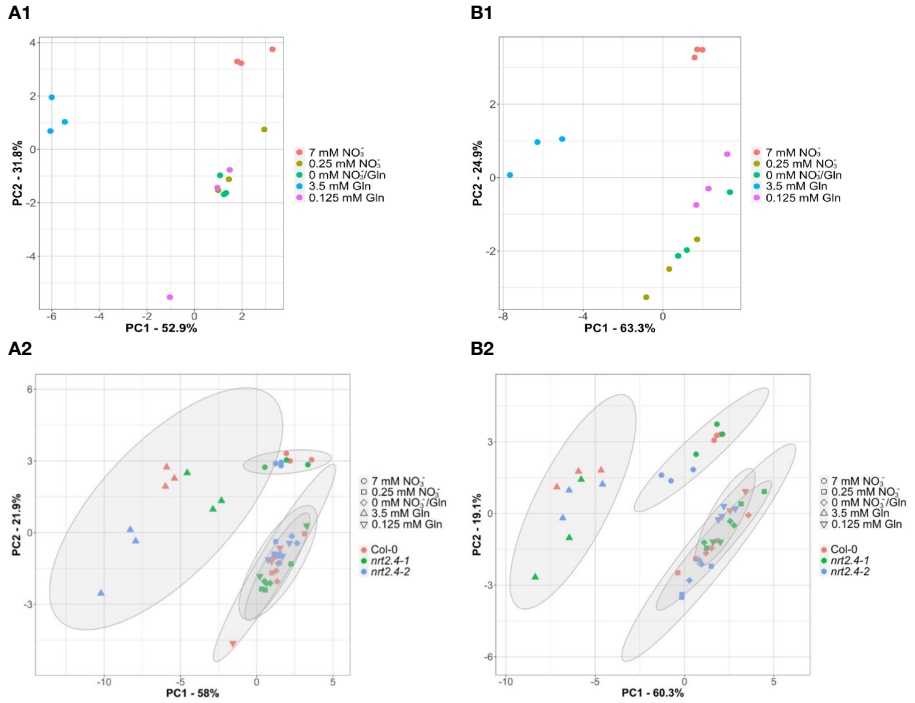

FIGURE 5
Principal component analyses (PCA) of free amino acid compositions in *Arabidopsis thaliana* shoots **(A)** and roots **(B)** during N starvation. The PCA score plot distinguishes the amino acid profiles of WT plants **(A1, B1)** or WT and mutant lines (Col-0; *nrt2.4-1; nrt2.4-2*) **(A2, B2)** grown under different treatments of N-starvation: N-free (0 mM NO_3^-/0 mM Gln), N-low (0.25 mM NO_3^-/0.125 mM Gln) and N-complete (7mM NO_3^-/3.5 mM Gln). **(A2, B2)** Amino acid profiles were separately analyzed after 10 d. The ellipses represent the multivariate normal distribution.

growth under low or no N-sources compared to *nrt2.4-1*. This can be seen in Figure 3 in the fresh weight of roots and shoots after 10 days of N deprivation.

Low exogenous Gln concentration (0.125 mM) as the only N-supply had similar effects on the AA pools as no or 0.25 mM NO_3^- (Figures 4, 5). As indicate by PCA, only the full N-sources (3.5 mM Gln, 7 mM NO_3^-) clustered differently, even from each other (Figure 5). This strongly suggests that low Gln concentrations have similar effects as comparable NO_3^- concentrations in contrast to higher Gln concentrations. Once the source of organic bound nitrogen is very high, the plants seemingly fill nitrogen stores. A particular strong and different effect on the AA pools was detected in WT and *nrt2.4* ko plants upon high Gln supply in both roots and even more pronounced in shoots (Figure 4; Supplementary Table S4). High exogenous Gln significantly increased the level of AAs containing two (Asn, Gln, Lys, Trp), three (His) or four (Arg) nitrogen in chemical structure in both shoots and roots suggesting a role of AA as N storage compounds (Figure 4). In particular Arg is also a precursor for the biosynthesis of oxidative stress-related NO production as well as for polyamines such as spermine, spermidine and putrescine. Various studies have demonstrated that polyamines are required for plant growth and development (Kawade et al., 2023).

Gln is the first nitrogen-containing organic compound, which is involved via transamination to generate other AAs. Root-to-shoot movement of AAs occurs in the xylem and xylem loading with Gln is known for a long time (Schobert and Komor, 1990). Gln and Arg are most abundant in the xylem sap, whereas all amino acids are transported through the phloem (Yao et al., 2020). Here, AA transporters of the AAP or LHT types might be involved (Guo et al., 2021). Another observation was the increase of minor AAs (e.g. Leu, Ile, Val, Pro, Tyr, Trp) when plant grew at low nitrogen (Figure 4). Not at least here, the question for the origin of these AAs raised, *de novo* or from protein degradation (Rhodes et al., 1986, Rhodes et al., 1987). A study of Huang and Jander (2017) demonstrated that in Arabidopsis abiotic stress, including nutrient deficiency was able to induce protein degradation and subsequently the accumulation of free AAs, in particular branched-chain amino acids (BCAAs). This protein degradation was depending on ABA. Moreover, it is suggested that nutrients such as nitrogen may function via a TOR-based pathway (Shi et al., 2018). For example, *Arabidopsis* seedlings overexpressing TOR are hyposensitive to high nitrate inhibition of roots. AAs may also activate TOR signaling pathways (Shi et al., 2018). Strikingly, ABA can repress TOR signaling by activation of SnRK2s, plant-specific serine/threonine kinases involved in response to abiotic stresses (Wang et al., 2018). Due to such findings, we chose an indirect approach and analyzed the ABA content in the different Arabidopsis lines and different nitrogen supply approaches (Figure S1). While in roots only minor changes in ABA contents were detectable, there was a clear increase of ABA in shoots upon growth on low nitrogen sources (Supplementary Figure S1B). These results suggest at least the involvement of protein degradation in shoots in particular in *nrt2.4-2* and supported by our finding of increase of BCAAs (Val, Ile, Leu) as well as of aromatic AAs (Tyr, Phe, Trp) (Figure 4; Supplementary Table S4). Huang and

Jander (2017) have found similar results upon nutrient deficiency. In order to find a clear explanation for the origin of the AAs that increased, more experiments with ^{15}N-labelled precursors of AAs synthesis should be performed (Rhodes et al., 1986; Rhodes et al., 1987). In addition, a connection between nitrogen deficiency, ABA and AAs increase, and TOR signaling is conceivable and needs further studies.

The reasons for the unexpected results concerning the affected *NRT2.5* expression in *nrt2.4-2* are not clear. From Kiba et al. (2012), it is known that both ko lines lack the *NRT2.4* transcript in RT-PCR. However, it is conceivable that due to the T-DNA insertion an unknown truncated protein is produced, which somehow affects *NRT2.5* gene expression. This could be a direct physical interaction as well as disturbance of regulatory processes. Since *NRT2.5* expression can be detected in *nrt2.4-1* plants but not in *nrt2.4-2*, it is more likely that only this latter mutant line has a side or off-target effect. Obviously, the additional effect on *NRT2.5* has more consequences for this particular plant line. Beside a slightly reduced growth (Figure 3) the content of various AAs in shoots is significantly different compared to WT and *nrt2.4-1* plants (Supplementary Table S4). For all these AAs, a higher level was detected in *nrt2.4-2* suggesting an impact on AA metabolism. This seems to be restricted to the shoots. Overall, but unfortunately beyond the scope of this study, it is necessary to find out the differences between the *nrt2.4-1* and *nrt2.4-2* mutant lines at the molecular level that cause their different nature.

Data availability statement

The original contributions presented in the study are included in the article/Supplementary Material. Further inquiries can be directed to the corresponding author.

Author contributions

NS: Conceptualization, Investigation, Methodology, Writing – original draft, Writing – review & editing. LZ: Formal analysis, Software, Visualization, Writing – review & editing. MR: Investigation, Writing – review & editing. VG: Data curation, Resources, Writing – review & editing. AM: Conceptualization, Funding acquisition, Supervision, Writing – original draft, Writing – review & editing.

Funding

The author(s) declare financial support was received for the research, authorship, and/or publication of this article. The VolkswagenStiftung (Funding for Refugee Scholars and Scientists from Ukraine; grant number A139316) supported NS with a fellowship; the International Max Planck Research School (IMPRS) supported LZ with a fellowship.

Acknowledgments

We thank Anne Krapp (Université Paris-Saclay, Institut Jean-Pierre Bourgin, Versailles, France) for providing the mutant lines, Andrea Lehr (MPI for Chemical Ecology, Jena) for technical support, and the MPI greenhouse team for growing plants. We moreover thank the VolkswagenStiftung and the Max Planck Society for supporting NS with a fellowship and the International Max Planck Research School (IMPRS) for supporting LZ.

Conflict of interest

The authors declare that the research was conducted in the absence of any commercial or financial relationships that could be construed as a potential conflict of interest.

Publisher's note

Supplementary material

The Supplementary Material for this article can be found online at: https://www.frontiersin.org/articles/10.3389/fpls.2024.1369543/full#supplementary-material

References

Alonso, J. M., Stepanova, A. N., Leisse, T. J., Kim, C. J., Chen, H., Shinn, P., et al. (2003). Genome-wide insertional mutagenesis of *Arabidopsis thaliana*. *Science* 301, 653–657. doi: 10.1126/science.1086391

Andrews, M., Raven, J. A., and Lea, P. J. (2013). Do plants need nitrate? The mechanisms by which nitrogen form affects plants. *Ann. Appl. Biol.* 163, 174–199. doi: 10.1111/aab.12045

Bonner, C. A., and Jensen, R. A. (1997). Recognition of specific patterns of amino acid inhibition of growth in higher plants, uncomplicated by glutamine-reversible 'general amino acid inhibition. *Plant Sci.* 130, 133–143. doi: 10.1016/S0168-9452(97)00213-6

Bonner, C. A., Williams, D., Aldrich, H. ,. C., and Jensen, R. A. (1996). Antagonism by L-glutamine of toxicity and growth inhibition caused by other amino acids in cell cultures of *Nicotiana silvestris*. *Plant Sci.* 113, 43–58. doi: 10.1016/0168-9452(95)04284-9

Chaput, V., Li, J., Séré, D., Tillard, P., Fizames, C., Moyano, T., et al. (2023). Characterization of the signalling pathways involved in the repression of root nitrate uptake by nitrate in *Arabidopsis thaliana*. *J. Exp. Bot.* 74, 4244–4258. doi: 10.1093/jxb/erad149

Chellamuthu, V. R., Ermilova, E., Lapina, T., Lüddecke, J., Minaeva, E., Herrmann, C., et al. (2014). A widespread glutamine-sensing mechanism in the plant kingdom. *Cell* 159, 1188–1199. doi: 10.1016/j.cell.2014.10.015

Crocoll, C., Mirza, N., Reichelt, M., Gershenzon, J., and Halkier, B. A. (2016). Optimization of engineered production of the glucoraphanin precursor dihomomethionine in *Nicotiana benthamiana*. *Front. Bioeng. Biotechnol.* 4. doi: 10.3389/fbioe.2016.00014

Dinkeloo, K., Boyd, S., and Pilot, G. (2018). Update on amino acid transporter functions and on possible amino acid sensing mechanisms in plants. *Semin. Cell Dev. Biol.* 74, 105–113. doi: 10.1016/j.semcdb.2017.07.010

El-Naggar, A., de Neergaard, A., El-Araby, A., and Høgh-Jensen, H. (2009). Simultaneous uptake of multiple amino acids by wheat. *J. Plant Nutr.* 32, 725–740. doi: 10.1080/01904160902787842

Fischer, W.-N., André, B., Rentsch, D., Krolkiewicz, S., Tegeder, M., Breitkreuz, K. E., et al. (1998). Amino acid transport in plants. *Trends Plant Sci.* 3, 188–195. doi: 10.1016/S1360-1385(98)01231-X

Forsbach, A., Schubert, D., Lechtenberg, B., Gils, M., and Schmidt, R. (2003). A comprehensive characterization of single-copy T-DNA insertions in the *Arabidopsis thaliana* genome. *Plant Mol. Biol.* 52, 161–176. doi: 10.1023/A:1023929630687

Forsum, O., Svennerstam, H., Ganeteg, U., and Näsholm, T. (2008). Capacities and constraints of amino acid utilization in Arabidopsis. *New Phytol.* 179, 1058–1069. doi: 10.1111/j.1469-8137.2008.02546.x

Gent, L., and Forde, B. G. (2017). How do plants sense their nitrogen status? *J. Exp. Bot.* 68, 2531–2539. doi: 10.1093/jxb/erx013

Gioseffi, E., de Neergaard, A., and Schjoerring, J. K. (2012). Interactions between uptake of amino acids and inorganic nitrogen in wheat plants. *Biogeosciences* 9, 1509–1518. doi: 10.5194/bg-9-1509-2012

Guo, N., Zhang, S., Gu, M., and Xu, G. (2021). Function, transport, and regulation of amino acids: What is missing in rice? *Crop J.* 9, 530–542. doi: 10.1016/j.cj.2021.04.002

Han, M., Xu, M., Wang, S., Wu, L., Sun, S., and Su, T. (2022). Effects of exogenous L-Glutamine as a sole nitrogen source on physiological characteristics and nitrogen use efficiency of poplar. *Plant Physiol. Biochem.* 172, 1–13. doi: 10.1016/j.plaphy.2021.12.032

Hao, D. L., Zhou, J. Y., Yang, S. Y., Qi, W., Yang, K. J., and Su, Y. H. (2020). Function and regulation of ammonium transporters in plants. *Int. J. Mol. Sci.* 21, 3557. doi: 10.3390/ijms21103557

Huang, T., and Jander, G. (2017). Abscisic acid-regulated protein degradation causes osmotic stress-induced accumulation of branched-chain amino acids in *Arabidopsis thaliana*. *Planta* 246, 737–747. doi: 10.1007/s00425-017-2727-3

Kan, C.-C., Chung, T.-Y., Juo, Y.-A., and Hsieh, M.-H. (2015). Glutamine rapidly induces the expression of key transcription factor genes involved in nitrogen and stress responses in rice roots. *BMC Genomics* 16, 731. doi: 10.1186/s12864-015-1892-7

Kawade, K., Tabeta, H., Ferjani, A., and Hirai, M. ,. Y. (2023). The roles of functional amino acids in plant growth and development. *Plant Cell Physiol.* 64, 1482–1493. doi: 10.1093/pcp/pcad071

Kiba, T., Feria-Bourrellier, A. B., Lafouge, F., Lezhneva, L., Boutet-Mercey, S., Orsel, M., et al. (2012). The Arabidopsis nitrate transporter NRT2. 4 plays a double role in roots and shoots of nitrogen-starved plants. *Plant Cell* 24, 245–258. doi: 10.1105/tpc.111.092221

Lardos, M., Marmagne, A., Bonadé Bottino, N., Caris, Q., Béal, B., Chardon, F., et al. (2024). Discovery of the biostimulant effect of asparagine and glutamine on plant growth in *Arabidopsis thaliana*. *Front. Plant Sci.* 14. doi: 10.3389/fpls.2023.1281495

Lee, K. T., Liao, H.-S., and Hsieh, M.-H. (2023). Glutamine metabolism, sensing and signaling in plants. *Plant Cell Physiol.* 64, 1466–1481. doi: 10.1093/pcp/pcad054

Lezhneva, L., Kiba, T., Feria-Bourrellier, A. B., Lafouge, F., Boutet-Mercey, S., Zoufan, P., et al. (2014). The Arabidopsis nitrate transporter NRT 2.5 plays a role in nitrate acquisition and remobilization in nitrogen-starved plants. *Plant J.* 80, 230–241. doi: 10.1111/tpj.12626

Liu, G., Ji., Y., Bhuiyan, N. H., Pilot, G., Selvaraj, G., Zou, J., et al. (2010). Amino acid homeostasis modulates salicylic acid–associated redox status and defense responses in Arabidopsis. *Plant Cell* 22, 3845–3863. doi: 10.1105/tpc.110.079392

Miller, A. J., Fan, X., Shen, Q., and Smith, S. J. (2008). Amino acids and nitrate as signals for the regulation of nitrogen acquisition. *J. Exp. Bot.* 59, 111–119. doi: 10.1093/jxb/erm208

Näsholm, T., Kielland, K., and Ganeteg, U. (2009). Uptake of organic nitrogen by plants. *New Phytol.* 182, 31–48. doi: 10.1111/j.1469-8137.2008.02751.x

Nazoa, P., Vidmar, J. J., Tranbarger, T. J., Mouline, K., Damiani, I., Tillard, P., et al. (2003). Regulation of the nitrate transporter gene AtNRT2.1 in *Arabidopsis thaliana*: responses to nitrate, amino acids and developmental stage. *Plant Mol. Biol.* 52, 689–703. doi: 10.1023/A:1024899808018

Noroozlo, Y. A., Souri, M. K., and Delshad, M. (2019). Stimulation effects of foliar applied glycine and glutamine amino acids on lettuce growth. *Open Agricult.* 4, 164–172. doi: 10.1515/opag-2019-0016

Okamoto, M., Vidmar, J. J., and Glass, A. D. (2003). Regulation of *NRT1* and *NRT2* gene families of *Arabidopsis thaliana*: Responses to nitrate provision. *Plant Cell Physiol.* 44, 304–317. doi: 10.1093/pcp/pcg036

Orsel, M., Filleur, S., Fraisier, V., and Daniel-Vedele, F. (2002). Nitrate transport in plants: which gene and which control? *J. Exp. Bot.* 53, 825–833. doi: 10.1093/jexbot/53.370.825

Ortiz-Lopez, A., Chang, H. C., and Bush, D. R. (2000). Amino acid transporters in plants. *Biochim. Biophys. Acta – Biomembr.* 1465), 275–280. doi: 10.1016/S0005-2736(00)00144-9

Pfaffl, M. W. (2001). A new mathematical model for relative quantification in real-time RT-PCR. *Nucleic Acids Res.* 29, e45. doi: 10.1093/nar/29.9.e45

R Core Team. (2018). R: A language and environment for statistical computing. Vienna, Austria: R Foundation for Statistical Computing. Available at: http://www.R-project.org/.

Rhodes, D., Deal, L., Haworth, P., Jamieson, G. C., Reuter, C. C., and Ericson, M. C. (1986). Amino acid metabolism of *Lemna minor* L. I. Responses to methionine sulfoximine. *Plant Physiol.* 82, 1057–1062. doi: 10.1104/pp.82.4.1057

Rhodes, D., Hogan, A. L., Deal, L., Jamieson, G. C., and Haworth, P. (1987). Amino acid metabolism of *Lemna minor* L. II. Responses to chlorsulfuron. *Plant Physiol.* 84, 775–780. doi: 10.1104/pp.84.3.775

Rognes, S. E., Wallsgrove, R. M., Kueh, J. S. H., and Bright, S. W. J. (1986). Effects of exogenous amino acids on growth and activity of four aspartate pathway enzymes in barley. *Plant Sci.* 43, 45–50. doi: 10.1016/0168-9452(86)90106-8

Schobert, C., and Komor, E. (1990). Transfer of amino acids and nitrate from roots into the xylem of *Ricinus communis* seedlings. *Planta* 181, 85–90. doi: 10.1007/BF00202328

Shi, L., Wu, Y., and Sheen, J. (2018). TOR signaling in plants: conservation and innovation. *Development* 145, dev160887. doi: 10.1242/dev.160887

Sivaguru, M., Pike, S., Gassmann, W., and Baskin, T. I. (2003). Aluminum rapidly depolymerizes cortical microtubules and depolarizes the plasma membrane: evidence that these responses are mediated by a glutamate receptor. *Plant Cell Physiol.* 44, 667–675. doi: 10.1093/pcp/pcg094

Svennerstam, H., Ganeteg, U., Bellini, C., and Näsholm, T. (2007). Comprehensive screening of Arabidopsis mutants suggests the lysine histidine transporter 1 to be involved in plant uptake of amino acids. *Plant Physiol.* 143, 1853–1860. doi: 10.1104/pp.106.092205

Svietlova, N., Reichelt, M., Zhyr, L., Majumder, M., Scholz, S. S., Grabe, V., et al. (2023). The beneficial fungus *Mortierella hyalina* modulates amino acid homeostasis in Arabidopsis under nitrogen starvation. *Int. J. Mol. Sci.* 24, 16128. doi: 10.3390/ijms242216128

Tegeder, M. (2012). Transporters for amino acids in plant cells: some functions and many unknowns. *Curr. Opin. Plant Biol.* 15, 315–321. doi: 10.1016/j.pbi.2012.02.001

Thornton, B. (2004). Inhibition of nitrate influx by glutamine in *Lolium perenne* depends upon the contribution of the HATS to the total influx. *J. Exp. Bot.* 55, 761–769. doi: 10.1093/jxb/erh066

Vidal, E. A., Alvarez, J. M., Araus, V., Riveras, E., Brooks, M. D., Krouk, G., et al. (2020). Nitrate in 2020: Thirty years from transport to signaling networks. *Plant Cell* 32, 2094–2119. doi: 10.1105/tpc.19.00748

Walch-Liu, P., Liu, L.-H., Remans, T., Tester, M., and Forde, B. G. (2006). Evidence that L-glutamate can act as an exogenous signal to modulate root growth and branching in *Arabidopsis thaliana*. *Plant Cell Physiol.* 47, 1045–1057. doi: 10.1093/pcp/pcj075

Wang, Y. Y., Hsu, P. K., and Tsay, Y. F. (2012). Uptake, allocation and signaling of nitrate. *Trends Plant Sci.* 17, 458–467. doi: 10.1016/j.tplants.2012.04.006

Wang, P., Zhao, Y., Li, Z., Hsu, C. C., Liu, X., Fu, L., et al. (2018). Reciprocal regulation of the TOR kinase and ABA receptor balances plant growth and stress response. *Mol. Cell* 69, 100–112.e6. doi: 10.1016/j.molcel.2017.12.002

Xuan, W., Beeckman, T., and Xu, G. (2017). Plant nitrogen nutrition: sensing and signaling. *Curr. Opin. Plant Biol.* 39, 57–65. doi: 10.1016/j.pbi.2017.05.010

Yao, X., Nie, J., Bai, R., and Sui, X. (2020). Amino acid transporters in plants: Identification and function. *Plants* 9, 972. doi: 10.3390/plants9080972

Zhuo, D., Okamoto, M., Vidmar, J. J., and Glass, A. D. (1999). Regulation of a putative high-affinity nitrate transporter (Nrt2;1At) in roots of *Arabidopsis thaliana*. *Plant J.* 17, 563–568. doi: 10.1046/j.1365-313X.1999.00396.x

Zoufan, P., and Shariati, M. (2009). The trend of HATS nitrate uptake in response to nitrate and glutamine in *Nicotiana plunbaginifolia* plant. *Res. J. Environ. Sci.* 3, 163–173. doi: 10.3923/rjes.2009.163.173

frontiers | Frontiers in Plant Science

TYPE Original Research
PUBLISHED 25 March 2024
DOI 10.3389/fpls.2024.1340336

OPEN ACCESS

EDITED BY
Néstor Fernández Del-Saz,
University of the Balearic Islands, Spain

REVIEWED BY
Jianlin Shen,
Chinese Academy of Sciences (CAS), China
Hanxi Wang,
Harbin Normal University, China
S.M. Mofijul Islam,
Bangladesh Rice Research Institute, Bangladesh

*CORRESPONDENCE
Zhen Zhang
zzhangal@scau.edu.cn;
zhangzhen_23102@163.com
Yongtao Li
yongtao@scau.edu.cn

†These authors have contributed equally to this work and share first authorship

RECEIVED 17 November 2023
ACCEPTED 08 March 2024
PUBLISHED 25 March 2024

CITATION
Chen T, Yang X, Zuo Z, Xu H, Yang X, Zheng X, He S, Wu X, Lin X, Li Y and Zhang Z (2024) Shallow wet irrigation reduces nitrogen leaching loss rate in paddy fields by microbial regulation and lowers rate of downward migration of leaching water: a ^{15}N-tracer study. *Front. Plant Sci.* 15:1340336. doi: 10.3389/fpls.2024.1340336

Shallow wet irrigation reduces nitrogen leaching loss rate in paddy fields by microbial regulation and lowers rate of downward migration of leaching water: a ^{15}N-tracer study

Tianyi Chen[1†], Xiaoming Yang[1†], Zheng Zuo[1], Huijuan Xu[1], Xingjian Yang[1], Xiangjian Zheng[1], Shuran He[2], Xin Wu[1], Xueming Lin[1], Yongtao Li[1*] and Zhen Zhang[1*]

[1]College of Natural Resources and Environment, Joint Institute for Environmental Research & Education, South China Agricultural University, Guangzhou, China, [2]College of Resources and Environment, Yunnan Agricultural University, Kunming, China

China consumes 35% of the world's fertilizer every year; however, most of the nitrogen fertilizers, which are essential for rice cultivation, are not used effectively. In this study, factors affecting the nitrogen leaching loss rate were studied in typical soil and rice varieties in South China. The effects of various irrigation measures on rice growth and nitrogen leaching loss were investigated by conducting experiments with eight groups. These groups included traditional irrigation (TI) and shallow wet irrigation (SWI). The TI is a common irrigation method for farmers in South China, maintaining a water layer of 5-8 cm depth. For SWI, after establishing a shallow water layer usually maintaining at 1-2 cm, paddy is irrigated when the field water level falls to a certain depth, then this process is then repeat as necessary. The nitrogen distribution characteristics were determined using ^{15}N isotope tracing. In addition, the effects of nitrification, denitrification, and microbial composition on soil nitrogen transformation at different depths were studied by microbial functional gene quantification and high-throughput sequencing. The results revealed that in the SWI groups, the total nitrogen leaching loss rate reduced by 0.3-0.8% and the nitrogen use efficiency (NUE) increased by 2.18-4.43% compared with those in the TI groups. After the ^{15}N-labeled nitrogen fertilizer was applied, the main pathways of nitrogen were found to be related to plant absorption and nitrogen residues. Furthermore, paddy soil ammonia-oxidizing archaea were more effective than ammonia-oxidizing bacteria for soil ammonia oxidation by SWI groups. The SWI measures increased the relative abundance of *Firmicutes* in paddy soil, enhancing the ability of rice to fix nitrogen to produce ammonium nitrogen, thus reducing the dependence of rice on chemical fertilizers. Moreover, SWI enhanced the relative abundance of *nirS* and *nosZ* genes within surface soil bacteria, thereby promoting denitrification in the surface soil of paddy fields. SWI

also promoted ammonia oxidation and denitrification by increasing the abundance and activity of *Proteobacteria*, *Nitrospirae*, and *Bacteroidetes*. Collectively, SWI effectively reduced the nitrogen leaching loss rate and increase NUE.

KEYWORDS

shallow wet irrigation, soil nitrogen transformation, nitrogen leaching loss, ^{15}N isotope tracer technique, microbial composition and function

1 Introduction

China, as one of the major rice-producing countries, accounts for one-fifth of the rice planting area and one-third of the rice production globally (Zhuang et al., 2019). Nitrogen fertilizers play a crucial role in rice cultivation. However, excessive irrigation can lead to low fertilizer use efficiency, and crops can only use 30%-40% of nitrogen fertilizers. About 50% of the applied nitrogen is lost to the environment due to ammonia volatilization, denitrification, runoff, and leaching. This situation has resulted in a range of serious environmental problems, such as soil acidification (Guo et al., 2010), groundwater pollution (Zhang et al., 2017), water eutrophication (Zhao et al., 2014, 2016), and air pollution (Wang et al., 2018; Cheng et al., 2021). Owing to the different water requirements of crops in each growth period, farmland irrigation water control can save water and improve crop quality and yield. The increasing studies related to the water-saving irrigation techniques have investigated grain yield, nitrogen use efficiency (NUE), denitrification, N_2O and NO gas emissions derived from fertilizer and water regimes. Islam et al. (2018b) reported that the urea deep placement (UDP) increased grain yields by 13% during the Aman season. Qi et al. (2020) found that the water-saving irrigation techniques can increase rice yield by reducing total infiltration water. Some studies found that the combination alternate wetting and drying (AWD) irrigation and UDP drastically reduced N losses and increases NUE (Gaihre et al., 2015; Islam et al., 2018a, Islam et al., 2018b). Several studies have demonstrated that water-saving irrigation techniques can significantly decrease nitrogen emissions and leaching loss in paddy fields (Mao, 2002; Peng et al., 2011, 2012; Tan et al., 2013; Qi et al., 2020). Some studies reported that the combination AWD and UDP reduced ammonia volatilization and N_2O emissions (Gaihre et al., 2015, 2018; Islam et al., 2018a). Shallow wet irrigation (SWI) is also a water-saving irrigation technology, and whether the use of SWI can reduce nitrogen loss and improve NUE. Additionally, nitrogen loss in paddy fields is influenced by microbial regulation. Therefore, it is necessary to understand the distribution, diversity, and abundance of microbial communities under SWI conditions, which can provide insights into microorganisms involved in nitrification in agricultural ecosystems.

Previous research indicated that nitrogen loss in paddy fields was regulated by soil microorganisms. Liu et al. (2020) found that irrigation greatly affected bacterial diversity. Das et al. (2016) reported that flooding might affect the composition and activity of rhizosphere microorganisms, consequently influencing the formation and accumulation of nitrogen forms in both rhizosphere soil and pore water. Soil aerobic conditions are important factors in determining the abundance of ammonia-oxidizing bacteria (AOB). Xu et al. (2020) found that dry-wet alternations increased soil oxygen content and further increased AOB abundance, which directly affected soil nitrification. Nitrification is the reaction of ammonia being converted into nitrite, which is in turn converted into nitrate by soil microorganisms; it is the dominant process of the soil nitrogen cycle. These processes of the nitrogen cycle are intricately connected to nitrogen loss. Compared with traditional irrigation methods, SWI treatment can provide better aerobic conditions for paddy soils. Whether SWI treatment can also increase the abundance of AOB, thereby reducing nitrogen loss in paddy fields. Meanwhile, understanding the response mechanisms of microbial communities to irrigation practices is vital for effectively preventing and controlling nitrogen loss.

In South China, the paddy growing season aligns with the summer rainy season, with an average annual precipitation of more than 1000 mm. Thus, runoff and leaching are the main processes of nitrogen loss (Chen et al., 2022). Currently, numerous studies have examined nitrogen runoff loss in paddy fields of South China (Ding et al., 2016; Issaka et al., 2019; Zeng et al., 2021). In our previous study, we found a 31.7% reduction in nitrogen loss from paddy field runoff in the SWI groups compared to that in the traditional irrigation (TI) groups (Zeng et al., 2021). However, limited studies are available on nitrogen leaching loss from paddy fields in South China. Paddy is a submerged crop, and leaching is one of the main ways of nitrogen loss. Owing to the limited number of studies in South China, quantifying the amount of leaching is difficult. Therefore, in the present study, we used a farmland underground leaching water collection device to conduct experiments with the following aims: (i) to monitor the effects of SWI measures on rice growth and nitrogen leaching loss; (ii) to analyze the mechanisms of nitrogen transport, distribution, and loss using ^{15}N isotope tracing; and (iii) to analyze the effects of microbial colony structures and functional gene compositions on soil nitrogen transformation using molecular biotechnology. In this study, the leaching loss of nitrogen in paddy was quantified. We believe that

this study provides a scientific basis and data to reduce the risk of nitrogen loss in paddy fields.

2 Materials and methods

2.1 Experimental site and soil characteristics

The experimental site was located at the South China Agricultural University, Guangzhou, Guangdong Province, China (23°15'N, 113°35'E). The South China Agricultural University is in the South China area. And this area is a densely populated and intensively farm region with a high cropping index (i.e., the average number of annual crop seasons). The experimental soil used was acid red soil, with a depth of 0 cm to 60 cm, which is a typical soil type in South China (Zeng et al., 2021). The topsoil had the following physicochemical characteristics: bulk density of 1.26 $g{\cdot}cm^{-3}$, soil pH of 5.83, soil organic matter of 15.49 $g{\cdot}kg^{-1}$, total phosphorus of 0.16 $g{\cdot}kg^{-1}$, and total nitrogen (TN) of 1.05 $g{\cdot}kg^{-1}$, with alkali-hydrolyzed nitrogen of 35.16 $g{\cdot}kg^{-1}$.

2.2 Experimental device

The experimental device used to collect underground leaching water from the farmland included a soil column tube, rainproof cover, and leaching collection box (Figure 1). The experiment is a pot experiment and its device is made of 5mm thick PVC material. The specific size of the device has been given in Supplementary Data (Supplementary Figure S1). The rainproof cover was equipped with a through-hole corresponding to the soil column tube, and the lower end of the soil column tube was connected to the leaching collection box. There was a dense hole partition between the soil column tube and the leaching collection box. The bottom of the leaching collection box was connected to a base, and the side wall of the leaching collection box was equipped with leaching sampling valves. At least two depth sampling valves were installed on the side wall of the soil column tube. During sampling, the depth sampling valves at different depths were opened, and syringes were used to collect water samples at different depths of the leachate. The leaching sampling valve was opened, and a measuring cylinder was used to quantitatively collect the leaching water. During rice plant growth, flooding in the soil column tube was controlled by switching the field control valve to set different flooding depths and moisture patterns.

2.3 Experiment design

The experiment was set up with eight treatment groups according to two irrigation patterns (TI and SWI) and four nitrogen fertilizer application rates (0%, 40%, 70%, and 100%) with three replicates for each treatment group. The experimental fertilizers application rate was based on the recommended fertilizers application rate of Guangdong Province testing soil for formulated fertilization. The application rates of N, P and K fertilizers were 148, 67, 114 $kg{\cdot}ha^{-1}$, respectively. The treatment groups were set at 0, 40, 70, and 100 in accordance with 0%, 40%, 70%, and 100% of the TN fertilizer applied to the individual units, respectively. The urea concentration used was 10 atoms% ^{15}N labeled urea. The amount of phosphate and potassium fertilizers applied was uniform for all the treatment groups. The specific experimental settings were shown in Table 1. The base fertilizer was applied to the rice seedlings before transplanting, the surface soil (0 cm -10 cm) was mixed thoroughly with minimal disturbance of the soil after fertilizer application. The tiller fertilizer was applied at the rice tillering stage to supply the required nutrients for late tillering and nodulation. The spike fertilizer was applied at the rice spike stage to supply nutrients required for flowering, fruiting, and fruit ripening. The tiller fertilizer and spike fertilizer were dissolved with 50 mL of pure water during application, and evenly applied to the surface soil.

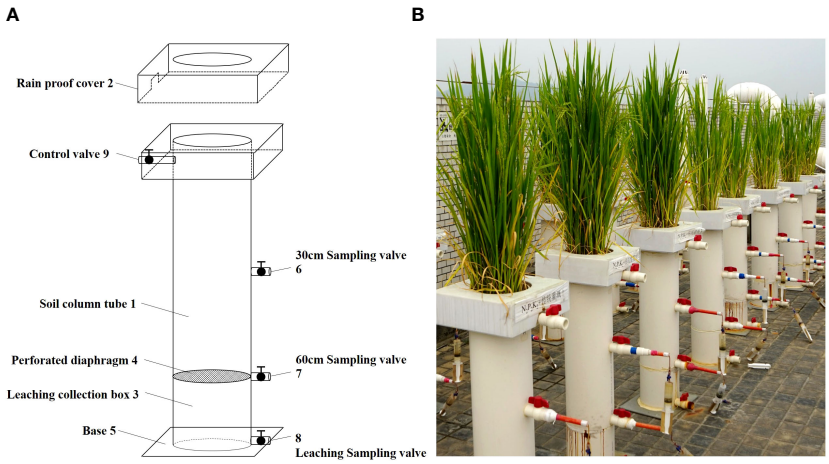

FIGURE 1
Schematic diagram of experimental device for collecting underground leaching water from farmland [**(A)** is design drawing and **(B)** is physical drawings].

10.3389/fpls.2024.1340336

TABLE 1 Experimental agricultural treatment design.

Treatment	Fertilizer application			Irrigation pattern
	N ($kg·ha^{-1}$)	P ($kg·ha^{-1}$)	K ($kg·ha^{-1}$)	
TI [a]-0	0	0	0	Conventional
TI-40	59	67	114	Conventional
TI-70	104	67	114	Conventional
TI-100	148	67	114	Conventional
SWI [b]-0	0	0	0	Shallow-Wet
SWI-40	59	67	114	Shallow-Wet
SWI-70	104	67	114	Shallow-Wet
SWI-100	148	67	114	Shallow-Wet

[a]TI refers to traditional irrigation group.
[b]SWI refers to shallow wet irrigation.

During the planting period, flooding in the installation was observed daily and supplemented according to the appropriate flooding conditions for SWI and TI. The water level of the TI treatment was supplemented to 8 cm when it fell below 5 cm, and a water level of 1 cm -2 cm was maintained for the SWI treatment.

2.4 Sample collection and analysis

2.4.1 Water sample collection and analysis

The method of collecting and preserving leaching water samples is shown in Supplementary Table S1. The leaching water was sampled regularly every week, kept separately, and labeled according to sampling time and depth. The measured water data were recorded according to time.

The TN concentration of the collected samples was determined using a Unico UV-2800 (Unicoi Systems, Atlanta, GA, USA) spectrophotometer after performing potassium peroxodisulfate digestion. The concentrations of NH_4^+-N and $NO_{3-}-N$ were analyzed using a continuous-flow analyzer (Skalar, Breda, the Netherlands).

$$V = \sum(V_i) \tag{1}$$

where V denotes the leaching volume of a single device (L) and V_i denotes the leaching volume of a single device in I sampling duration (L).

$$V_L = \frac{V}{R_t \times R_s} \times 10^{-3} \tag{2}$$

where V_L denotes the volume of leaching loss ($t·hm^{-2}·yr^{-1}$); R_t refers to the planting time accounts for a proportion of the year, and R_s denotes the proportion of area per hectare of a single device.

$$NLV_i = \frac{\sum C_{Ni}}{V} \times 10^{-3} \tag{3}$$

where NLV_i represents the concentration of TN in leaching (g), and C_{Ni} denotes the concentration of TN in leaching of a single device in I sample duration ($mg·L^{-1}$).

$$NLL = \frac{NLV_1 - NLV_2}{W_N} \times 100 \tag{4}$$

where NLL denotes the loss rate of TN through leaching (%); NLV_i and NLV_0 refer to NLV of N applied and N without applied, respectively, and W_N denotes the amount of N applied.

2.4.2 Soil and plant sample collection and analysis

The whole rice growth period was divided into three soil sampling periods as follows: before the application of the tiller fertilizer, before the application of the spike fertilizer, and before harvest. Soil samples were sampled at 3-5 points using soil sampling tubes and then mixed and bagged. The samples were stored separately according to sampling depth and were categorized as wet and dry. Soil samples that needed to be air-dried were stored in a cool and ventilated place after natural air-drying, whereas fresh soil was stored at -80°C. Plant samples were collected only at harvest time. Further, plant samples from each device were cut flush, measured for wet weight, dried in a 70°C oven, cooled, weighed for dry weight, and finally crushed, ground, and stored in bags.

The TN content of soil was analyzed using the Kjeldahl method, and the nitrogen contents of both the soil and plant samples were measured using an elemental analyzer (Vario MICRO cube, Elementar, Germany). The alkali-hydrolyzed nitrogen content of soil was analyzed using the alkaline hydrolysis method. The NH_4^+-N and $NO_{3-}-N$ concentrations were analyzed using a continuous-flow analyzer (Skalar, Breda, the Netherlands) (Wang D. et al., 2021). The nitrogen content of the plant samples was measured using an elemental analyzer (Vario MICRO cube, Elementar, Germany).

2.4.3 Isotope abundance determination

The atom% ^{15}N abundance was analyzed using a stable isotope mass spectrometer (IsoPrime 100, Elementar, Germany). The proportion of the isotopes to the fertilizer (Ndff) was calculated based on the natural abundance of isotopes, and the Plant ^{15}N use efficiency, Soil ^{15}N residue rate, ^{15}N leaching loss rate are calculated with reference to the method of Wang D. et al. (2017) and Li P. et al. (2018). The background of ^{15}N abundance in soil was 0.368 atom%. *Ndff* was calculated as follows:

$$Ndff(\%) = \frac{a-b}{c-d} \times 100 \tag{5}$$

where a is atom% ^{15}N abundance in the plant/soil/water samples, b is atom% ^{15}N abundance in the control plant/soil/water samples, c is atom% ^{15}N abundance of the fertilizer, and d is natural atom% ^{15}N abundance (0.368 atom% ^{15}N).

Plant ^{15}N use efficiency was calculated as follows:

$$\text{Plant } ^{15}\text{N use efficiency}(\%) = \frac{Ndff \times e_p \times W_p}{f} \times 100 \tag{6}$$

where e_p is the ^{15}N concentration of the plant (%), W_p is plant dry weight (g), and f is the amount of fertilizer (g).

Soil ^{15}N residue rate was calculated as follows:

$$\text{Soil } ^{15}\text{N residue rate } (\%) = \frac{Ndff \times e_s \times W_s}{f} \times 100 \quad (7)$$

where e_s is the ^{15}N concentration of plant (%), and W_s is the soil dry weight (g).

^{15}N leaching loss was calculated as follows:

$$^{15}\text{N leaching loss rate } (\%) = \frac{Ndff \times e_L \times W_L}{f} \times 100 \quad (8)$$

where e_L is the ^{15}N concentration of leaching (%), and W_L is the leaching weight (g).

2.4.4 High-throughput sequencing and functional gene quantification of soil microorganisms

The genomic DNA was extracted from the soil using the FastDNA® SPIN Kit for Soil (MP Biomedicals, CA, USA). The concentration of DNA was measured using a NanoDrop2000 spectrophotometer. Polymerase chain reaction (PCR) of the rRNA gene was conducted using the universal 16S rRNA primers (338F: ACTCCTACGGGAGGCAGCAG and 806R: GGACTACHVGGGTWTCTAAT). The 16s raw data were deposited in the National Center for Biotechnology Information (NCBI) Sequence Reads Archive (SRA) (accession number: PRJNA1087108). The resulting product was detected using 2% agarose gel electrophoresis. The PCR product was purified and quantified using the Quantus™ Fluorometer and AxyPrep DNA Gel Extraction Kit, respectively. The DNA library was built using the NEXTFLEX Rapid DNA-Seq Kit and sequenced using the Miseq PE300 platform (Illumina, California, USA). The original sequencing sequence was subjected to quality control using Trimmomatic software. The sequences were clustered into operational taxonomic units (OTU) using UPARSE software (version 7.1 http://drive5.com/uparse/) based on 97% similarity. Chimeras were removed from the dataset using UCHIME software. Species classification annotations were assigned to each sequence using RDP classifiers. The alignment threshold was set to 70% based on the Silva database (SSU128).

Functional gene quantitative primer information and amplification system conditions for bacteria and archaea are shown in Supplementary Tables S2 and S3. Genomic DNA was extracted using the Magnetic Bead Method Soil and Fecal Genomic DNA Extraction Kit. After the genomic DNA was photographed in a gel imaging analyzer using Beijing Liuyi DYY-6C at a concentration of 1%, a voltage of 120 V, and an electrophoresis time of 20 min, the DNA concentration and purity were detected using Thermo NANo DROP8000. The standard quality granules were provided by Wuhan Tianyi Huiyuan Biotechnology Co., Ltd. and diluted 10-fold to obtain six concentration gradients of 1E9, 1E8, 1E7, 1E6, 1E5, 1E4, and 1E3, and the reactions were prepared using qPCR96Well and SYBR® Select Master Mix (2X) kits, with each sample analyzed in triplicate.

The samples were quantified on an Applied Biosystems StepOnePlusTM Real-Time System and Bio-Rad CFX96 Real-Time System, and the same primers and conditions were applied according to the standard curve for quantitative PCR 3-well detection. A 96-well plate with standard mass pellets was used as a positive control for error correction, and no template control (NTC)was used as a negative control. The test results were analyzed usin StepOne v2.3 and BioRadCFXManager software. Refer to the research of Liu et al. (2022) and Man et al. (2022), the relative abundance of functional genes was calculated as:

$$\text{Relative abundance of bacteria } amoA \text{ genes} = \frac{\text{Bacterial } amoA \text{ gene copy numbers}}{\text{Bacterial 16S gene copy numbers}} \quad (9)$$

$$\text{Relative abundance of archaeal } amoA \text{ genes} = \frac{\text{Archaeal } amoA \text{ gene copy numbers}}{\text{Archaeal 16S gene copy numbers}} \quad (10)$$

$$\text{Relative abundance of bacteria } nirS \text{ genes} = \frac{\text{Bacterial } nirS \text{ gene copy numbers}}{\text{Bacterial 16S gene copy numbers}} \quad (11)$$

$$\text{Relative abundance of bacteria } nosZ \text{ genes} = \frac{\text{Archaeal } nosZ \text{ gene copy numbers}}{\text{Bacterial 16S gene copy numbers}} \quad (12)$$

2.4.5 Statistical analysis

All experiments were conducted in triplicate, and the data were presented as the arithmetic mean values. Statistical analysis was conducted using SPSS statistics version 20.0. The experimental data were plotted using Origin 2022 software. In each case, the data were statistically analyzed using a one-way analysis of variance, with the minimum level of significance set at $p < 0.05$.

3 Results

3.1 Physicochemical properties of soil and rice plants

The changes of soil nitrogen content at different depths of rice under different treatments were shown in Figure 2. The ammonium nitrogen content under TI treatment was significantly higher than that under SWI treatment at different growth stages and depths ($p<0.05$, Figures 2A, B). The changes of soil ammonium nitrogen content in 30-60 cm depth soil layers of paddy under different irrigation measures were similar to those in 0-30 cm depth. Overall, nitrate nitrogen content is higher in 0-30 cm depth soil layers than in 30-60 cm depth. During the same fertilization period, the nitrate

nitrogen content of the SWI treatment was higher than that of the TI treatment ($p<0.05$, Figures 2C, D). The alkali-hydrolyzed nitrogen content of SWI treatment was significantly higher than that of TI treatment ($p<0.05$, Figures 2E, F). Under two different soil depths, with the increase of N fertilizer application in the treatment group, the contents of ammonia nitrogen, nitrate nitrogen and alkali-hydrolyzed nitrogen in soil will also increase. The soil nitrogen content after basal and tillering in the treatments of SWI-40, SWI-70, and SWI-100 were significantly higher than that of other treatments($p<0.05$). The peak value of soil nitrogen content was SWI-70 treatment in 0-30 cm depth soil (0.09%) during panicle (Figures 2G, H).

The physicochemical properties of rice plants under different treatments were shown in Table 2. The growth differences of paddy in different treatment groups were shown in Supplementary Figure S2. Compared with TI treatment, SWI treatment could increase rice yield, seed setting rate and plant nitrogen content. The nitrogen content of plants was significantly increased with high nitrogen fertilizer application of SWI-70 and SWI-100 ($p<0.05$).

3.2 Leaching loss concentration and loss volume

The dynamic changes of rice leaching nitrogen concentration under different irrigation measures were shown in Figure 3. The increase of fertilization rate can increase the concentration of leaching total nitrogen loss. The SW-100 and TI-100 treatment had the highest concentrations of leached total nitrogen, which were 1.30-5.41 $mg{\cdot}L^{-1}$ and 1.89-5.25 $mg{\cdot}L^{-1}$. The effect of each fertilization on the total nitrogen concentration in 30-60 cm depth soil layers was less abrupt than in 0-30 cm depth, and the concentration of total nitrogen increased first and then decreased slowly with the growth of rice (Figures 3A, B).

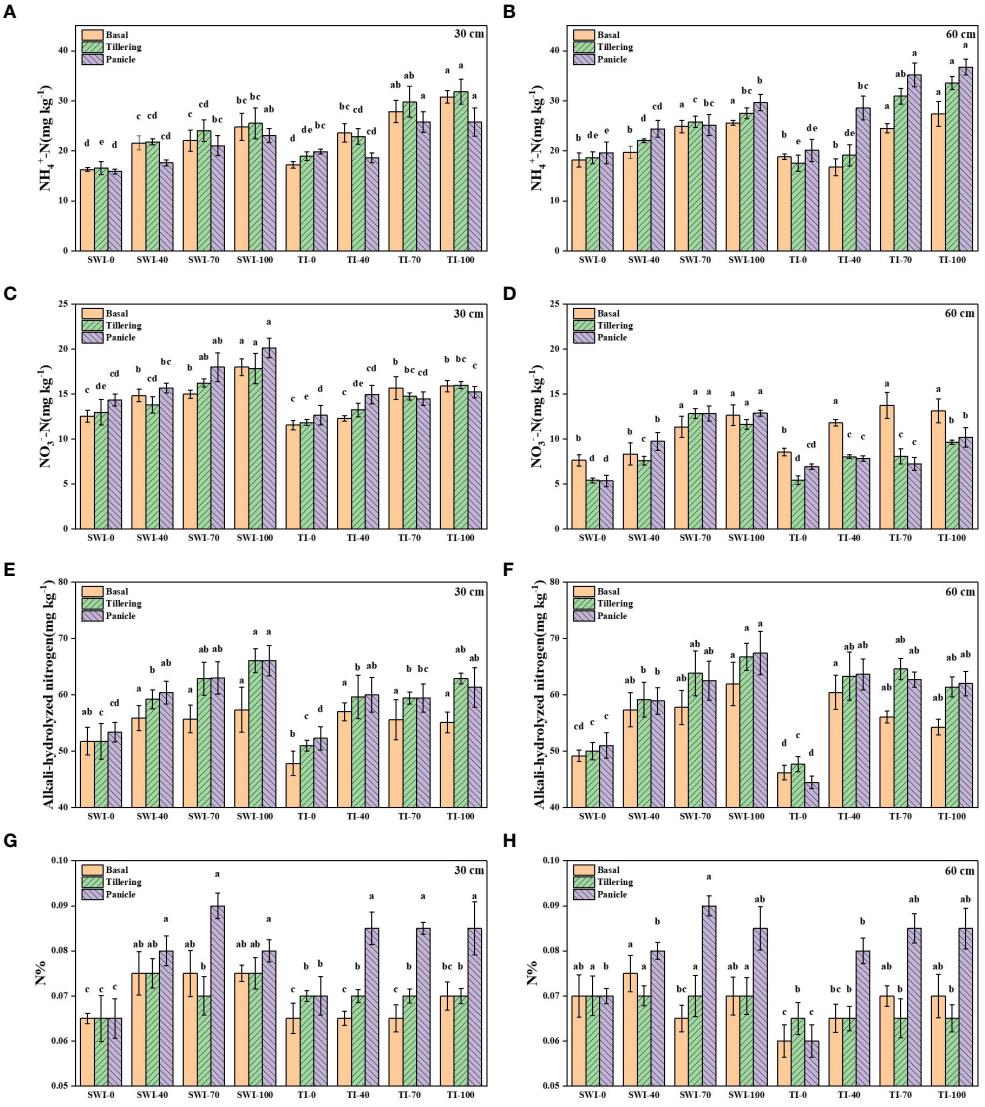

FIGURE 2
The contents of NH_4^+-N **(A, B)**, NO_3^--N **(C, D)**, alkali-hydrolyzed nitrogen **(E, F)** and nitrogen contents **(G, H)** in 0–30 cm and 30–60 cm soil layers of rice under different treatments. Means within the same item followed by different letters are significantly different (LSD, $p < 0.05$).

TABLE 2 Physicochemical properties of rice plants under different treatments.

Treatment	Plant height (cm)	Grain yield (g)	Straw yield (g)	Seed-setting rate (%)	Nitrogen content (%)
TI [a]-0	86.91 ± 1.81c	6.21 ± 0.94d	19.06 ± 1.50d	65.50 ± 1.50de	0.92 ± 0.03c
TI-40	91.02 ± 1.88bc	15.37 ± 2.77cd	46.17 ± 4.96c	70.00 ± 1.75d	0.96 ± 0.04c
TI-70	102.61 ± 2.44ab	42.91 ± 5.84b	67.76 ± 3.41b	81.50 ± 1.40c	1.02 ± 0.08bc
TI-100	104.38 ± 5.64a	75.61 ± 7.18a	88.06 ± 5.23a	85.00 ± 1.50ab	1.16 ± 0.02a
SWI [b]-0	91.34 ± 2.85bc	5.68 ± 0.34d	19.34 ± 0.66d	64.00 ± 1.00e	0.95 ± 0.01c
SWI-40	93.85 ± 2.44b	18.64 ± 2.67c	45.52 ± 2.04c	68.00 ± 3.25de	1.22 ± 0.09a
SWI-70	101.14 ± 3.61ab	45.15 ± 4.85b	68.77 ± 5.41b	82.25 ± 2.50bc	1.11 ± 0.01ab
SWI-100	105.61 ± 3.11a	76.41 ± 5.81a	94.45 ± 8.75a	88.00 ± 0.75a	1.14 ± 0.00a

[a]TI refers to traditional irrigation group.
[b]SWI refers to shallow wet irrigation group.
Means (n = 3) within a column followed by different letters are significantly different (LSD, $p < 0.05$).

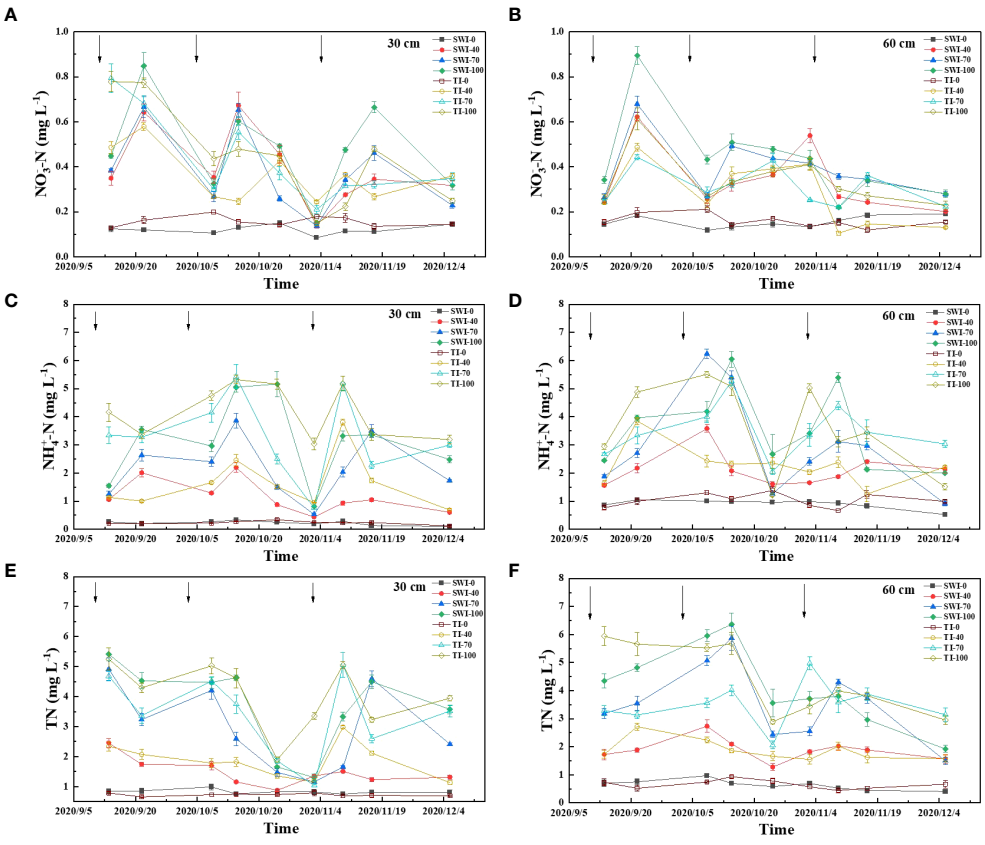

FIGURE 3
Dynamics of leached NO_3^--N **(A, B)**, NH_4^+-N **(C, D)** and TN **(E, F)** concentrations in rice under different water fertilizer management practices (Arrows represent fertilization).

The concentration of leached ammonium nitrogen was similar to that of total nitrogen, and the main form of soil nitrogen leaching was ammonium nitrogen (Figures 3C, D). The leaching ammonium nitrogen concentration responded quickly to the three nitrogen fertilizer applications and had a large range. The TI-100 and TI-70 were the most obvious treatments with concentrations ranging from 3.04-5.32 mg·L^{-1} and 0.76-5.42 mg·L^{-1}. The content of leaching nitrate in each treatment was significantly lower than that of ammonium nitrogen, and the content of leaching nitrate in each treatment fluctuatingly decreased with the growth period (Figures 3E, F).

The changes of total nitrogen loss in leaching (Equation 3) of rice under different treatments are shown in Figure 4. At the same time, the leaching loss volume of SWI treatment was significantly lower

than that of TI treatment (Equations 1, 2; $p<0.05$, Supplementary Figure S3). The total nitrogen leaching loss rate (Equation 4) of each treatment was 4.60-6.32%, and the TI-100 and TI-70 were the highest treatments. Compared with the TI treatment, although the total leaching nitrogen concentration of SWI treatment was slightly higher than that of TI treatment, the total nitrogen leaching loss of SWI treatment was significantly lower. Therefore, the total nitrogen loss rate of SWI treatment was low, indicating that SWI treatment could effectively reduce nitrogen loss.

3.3 Distribution of ^{15}N in the soil-plant-water system after fertilization

The residue and leaching loss rate of ^{15}N labeled nitrogen fertilizer in rice soil under different treatments is shown in Figure 5. After the basal, the soil nitrogen residue rate of SWI treatment decreased with the increase of fertilizer rate, while that of TI was the opposite. After the tillering and panicle, the nitrogen residue rate of SWI treatment (Equations 5, 7) in 0-30 cm depth soil layers was increased (Figure 5A). After the panicle, the SWI-100 was the treatment with the highest residue rate, reaching 38.25%. Analyzing the soil nitrogen residue rate in two depth soil layers, it was found that nitrogen fertilizer in the SWI treatment was more likely to accumulate in 0-30 cm depth soil layers, while nitrogen fertilizer in the TI treatment was similar at two depths soil layers (Figures 5A, B).

On the whole, the leaching loss rate of nitrogen fertilizer in 30-60 cm depth soil layers (1.06-4.63%) under TI treatment was higher than that in 0-30 cm depth (0.99-2.95%). Increasing the nitrogen fertilizer application rate has a tendency to widen the gap between the leaching loss rate (Equations 5, 8) of nitrogen fertilizer in the two depths. However, compared with TI treatment, the difference in the leaching loss rate of nitrogen fertilizer in the SWI treatment was lower between the two depths (Figure 5C). From Figure 5D, it can be seen that the fertilizer NUE (Equations 5, 6) of each treatment ranged from 19.28-28.50%, with the peak value of SWI-70 treatment. Under different irrigation measures, the fertilizer NUE with 70% nitrogen application rate was the highest. Compared with TI treatment, the SWI treatment could increase the NUE by 2.18-4.43% under the same nitrogen application rate.

3.4 Changes in soil microbial communities

The diversity index analysis of soil bacterial communities in each treatment was shown in Supplementary Table S4. The Chao1 and ACE indices of the 0-30 cm depth soil in the SWI groups were greater than those of the 30-60 cm depth soil, indicating that the microbial community richness of the 0-30 cm depth soil in the SWI groups was higher than that of the 30-60 cm depth soil. The Shannon index of the SWI groups was generally smaller than that of the TI groups, and the Shannon index of the 0-30 cm depth soil was generally smaller than that of the 30-60 cm depth soil. The Simpson index was higher in the SW-0 group compared to that in the TI-0 group, whereas the other SW groups showed lower Simpson indices than the TI groups. Therefore, the SWI measures enhanced both the homogeneity of soil microorganisms and the diversity of soil microbial communities.

High-throughput sequencing of soil microorganisms was used to analyze the microbial community at the phylum level. (Figure 6A). In the relative abundance of *Proteobacteria*, the vast majority of the 0-30 cm depth soil was higher than that in the 30-60 cm depth soil, with the SWI-100 groups demonstrating the highest relative abundance (25.47%). The SWI groups exhibited a higher relative abundance of *Firmicutes* than the TI groups. Changes in the microbial community at the genus level are shown in Figure 6B. In the SWI-0 and SWI-100 groups, the relative abundance of *Bacillus*, *Clostridium*, and *Anaeromyxobacter* was higher compared to those in the TI-0 and TI-100 groups.

The redundancy analysis (RDA) revealed (Figure 6C) that the differences between the bacterial communities of soils at the two depths in the SWI groups were greater. At the 0-30 cm depth, the bacterial communities showed a positive correlation with the soil nitrate content and a negative correlation with the soil alkaline and ammonium nitrogen content, while the opposite trend was observed at the 30-60 cm depth. This indicated that the form of nitrogen in the soil at different depths were related to soil microbial communities. Differences in soil microbial communities at the 0-30 cm depth were closely related to nitrogen forms. This indicated that the fate of nitrogen in the paddy soil was closely linked to the microbial communities in the surface soil. The SWI measures could promote this phenomenon.

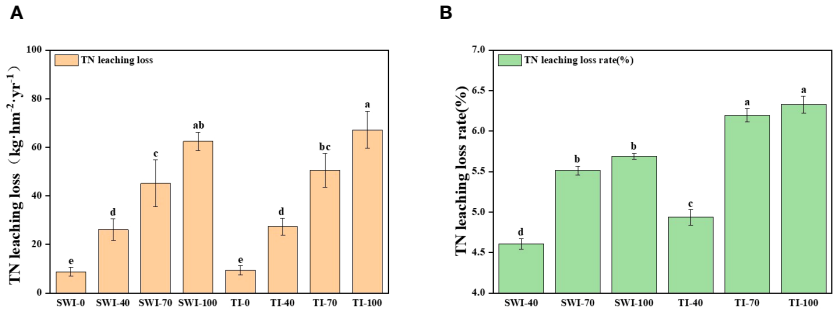

FIGURE 4
Changes in the amount **(A)** and rate **(B)** of total nitrogen loss from rice leaching under different treatments.

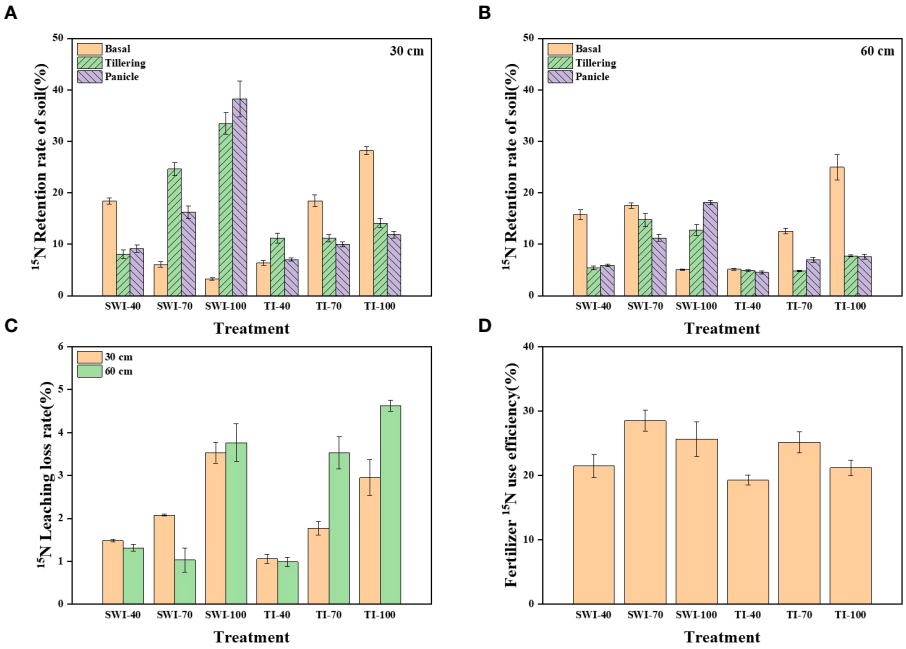

FIGURE 5
(A) Residual rate of ^{15}N-labeled nitrogen fertilizer in rice 0-30 cm soil layer under different treatments; **(B)** Residual rate of ^{15}N-labeled nitrogen fertilizer in 30-60 cm soil layer; **(C)** ^{15}N leaching loss rate of rice nitrogen fertilizer under different treatments; **(D)** NUE of ^{15}N-labeled nitrogen fertilizer under different treatments.

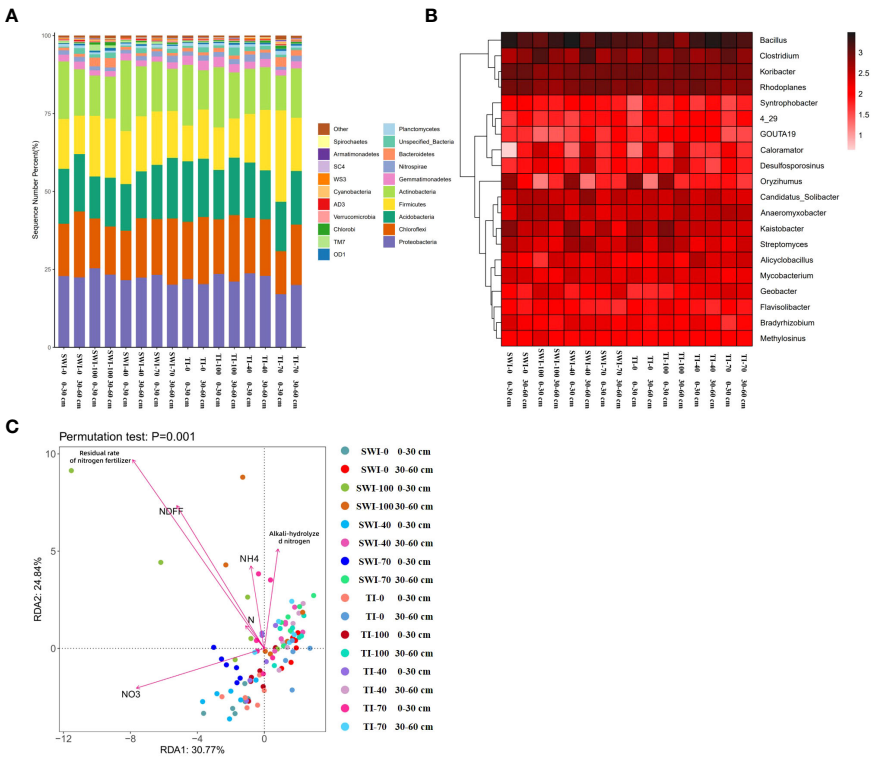

FIGURE 6
(A) Relative abundance composition of bacterial communities in each treatment group based on phylum levels; **(B)** Relative abundance composition of bacterial communities in each treatment group based on genus level; **(C)** Redundancy analysis (RDA) of NH_4^+-N, NO_{3-} – N, alkali-hydrolyzed nitrogen, nitrogen content (N%), Ndff and nitrogen fertilizer residual rate under different irrigation and fertilization treatment conditions.

10.3389/fpls.2024.1340336

3.5 Changes in the soil microbial functional gene abundance

Figure 7 shows the results of soil microbial functional gene abundance determination. The 16S gene copy numbers of soil bacteria and archaea at the 0-30 cm depth were larger than those at the 30-60 cm depth. The 16S gene copy numbers of soil bacteria were 1-2 orders of magnitude larger than that of archaea. This indicated that the surface or rhizosphere soil exhibits the most concentrated distribution of soil microorganisms. The analysis of the abundance of soil ammonia-oxidizing microbial functional genes showed that the relative abundance of the bacterial *amoA* gene in the SWI groups was significantly higher than that in the TI groups (Equation 9). After fertilization with the tiller fertilizer, the relative abundances of the *amoA* gene in the 0-30 cm and 30-60 cm depth soils were 4.30×10^{-4} and 6.07×10^{-4}, respectively, in the SWI-100 groups. After the fertilization of the panicle fertilizer, the relative abundance of the soil bacterial *amoA* gene in the SWI

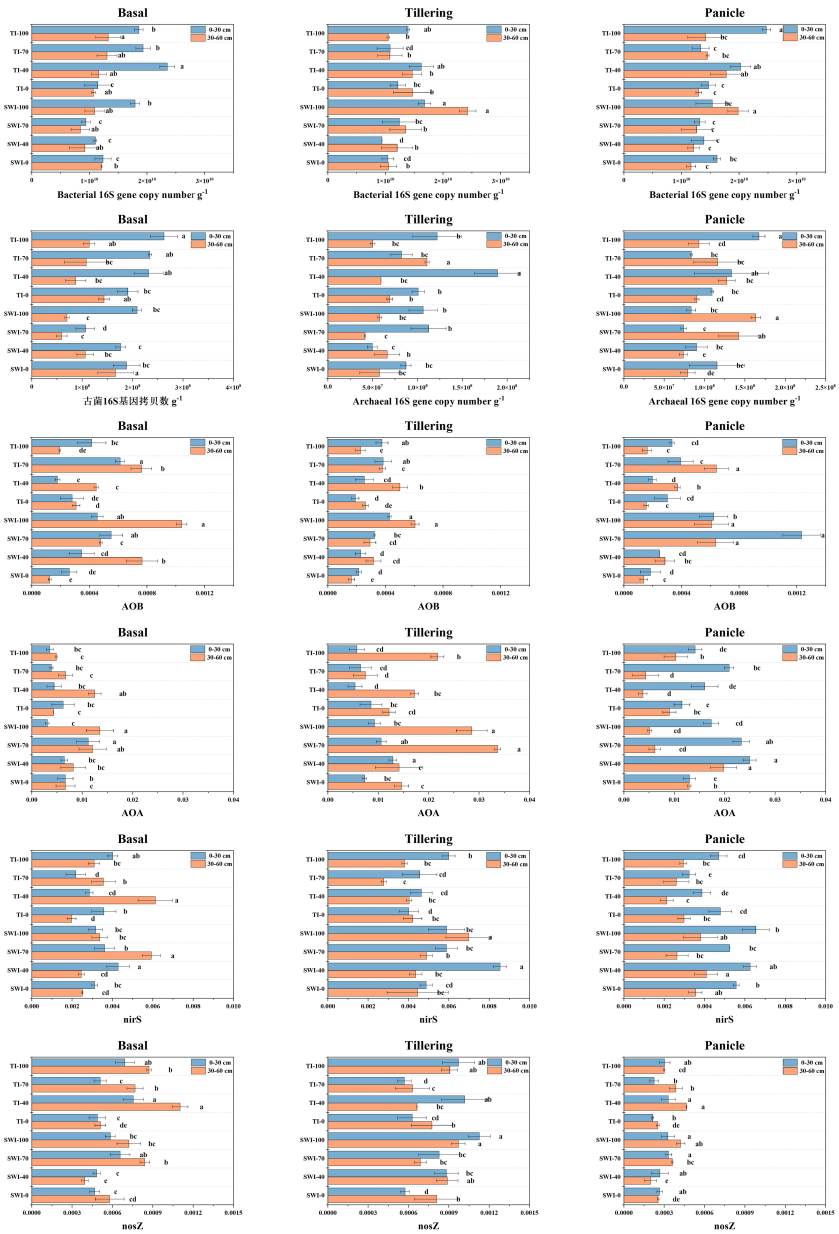

FIGURE 7
Changes in the copy number of soil bacteria 16S gene, copy number of soil archaea 16S gene, relative abundance of soil bacteria amoA gene, relative abundance of soil archaea amoA gene, relative abundance of soil bacteria *nirS* and *nosZ* gene at 0-30 cm and 30-60 cm soil in three reproductive periods.

groups was significantly higher compared to the TI groups. The relative abundance of soil archaea genes (Equation 10) was approximately ten times higher compared to that of the bacterial *amoA* gene.

The analysis of soil denitrifying bacterial functional genes showed that there was a higher relative abundance of the soil bacterial *nirS* gene in the SWI groups than that in the TI groups (Equation 11). After each fertilization, the relative abundance of the soil bacterial *nirS* gene in the SWI groups increased, whereas that in the TI groups decreased during the later stage of rice growth. The SWI measure resulted in an increase in the relative abundance of the bacterial *nirS* gene both in the surface soil and in the deep soil during the middle stage of rice growth in paddy fields.

4 Discussion

4.1 Changes in physical and chemical properties of soils and rice plants

In this study, the SWI treatment increased the NO_3^--N content and decreased the NH_4^+-N content of the paddy soil. These findings align with the research conducted by Wang and Huang (2021) on nitrogen content in paddy soils under water-saving irrigation practices. Soil ammonium nitrogen and nitrate nitrogen tended to migrate to deep soil; however, the migration rate of ammonium nitrogen was slower than that of nitrate nitrogen. Soil ammonium nitrogen was prone to adsorption onto soil colloidal particles, leading to its slower migration, whereas ammonium nitrogen converted into nitrate nitrogen was easier to move with water (Wang et al., 2019). After the application of nitrogen fertilizer, SWI measure can slightly increase the content of alkali-hydrolyzable nitrogen and soil nitrogen in paddy soil, indicating that reducing irrigation water will increase the content of soil organic matter and alkali-hydrolyzable nitrogen (Ma, 2018), and the increase is positively correlated with the amount of fertilizer applied.

The SWI treatment and increasing nitrogen fertilizer application rate could increase rice yield, seed setting rate and nitrogen content, but had little effect on the increase of rice plant height. This is similar to the research of Islam et al. (2016) that studying the alternate wetting and drying irrigation increased grain yield by 16%. The leaf size, tillering number and heading status of rice with 70% nitrogen application rate were significantly better than those with 40% nitrogen application rate. Postponing and reducing the application of nitrogen fertilizer can reduce the rate of nitrogen transfer in leaves, delay leaf senescence, and lead to high nitrogen accumulation in rice (Ye et al., 2013).

4.2 Dynamic changes in leaching loss concentration and loss volume

The leaching TN concentration of the SWI-100 treatment groups was found to be higher compared to that of the TI-100 treatment groups, which might be because of less water input and less dilution of nitrogen under SWI. The leaching NH_4^+-N concentration of the SWI-100 treatment groups was lower than that of the TI-100 treatment groups, which might be because of the reduction of the surface soil under TI. This hindered the nitrification of NH_4^+-N, and the applied urea was more easily converted and accumulated into NH_4^+-N (Valerie et al., 2023). Simultaneously, there was a posterior shift in the peak concentration of leaching NH_4^+-N in the SWI treatment groups. NH_4^+-N may be easily adsorbed by soil colloids, resulting in a slower rate of migration. Moreover, the leaching effect of the SWI treatment was weaker than that of the TI treatment, resulting in a slower downward migration of NH_4^+-N with gravity water. The predominant form of nitrogen leaching loss in paddy fields was NH_4^+-N, with a significantly higher concentration than NO_3^--N. This was consistent with the findings of Ji et al. (2011), which indicated that NH_4^+-N was the primary form of nitrogen leaching loss, constituting 39.70% of the TN loss. Root uptake is the main way for rice to absorb nitrogen (Yang et al., 2023). Zhang et al. (2016) found that rice roots had a strong preference for NH_4^+-N absorption. Supplying NH_4^+-N fertilizers to ammonium-loving crops can improve the NUE of paddy and supplying both NH_4^+-N and NO_3^--N can promote nitrogen absorption and root growth (Dong et al., 2023). Therefore, controlling moisture in paddy fields can slow down the rate of nitrogen leaching. Simultaneously, fertilizer-converted nitrogen remained in the soil of rice roots for a longer time during downward migration, promoting more forms of nitrogen to be absorbed by the plants and thus limiting nitrogen leaching losses.

The TN leaching losses in the SWI-100 and TI-100 treatment groups were 62.45 and 67.21 $kg{\cdot}hm^{-2}{\cdot}yr^{-1}$, respectively. Compared with the TI treatment groups, the SWI groups could reduce leaching water in the paddy field. This is similar to the study of Qi et al. (2020), which showed that dry-wet alternations significantly reduced leaching water by 21.90%. SWI reduced the amount of leaching loss by 3.0-15%, thereby reducing the TN leaching loss by 5.0-11% and the TN leaching loss rate by 0.30-0.80%. Therefore, SWI may be an effective method to reduce nitrogen leaching in paddy fields.

4.3 Distribution of ^{15}N in the soil-plant-water system after fertilization

Figure 8 shows the nitrogen flow trend of paddy fields with ^{15}N nitrogen fertilizer. Plant uptake (19.28-28.50%) and soil nitrogen residue were the main destinations of nitrogen fertilizer. SWI treatment could increase NUE by 2.18-4.43% under the same nitrogen application rate. Under the same irrigation measures, the NUE of 70% nitrogen application rate was the highest, which was 28.50%. Too high or too low nitrogen application rate would reduce the NUE, which was similar to the result that Zhang et al. (2012) found that the ^{15}N-labeled NUE of rice plants was 26-30%. The accumulation of nitrogen fertilizer in soil under SWI treatment mainly occurred in the middle and late stages of rice growth (after the application of tillering or panicle), while TI treatment mainly occurred in the early stage of rice growth (after the application of

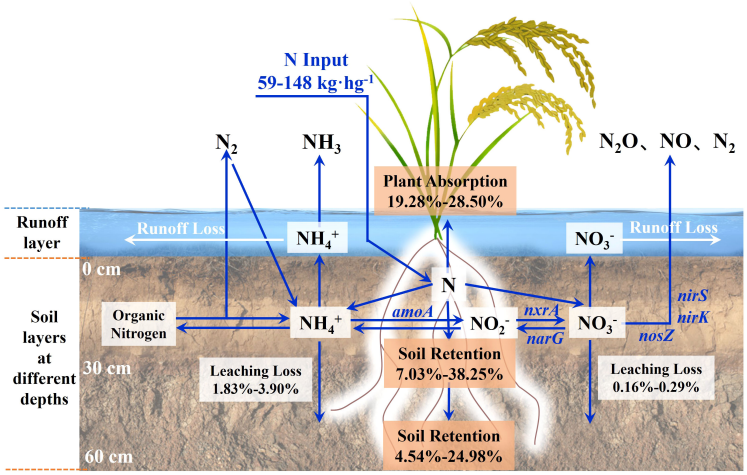

FIGURE 8
Nitrogen fate of ^{15}N-labeled nitrogen fertilizer.

basal), which is consistent with previous studies. Li G. et al. (2018) found that 10.30-36.40% of the basal remained in paddy soil. The leaching loss of nitrogen in various forms accounted for only 1.31-4.63% of nitrogen fertilizer. This was similar to that of many previous studies, such as the studies of Ji et al. (2011); Peng et al. (2011); Zhang et al. (2017); Han et al. (2021), and their leaching loss rates of nitrogen fertilizer were 3.50-5.40%, 3.50-5.40%, 1.40-6.40% and 0.66-2.28%, respectively. It was due to the high rainfall, low soil organic matter content and large surface runoff in South China (Zeng et al., 2021), which leads to the low rate of nitrogen fertilizer leaching. With the increase of nitrogen fertilizer application, the nitrogen leaching loss rate also showed an increasing trend, which was similar to the previous study (Shen et al., 2022; Zhang et al., 2021). This is also similar to the result of total nitrogen leaching loss in Section 3.2, indicating that appropriately reducing the nitrogen application rate in agricultural production can effectively reduce the risk of nitrogen leaching loss in paddy fields. Nitrogen fertilizer from SWI treatment is more likely to accumulate in 0-30 cm depth soil layers, which is the same as the finding of Zhang et al. (2012). Increasing the fertilization rate could significantly increase the nitrogen residue rate in 0-30 cm depth soil layers under SWI treatment and in 30-60 cm depth soil layers under TI treatment. The difference verifies that SWI treatment can effectively reduce soil nitrogen leaching loss in paddy fields.

4.4 Effects of different fertilization measures on soil bacterial community composition

The SWI measures enhanced both the homogeneity of soil microorganisms and the diversity of soil microbial communities (Supplementary Table S4). The SWI measures could increase the relative abundance of *Proteobacteria* in the surface soil. Kowalchuk and Stephen (2001) found that the first step of the nitrification process, that is, the oxidation of ammonia to nitrite was the limiting step in the cycle. This stage was usually carried out by AOB of *β-Proteobacteria* and *γ-Proteobacteria* (Schleper et al., 2005). The SWI increased the relative abundance of *Firmicutes* in the paddy soil. Additionally, *Firmicutes* were found to have the ability to fix nitrogen and produce a large amount of ammonium nitrogen during rice growth (Wang J. et al., 2017). This may complement the relatively low NH_4^+-N content in the paddy soil and water under SWI measures, reducing the dependence of rice on chemical fertilizers, and thereby increasing the NUE. Among them, Mevel and Prieur (2000) found that *Bacillus* could improve heterotrophic nitrification activity under aerobic conditions. Simultaneously, *Clostridium* and *Anaeromyxobacter* could promote nitrogen fixation under anaerobic conditions (Masuda et al., 2020; Han et al., 2021). The relative abundance of *Nitrospirae* in 0-30 cm soils was smaller than that in 30-60 cm soils under SWI treatment. Previous studies have found that the *Comammox Nitrospira* strain can oxidize ammonium nitrogen to nitrate (Daims et al., 2015). This may be the reason for the smaller ^{15}N leaching loss rate of 0-30 cm than 30-60 cm soil under SWI treatment. Therefore, the SWI treatment could enhance the NUE of paddy by increasing the relative abundance of microbial communities such as *Bacillus*, *Clostridium*, and *Anaeromyxobacter*.

4.5 Effects of different fertilization measures on microbial functional gene abundance

Ammonia-oxidizing archaea (AOA) in the paddy soil may exert a greater effect on soil ammonia oxidation than that exerted by AOB. It was found that the number of AOA in the soil could be up to 3000 times that of AOB (Leininger et al., 2006; He et al., 2007; Shen et al., 2008). This indicated that AOA was the dominant ammonia-oxidizing microorganism in the soil compared to AOB. The relative abundance of AOA and AOB in the SWI groups was higher compared to that in the TI groups during the growth and

development of paddy. Additionally, SWI measures were found to increase the NO_3^--N content in both the soil and leaching water (Sections 3.1 and 3.2). The increase of AOA and AOB in the SWI groups promoted the soil nitrification process, thereby increasing NO_3^--N content. The abundances of AOA and AOB during the middle and later stages of paddy planting were higher compared to those during the early stage. This indicated that nitrification is stronger during the middle and late stages of paddy planting, and that NH_4^+-N converted by urea was more easily converted into NO_3^--N. The relative abundance of the *nosZ* gene (Equation 12) was lower than that of the *nirS* gene, which may lead to the activity of NO_2^- reduction to NO, which was higher than that of N_2O reduction to N_2.

4.6 Fate of ^{15}N in the soil-plant-water system and environmental implication

In this study, the amount of nitrogen fertilizers applied to plants, soil, and leaching loss in the paddy field system was tracked by adding ^{15}N-labeled urea. Figure 8 shows the fate of ^{15}N in the soil-plant-water system after fertilization. It was found that plant absorption and soil residue were the main pathways of the nitrogen fertilizers. The same results were described in Section 3.4. The SWI measures increased the relative abundance of *Firmicutes* in the paddy soil, thereby increasing the ability of nitrogen fixation to produce ammonium nitrogen. Simultaneously, the relative abundances of *Bacillus*, *Clostridium*, and *Anaeromyxobacter* in the paddy soil were increased by SWI measures. *Bacillus* could improve heterotrophic nitrification activity under aerobic conditions (Mevel and Prieur, 2000). *Clostridium* and *Anaeromyxobacter* could promote nitrogen fixation under anaerobic conditions (Masuda et al., 2020; Han et al., 2021). This indicated that the SWI measures could effectively increase the NUE of paddy. Nutrients dissolved in water flow into groundwater as the paddy field is vertically leached. The SWI treatment reduced the amount of leaching water by reducing the amount of irrigation water while ensuring the yield, thereby reducing the loss of nitrogen. This improved the NUE and reduced the risk of non-point source pollution.

During the middle and late stages of rice growth, the SWI groups resulted in higher abundance of AOA and AOB. Therefore, the nitrification was more intense in the SWI group. At this time, the ammonium nitrogen converted from urea is more easily converted to nitrate nitrogen through nitrification. The nitrogen leaching loss in paddy fields is mainly caused by ammonium nitrogen (Figure 7). Thus, the SWI measures can effectively reduce the nitrogen leaching loss in paddy fields by controlling ammonium nitrogen.

5 Conclusions

The main conclusions of this paper are as follows:

- The SWI treatment promoted the absorption of nitrogen fertilizer by rice through increasing the NO_3^--N content in red soil and inhibiting the migration of nitrogen. Further experiments revealed that SWI treatment increased the relative abundance of *Firmicutes* in the paddy red soil, which were found to be capable of fixing nitrogen and producing ammonium nitrogen during rice growth. This may complement the NH_4^+-N content for paddy under SWI treatment.
- In South China with red soil as the main soil type, the SWI treatment could reduce the leaching loss rate of nitrogen fertilizer in the deep soil by 0.30-0.80% and improve the NUE by 2.18-4.43%. Nitrogen fertilizer from SWI treatment tend to accumulate in the surface layer (0-30 cm) of the soil. Plant absorption and nitrogen fertilizer residue were the main pathways of nitrogen fertilizer. After applying the ^{15}N-labeled nitrogen fertilizer to the paddy soil, plant absorption accounted for 19.28-28.50% of the nitrogen fertilizer, whereas the leaching loss of each form of the nitrogen fertilizer only accounted for 1.31-4.63%.
- The SWI measure can enhance nitrification and promote nitrate nitrogen accumulation and ammonium nitrogen transformation in red soil. The SWI measure and nitrogen fertilizer application increased the relative abundance of *nirS* and *nosZ* genes and promoted denitrification in the surface red soil of paddy. The SWI measures promoted ammonia oxidation and denitrification through the promotion of *Proteobacteria*, *Nitrospirae*, and *Bacteroidetes* abundance and activity. Compared to AOB, AOA in the paddy soil might have a greater effect on soil ammonia oxidation.

The outcomes from this study are expected to advance the understanding the nitrogen transformation and microbial regulation mechanisms in paddy field systems under different water and fertilizer management conditions. However, limitations still exist in (i) the lack of studying gaseous nitrogen loss in paddy fields; (ii) the absence of data to deeper analysis that the soil moisture content is consistent with the same treatment. Therefore, further studies are needed to quantify the gaseous loss and fate of nitrogen fertilizers throughout the paddy system. At the same time, soil-water potential data and water depth data throughout the crop-growing season need to be analyzed to eliminate the influence of soil moisture content on different irrigational measures.

Data availability statement

The 16S raw data were deposited in the National Center for Biotechnology Information (NCBI) Sequence Reads Archive (SRA) (accession number: PRJNA1087108).

Author contributions

TYC: Data curation, Formal analysis, Writing – original draft, Writing – review & editing. XMY: Data curation, Investigation, Visualization, Writing – review & editing. ZZu: Data curation,

Investigation, Visualization, Writing – review & editing. HJX: Writing – review & editing, Investigation. XJY: Investigation, Writing – review & editing. XJZ: Investigation, Writing – review & editing. SRH: Investigation, Writing – review & editing. XW: Investigation, Writing – review & editing. XML: Investigation, Writing – review & editing. YTL: Conceptualization, Funding acquisition, Methodology, Resources, Supervision, Writing – review & editing. ZZh: Conceptualization, Funding acquisition, Methodology, Resources, Supervision, Writing – review & editing.

Funding

The author(s) declare that financial support was received for the research, authorship, and/or publication of this article. This work was supported by the National Natural Science Foundation of China (grant number 42077359), National Key Research and Development Program of China (No. 2023YFD1901305), Guangdong Provincial Key R&D Program (grant number 2023B0202030001), and Science and Technology Planning Project of Guangzhou (202201010505).

Conflict of interest

The authors declare that the research was conducted in the absence of any commercial or financial relationships that could be construed as a potential conflict of interest.

Publisher's note

Supplementary material

The Supplementary Material for this article can be found online at: https://www.frontiersin.org/articles/10.3389/fpls.2024.1340336/full#supplementary-material

References

Chen, K., Yu, S. E., Ma, T., Ding, J., He, P., Dai, Y., et al. (2022). Effects of water and nitrogen management on water productivity, nitrogen use efficiency and leaching loss in rice paddies. *Water* 14, 1596. doi: 10.3390/w14101596

Cheng, Y., Zhang, H., Chen, Z., Wang, J., Cai, Z., Sun, N., et al. (2021). Contrasting effects of different pH-raising materials on N_2O emissions in acidic upland soils. *Eur. J. Soil Sci.* 72, 432–445. doi: 10.1111/ejss.12964

Daims, H., Lebedeva, E. V., Pjevac, P., Han, P., Herbold, C., Albertsen, M., et al. (2015). Complete nitrification by Nitrospira bacteria. *Nature* 528, 504. doi: 10.1038/nature16461

Das, S., Chou, M., Jean, J., Liu, C., and Yang, H. (2016). Water management impacts on arsenic behavior and rhizosphere bacterial communities and activities in a rice agro-ecosystem. *Sci. Total Environ.* 542, 642–652. doi: 10.1016/j.scitotenv.2015.10.122

Ding, J., Jiang, Y., Liu, Q., Hou, Z., Liao, J., Fu, L., et al. (2016). Influences of the land use pattern on water quality in low-order streams of the Dongjiang River basin, China: A multi-scale analysis. *Sci. Total Environ.* 551-552, 205–216. doi: 10.1016/j.scitotenv.2016.01.162

Dong, Y., Sun, C., and Dong, Q. (2023). Effects of different ratios of ammonium and nitrate fertilizers on rice seedling quality and soil nutrient changes. *Southwest Agric. J.* 36, 2183–2190. doi: 10.16213/j.cnki.scjas.2023.10.014

Gaihre, Y. K., Singh, U., Islam, S. M. M., Huda, A., Islam, M. R., Satter, M. A., et al. (2015). Impacts of urea deep placement on nitrous oxide and nitric oxide emissions from rice fields in Bangladesh. *Geoderma* 259-260, 370–379. doi: 10.1016/j.geoderma.2015.06.001

Gaihre, Y. K., Singh, U., Islam, S. M. M., Huda, A., Islam, M. R., Sanabria, J., et al. (2018). Nitrous oxide and nitric oxide emissions and nitrogen use efficiency as affected by nitrogen placement in lowland rice fields. *Nutr. Cyc. Agroecosys.* 110, 277–291. doi: 10.1007/s10705-017-9897-z

Guo, H., Liu, J., Zhang, Y., Shen, J., Han, X., Zhang, W., et al. (2010). Significant acidification in major Chinese croplands. *Science* 5968), 1008–1010. doi: 10.1126/science.1182570

Han, H., Gao, R., Cui, Y., and Gu, S. (2021). Transport and transformation of water and nitrogen under different irrigation modes and urea application regimes in paddy fields. *Agric. Water Manage.* 255, 107024. doi: 10.1016/j.agwat.2021.107024

He, J., Shen, J., Zhang, L., Zhu, Y., Zheng, Y., Xu, M., et al. (2007). Quantitative analyses of the abundance and composition of ammonia-oxidizing bacteria and ammonia-oxidizing archaea of a Chinese upland red soil under long-term fertilization practices. *Environ. Microbiol.* 9, 2364–2374. doi: 10.1111/j.1462-2920.2007.01358.x

Islam, S. M. M., Gaihre, Y. K., Biswas, J. C., Jahan, M. S., Singh, U., Adhikary, S., et al. (2018a). Different nitrogen rates and methods of application for dry season rice cultivation with alternate wetting and drying irrigation: Fate of nitrogen and grain yield. *Agric. Water Manage.* 196, 144–153. doi: 10.1016/j.agwat.2017.11.002

Islam, S. M. M., Gaihre, Y. K., Biswas, J. C., Singh, U., Ahmed, M. N., Sanabria, J., et al. (2018b). Nitrous oxide and nitric oxide emissions from lowland rice cultivation with urea deep placement and alternate wetting and drying irrigation. *Sci. Rep.* 8 (1), 1–10. doi: 10.1038/s41598-018-35939-7

Islam, S. M. M., Gaihre, Y. K., Shah, A. L., Singh, U., Sarkar, M. I. U., Satte, M. A., et al. (2016). Rice yields and nitrogen use efficiency with different fertilizers and water management under intensive lowland rice cropping systems in Bangladesh. *Nutr. Cycl. Agroecosys.* 106, 143–156. doi: 10.1007/s10705-016-9795-9

Issaka, F., Zhang, Z., Zhao, Z., Asenso, E., Li, J., Li, Y.-T., et al. (2019). Sustainable conservation tillage improves soil nutrients and reduces nitrogen and phosphorous losses in maize farmland in Southern China. *Sustainability* 11, 2397. doi: 10.3390/su11082397

Ji, X., Zheng, S., Shi, L., and Liu, Z. (2011). Systematic studies of nitrogen loss from paddy soils through leaching in the Dongting Lake area of China. *Pedosphere* 06, 753–762. doi: 10.1016/S1002-0160(11)60179-3

Kowalchuk, G. A., and Stephen, J. R. (2001). AMMONIA-OXIDIZING BACTERIA: A model for molecular microbial ecology. *Annu. Rev. Microbiol.* 55, 485–529. doi: 10.1146/annurev.micro.55.1.485

Leininger, S., Urich, T., Schloter, M., Schwark, L., Qi, J., Nicol, G., et al. (2006). Archaea predominate among ammonia-oxidizing prokaryotes in soils. *Nature* 442, 806–809. doi: 10.1038/nature04983

Li, G., Lin, J., Xue, L., Ding, Y., Wang, S., and Linzhang, Y. (2018). Fate of basal N under split fertilization in rice with ^{15}N isotope trace. *Pedosphere* 28, 135–143. doi: 10.1016/S1002-0160(17)60407-7

Li, P., Li, X., Hou, W., Ren, T., and Cong, R. (2018). Studying the fate and recovery efficiency of controlled release urea in paddy soil using ^{15}N tracer technique. *Scientia Agricultura Sin.* 51, 3961–3971. doi: 10.3864/j.issn.0578-1752.2018.20.014

Liu, H., Huang, X., Tan, W., Di, H., Xu, J., Li, Y., et al. (2020). High manure load reduces bacterial diversity and network complexity in a paddy soil under crop rotations. *Soil Ecol. Lett.* 2, 104–119. doi: 10.1007/s42832-020-0032-8

Liu, Y., Chi, Q., Cheng, H., Ding, H., Wen, T., Zhao, J., et al. (2022). Comparative microbial nitrogen functional gene abundances in the topsoil vs. Subsoil of three grassland habitats in northern China. *Front. Plant Sci.* 12. doi: 10.3389/fpls.2021.792002

Ma, Y. (2018). Effects of water regulation on yield, quality and soil environment of alfalfa under subsurface drip irrigation in desert irrigation area. *Gansu Agric. University*.

Man, Y., Li, W., Wang, J., Tam, N., Tai, Y., Tao, R., et al. (2022). Plants inhibit the relative abundance of sulfonamide resistance genes and class 1 integron by influencing bacterial community in rhizosphere of constructed wetlands. *Sci. Total Environ.* 824, 153977–153977. doi: 10.1016/j.scitotenv.2022.153977

Mao, Z. (2002). Water saving irrigation for rice and its effect on environment. *Eng. Sci.* 4, 8–16.

Masuda, Y., Yamanaka, H., Xu, Z. X., Shiratori, Y., Aono, T., Amachi, S., et al. (2020). Diazotrophic anaeromyxobacter isolates from soils. *Appl. Environ. Microbiol.* 86. doi: 10.1128/AEM.00956-20

Mevel, G., and Prieur, D. (2000). Heterotrophic nitrification by a thermophilic Bacillus species as influenced by different culture conditions. *Can. J. Microbiol.* 46, 465–473. doi: 10.1139/w00-005

Peng, S., Luo, Y., Xu, J., Khan, S., Jiao, X., and Wang, W. (2012). Integrated irrigation and drainage practices to enhance water productivity and reduce pollution in a rice production system. *Irrigation Drainage* 61, 285–293. doi: 10.1002/ird.684

Peng, S., Yang, S., Xu, J., Luo, Y., and Hou, H. (2011). Nitrogen and phosphorus leaching losses from paddy fields with different water and nitrogen managements. *Paddy Water Environ.* 9, 333–342. doi: 10.1007/s10333-010-0246-y

Qi, D., Wu, Q., and Zhu, J. (2020). Nitrogen and phosphorus losses from paddy fields and the yield of rice with different water and nitrogen management practices. *Sci. Rep.* 10. doi: 10.1038/s41598-020-66757-5

Schleper, C., Jurgens, G., and Jonuscheit, M. (2005). Genomic studies of uncultivated archaea. *Nat. Rev. Microbiol.* 3, 479–488. doi: 10.1038/nrmicro1159

Shen, J., Li, Y., Wang, Y., Li, Y., Zhu, X., Jiang, W., et al. (2022). Soil nitrogen cycling and environmental impacts in the subtropical hilly region of China. *Front. Agric. Sci. Eng.* 03), 407–424.

Shen, J., Zhang, L., Zhu, Y., Zhang, J., and He, J. (2008). Abundance and composition of ammonia-oxidizing bacteria and ammonia-oxidizing archaea communities of an alkaline sandy loam. *Environ. Microbiol.* 10, 1601–1611. doi: 10.1111/j.1462-2920.2008.01578.x

Tan, X., Shao, D., Liu, H., Yang, F., Xiao, C., Yang, H., et al. (2013). Effects of alternate wetting and drying irrigation on percolation and nitrogen leaching in paddy fields. *Paddy Water Environ.* 11, 381–395. doi: 10.1007/s10333-012-0328-0

Valerie, S., Andre, V., Wolfgang, W., Catarina, H., Nils, P., Gerd, W., et al. (2023). Nitrogen release from different polymer-coated urea fertilizers in soil is affected by soil properties. *Soil Use Manage.* 4, 1477–1490.

Wang, M., Fu, Y., Wang, Y., Li, Y., Shen, J., Liu, X., et al. (2021). Pathways and mechanisms by which biochar application reduces nitrogen and phosphorus runoff losses from a rice agroecosystem. *Sci. Total Environ.* 797, 149193. doi: 10.1016/j.scitotenv.2021.149193

Wang, L., and Huang, D. (2021). Nitrogen and phosphorus losses by surface runoff and soil microbial communities in a paddy field with different irrigation and fertilization managements. *PloS One* 16, e254227. doi: 10.1371/journal.pone.0254227

Wang, C., Liu, D., and Bai, E. (2018). Decreasing soil microbial diversity is associated with decreasing microbial biomass under nitrogen addition. *Soil Biol. Biochem.* 120, 126–133. doi: 10.1016/j.soilbio.2018.02.003

Wang, R., Min, J., Kronzucker, H. J., Li, Y., and Shi, W. (2019). N and P runoff losses in China's vegetable production systems: Loss characteristics, impact, and management practices. *Sci. Total Environ.* 663, 971–979. doi: 10.1016/j.scitotenv.2019.01.368

Wang, J., Song, Y., Ma, T., Raza, W., Li, J., Howland, J. G., et al. (2017). Impacts of inorganic and organic fertilization treatments on bacterial and fungal communities in a paddy soil. *Appl. Soil Ecol.* 112, 42–50. doi: 10.1016/j.apsoil.2017.01.005

Wang, D., Xu, C., Yan, J., Zhang, X., Chen, S., Chauhan, B. S., et al. (2017). 15 N tracer-based analysis of genotypic differences in the uptake and partitioning of N applied at different growth stages in transplanted rice. *Field Crops Res.* 211, 27–36. doi: 10.1016/j.fcr.2017.06.017

Xu, C., Chen, L., Chen, S., Chu, G., Wang, D., and Zhang, X. (2020). Rhizosphere aeration improves nitrogen transformation in soil, and nitrogen absorption and accumulation in rice plants. *Rice Sci.* 02), 162–174.

Yang, J., Guo, W., Yang, W., Zhou, B., and Xing, S. (2023). Effects of milk vetch on leaching and loss of dissolved organic carbon and nitrogen in different types of paddy soils. *J. Agro-Environment Sci.* 1–10.

Ye, Y., Liang, X., Chen, Y., Liu, J., Gu, J., Guo, R., et al. (2013). Alternate wetting and drying irrigation and controlled-release nitrogen fertilizer in late-season rice. Effects on dry matter accumulation, yield, water and nitrogen use. *Field Crops Res.* 144, 212–224. doi: 10.1016/j.fcr.2012.12.003

Zeng, F., Zuo, Z., Mo, J., Chen, C., Yang, X., Wang, J., et al. (2021). Runoff losses in nitrogen and phosphorus from paddy and maize cropping systems: A field study in Dongjiang basin, South China. *Front. Plant Sci.* 12. doi: 10.3389/fpls.2021.675121

Zhang, M., Tian, Y., Zhao, M., Yin, B., and Zhu, Z. (2017). The assessment of nitrate leaching in a rice–wheat rotation system using an improved agronomic practice aimed to increase rice crop yields. *Agriculture Ecosyst. Environ.* 241, 100–109. doi: 10.1016/j.agee.2017.03.002

Zhang, J., Wang, J., Müller, C., and Cai, Z. (2016). Ecological and practical significances of crop species preferential N uptake matching with soil N dynamics. *Soil Biol. Biochem.* 103, 63–70. doi: 10.1016/j.soilbio.2016.08.009

Zhang, X., Xiao, G., Bol, R., Wang, L., Zhuge, Y., Wu, W., et al. (2021). Influences of irrigation and fertilization on soil N cycle and losses from wheat-maize cropping system in northern China. *Environ. Pollut.* 278, 116852–116852. doi: 10.1016/j.envpol.2021.116852

Zhang, Q., Yang, Z., Zhang, H., and Yi, J. (2012). Recovery efficiency and loss of ^{15}N-labelled urea in a rice-soil system in the upper reaches of the Yellow River basin. *Agriculture Ecosyst. Environ.* 158, 118–126. doi: 10.1016/j.agee.2012.06.003

Zhao, Z., Sha, Z., Liu, Y., Wu, S., Zhang, H., Li, C., et al. (2016). Modeling the impacts of alternative fertilization methods on nitrogen loading in rice production in Shanghai. *Sci. Total Environ.* 566-567, 1595–1603. doi: 10.1016/j.scitotenv.2016.06.055

Zhao, Z., Zhang, H., Li, C., Zhao, Q., and Cao, L. (2014). Quantifying nitrogen loading from a paddy field in Shanghai, China with modified DNDC model. *Agriculture Ecosyst. Environ.* 197, 212–221. doi: 10.1016/j.agee.2014.08.002

Zhuang, Y., Zhang, L., Li, S., Liu, H., Zhai, L., Zhou, F., et al. (2019). Effects and potential of water-saving irrigation for rice production in China. *Agric. Water Manage.* 217, 374–382. doi: 10.1016/j.agwat.2019.03.010

frontiers | Frontiers in Plant Science

TYPE Original Research
PUBLISHED 05 June 2024
DOI 10.3389/fpls.2024.1387977

OPEN ACCESS

EDITED BY
Enrique Ostria-Gallardo,
University of Concepcion, Chile

REVIEWED BY
Yahui Guo,
Central China Normal University, China
Evans Asenso,
University of Ghana, Ghana

*CORRESPONDENCE
Ruipeng Tang
22057874@siswa.um.edu.my

RECEIVED 19 February 2024
ACCEPTED 08 May 2024
PUBLISHED 05 June 2024

CITATION
Tang R, Wei S, Jianxun T, Aridas NK and Talip MSA (2024) A method for durian precise fertilization based on improved radial basis neural network algorithm. *Front. Plant Sci.* 15:1387977. doi: 10.3389/fpls.2024.1387977

A method for durian precise fertilization based on improved radial basis neural network algorithm

Ruipeng Tang[1*], Sun Wei[1], Tang Jianxun[2], Narendra Kumar Aridas[1] and Mohamad Sofian Abu Talip[1]

[1]Faculty of Engineering, University of Malaya, Kuala Lumpur, Malaysia, [2]Faculty of Electronics and Electrical Engineering, Zhaoqing University, Zhaoqing, Guangdong, China

Introduction: Durian is one of the tropical fruits that requires soil nutrients in its cultivation. It is important to understand the relationship between the content of critical nutrients, such as nitrogen (N), phosphorus (P), and potassium (K) in the soil and durian yield. How to optimize the fertilization plan is also important to the durian planting.

Methods: Thus, this study proposes an Improved Radial Basis Neural Network Algorithm (IM-RBNNA) in the durian precision fertilization. It uses the gray wolf algorithm to optimize the weights and thresholds of the RBNNA algorithm, which can improve the prediction accuracy of the RBNNA algorithm for the soil nutrient content and its relationship with the durian yield. It also collects the soil nutrients and historical yield data to build the IM-RBNNA model and compare with other similar algorithms.

Results: The results show that the IM-RBNNA algorithm is better than the other three algorithms in the average relative error, average absolute error, and coefficient of determination between the predicted and true values of soil N, K, and P fertilizer contents. It also predicts the relationship between soil nutrients and yield, which is closer to the true value.

Discussion: It shows that the IM-RBNNA algorithm can accurately predict the durian soil nutrient content and yield, which is benefited for farmers to make agronomic plans and management strategies. It uses soil nutrient resources efficiently, which reduces the environmental negative impacts. It also ensures that the durian tree can obtain the appropriate amount of nutrients, maximize its growth potential, reduce production costs, and increase yields.

KEYWORDS

durian precise fertilization, durian soil nutrient management, precise nutrient supply, durian planting, durian yield prediction

1 Introduction

As one of the representatives in tropical fruits, durian is popular for its unique flavor and high nutritional value. The formulation of fertilization strategies is the key issues of agricultural production in durian cultivation. However, the durian fertilization decisions mainly rely on farmers' experience and traditional agricultural methods, which is subjective and lacks scientific basis. It leads to the effectiveness of fertilization and poses a threat to farmers' economic benefits and the stability of the supply chain. However, soil properties vary from different regions; traditional fertilization programs fail to consider soil heterogeneity, which leads to unscientific fertilization. It affects the durian growth and quality and negatively impacts land health and sustainability. Therefore, it is important to collect the durian growth data and soil conditions and use relevant algorithms to learn the complex relationship of durian growth for reducing the fertilizer waste and production costs (Zhou et al., 2021; Chanachot et al., 2023).

Precise fertilization decisions can control the input of agricultural production materials and improve the yield and quality of crops. Therefore, some scholars have made some achievements in some crops. Guo et al. (2021) proposed an integrated phenology and climate in rice yields prediction using machine learning methods. It tested 11 phenological, climate, and geographical data and three machine learning methods to predict site-based rice yield, thereby improving the accuracy of rice yield prediction under climate change conditions using integrated machine learning methods. Hossain et al. (Hossain and Siddique, 2020) proposed an online fertilizer recommendation system (OFRS). It analyzed Bangladesh's national soil database to generate site-specific fertilizer recommendations for selected crops using recommended doses of fertilizer calculated based on soil test values. Kuzman et al. (2021) established a prediction method through an adaptive neuro-fuzzy inference system (ANFIS) to determine the impact of temperature, moisture, humidity, soil type, crop type, nitrogen, potassium, and phosphorus on fertilizer prediction, thereby reducing process costs. Guo et al. (2022) proposed a machine learning-based approach for predicting spad values of maize using multi-spectral images. It used the Mini MCA 6 camera of the drone platform to collect images of corn at different growth stages and established a linear regression model with the spectrum and texture index of different growth stages to accurately monitor the growth and nutritional status of corn for better subsequent fertilization management.

Kanuru et al. (2021) used Global Positioning System (GPS) modules and Internet of Things (IoT) technology to determine the properties of the soil and the types and amounts of pesticides and fertilizers used in effective methods, improving the efficiency of pesticide and fertilizer use to achieve optimal economic benefits. Guo et al. (2023) used hyperspectral images collected by drones, explored multispectral images using the formed dual-band (2D) vegetation index (VI) and 2D texture index (TI), and used five deep learning methods to accurately monitor corn growth, which can help adjust fertilization strategies and achieve precise fertilization. Ahmed et al. (2021) proposed a soil fertilization nutrient recommendation system based on evolutionary calculation. It improves the Genetic Algorithm (IGA) and uses time-series sensor data to make recommendations for various crop nutrient settings. Neighborhood-based strategies were also proposed to handle exploration and exploitation to optimize parameters for maximum yield. Sujatha et al. (2023) proposed a soil fertility classification and fertilization method based on the one-dimensional convolutional neural network. It utilized 1D-CNN to classify soil based on fertility. Classification results were used to specify fertilizers for rice, areca nut, and black/green grams. It also adopted the MinMax normalization and Synthetic Minority Oversampling Technology (SMOTE) to improve the classification efficiency. Lucas et al. (Benedet et al., 2021) used X-ray fluorescence (pXRF) spectrometer to analyze the fertility and element content of 1,975 different soil samples and used a random forest algorithm to establish a spatial distribution model of soil fertility characteristics to achieve soil fertility prediction.

Although the above studies has achieved good results in precise fertilization for some crops, but they are used for other crops and cannot be used for durian because the durian has higher requirements for the growth environment and is quite different from other crops,which is relianced on the information technology infrastructure and the difficulty of equipment maintenance. These methods are mainly the fertilizer effect and nutrient balance. The former has a complex nonlinear relationship between the soil fertilizer amount and multiple soil factors, which does not consider the soil nutrient content. The nutrient balance method needs to keep the dynamic balance, which is corrected. The difficulty of the coefficient is higher. Dong et al. (2020) proposed a method for precise corn fertilization based on wavelet BP neural network, which used wavelet decomposition and reconstruction methods to calculate the yield. However, the combination of wavelet analysis and BP neural network increases the complexity of the model, requiring more computing resources and time for training and verification. Thus, this study proposes an Improved Radial Basis Neural Network Algorithm (IM-RBNNA) in the durian precision fertilization. It extracts and processes the soil sample data and introduces the gray wolf algorithm to improve the Improved Radial Basis Neural Network Algorithm (IM-RBNNA) for calculating the weight ratio, fertilizer amount, and yield of nitrogen, phosphorus, and potassium fertilizers (Song et al., 2020). By comparison, it shows that the IM-RBNNA algorithm can predict the relationship between durian soil nutrient content and yield, which allows durian managers to carry out scientific fertilization based on the prediction results. It reduces fertilizer waste and production costs, achieving sustainability durian planting.

2 Algorithms and models design

2.1 Radial basis neural network algorithm

RBNNA is a forward neural network with good performance. It maps nonlinear problems to linear space, transforms them into the adaptive algorithm processing, and maintains the high accuracy and efficiency of the algorithm. RBNNA is a three-layer feedforward neural network consisting of an input, hidden, and output layer

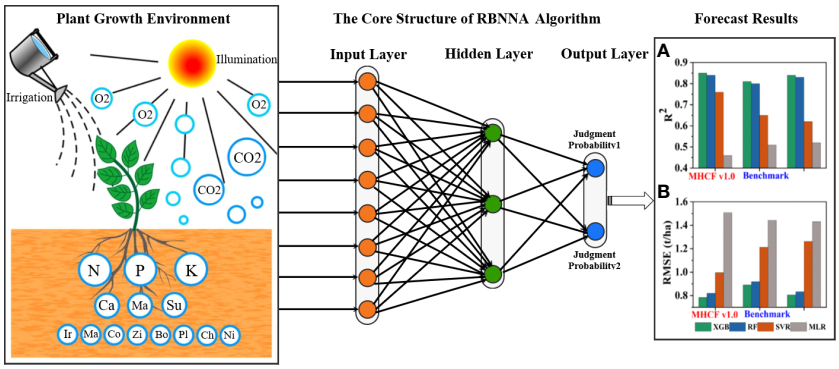

FIGURE 1
The prediction process of the RBNNA algorithm.

(Wang et al., 2023). The input layer is the node that receives the original input data, and each node corresponds to the input feature. The hidden layer is a set of nodes for radial basis functions, which is used to measure the distance between input data and some centers. The output layer produces the final output, which is a linear layer that combines the outputs of the hidden layers. Figure 1 shows the prediction process of the RBNNA algorithm. The core of RBFNN lies in the radial basis function of the hidden layer, which is a Gaussian or other symmetric function. Gaussian is one of the radial basis functions, which is expressed by Equation 1:

$$G_s(\rho) = \exp(-|\rho - o_s|^2/2\sigma_s^2) \tag{1}$$

In Equation 1, $G_s(\rho)$ represents the output of the s-th basis function, o_s represents the center of the basis function, and σ_s^2 represents the width parameter.

2.2 Gray wolf algorithm

The gray wolf algorithm is a meta-heuristic algorithm proposed by Mirjalili et al (Li et al., 2021), which is derived from gray wolves' social hierarchy and hunting strategy. In this algorithm, the population is divided into levels A–D. Wolves A control all actions of the wolf pack, which are the supreme leader of the wolf pack. Wolves B assist wolf A in making some decisions, which are some experienced wolves (Xu et al., 2023). Wolves C are responsible for the reconnaissance of the wolf pack, which are responsible for guarding and caring cubs. Wolves D belong to the lowest level of gray wolves and obey the commands of gray wolves from other classes, which are accounting for the vast majority. The best wolves are A, B, and C. They help wolves D to find the favorable area (Verma et al., 2022). First, the wolves need to locate their prey and surround it. The process is shown in Equation 2:

$$\text{Dist} = \left|N \times W_\varphi(k) - W(k)\right| \tag{2}$$

In Equation 2, D represents the distance between the gray wolf and the prey, N represents the coefficient vector, $W_\varphi(k)$ represents the position vector of the prey, $W(k)$ represents the position vector of the gray wolf, and k represents the number of iterations. The position of k +1 wolves is shown in Equation 3:

$$W(k+1) = W_\varphi(k) - M \times \text{Dist} \tag{3}$$

In Equation 3, M represents the coefficient vector; other parameters have the same meaning as Equation 2. N represents the calculation process of the coefficient vector sum, which is shown in Equations 4, 5:

$$M = 2\omega \times p_1 - \omega \tag{4}$$

$$N = 2p_2 \tag{5}$$

In Equations 4, 5, ω represents the convergence factor, which decreases linearly from 2 to 0 as k increases; p_1 and p_2 represent the random number with a value range of (0,1). When the prey is surrounded, the wolves start hunting. The hunting process is carried out under the leadership of wolves A, B, and C. They guide wolves D to track the prey location. The calculation process is as shown in Equations 6–8:

$$A(Dist) = |N_1 \times W_a - W| \tag{6}$$

$$B(Dist) = |N_2 \times W_b - W| \tag{7}$$

$$C(Dist) = |N_3 \times W_c - W| \tag{8}$$

In Equations 6–8, $A(Dist)$, $B(Dist)$, and $C(Dist)$ represent the distance between the three wolves and other individuals; W_a, W_b, and W_c represent the current positions of the three wolves; N_1, N_2, and N_3 represent the random vectors; and W represents the current position of the gray wolf. The vectors of wolves D in the wolf pack moving toward wolves A, B, and C are represented by W_1, W_2, and W_3. The calculation process is as shown in Equations 9–11:

$$W_1 = W_a - M_1 \times A(Dist) \tag{9}$$

$$W_2 = W_b - M_2 \times B(Dist) \tag{10}$$

$$W_3 = W_c - M_3 \times C(Dist) \tag{11}$$

In Equation 9, Equation 10, Equation 11, according to the calculation results of W_1, W_2, and W_3, the final position of wolves D can be determined. The calculation process is shown in Equation 12:

$$D(Dist) = (W_1 + W_2 + W_3)/3 \quad (12)$$

Finally, the hunt is completed by attacking the prey when it cannot move. The processing of gray wolf algorithm is shown in Figure 2.

2.3 Improved radial basis neural network algorithm

In order to enhance the predicting accuracy of the RBNNA algorithm, this study proposes an IM-RBNNA algorithm. It uses the gray wolf algorithm to optimize the weights and thresholds of the RBNNA algorithm so that the weights and threshold are optimal. When the output result is different from the expected value, the principle of backpropagation is used to optimize. The threshold and weight of the gray wolf algorithm are used as the weight and threshold of the RBNNA algorithm (Liu and Wang, 2020). The relative error value between the predicted and true value of soil nutrient content is used as the fitness value. The continuous iterative update of the gray wolf algorithm is used to adjust the weights and thresholds of the RBNNA algorithm. The advantages with better global effects can improve the model's prediction accuracy (Feng et al., 2023). Figure 3 shows the processing of the gray wolf algorithm for optimizing the RBNNA algorithm.

3 Experimental design

3.1 Experimental environment

This study is conducted in Area 2 of a durian orchard in Penang, Malaysia. It is located in Sungai Pinang Balik Pulau, Penang, which coveres an area of 3,200 acres. The rows of planting density is 5.0 m × 4.0 m. Every acre has 30 plants. The durian trees in this area are all in the peak production period of 15–20 years. During this period, the durian trees have fully developed, so the canopy is dense, which can produce more durian fruits. This area has a tropical rainforest climate, with an average annual temperature of 28°C, an average annual precipitation of 2,525.3 mm, and an annual sunshine count of 2,076.9 h. The study area has significant spatial differences in the growth and yield of durian, which is suitable for the precise fertilization, so this site is chosen to study the precise fertilization. Four experiments are set up in the research area to verify the differences of soil fertility under different algorithms (Portela et al., 2011). From west to east are areas A, B, C, and D, which are used for experiments on different fertilization decision-making methods. Each area is 5 acres. In this plantation soil, the alkaline hydrolyzed nitrogen is 21.5 ± 3.0 mg/kg (low), the available phosphorus is 47.1 ± 0.6 mg/kg (high), the available potassium is 117.7 ± 20.9 mg/kg (low), and the pH is 7.6 ± 0.1 (alkaline). All plots are used for unified measures. Figure 4 shows the design of soil sampling locations for this experiment.

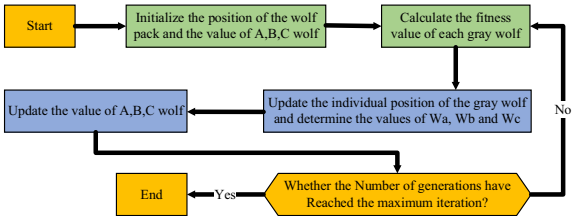

FIGURE 2
The processing of gray wolf algorithm.

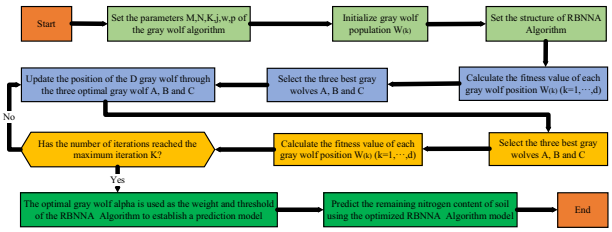

FIGURE 3
The processing of the gray wolf algorithm for optimizing the RBNNA algorithm.

3.2 Data extraction and processing

In order to get the nutrient information of durian soil, five samples are collected within 20 m of the sampling center in each sampling point. The corresponding network of the plot is determined by using manual measurement. The plum blossom sampling method is used in each grid (Zhou and Staver, 2019). Five points of the soil sampling samples are mixed into labeling bags, which have 5,000 sampling points and 150 plots. The sampling time is from February to August 2022. The sample depth is 0–20 cm. These samples are mixed and labeled as soil samples at that point. RTK (real-time kinematic) is used to collect and record the longitude and latitude of the sample point. After the soil samples are naturally air-dried and sieved, the pH is measured to use an electrode method with a water-to-soil volume ratio of 1:1; the organic matter is measured to use the dichromic acid. The potassium method is used to measure the total nitrogen; the copper sulfate digestion method is used to measure the total nitrogen; and the available phosphorus is measured to use the suitable method for neutral and calcareous soils. The soil is measured to use the sodium bicarbonate; the available potassium is measured to use the flame photometry. The fertilizer amount is calculated based on the soil nutrient data, which is obtained from laboratory tests (Liu and Feng, 2017) by using the fertilizer balance model of the target yield method. The physical and chemical properties of the soil are measured through the above laboratory methods to obtain the various nutrient data for each plot (Kim, 2018). Table 1 shows the nutrient data of some sampling points in the durian orchard.

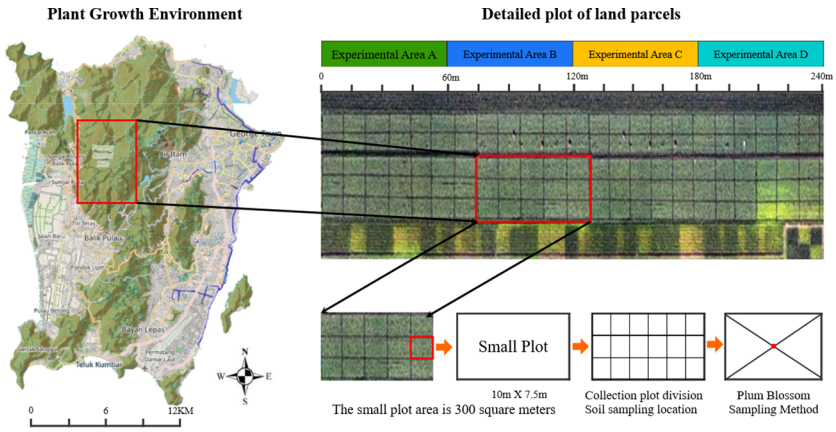

FIGURE 4
The design of soil sampling locations for this experiment.

The nutrient contents of alkaline hydrolyzable nitrogen, available phosphorus, and available potassium in the soil vary greatly. For example, the potassium is approximately 200 mg/kg, but the phosphorus is approximately 10 mg/kg. When the cluster analysis is performed, the impact of available phosphorus is almost negligible, which is difficult not to meet the requirements of the soil similarity calculation. In order to solve these problems, this study standardized the data by using the same standard. The normal standardization subtracts each attribute of each data object from the average value of the attribute and then divides it by the variance of the attribute (Mykhailenko et al., 2020). The data standardized by this method reach the standard normal distribution. The data have a mean of 0 and a variance of 1, which is shown in Equation 13.

$$\overline{H_i} = (H_i - R)/\alpha_h \tag{13}$$

In Equation 13, $\overline{H_i}$ represents the i-th standardized data attribute value, H_i represents the i-th data attribute value to be standardized, R represents the mean value of the attribute, and α_h represents the variance of the attribute. The standardized value of the soil nutrient content is calculated. Table 2 shows the standardized results of the soil nutrient data in Table 1.

3.3 Model establishment and evaluation

The Inter@core i7–9700K processor was used in this study, the graphics card is NVIDIA Geforce GTX3080 32GB, the memory is 64GB, the operating system is Ubuntu19.04 64-bit, the deep learning framework is Pyotrch1.9.2, the programming language is Python3.7.1, the integrated development environment is PycharmCE2023, and the drawing tool is Matplotlib 3.1.0. In order to ensure that the data distribution is representative, this study trains 5,000 samples according to the validation set =7:3, which is divided in 3,500 training and 1,500 validation sets. The deep learning network algorithm needs to preset hyperparameters before training, so this study set the hyper parameters to batch after

TABLE 1 The nutrient data of some sampling points in the durian orchard.

Plot	Alkaline hydrolysis nitrogen N (mg/kg)	Available phosphorus P (mg/kg)	Available potassium K (mg/kg)	P application amount (kg/ha)	Amount of N application (kg/ha)	Amount of K application (kg/ha)	Actual output (kg)
2-A1	22.74	5.23	64.1	162.61	76.39	167.05	162.65
2-A2	22.53	6.4	60.8	170.53	82.66	180.97	153.81
2-A3	20.78	5.95	66.17	188.64	79.85	171.99	160.81
2-A4	23.52	5.62	74.65	170.2	86.42	177.48	178.93
2-A5	21.89	8.59	77.06	170.52	72.53	184.26	173.38
2-B1	22.68	5.92	58.27	177.08	73.94	179.42	165.55
2-B2	20.01	7.18	63.35	158.52	80.09	174.23	185.35
2-B3	22.36	6.08	85.2	165.77	88	183.21	157.33
2-B4	24.74	5.92	71.92	161.47	75.21	169.92	163.21
2-B5	24.92	7.64	79.59	182.95	84.26	181.62	182.03

TABLE 2 The standardized results of the soil nutrient data in Table 1.

Plot	Standardized alkaline hydrolysis nitrogen	Standardized available phosphorus	Standardized available potassium	Standardized application amount	Standardized dosage	Standardized application amount	Standardized measured yield
2-A1	−0.29	−0.77	−0.61	−0.39	−0.33	−0.41	−0.38
2-A2	−0.30	−0.06	−0.83	−0.31	−0.15	−0.24	−0.48
2-A3	−0.52	−0.33	−0.45	−0.10	−0.21	−0.35	−0.24
2-A4	−0.05	−0.55	0.14	−0.32	0.10	−0.14	0.38
2-A5	−0.36	1.37	0.32	−0.31	−0.57	0.06	0.24
2-B1	−0.31	−0.37	−1.17	−0.22	−0.49	−0.08	−0.16
2-B2	−0.72	0.20	−0.69	−0.53	0.08	−0.24	0.58
2-B3	−0.17	−0.23	1.24	−0.38	0.35	0.04	−0.62
2-B4	0.26	−0.37	0.00	−0.47	−0.30	−0.52	−0.36
2-B5	0.29	0.44	0.62	−0.12	0.23	0.25	0.52

comparison. The number of samples is 6, the epoch is 100, the learning rate optimizer uses the SGD algorithm (Stochastic Gradient Descent) (Thuwajit et al., 2021) to update the weights, the initial learning rate is 0.01, the learning rate decay is 0.001, the activation function uses the Sigmoid function, and the model classifier uses SVM (support vector machine) (Dou et al., 2023).

This study uses the mean relative error (MAPE), the mean absolute error (MAE), and the coefficient of determination (R^2) to evaluate the performance of the IM-RBNNA and other similar algorithms (Li et al., 2020). The MAPE is used to calculate the relative difference between the actual and predicted values. MAPE is used to calculate the percentage error of each observed value relative to the actual value and then averages it. The smaller the value of MAPE, the better the model's performance. The MAE is used to calculate the average of the absolute differences between actual and predicted values. The R^2 measures how well a model fits the data and represents the model's ability to explain the variation in the dependent variable. In these calculation formula, U_j represents the actual value of the soil nitrogen content; $\overline{U_j}$ represents the predicted average value of the soil nitrogen content; and U represents the predictive value of the soil nitrogen content. t represents the number of samples. The calculation formula is Equations 14–16, which are as follows:

$$f(mape) = \frac{1}{t}\sum_{j=1}^{t}\left|\frac{U_j - \overline{U_j}}{U_j}\right| \times 100 \tag{14}$$

$$f(mae) = \frac{1}{t}\sum_{j=1}^{t}\left|U_j - \overline{U_j}\right| \tag{15}$$

$$f(R^2) = 1 - \frac{\sum_{j=1}^{t}(U_j - \overline{U_j})^2}{\sum_{j=1}^{t}(U_j - \bar{U})^2} \tag{16}$$

The target yield is the key to durian fertilization recommendations. This study uses the multiple linear stepwise regression methods to determine the durian yield (Sardoei et al., 2023). It determines an initial set containing multiple independent variables and builds a multiple regression formula that does not include this factor. It will run until no more independent variables X can be introduced. The soil nutrient content of the alkaline hydrolyzable nitrogen, available phosphorus, and available potassium are important factors to affect the durian yield, which is relatively in line with the requirements of the above method. The calculation process of the model is shown in Equation 17:

$$Y = e_0 + e_1 \times X_1 + e_2 \times X_2 + \ldots + e_z \times X_z \tag{17}$$

In Equation 17, X represents the independent variable, Y represents the dependent variable, z represents the number of independent variables, and e represents the regression coefficient of each variable. The training of the multiple linear stepwise regression algorithm in this study is conducted in IBMSPSS Statistics 25.

3.4 Experimental results

In order to compare the performance of the IM-RBNNA algorithm, this study introduces three methods for comparison: the RBNNA, Backpropagation Neural Network (BPNN) (LI et al., 2019), and Nutrient Balance Calculation Algorithm (NUBCA) (Nannan et al., 2021). The NUBCA algorithm keeps balance between the plants receiving adequate nutrients and their nutrient needs with the available nutrients in the soil. The BPNN algorithm builds the relationship between the plant growth and soil conditions, which uses the backpropagation algorithm for model training and reduces prediction errors by adjusting the weights and biases. This experiment also measures the performance of the four algorithms from three indicators: mean absolute percentage error (MAPE), mean absolute error (MAE), and coefficient of determination(R^2).

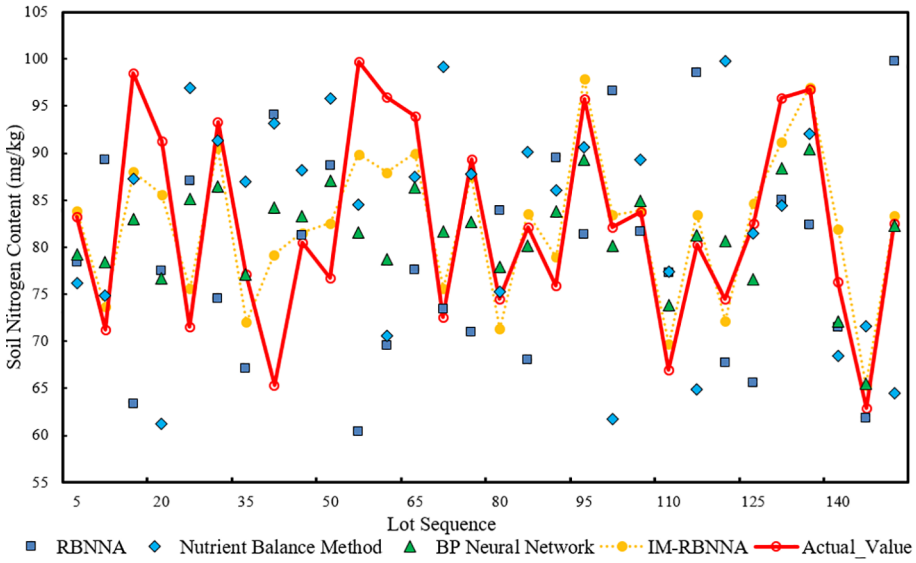

FIGURE 5
The comparative distribution of predicted alkaline hydrolyzable nitrogen of each algorithm.

3.4.1 The prediction of alkaline hydrolyzable nitrogen in the soil content

Figure 5 shows the comparative distribution of predicted alkaline hydrolyzable nitrogen of each algorithm. It shows that the maximum, minimum, and average values predicted by the IM-RBNNA algorithm are 97.02 mg/kg, 65.31 mg/kg, and 80.74 mg/kg. The maximum, minimum, and average values in the real soil content are 99.70 mg/kg, 62.93 mg/kg, and 80.50 mg/kg, respectively. Table 3 shows the performance of different algorithms in predicting soil alkaline hydrolyzable content. By comparing the RBNNA, NUBCA, and BPNN algorithms, the MAPE value of the IM-RBNNA algorithm is 1.61%, which is reduced by 69.41%, 80.26%, and 66.60%; the MAE value of the IM-RBNNA algorithm is 1.403, which is reduced by 57.34%, 76.38%, and 57.99%; and the R^2 value of the IM-RBNNA algorithm is 0.977, which is increased by 8.23%, 28.10%, and 11.17%. It shows that the IM-RBNNA algorithm is more stable than the other three algorithms, which has a smaller fluctuation amplitude, and is closer to the 0-bit horizontal axis. Its prediction effect is better than the other three algorithms, so it can more accurately predict the alkaline hydrolyzable content of durian soil, which is convenient for durian farmers to precise fertilize.

3.4.2 The prediction of available phosphorus in the soil content

Figure 6 shows the comparative distribution of predicted available phosphorus of each algorithm. It shows that the maximum, minimum, and average values predicted by the IM-RBNNA algorithm are 41.93 mg/kg, 15.12 mg/kg, and 29.76 mg/kg. The maximum, minimum, and average values in the real soil content is 39.67 mg/kg, 18.30 mg/kg, and 29.20 mg/kg, respectively. Table 4 shows the performance of different algorithms in predicting soil available phosphorus content. By comparing the RBNNA, NUBCA, and BPNN algorithms, the MAPE value of the IM-RBNNA algorithm is 10.46%, which is reduced by 35.04%, 47.73%, and 21.66%; the MAE value of the IM-RBNNA algorithm is 3.641, which is reduced by 20.65%, 44.86%, and 24.00%; and the R^2 value of the IM-RBNNA algorithm is 0.835, which is increased by 16.77%, 46.66%, and 18.89%. It shows that the IM-RBNNA algorithm is more stable than the other three algorithms, which has a smaller fluctuation amplitude and is closer to the 0-bit horizontal axis. Its prediction effect is better than the other three algorithms, so it can more accurately predict the available phosphorus content of durian soil, which is convenient for durian farmers to precise fertilize.

TABLE 3 The performance of different algorithms in predicting soil alkaline hydrolyzable content.

Algorithm name / Error index	RBNNA	NUBCA	BPNN	IM-RBNNA
MAPE	5.26%	8.17%	4.82%	1.61%
MAE	3.097	5.94	3.696	1.403
R^2	0.903	0.762	0.877	0.977

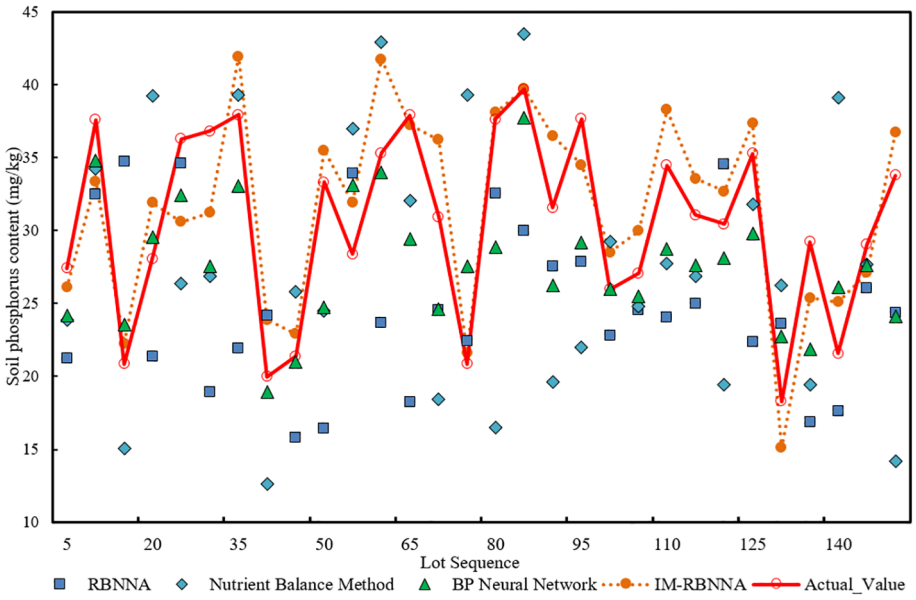

FIGURE 6
The comparative distribution of predicted available phosphorus of each algorithm.

3.4.3 The prediction of available potassium in the soil content

Figure 7 shows the comparative distribution of predicted available potassium of each algorithm.. It shows that the maximum, minimum, and average values predicted by the IM-RBNNA algorithm are 307.73 mg/kg, 157.10 mg/kg, and 228.11 mg/kg. The maximum, minimum, and average values in the real soil content are 307.31 mg/kg, 158.38 mg/kg, and 229.62 mg/kg, respectively. Table 5 shows the performance of different algorithms in predicting soil available potassium content. By comparing the RBNNA, NUBCA, and BPNN algorithms, the MAPE value of the IM-RBNNA algorithm is 10.46%,which is reduced by 34.95%, 84.36%, and 29.74%; the MAE value of the IM-RBNNA algorithm is 3.641, which is reduced by 13.20%, 21.44%, and 4.20%; and the R^2 value of the IM-RBNNA algorithm is 0.835, which is increased by 8.62%,18.32%, and 4.58%. It shows that the IM-RBNNA algorithm is more stable than the other three algorithms, which has a smaller fluctuation amplitude and is closer to the 0-bit horizontal axis. Its prediction effect is better than the other three algorithms, so it can more accurately predict the available potassium content of durian soil, which is convenient for durian farmers to precise fertilize.

3.4.4 Prediction of the relationship between soil nutrients and yield

In this study, the multiple linear stepwise regression method determines the fertilizer amount and target yield predicted by four algorithms: RBNNA, NUBCA, BPNN, and IM-RBNNA. The predict time is the annual output of each mature durian tree from 2013 to 2022. The MAPE, MAE, and R^2 between the four algorithms and the real yield is calculated based on the historical data. In Figure 7, the maximum, minimum, and average values predicted by the IM-RBNNA algorithm is 297.75kg/tree, 177.58 kg/tree, and 224.58 kg/tree, respectively. The maximum, minimum, and average values in the real yield is 302.32 kg/tree, 175.87 kg/tree, and 219.21 kg/tree, respectively. Table 6 shows the performance of different algorithms in predicting the durian yield. By comparing the RBNNA, NUBCA, and BPNN algorithms, the MAPE value of the IM-RBNNA algorithm is 8.28%, which is reduced by 45.09%, 49.13%, and 49.67%; the MAE value of the IM-RBNNA algorithm is 18.56, which is reduced by 41.18%, 43.94%, and 42.22%; and the R^2 value of the IM-RBNNA algorithm is 0.934, which is increased by 14.99%, 21.56%, and 21.08%. It shows that the yield predicted by the IM-RBNNA algorithm based on soil nutrient fertilization is closer to the true value, which helps durian farmers understand the

TABLE 4 The performance of different algorithms in predicting soil available phosphorus content.

Algorithm name / Error index	RBNNA	NUBCA	BPNN	IM-RBNNA
MAPE	16.09%	19.99%	13.36%	10.46%
MAE	5.061	6.306	4.781	3.641
R^2	0.715	0.572	0.702	0.835

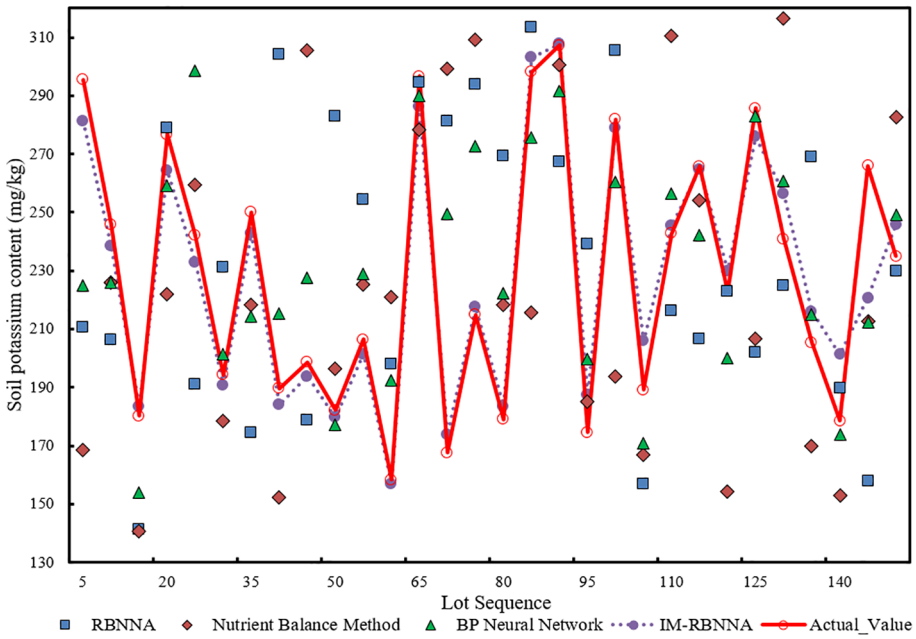

FIGURE 7
The comparative distribution of predicted available potassium of each algorithm.

relative contributions of alkali-hydrolyzable nitrogen, available phosphorus, and available potassium to the durian yield. It also makes reasonable decisions based on the prediction results to achieve the goal of maximizing yields.

4 Discussion

Although the IM-RBNNA algorithm proposed in this study provides an advanced method for precise durian fertilization, it has some limitations. It is highly dependent on the quality and detail of input data, such as soil nutrient levels and historical yields. Poor data quality or insufficient data volume can significantly reduce the predictive accuracy of the model. However, the comprehensive collection of soil samples and yield data in different growing seasons requires a large cost, so the algorithm needs to be applied for a period of time to gradually improve the accuracy. In addition, the study did not take into account the impact of environmental factors such as soil temperature and humidity, pests, and diseases on durian yield. Take soil moisture as an example; it is an important component of the terrestrial water cycle, which affects the surface material exchange, energy balance, and durian yield (Fang et al., 2020).

In order to improve the yield prediction of the IM-RBNNA algorithm, subsequent studies will collect the soil moisture data and measure it with the TZS-IIW200 soil moisture meter. After setting the sampling points in the laboratory, the field sampling is carried out, and the soil moisture is measured. The latitude and longitude of the sampling points are recorded. The soil moisture data at two different depths of 0–5 cm and 15–20 cm are obtained. The typical slopes of durian topographic undulating sections will be selected. The soil temperature and humidity sensors will be deployed (see Figure 8), which obtains soil data at two soil depths of 0–20 cm and 20–30 cm. Two underground plots will be installed. There are 14 sensors, from south to north numbered in sequence. The soil temperature and humidity sensor is TESLA-600. The soil moisture testing accuracy is ± 1%, the soil temperature testing accuracy is ± 0.3°C, and the soil conductivity testing accuracy is ± 2%. The sensor has built the wireless network transmission, which transmits data every hour, works around the day, and records the environmental information in real time. Figure 9 shows the nutrient and soil temperature and moisture sensors.

TABLE 5 The performance of different algorithms in predicting soil available potassium content.

Algorithm name / Error index	RBNNA	NUBCA	BPNN	IM-RBNNA
MAPE	11.39	15.56	10.95	8.44
MAE	21.01	22.54	19.34	18.56
R^2	0.838	0.749	0.875	0.917

TABLE 6 The performance of different algorithms in predicting soil potassium content.

Algorithm name / Error index	RBNNA	NUBCA	BPNN	IM-RBNNA
MAPE	15.08	16.29	16.44	8.28
MAE	31.56	33.16	32.14	18.56
R^2	0.812	0.769	0.767	0.934

In addition, climatic conditions play a vital role in durian production, which includes temperature, humidity, rainfall, and sunlight exposure. For example, temperature is the key factors to the durian growth and fruit development. Warm temperatures is the best environment in for growth durians. The warmer climate aids the flower formation and fruiting process, which increases durian yields (Amran et al., 2023). The proper humidity helps durian plants thrive and enhances pollination, which is crucial for fruit formation. Additionally, durian trees require consistent and evenly distributed rainfall, especially during critical growth stages. The insufficient rainfall causes water stress, which affects the development of flowers and fruits. The excessive rainfall causes waterlogged soil, which affects the root health and nutrient uptake. Finally, sunlight is the key factor affecting photosynthesis. The

FIGURE 8
Comparative distribution of predicted values and real values of each algorithm.

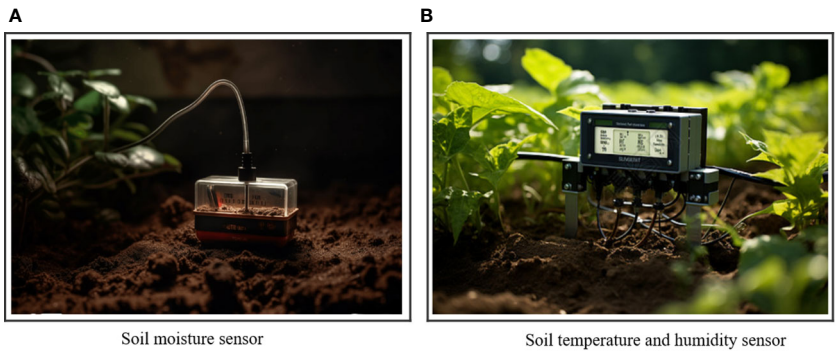

FIGURE 9
The nutrient and soil temperature and humidity sensor.

adequate sunlight is crucial for the healthy growth of durian trees. The insufficient light may weaken the photosynthetic activity, which affects the overall vigor and yield. Through comprehensive training of the above factors and combined with the IM-RBNNA algorithm, the complex relationship between climate conditions and durian yield can be explored, and fertilization strategies can be adjusted according to meteorological changes and soil conditions in different periods. It will help the address climate change, which improves agricultural production capabilities and scientific accuracy of fertilization decisions.

5 Conclusions

This study proposes an IM-RBNNA algorithm for the durian precision fertilization. It introduces the gray wolf algorithm to optimize the weights and thresholds of the RBNNA algorithm to enhance the ability to search for optimal solutions and prediction accuracy. It is compared with the RBNNA, NUBCA, and BPNN algorithm. The experimental results show that the IM-RBNNA algorithm is better than the other three algorithms in predicting alkaline hydrolyzable nitrogen, available phosphorus, and available potassium of the soil content. The prediction results between soil nutrients and yield are closer to the true values. The IM-RBNNA algorithm ensures that durian trees obtain the appropriate amount of nutrients and avoid the problem of excess or insufficient nutrients. It helps durian farmers to make the scientific planting plans and management strategies, which can improve the soil fertility utilization. It also reduces production costs and avoids resource waste, which maximizes the growth potential of durian and improves the economic benefits of durian planting.

Data availability statement

The original contributions presented in the study are included in the article/Supplementary Material. Further inquiries can be directed to the corresponding author.

Author contributions

RT: Writing – review & editing, Writing – original draft, Visualization, Software, Methodology, Investigation, Validation, Formal analysis, Conceptualization, Data curation. SW: Writing – review & editing, Methodology, Validation, Resources, Formal analysis, Conceptualization. TJ: Writing – review & editing, Data curation, Formal analysis, Investigation, Software, Visualization. NA: Writing – review & editing, Project administration, Funding acquisition. MSAT: Writing – review & editing, Supervision, Resources.

Funding

The author(s) declare that no financial support was received for the research, authorship, and/or publication of this article.

Conflict of interest

The authors declare that the research was conducted in the absence of any commercial or financial relationships that could be construed as a potential conflict of interest.

Publisher's note

All claims expressed in this article are solely those of the authors and do not necessarily represent those of their affiliated organizations, or those of the publisher, the editors and the reviewers. Any product that may be evaluated in this article, or claim that may be made by its manufacturer, is not guaranteed or endorsed by the publisher.

Supplementary material

The Supplementary Material for this article can be found online at: https://www.frontiersin.org/articles/10.3389/fpls.2024.1387977/full#supplementary-material

References

Ahmed, U., Lin, J. C. W., Srivastava, G., and Djenouri, Y. (2021). A nutrient recommendation system for soil fertilization based on evolutionary computation. *Comput. Electron. Agric.* 189, 106407. doi: 10.1016/j.compag.2021.106407

Amran, A., Ariffin, M. R., Isa, I. M., Ahmed, O. H., Herman, G., Muhamad, S. H., et al. (2023). Physicochemical properties of soil cultivated with durian (Durio zibethinus murr.) in Gua Musang, Kelantan. *AGRIVITA J. Agric. Sci.* 45, 278–287. doi: 10.17503/agrivita

Benedet, L., Acuña-Guzman, S. F., Faria, W. M., Silva, S. H. G., Mancini, M., dos Santos Teixeira, A. F., et al. (2021). Rapid soil fertility prediction using X-ray fluorescence data and machine learning algorithms. *Catena* 197, 105003. doi: 10.1016/j.catena.2020.105003

Chanachot, K., Saechua, W., Posom, J., and Sirisomboon, P. (2023). A geographical origin classification of durian (cv. monthong) using near-infrared diffuse reflectance spectroscopy. *Foods* 12 (20), 3844. doi: 10.3390/foods12203844

Dong, Y., Fu, Z., Peng, Y., Zheng, Y., Yan, H., and Li, X. (2020). Precision fertilization method of field crops based on the Wavelet-BP neural network in China. *J. cleaner production* 246, 118735. doi: 10.1016/j.jclepro.2019.118735

Dou, Z., Han, R., and Wang, Y. (2023). A prediction method of failure depth of coal seam floor based on FA-GWO-SVM model. *J. Eng. Sci. Technol. Rev.* 16, 161–169. doi: 10.25103/jestr

Fang, Q., Wang, G., Liu, T., Xue, B., Sun, W., and Shrestha, S. (2020). Unraveling the sensitivity and nonlinear response of water use efficiency to the water–energy balance and underlying surface condition in a semiarid basin. *Sci. total Environ.* 699, 134405. doi: 10.1016/j.scitotenv.2019.134405

Feng, X., Li, Y., Zhao, Y., and Chen, J. (2023). Spatial variability analysis of wheat nitrogen yield response: A case study of Henan province, China. *Agronomy* 13, 1796. doi: 10.3390/agronomy13071796

Guo, Y., Chen, S., Li, X., Cunha, M., Jayavelu, S., Cammarano, D., et al. (2022). Machine learning-based approaches for predicting SPAD values of maize using multi-spectral images. *Remote Sens.* 14, 1337. doi: 10.3390/rs14061337

Guo, Y., Fu, Y., Hao, F., Zhang, X., Wu, W., Jin, X., et al. (2021). Integrated phenology and climate in rice yields prediction using machine learning methods. *Ecol. Indic.* 120, 106935. doi: 10.1016/j.ecolind.2020.106935

Guo, Y., Xiao, Y., Hao, F., Zhang, X., Chen, J., de Beurs, K., et al. (2023). Comparison of different machine learning algorithms for predicting maize grain yield using UAV-based hyperspectral images. *Int. J. Appl. Earth Observation Geoinformation* 124, 103528. doi: 10.1016/j.jag.2023.103528

Hossain, M. A., and Siddique, M. N. A. (2020). Online Fertilizer Recommendation System (OFRS): A step towards precision agriculture and optimized fertilizer usage by smallholder farmers in Bangladesh: online fertilizer recommendation. *Eur. J. Environ. Earth Sci.* 1. doi: 10.24018/ejgeo.2020.1.4.47

Kanuru, L., Tyagi, A. K., Aswathy, S. U., Fernandez, T. F., Sreenath, N., and Mishra, S. (2021). "Prediction of pesticides and fertilizers using machine learning and Internet of Things," in *2021 International Conference on Computer Communication and Informatics (ICCCI)*. 1–6 (IEEE). doi: 10.1109/ICCCI50826.2021.9402536

Kim, H. C. (2018). Photostimulation of sequential degradation and assimilation of recalcitrant carbonaceous organics in Scenedesmus quadricauda. *Process Biochem.* 65, 172–177. doi: 10.1016/j.procbio.2017.11.014

Kuzman, B., Petković, B., Denić, N., Petković, D., Ćirković, B., Stojanović, J., et al. (2021). Estimation of optimal fertilizers for optimal crop yield by adaptive neuro fuzzy logic. *Rhizosphere* 18, 100358. doi: 10.1016/j.rhisph.2021.100358

Li, S. H., Wu, L. Z., Chen, J. J., and Huang, R. Q. (2020). Multiple data-driven approach for predicting landslide deformation. *Landslides* 17, 709–718. doi: 10.1007/s10346-019-01320-6

LI, W., Sun, J., and Chen, W. (2019). Real-time obstacle avoidance algorithm for robots based on BP neural network. *Chin. J. Sci. instrument* 40, 204–211.

Li, Y., Lin, X., and Liu, J. (2021). An improved gray wolf optimization algorithm to solve engineering problems. *Sustainability* 13, 3208. doi: 10.3390/su13063208

Liu, P., and Feng, C. (2017). Application of dimensionless processing of normal standardized data in factor analysis. *J. Neijiang Normal Univ.* 32, 54–58.

Liu, C., and Wang, Y. (2020). Grey Wolf algorithm based on S-function and particle swarm optimization. *J. Physics: Conf. Ser.* 1453, 012021. doi: 10.1088/1742-6596/1453/1/012021

Mykhailenko, O., Gudžinskas, Z., Kovalyov, V., Desenko, V., Ivanauskas, L., Bezruk, I., et al. (2020). Effect of ecological factors on the accumulation of phenolic compounds in Iris species from Latvia, Lithuania and Ukraine. *Phytochemical Analysis* 31 (5), 545–563. doi: 10.3390/plants10081599

Nannan, W., Chunfeng, Z., Qingying, M., Baoguo, Z., Yu, L., Hongquan, Z., et al. (2021). Design of formula fertilization system based on nutrient balance fertilization method. *J. Agric.* 11, 92. doi: 10.11923/j.issn.2095-4050.cjas2020-0100

Portela, E. A. C., Ferreira-Cardoso, J. V., and Louzada, J. L. (2011). Boron application on a chestnut orchard: Effect on yield and quality of nuts. *J. Plant Nutr.* 34, 1245–1253. doi: 10.1080/01904167.2011.580812

Sardoei, A. S., Sharifani, M., Sarmast, M. K., and Ghasemnejhad, M. (2023). Stepwise regression analysis of citrus genotype under cold stress. *Gene Cell Tissue* 10. doi: 10.5812/gct-126518

Song, Z., Liu, S., Wang, X., and Hu, Z. (2020). Optimization and prediction of volume shrinkage and warpage of injection-molded thin-walled parts based on neural network. *Int. J. Advanced Manufacturing Technol.* 109, 755–769. doi: 10.1007/s00170-020-05558-6

Sujatha, M., Jaidhar, C. D., and Lingappa, M. (2023). 1D convolutional neural networks-based soil fertility classification and fertilizer prescription. *Ecol. Inf.* 78, 102295. doi: 10.1016/j.ecoinf.2023.102295

Thuwajit, P., Rangpong, P., Sawangjai, P., Autthasan, P., Chaisaen, R., Banluesombatkul, N., et al. (2021). EEGWaveNet: Multiscale CNN-based spatiotemporal feature extraction for EEG seizure detection. *IEEE Trans. Ind. Inf.* 18, 5547–5557. doi: 10.1109/TII.2021.3133307

Verma, R. K., Sivakkumar, M., and Namdeo, V. (2022). "Robust image watermarking using LWT transform and stacking ensemble classifier," in *Soft Computing for Security Applications: Proceedings of ICSCS 2021*. 621–634 (Singapore: Springer). doi: 10.1016/j.image.2020.116019

Wang, G., Wang, J., Wang, J., Yu, H., and Sui, Y. (2023). Study on prediction model of soil nutrient content based on optimized BP neural network model. *Commun. Soil Sci. Plant Anal.* 54, 463–471. doi: 10.1080/00103624.2022.2118291

Xu, C., Yang, J., Zhang, T., Li, K., and Zhang, K. (2023). Adaptive parameter selection variational mode decomposition based on a novel hybrid entropy and its applications in locomotive bearing diagnosis. *Measurement* 217, 113110. doi: 10.1016/j.measurement.2023.113110

Zhou, X. W., Pan, J. R., Wu, H., Chen, H. Q., Yan, Z., Jin, B. H., et al. (2021). Discrimination of durian from different geographical origins based on mineral element fingerprint characteristics. *Food Science* 42, 255–262. doi: 10.3864/j.issn.0578-1752.2022.21.012

Zhou, Y., and Staver, A. C. (2019). Enhanced activity of soil nutrient-releasing enzymes after plant invasion: a meta-analysis. *Ecology* 100, e02830. doi: 10.1002/ecy.2830

frontiers | Frontiers in Plant Science

TYPE Original Research
PUBLISHED 01 August 2024
DOI 10.3389/fpls.2024.1416397

OPEN ACCESS

EDITED BY
Enrique Ostria-Gallardo,
University of Concepcion, Chile

REVIEWED BY
Hongmei Cai,
Huazhong Agricultural University, China
Catalina Castro,
Universidad de Concepción, Chile

*CORRESPONDENCE
Wanjun Feng
fengwj123@sxau.edu.cn
Baoguo Chen
bgchen108@sina.com

†These authors have contributed equally to this work

RECEIVED 18 April 2024
ACCEPTED 17 July 2024
PUBLISHED 01 August 2024

CITATION
Feng W, Xue W, Zhao Z, Shi Z, Wang W, Bai Y, Wang H, Qiu P, Xue J and Chen B (2024) Nitrogen fertilizer application rate affects the dynamic metabolism of nitrogen and carbohydrates in kernels of waxy maize. *Front. Plant Sci.* 15:1416397. doi: 10.3389/fpls.2024.1416397

Nitrogen fertilizer application rate affects the dynamic metabolism of nitrogen and carbohydrates in kernels of waxy maize

Wanjun Feng[1*†], Weiwei Xue[2†], Zequn Zhao[2†], Zhaokang Shi[2], Weijie Wang[2], Yu Bai[2], Haoxue Wang[2], Peng Qiu[1], Jianfu Xue[2] and Baoguo Chen[2*]

[1]Sorghum Research Institute, Shanxi Agricultural University, Yuci, Shanxi, China, [2]College of Agriculture, Shanxi Agricultural University, Taigu, Shanxi, China

Introduction: Nitrogen (N) plays a pivotal role in the growth, development, and yield of maize. An optimal N application rate is crucial for enhancing N and carbohydrate (C) accumulation in waxy maize grains, which in turn synergistically improves grain weight.

Methods: A 2-year field experiment was conducted to evaluate the impact of different N application rates on two waxy maize varieties, Jinnuo20 (JN20) and Jindannuo41 (JDN41), during various grain filling stages. The applied N rates were 0 (N0), 120 (N1), 240 (N2), and 360 (N3) kg N ha^{-1}.

Results: The study revealed that N application significantly influenced nitrogen accumulation, protein components (gliadin, albumin, globulin, and glutelin), carbohydrate contents (soluble sugars, amylose, and amylopectin), and activities of enzymes related to N and C metabolism in waxy maize grains. Notable varietal differences in these parameters were observed. In both varieties, the N2 treatment consistently resulted in the highest values for almost all measured traits compared to the other N treatments. Specifically, the N2 treatment yielded an average increase in grain dry matter of 21.78% for JN20 and 17.11% for JDN41 compared to N0. The application of N positively influenced the activities of enzymes involved in C and N metabolism, enhancing the biosynthesis of grain protein, amylose, and amylopectin while decreasing the accumulation of soluble sugars. This modulation of the C/N ratio in the grains directly contributed to an increase in grain dry weight.

Conclusion: Collectively, our findings underscore the critical role of N in regulating kernel N and C metabolism, thereby influencing dry matter accumulation in waxy maize grains during the grain filling stage.

KEYWORDS

waxy corn, nitrogen application, protein components, carbohydrate content, enzyme activity

1 Introduction

Waxy maize (*Zea mays* L. var. *ceratina* Kulesh) is a subspecies of maize, also called sticky maize, and is characterized by its viscosity and digestibility. It emerged in southwest China in the early 20th century (Collins, 1909). Due to the mutation of the *waxy* gene (*Wx*), almost all the starch synthesized in the kernels of waxy corn is amylopectin (Schwartz and Whistler, 2009). In recent decades, waxy maize has gained popularity among consumers and farmers in Asia due to its unique taste, high nutritional and economic value, and ease of processing (Yang et al., 2021). In addition, it is also an important industrial raw for the textile, adhesive, brewing and paper industries (Klimek-Kopyra et al., 2012; Liu et al., 2021).

Nitrogen (N) is an essential mineral element for plants and an important regulatory factor for plant growth, development and yield production (Kant, 2018). In fact, the increasing use of N fertilizers over the last half century has contributed significantly to significantly improving global food production (Foley et al., 2011). However, excessive N application often occurs in crop production around the world, resulting in lower N use efficiency (NUE) for plants (Zhang et al., 2015). According to field research experiments, the NUE ranges from 10 and 60%, which is lower than other cereals (Cui et al., 2010; Ladha et al., 2016; Morris et al., 2018). In addition, large N fertilizer loss also leads to adverse effects on crop quality, soil acidification, greenhouse effect, environmental pollution and human health (Guo et al., 2010; Mueller et al., 2012; Liu et al., 2020). Therefore, to address the triple challenges of climate change, environmental degradation and food security, increasing crop NUE can be a useful tactic (Zhang et al., 2015).

Nitrogen and carbohydrate metabolism in corn kernels is closely related to the synthesis and accumulation of storage proteins, starch, and other compounds. Compared to other maize, waxy maize lacks the production of amylose, resulting in different carbohydrate metabolism as starch composed vast majority of amylopectin. Meanwhile, previous studies demonstrated that N and carbohydrate metabolism have interaction in maize kernels (Swank et al., 1982; He et al., 2004; Li et al., 2022). Hence, it is believed that carbon and nitrogen metabolism in kernels between waxy maize and other maize may be significant differently. Starch and protein are two important nutritional components of cereal grains, and the dynamics of their content and accumulation influence grain yield and quality (Lu et al., 2014; Zhang et al., 2021). The process of starch and protein biosynthesis in cereal grains is complicated and relies on the synchronized activity of lots of enzymes (Ran et al., 2020). In the process of N assimilation, nitrate reductase (NR), nitrite reductase (NiR), glutamine synthetase (GS), and glutamine-2-oxoglutarate aminotransferase (GOGAT, also known as glutamate synthase) are the most important enzymes (Liu et al., 2022). Soluble starch synthase (SSS), granule bound Starch Synthase (GBSS), starch branching enzyme (SBE) and starch debranching enzyme (SDBE) are involved in starch synthesis in cereal grains and play crucial roles in the metabolic processes of grain development and yield formation, and ADP-glucose pyrophosphorylase (AGPase) is responsible for converting ADP-glucose into starch polymers, providing energy and building blocks for grain development (Smith and Zeeman, 2020).

It is clear that N fertilization affects the nitrogen metabolism in plant, influencing the synthesis of proteins and amino acids, as well as the translocation and allocation of N in maize (Chen et al., 2015; Mueller and Vyn, 2016). It has long been suggested that grain protein content (GPC) can be increased with an appropriate amount of N fertilizer (Qi et al., 2006). Furthermore, N availability can also impact the photosynthetic activity and carbohydrate metabolism in grains, thereby influencing the accumulation of starch and other carbohydrates is crucial for kernel development and yield formation (Mueller and Vyn, 2016). However, the specific impacts on the dynamic metabolism of nitrogen and carbohydrates in waxy maize kernels remain relatively understudied. Understanding the intricate biochemical and physiological processes underlying the response of waxy maize kernels to varying N fertilizer application rates is crucial for optimizing agricultural practices and enhancing waxy maize yield and quality. In this study, we aim to investigate the effects of nitrogen fertilization on the metabolism of nitrogen and carbohydrates in waxy maize kernels at different days after pollination (DAP), with a focus on elucidating the regulatory mechanisms that govern waxy maize yield, to provide valuable insights into the physiological and biochemical basis for optimizing nitrogen management strategies to maximize waxy maize yield and quality.

2 Materials and methods

2.1 Material planting and preparing

Two waxy maize varieties (Jinnuo20 (JN20), a purple waxy maize variety; and Jindannuo41 (JDN41), a yellow waxy maize variety) were used as experimental materials, the seeds of which were purchased from Shanxi Dafeng Seed Industry Co., LTD. The field experiment was conducted in Dongshan bottom Village (37° 22'28" N, 12°35'8" E), Taigu County, Shanxi Province, China, in 2018 and 2019. The field had been planted with trees for five years without planting crops or fertilizing before the trial began. Prior to conducting the experiment, the tested topsoil (0–20 cm) was sandy loam with pH value of 6.1, and the soil nutrient content prior to sowing was as follows: the contents of total N, alkaline hydrolyzable N, available phosphorus (P), exchangeable potassium (K) and organic substances were 0.66 g kg^{-1}, 30.24 mg kg^{-1}, 20.02 mg kg^{-1}, 114.11 mg kg^{-1} and 18.10 g kg^{-1}, respectively.

The experiment employed a split-plot design, incorporating three replicates. Main plots were allocated to two varieties of waxy maize, while subplots were designated to four nitrogen (N) fertilizer application rates: 0, 120, 240, and 360 kg ha^{-1} of pure N, referred to as N0, N1, N2, and N3, respectively. Maize planting occurred in late May for two consecutive years, utilizing a randomized plot arrangement with triple replicates. Each plot measured 40 m^2 (4 m x 10 m) and contained 8 rows, with a planting density of 60,000

plants ha^{-1}. Fertilizers used included urea (46% N) for nitrogen, superphosphate (12% P_2O_5) for phosphorus, and potassium chloride (60% K_2O) for potassium. Nitrogen was applied in a 3:5:2 ratio at the jointing, booting, and anthesis-silking stages. Additionally, 120 kg ha^{-1} of pure phosphorus (P_2O_5) and 240 kg ha^{-1} of pure potassium (K_2O) were administered in a 1:1 ratio at sowing and jointing stages. Corn cultivation followed standard field management practices.

The harvested ears were manually bagged to ensure pollination occurred without external pollen contamination. Sampling was conducted from 15 to 35 days after pollination (DAP), at five-day intervals. In each of the three replicates across all treatment groups, five uniformly growing ears were selected for seed extraction. Some seeds were blanched in an oven at 120 ° for 30 min, and dried at 80 ° to constant weight, and used to determine the biomass, nitrogen content, protein content and its fractions, and soluble sugar and starch content of the other seeds frozen in liquid nitrogen and quickly stored in an ultra-low temperature refrigerator of -80°C for measuring the activity of N and carbohydrate metabolic enzymes. All measurements were taken in three biological replicates.

2.2 Total nitrogen content assay

Total nitrogen content in the seeds was measured by a modified Kjeldahl digestion method (Nelson and Sommers, 1962). In brief, 0.5 g of dry grain flour was deboiled by H_2SO_4 for 10 min, and then heated for 5-10 min to remove the remaining H_2O_2. Later, the decocting liquid was fixed to 100 mL with distilled water, and 1.0 mL of the diluted solution was absorbed and added 1 mL EDTA-methyl red solution adjusting with NaOH (0.3 mo1 L^{-1}) to pH value for 6.0, and 5 mL phenol solution and 5 mL sodium hypochlorite solution were added in turn. After 1 h, the optical density (OD) was measured using a UV spectrophotometer (Shanghai Metash Instruments Co., Ltd., Shanghai, China) at 625 nm. The blank test solution was used to adjust zero point of instrument absorption value. After measuring the absorption value, the working curve was drawn to calculate the nitrogen content of samples.

2.3 Protein quantification

Protein content was assayed using the Coomassie brilliant blue G-250 method (Li and Li, 2000). Initially, a Coomassie brilliant blue G-250 and standard protein solutions were prepared. Using a mortar and pestle, 0.5 g of dry seeds were ground with 10 mL of distilled water. After centrifugation of the solution at 4000 × g at 4°C for 10 min, the supernatant was transferred to a clean tube and total protein content measured as the change in absorbance at 595 nm. Then, prepare a BSA protein standard at 1 mg mL^{-1} concentration in duplicate and dilute the protein standard in a volume of 20 µL to give 5 concentrations over a range of 10 to 50 µg protein. Add 20 µL of protein solution to 1 mL of dye reagent, mix, incubate for 2 min at room temperature and measure the absorbance in a cuvette. Subsequently, a calibration curve was plotted to depict the relationship between the absorbance values at 595 nm and the known protein concentrations. The protein concentration of the unidentified sample was deduced by aligning its absorbance value with the established calibration curve.

2.4 Determination of protein components

Protein components were determined using a previous method with slight modifications (Ju et al., 2001). 0.5 g fresh sample was ground into a homogeneous slurry in an ice bath and transferred to a 5 mL centrifuge tube. The slurry was then mixed with 5 mL of distilled water and agitated for 30 min. The mixture was centrifuged at 2000 rpm at 4 ˚C for 5 min, after which the supernatant was decanted, and the pellet was resuspended in 5 mL of distilled water for precipitation. This process was repeated twice, and the collected supernatant was adjusted to a final volume of 50 mL for the purpose of albumin quantification. Subsequently, 5 mL of a 10% sodium chloride solution was added to the residue within the centrifuge tube to facilitate albumin extraction. After the subsequent extraction method of albumin, centrifuge at 3000 g for 0.5 h and repeat three times to obtain the globulin fraction in the supernatant. The pellet from the previous step was dissolved with 5 mL of NaCl solution (10%) and centrifuge at 3000 g for 0.5 h at 4 ˚C. Following this centrifugation, the albumin extraction methodology was employed, and the procedure was repeated twice to further isolate the globulin component from the supernatant. For the extraction of the glutelin fraction, the precipitate remaining in the centrifuge tube was treated with 0.1 M NaOH (400 mL) at room temperature and subsequently centrifuged at 3000 g for 30 min. To isolate the gliadin fraction, the precipitate was then extracted with 70% ethanol (400 mL) under ambient conditions and centrifuged at 3000 g for 30 min.

The quantification of the extracted total proteins, albumins, globulins, gliadins, and glutelins was performed utilizing a UV spectrophotometer, with Bovine Serum Albumin (BSA) serving as the calibration standard. To establish a calibration curve, six standard solutions were prepared, comprising 0, 2.5, 5, 10, 15, and 20 µL of a BSA stock solution (1 mg mL^{-1}) each diluted in 1 mL of Bradford reagent. For the assay, 2 µL of each protein extract was combined with 1 mL of Bradford reagent. The tubes were then thoroughly mixed by inversion before the absorbance was measured at 595 nm using a UV spectrophotometer (Shanghai Metash Instruments Co., Ltd., Shanghai, China) (Marion, 1976). The standard linear curve of six points was created by using MS excel and concentrations of protein samples were calculated.

2.5 Starch content

The amylose content and amylopectin content were spectrophotometrically determined by the double-wavelength method (Dong et al., 2003). For the determination, 0.1 g of milled grains were stirred with 10 mL of 0.5 M KOH for 30 min at 90°C and then diluted to a volume of 50 mL with distilled water. From this, 2.5 ml was removed to a fresh tube containing 20 mL distilled water. The solution was adjusted to pH 3.5 with 0.1 M HCl, and 500 µL of I_2-KI reagent added. Finally, this solution was diluted to a

final volume of 50 mL with distilled water. After standing for 20 min, the absorbance of the mixture was measured with a UV spectrophotometer (Shanghai Metash Instruments Co., Ltd., Shanghai, China) at 480, 550, 630, and 735 nm, respectively. The total starch content was defined as the sum of amylose and amylopectin content.

2.6 Soluble sugars content

Soluble sugars were extracted according to a previous method (Adney and Baker, 1996). After being ground and homogenized with 10 mL of deionized water, 500 mg samples along with 5 mL of an 80% ethanol (C_2H_6O) solution were placed in a water bath at 45° C for 20 minutes. Following this, the samples were allowed to cool to room temperature. The homogenate was then centrifuged twice at 6000 rpm for 10 minutes at 15°C. Next, 2 mL of the supernatant was combined with 2 mL of 3,5-dinitrosalicylic acid reagent, thoroughly mixed, and then boiled in a water bath for 5 min. After boiling, the mixture was cooled to room temperature in a water-ice bath. The supernatant was collected for the determination of soluble sugar content using a UV spectrophotometer at 540 nm (Shanghai Metash Instruments Co., Ltd., Shanghai, China). Distilled water was used as a control, and glucose was employed to create a standard curve. The C/N ration was calculated by the formula: C/N ration = (Soluble sugar content + Starch content)/ Total nitrogen content.

2.7 Enzyme activities

Nitrate reductase (NR) was extracted and measured using a Nitrate Reductase (NR) Assay Kit (BC0080, Solarbio, Beijing, China). In brief, 0.1 g of fresh seed powder that frozen and grinded in liquid nitrogen was extracted in 1 mL extraction solution, and the mixture was centrifuged at 4000 × g at 4 ° for 10 min. The supernatant was absorbed for analyzing the OD value, and the absorbance at 520 nm was used for the calculation of NR activity.

Glutamine synthetase (GS) was extracted and measured using a Glutamine Synthetase (GS) Assay Kit (BC0915, Solarbio, Beijing, China). Briefly, 0.1 g of fresh seed powder frozen and ground in liquid nitrogen was extracted with 1 mL extraction buffer. The mixture was centrifuged for 10 min at 8000 × g at 4°C. Finally, the supernatant was collected after centrifugation for analysis of OD value and the absorbance at 520 nm was used to calculate GS activity.

The preparation procedure was according to a previous method (Nakamura et al., 1989). For the assays of enzymes, 5-10 g frozen grains were weighed and homogenized with a pestle in a pre-cooled mortar containing 10 mL ice-cooled extraction buffer (50 mM Hepes-NaOH [pH 7.5], 2 mM KCl, 5 mM EDTA, 1 mM DTT [Dithiothreitol], 1% (w/v) PVP [polyvinylpyrrolidone-30]). An aliquot of the homogenate (30 µL) was mixed with 1.8 mL extraction buffer and then centrifuged at 2000 g at 4°C. The homogenate was centrifuged at 10000 g for 0.5 h at 4°C, and the resulting supernatant was used for the determination of AGPase, SSS, SBE and DBE activities. The precipitate was re-suspended in 0.5 mL extraction solution and used for the determination of GBSS activity. Meanwhile, 50.0 µL of crude enzyme solution was taken and added to boiling water for 60 s in advance. The check procedure was then carried out as above. The production of NADH was monitored spectrophotometrically at 340, 540 and 660 nm using a UV spectrophotometer (Shanghai Metash Instruments Co., Ltd., Shanghai, China).

2.8 Data analysis

Statistical analysis was performed using Excel (Microsoft Office 2016) and SPSS v.26 statistical package (SPSS, Chicago, IL, USA). The test of normal distribution was conducted using the "nortest" packages in Rstudio software. Differences of above testing parameters, as affected by N application rate, harvest period, year and their interactions, were examined using a three-factor model of analysis of variances (ANOVA). When the ANOVA was proved significant for any parameter, a least significant difference (LSD) test was assayed for multiple comparisons at $P \leq 0.05$. Correlation analysis was performed using the Origin2022 software (OriginLab Corporation, Northampton, MA, USA). Regression analysis was performed using the "ggplot2" and "ggsignif" packages in Rstudio software. A structural equation model (SEM) was used to analyze the effects of N fertilizer application on detected characteristics of waxy maize grains using the "lavaan" package in Rstudio software. Data in figures were the average of three biological replicates.

3 Results

3.1 Effects of nitrogen level on the dynamic accumulation of kernel dry matter

The ANOVA analysis indicated that grain dry weight (GDW) was significantly affected by year (Y), filling time (T), variety (V), nitrogen level (NL), V×T and T×NL, but other interactions between the two or three factors had no significant effects on the GDW (Figure 1; Supplementary Figure 1). The effects of four nitrogen levels on GDW of Jinnuo20 (JN20) and Jindannuo 41 (JDN41) at different days after pollination (DAP) were similar and consistent in two years, all showing N2≥N3>N1>N0. In detail, the JN20 GDW under N1, N2 and N3 treatments raised with ranges of 1.11%-40.04%, 5.95%-55.80% and 3.72%-58.07% compared to N0 at different DAP over the two years, respectively. And the GDW of JDN41 under N1, N2 and N3 treatments increased with ranges of 2.67%-24.43%, 4.69%-33.00% and 3.05%-33.45% compared to N0 based on the five filling time points within the two years, respectively. Furthermore, the GDW of JN20 and JDN41 both raised gradually from 15 to 35 DAP under four N treatments, and the GDW of JN20 and JDN41 increased by an average of 94.68% and 81.83%, 173.26% and 133.43%, 229.60% and 166.67%, and 261.55% and 186.38% at 20, 25, 30, and 35 DAP, compared to 15 DAP, respectively, over the four N treatments within two years.

10.3389/fpls.2024.1416397

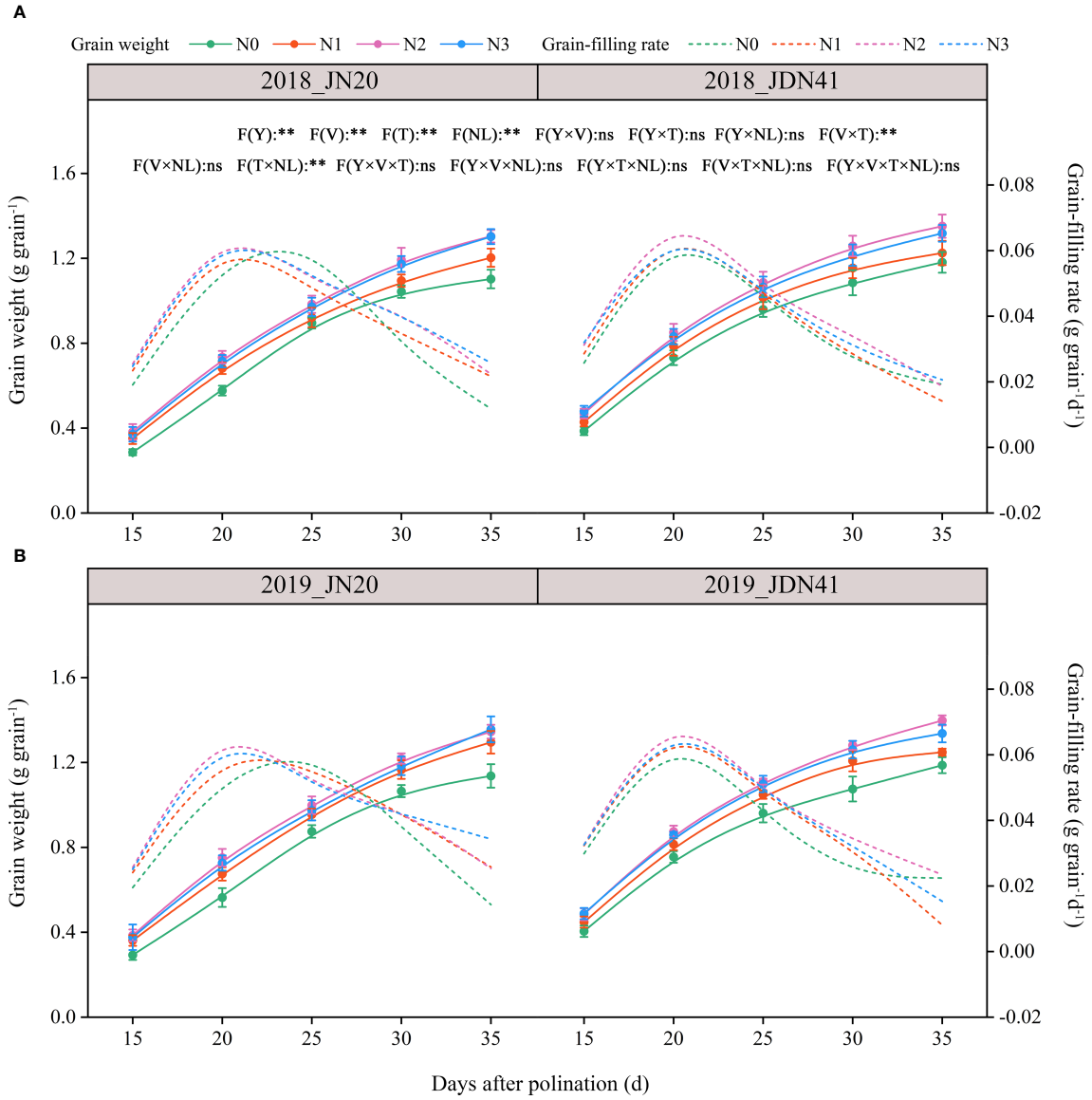

FIGURE 1
Effects of nitrogen rate on the grain weight dynamics and filling rate of two waxy maize varieties at different days after pollination in 2018 **(A)**, 2019 **(B)**. The grain filling rate is the derivative of the grain weight accumulation. ns indicates no significant differences, and * and ** indicate significant differences at $P < 0.05$, and $P < 0.01$ level, respectively. The error bar indicates standard error based on 3 data.

Obviously, nitrogen level also had significant effect on grain filling rate (GFR) of JN20 and JDN41 (Figure 1; Supplementary Figure 1). The GFR of JN20 under N1, N2 and N3, and that of JDN41 under N0, N1, N2 and N3, all reached a peak at 20 DAP, but that of JN20 under N0 delayed to 25 DAP, indicating that nitrogen levels had different effects on the GFR within maize varieties. Except for JN20 at 25 DAP, which was higher under N0 than other three N treatments, the GFR of JD20 under N1, N2 and N3 treatments all enhanced with ranges of 2.22% (15 DAP)-1129.13% (35 DAP), 2.20% (15 DAP)-891.26% (35 DAP) and 1.37% (15 DAP)-659.22% (35 DAP) compared to N0 over the five filling time points within the two years, respectively. For JDN41, the GFR at 35 DAP showed the higher values under N0 compared with other N treatments, but that of JDN41 at other grain filling stages all increased with ranges of 5.38%-104.08%, 7.30%-167.53% and 5.14%-119.00%, respectively.

3.2 Effects of nitrogen level on the dynamic metabolism of grain nitrogen

3.2.1 Grain nitrogen content

The GNC was significantly affected by factors Y, T, V, NL, and Y×V, but the other interactions between the two or three factors had no significant effects on the GNC (Figure 2; Supplementary Figure 2). The effects of four nitrogen levels on GNC of JN20 and JDN41 at different DAP were similar and constant within the two years, almost

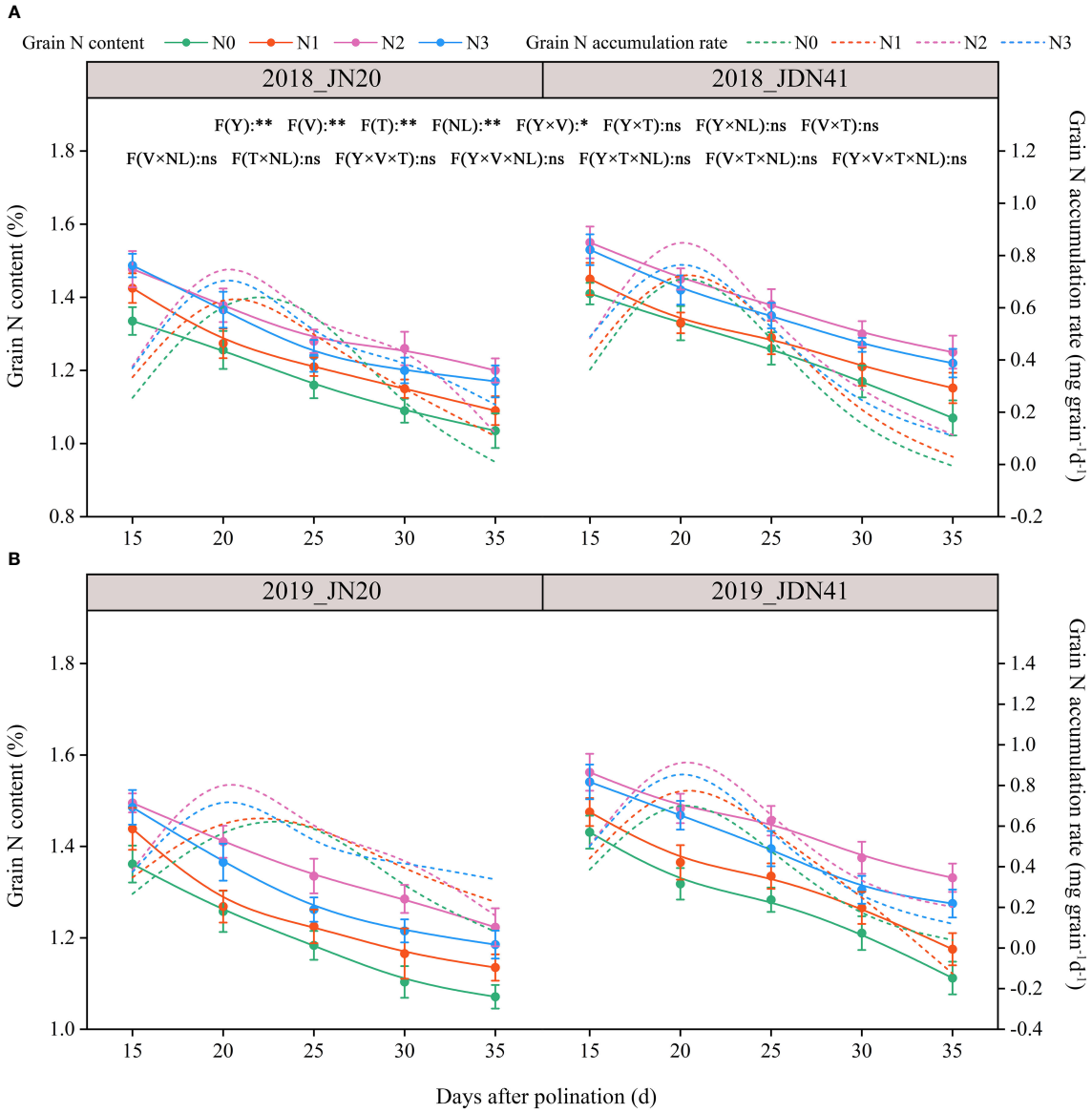

FIGURE 2
Effects of nitrogen rate on the grain N content and accumulation rate of two waxy maize varieties at different days after pollination in 2018 **(A)**, 2019 **(B)**. The grain N accumulation rate is the derivative of the grain N content accumulation. ns indicates no significant differences, and * and ** indicate significant differences at $P < 0.05$, and $P < 0.01$ level, respectively. The error bar indicates standard error based on 3 data.

showing a trend of N2>N3>N1>N0. The JN20 GNC under N1, N2, and N3 treatments grew by different ranges compared to N0 over two years. Specifically, the increases were between 0.26% and 14.46%, 4.22% and 21.58%, and 1.82% and 14.67%. Similarly, the JDN41 GNC increased by ranges of 1.29% to 14.81%, 5.13% to 24.49%, and 4.21% to 18.50%, respectively. In addition, the GNC of JN20 and JDN41 both dropped gradually from 15 to 35 DAP under four N treatments, which decreased by an average of 8.03% and 6.57%, 13.96% and 10.06%, 17.72% and 15.45%, and 20.84% and19.85% at 20, 25, 30, and 35 DAP compared to 15 DAP, respectively, over the four N treatments within two years.

In consistent with GFR, the grain N accumulation rate (GNAR) of JN20 under N1, N2 and N3, and that of JDN41 under four nitrogen levels, all reached a peak close to 20 DAP, but that of JN20 under N0 delayed close to 25 DAP (Figure 2; Supplementary Figure 2), indicating that nitrogen level also had significant effect on GNAR of both JN20 and JDN41, but with different effects within varieties. For instance, the GNAR of JN20 and JDN41 had the greatest values under N2 treatment, increasing by an average of 431.21% and 131.39% compared to N0 during the five filling time points over the two years.

3.2.2 Nitrate reductase and glutamine synthetase activity

As shown in Figure 3, the NR activity in JDN41 grains was much higher than that of JN20 under the same N level and at the same time point. The NR activity in the grains of both genotypes decreased gradually from 15-35 DAP under four N application rates

10.3389/fpls.2024.1416397

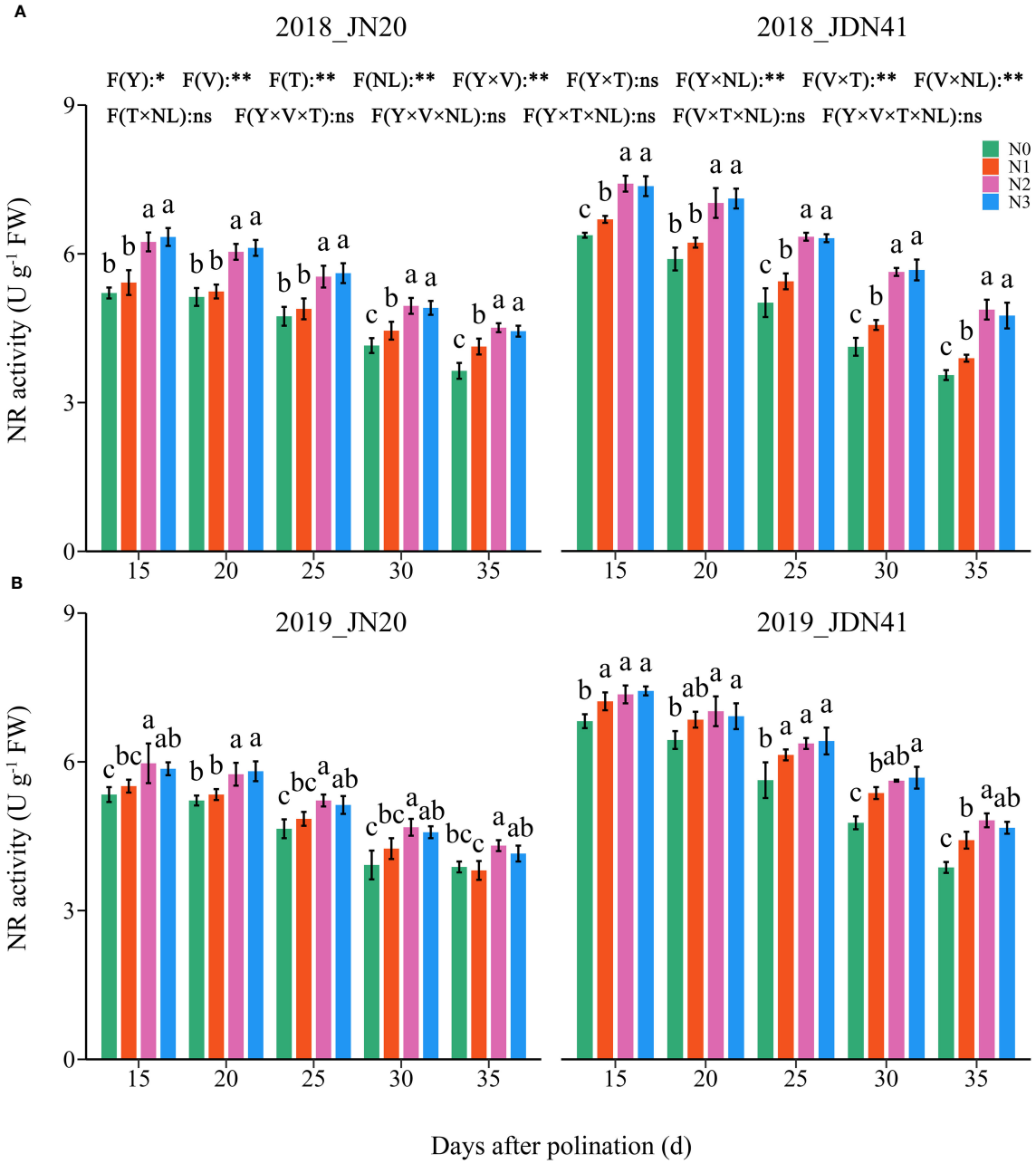

FIGURE 3
Effects of nitrogen rate on nitrate reductase (NR) activity of two waxy maize varieties at different days after pollination in 2018 **(A)**, 2019 **(B)**. ns indicates no significant differences, and * and ** indicate significant differences at $P < 0.05$, and $P < 0.01$ level, respectively. The different small letters above the error bars indicate significant differences between different treatments at the $P < 0.05$ level. The error bar indicates standard error based on 3 data.

within two years. The effects of N level on NR activity of both genotypes at different DAP were similar and consistent within two years. At any individual time point, the NR activity in the grains of both genotypes showed N3≥N2>N1≥N0. In detail, the NR activity of JN20 rose by 0.25%-23.12%, 4.58%-34.26%, and 4.06%-30.64% after N1, N2, and N3 treatments compared to N0 over the two-year period. And JDN41's values increased by 1.01%-16.80%, 2.88-45.93%, and 3.59%-45.64%, respectively (Supplementary Figure 3).

In contrast, the GS activity was unobvious between the two genotypes under the same N level and at the same time point (Figure 4; Supplementary Figure 3). Similarly, the GS activity in the grains of both genotypes decreased gradually from 15-35 DAP under four N levels within two years. The effects of N level on GS activity of both genotypes at different DAP were similar and consistent within two years. At the same grain filling stage, the GS activity in the grains of both genotypes showed a trend of N3≥N2>N1≥N0. In detail, the GS activity of JN20 under N1, N2 and N3 treatments increased by an average of 6.04%, 11.44% and 14.94% compared to N0 over five time points within two years, respectively. And that of JDN41 increased by an average of 6.52%,

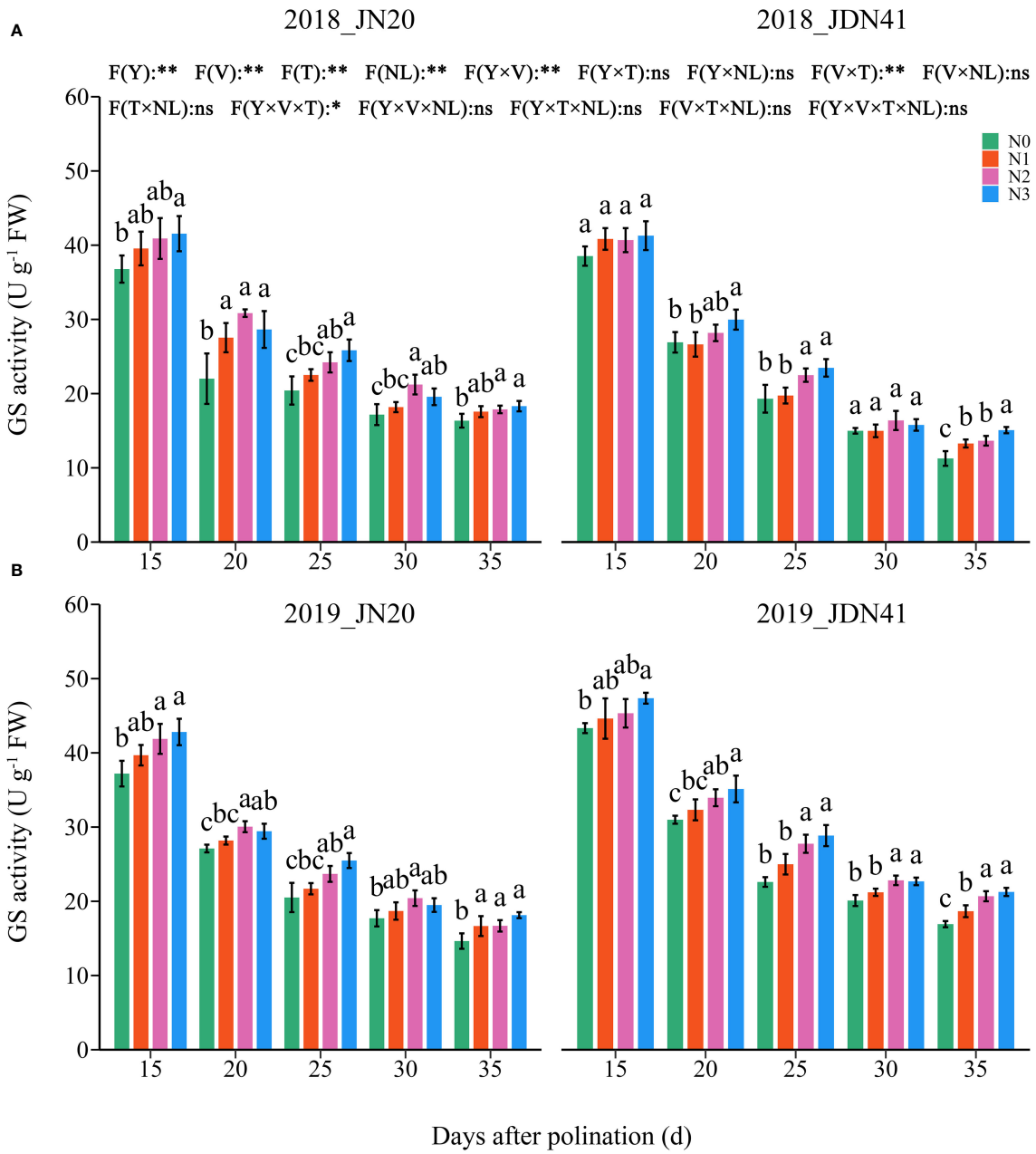

FIGURE 4
Effects of nitrogen rate on glutamine synthetase (GS) activity of two waxy maize varieties at different days after pollination in 2018 **(A)**, 2019 **(B)**. ns indicates no significant differences, and * and ** indicate significant differences at $P < 0.05$, and $P < 0.01$ level, respectively. The different small letters above the error bars indicate significant differences between different treatments at the $P < 0.05$ level. The error bar indicates standard error based on 3 data.

12.80% and 16.49%, respectively. Above results indicated that increasing N rate would induce the NR and GS activity.

3.2.3 Protein components content

The protein components in maize kernels are complex, which classified as gliadin (also called zeins), albumin, globulin and glutelin according to their solubility. As shown in Figure 5, the total protein content of JDN41 was higher than that of JN20 at any time point under four nitrogen levels in two years. Over time, the levels of albumin, globulin, and other protein components of both genotypes gradually decreased under the four nitrogen levels. On the contrary, both gliadin and glutelin content of the two genotypes showed a gradually increasing trend. The effects of N level on all protein components of both genotypes at any grain filling stage were almost coincident within two years, all showing N2≥N3>N1>N0. In detail, the grain albumin content of JN20 under N0, N1, N2 and N3 decreased from 3.55%, 3.67%, 3.82% and 3.87% at 15 DAP to 1.31%, 1.27%, 1.35% and 1.20% at 35 DAP over the two years, while that of JDN41 declined from 3.84%, 3.73%, 3.77% and 3.86% at 15 DAP to 1.42%, 1.42%, 1.49% and 1.32% at 35

10.3389/fpls.2024.1416397

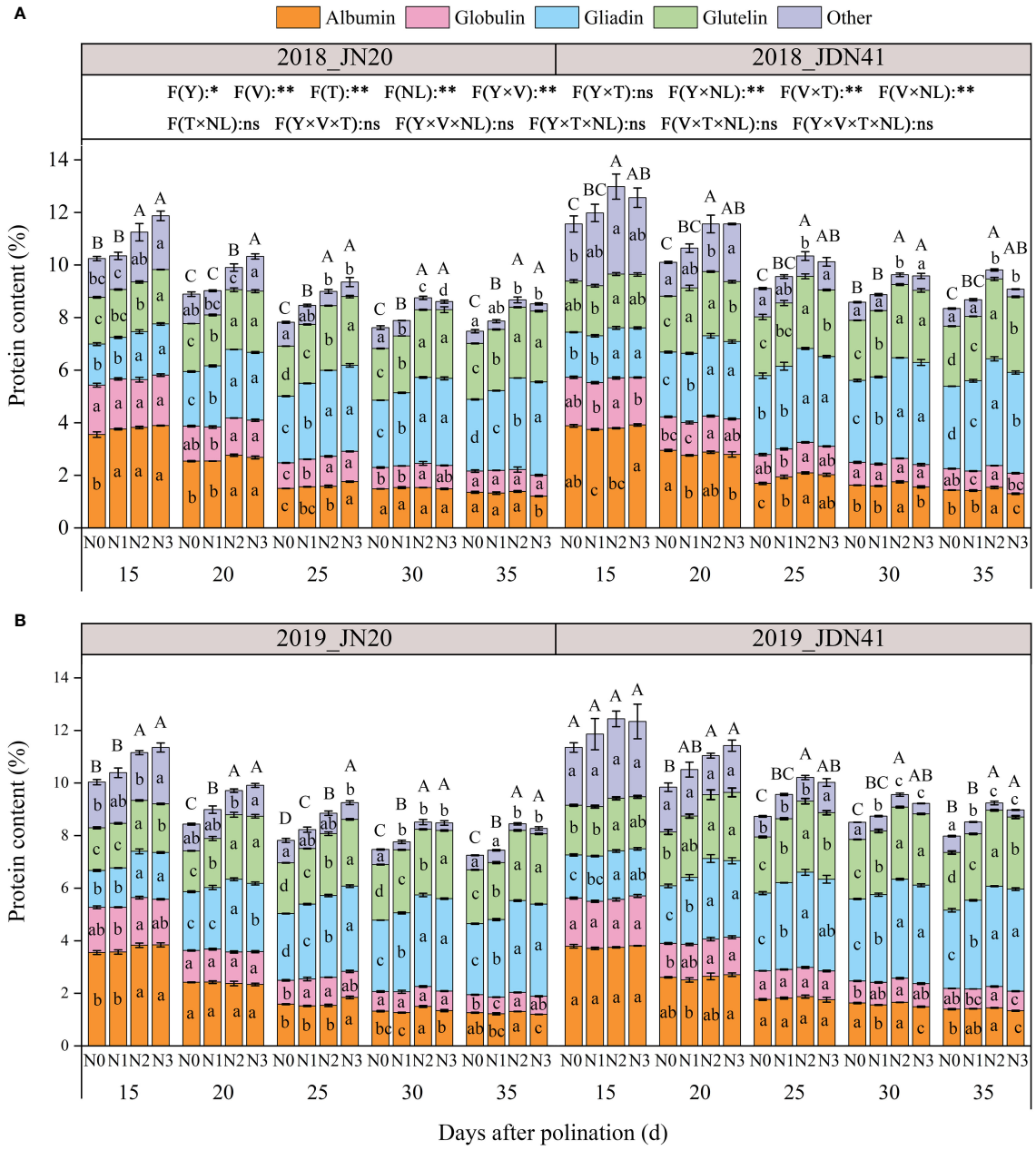

FIGURE 5
Effects of nitrogen rate on protein content and components of two waxy maize varieties at different days after pollination in 2018 **(A)**, 2019 **(B)**. ns indicates no significant differences, and * and ** indicate significant differences at $P < 0.05$, and $P < 0.01$ level, respectively. Different lowercase and capital letters indicate significant differences in protein components and protein content between different treatments at the $P<0.05$ level, respectively. The error bar indicates standard error based on 3 data.

DAP, respectively (Figure 5; Supplementary Figure 4). For the grain globulin content of JN20, it diminished from 1.80%, 1.80%, 1.82% and 1.83% at 15 DAP to 0.74%, 0.75%, 0.78% and 0.74% at 35 DAP, while that of JDN41 declined from 1.84%, 1.78%, 1.87% and 1.85% at 15 DAP to 0.80%, 0.75%, 0.82% and 0.76% at 35DAP under N0, N1, N2 and N3, respectively. However, the grain gliadin content of JN20 under N0, N1, N2 and N3 improved from 1.48%, 1.54%, 1.79% and 1.86% at 15 DAP to 2.71%, 2.99%, 3.49% and 3.53% at 35 DAP over the two years, while that of JDN41 promoted from 1.68%, 1.75%, 1.88% and 1.84% at 15 DAP to 3.06%, 3.40%, 3.94% and 3.86% at 35 DAP, respectively. The grain glutelin content of JN20 increased from 1.70%, 1.76%, 1.91% and 1.96% at 15 DAP to 2.09%, 2.25%, 2.68% and 2.68% at 35 DAP, while that of JDN41 decreased from 1.92%, 1.89%, 2.02% and 2.01% at 15DAP to 2.24%, 2.49%, 2.96% and 2.81% at 35DAP, respectively. These results demonstrated that the albumin and globulin were preferentially synthesized at the early grain filling stage, while gliadin and glutelin were mainly accumulated at the later grain filling stage, and N had significant effects on the synthesis of protein components, especially on gliadin and glutelin synthesis.

10.3389/fpls.2024.1416397

3.2.4 Regression analysis

Both JN20 and JDN41 GNC were significantly positively correlated with the NR activity (R^2 of JN20 and JDN41 was 0.74 and 0.84), GS activity (R^2 of JN20 and JDN41 was 0.78 and 0.68) (Supplementary Figure 5), albumin content (R^2 of JN20 and JDN41 was 0.72 and 0.61) and globulin content (R^2 of JN20 and JDN41 was 0.72 and 0.66) (Supplementary Figure 6). On the contrary, both JN20 and JDN41 GNC were significantly negatively correlated with the gliadin content (R^2 of JN20 and JDN41 was 0.30 and 0.28), and the relationship between GNC and glutelin content of both genotypes was nonlinear (Supplementary Figure 6).

3.3 Effects of nitrogen level on the dynamic metabolism of grain carbohydrates

3.3.1 Carbohydrate content

To detect the dynamic metabolism of grain C in waxy corn under different N application rates, the contents of three kinds of carbohydrates were determined, including amylose, amylopectin and soluble sugar. The ANOVA analysis showed that the overall content of three carbohydrates was strongly influenced by specific factors and their interactions, as illustrated in Figure 6. As shown in

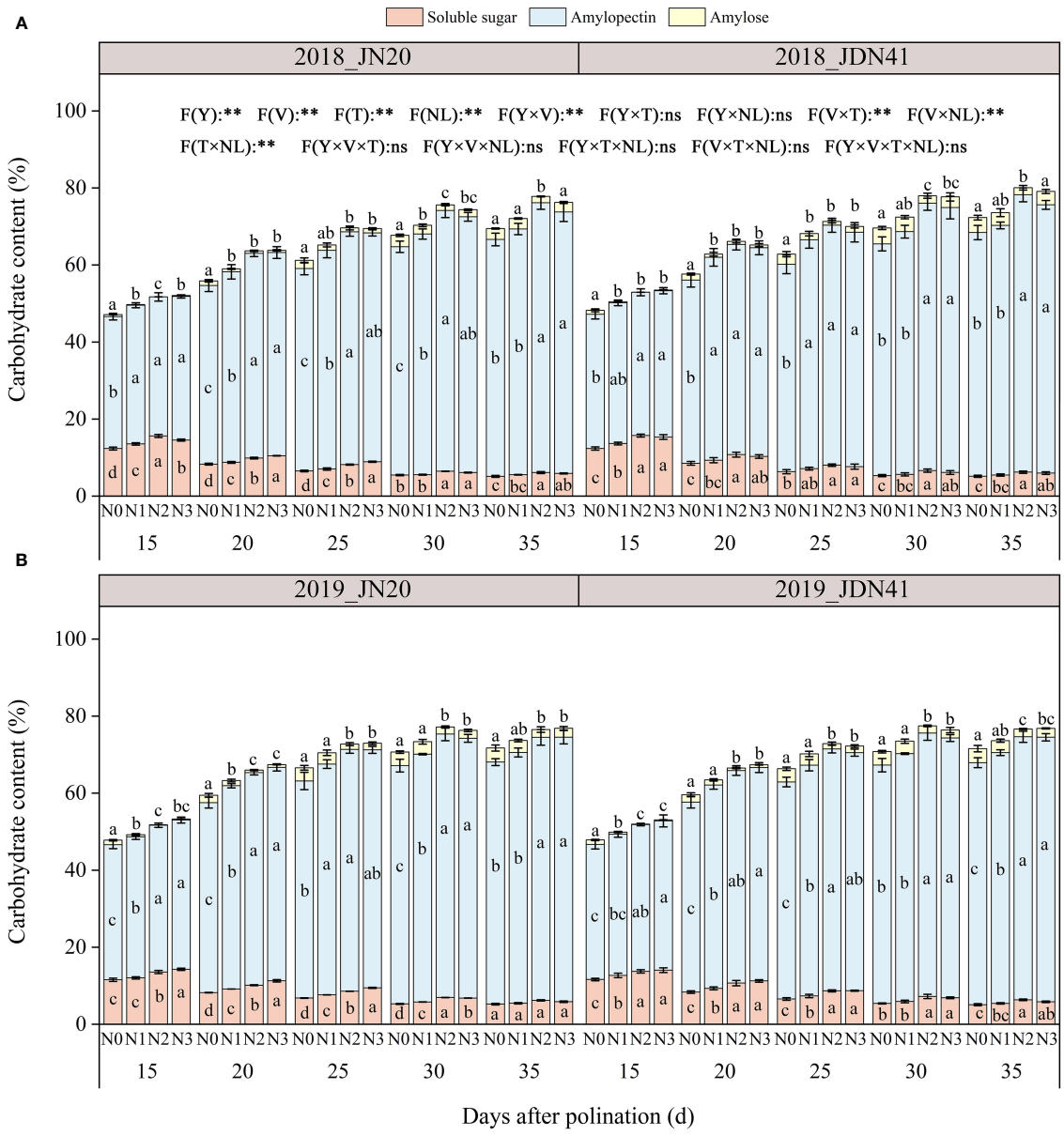

FIGURE 6
Effects of nitrogen rate on carbohydrate content of two waxy maize varieties at different days after pollination in 2018 **(A)**, 2019 **(B)**. ns indicates no significant differences, and * and ** indicate significant differences at $P < 0.05$, and $P < 0.01$ level, respectively. Different lowercase letters indicate significant differences between nitrogen rates at the $P<0.05$ level. The error bar indicates standard error based on 3 data.

Figure 6, the total C content of JDN41 was lower than that of JN20 at any time point under four nitrogen levels in two years. As time goes by, the levels of total C, amylose and amylopectin content of both genotypes promoted sharply from 15 to 30 DAP, and almost ceased from 30 to 35 DAP under the four N levels. The soluble sugar content of the two genotypes showed the opposite change trend compared to amylopectin content and amylose content. In addition, the effects of N level on all C components of both genotypes at any grain filling stage were almost consistent within two years, all showing N2≥N3>N1>N0.

In detail, the soluble sugar content of JN20 and JDN41 decreased over two years from 15 DAP to 35 DAP under different nitrogen levels. The amylopectin content in grain increased with time for both JN20 and JDN41 varieties, with JN20 showing an increase from 34.54% to 62.40% at 15 DAP and 35 DAP, respectively, and JDN41 increasing from 35.06% to 62.84% during the same period (Figure 6). The amylose content in JN20 grains increased from 0.78%, 0.24%, 0.06%, and 0.19% at 15 DAP to 3.34%, 3.02%, 1.74%, and 2.98% at 35 DAP under N0, N1, N2, and N3. For JDN41, the amylose content increased from 1.19%, 0.54%, 0.10%, and 0.25% at 15 DAP to 3.65%, 3.10%, 2.02%, and 2.30% at 35 DAP. These results demonstrated that increasing N dose had significantly negative effects on the soluble sugar metabolism and positive effects on the amylopectin and amylose biosynthesis in waxy maize grains.

3.3.2 C metabolism enzymes

Five C metabolism enzymes in the waxy corn grains, including soluble starch synthase (SSS), granule bound starch synthase (GBSS), starch branching enzyme (SBE), starch debranching enzyme (SDBE) and ADP-glucose pyrophosphorylase (AGPase) were determined. Significant variations in the activities of SBE and DBE enzymes were seen across genotypes throughout different time points, nitrogen application rates, and years. However, the activities of AGPase and SSS only displayed noticeable differences between the two genotypes in 2019 (Figure 7; Supplementary Figure 7). Over time, the activities of GBSS and DBE declined progressively, while the activities of AGPase, SSS, and SBE increased from 15 to 20 DAP and then fell gradually. Furthermore, the application of N enhanced the activity of AGP and SSS, while it suppressed the activity of GBSS and SBE. The impacts of nitrogen application on DBE activity were relatively complex. The N effects for DBE activity of both genotypes were not significant from 15 to 25 DAP in 2018, but applying N apparently enhanced the activity of DBE of both genotypes from 25 to 35 DAP. Meanwhile, N application had a significant impact on DBE activity of both genotypes in 2019. For example, the JN20's AGPase activity raised by 1.91%-20.85%, 4.36%-26.82%, and 1.29%-29.68% with N1, N2, and N3 treatments compared to N0 over the five grain filling stages over two years, respectively. The JDN41 values increased by 0.15%-14.53%, 0.14%-17.53%, and 1.51%-17.66%, respectively. In contrast, the GBSS activity of JN20 under N1, N2 and N3 treatments diminished with ranges of 0.64%-23.01%, 7.21%-58.81% and 2.57%-24.34% compared to N0 over the five grain filling stages within the two years, respectively. And that of JDN41 dropped with ranges of 0.26%-14.59%, 5.56%-34.26% and 2.42%-28.70%, respectively.

3.3.3 Regression analysis

Regression analysis results showed that both JN20 and JDN41 GNC were significantly positively correlated with the soluble sugar content, and R^2 of which was 0.80 and 0.79, respectively (Supplementary Figure 8). However, both JN20 and JDN41 GNC were significantly negatively correlated with the amylose content (R^2 of 0.65 and 0.73, respectively) and amylopectin content (R^2 of JN20 and JDN41 was 0.47 and 0.42, respectively).

Considering that SSS, SBE and SDBE participate in amylopectin synthesis, GBSS plays crucial role in amylose synthesis and AGPaseis is responsible for converting soluble sugar to starch (Smith and Zeeman, 2020). Therefore, we further analyzed the linear relationship between the relevant enzymes and carbohydrates (Figure 8). It showed that AGPase activity and soluble sugar content had a highly significant positive correlation in both genotypes, and SBE and DBE activity of both genotypes had extremely significant negative correlation with amylopectin content, while GBSS activity and amylopectin content was significantly correlated only in JN20. Furthermore, the correlation between SSS activity and amylopectin content was a univariate quadratic relationship, showing a positive correlation between SSS activity at low amylopectin content and a negative correlation at high amylopectin content.

3.4 Effects of nitrogen level on the dynamic C/N ratio

The ANOVA analysis revealed that C/N ratio in waxy corn grains was significantly influenced by V, T, NL, Y×V, V×T and T×NL, but Y and other interactions between the two or three factors had no significant effects on the C/N ratio (Figure 9). The C/N ratio of both genotypes was similar at same time point and under same N levels within two years. With time, the C/N ratio of both genotypes increased gradually under the four N levels within two years, indicating that the N accumulation in waxy corn grains occurs earlier than the C accumulation. In comparison, the C/N ratio of JN20 and JDN41 at 20, 25, 30, and 35 DAP gradually grew by an average of 32.49% and 35.78%, 54.16% and 55.13%, 75.47% and 74.26%, and 87.09% and 84.25% compared to 15 DAP, respectively, over the four N treatments within two years.

In addition, it showed that applying N had no effect on the C/N ratio at the early grain filling stages (15-25 DAP), but it caused a decrease in the C/N ratio at the later grain filling stages (30-35 DAP) (Figure 9). In detail, the JN20 C/N ratio under N1 and N3 treatments increased with ranges of 0.27%-9.56%, and 0.40%-12.35% compared to N0 over the five grain filling stages within the two years, respectively. And the C/N ratio of JDN41 under N1 and N3 treatments increased with ranges of 0.31%-11.28%, and 0.12%-7.95% compared to N0 over the five grain filling stages within the two years, respectively. However, the C/N ratio of JN20 and JDN41 under N2 treatments decreased with ranges of 0.17%-7.79%, and 0.09%-14.50% compared to N0 over the five grain filling stages within the two years, respectively.

10.3389/fpls.2024.1416397

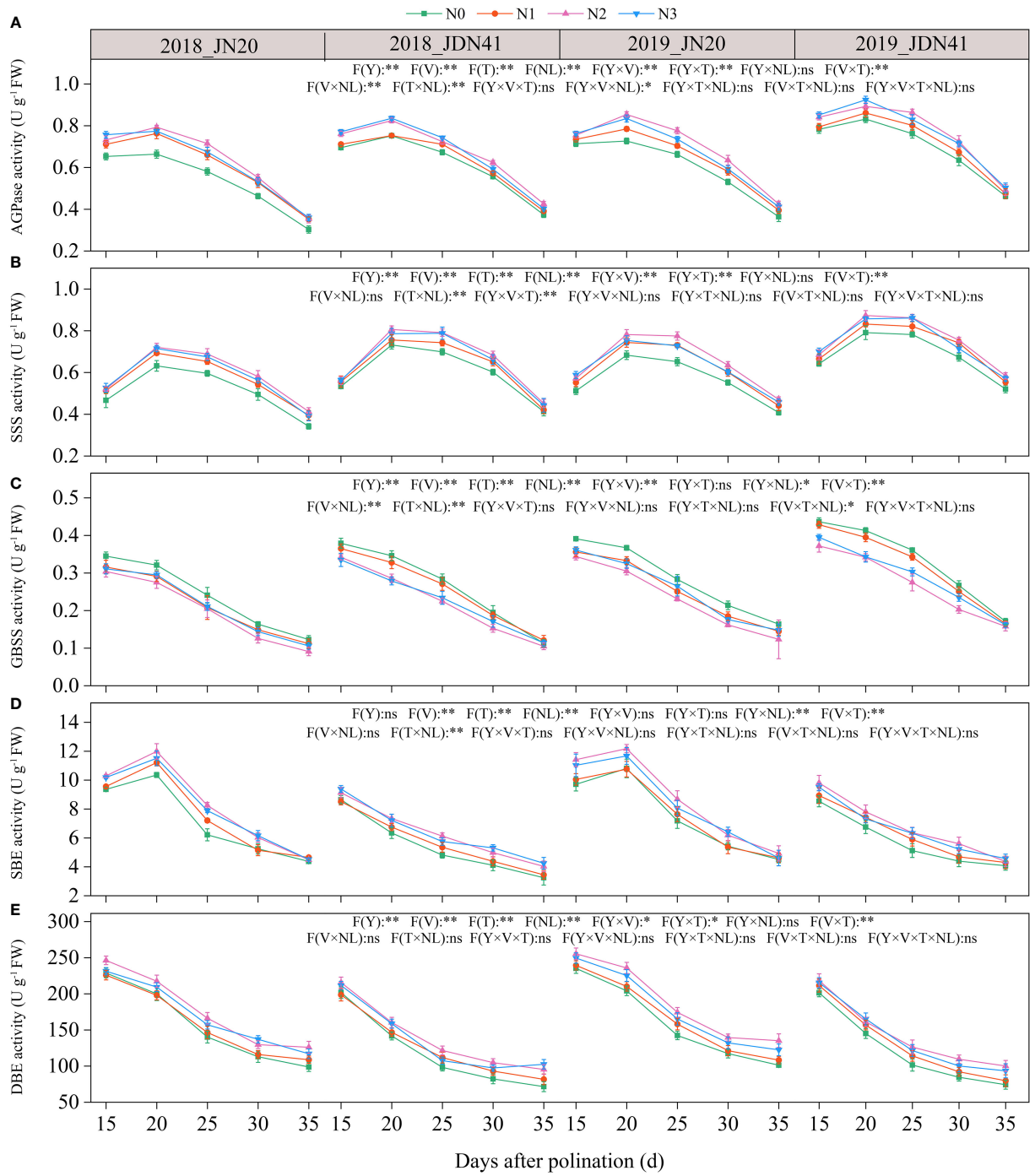

FIGURE 7
Effects of nitrogen rate on the enzymatic activity of carbon metabolism of two waxy maize varieties at different days after pollination. ns indicates no significant differences, and * and ** indicate significant differences at $P < 0.05$, and $P < 0.01$ level, respectively. The error bar indicates standard error based on 3 data. **(A-E)** ADP-glucose pyrophosphorylase (AGPase) activity, soluble starch synthase (SSS) activity, granule bound starch synthase (GBSS) activity, starch branching enzyme (SBE) activity and starch-debranching enzyme (DBE) activity of two waxy maize varieties at different days after pollination in 2018 and 2019, respectively.

3.5 Structural equation model analysis

SEM analysis showed that N application rate had significant positive influences on the enzyme activities related to C and N metabolism at 15-35 DAP directly (Figure 10). The enzymatic activities associated with carbohydrate metabolism exerted a markedly negative impact on the contents of amylose and amylopectin, whilst manifesting a significantly positive influence on the concentration of soluble sugars. In contrast, the contents of amylose and amylopectin were found to significantly bolster the overall starch content. Furthermore, the enzymatic processes integral to nitrogen metabolism were observed to substantially

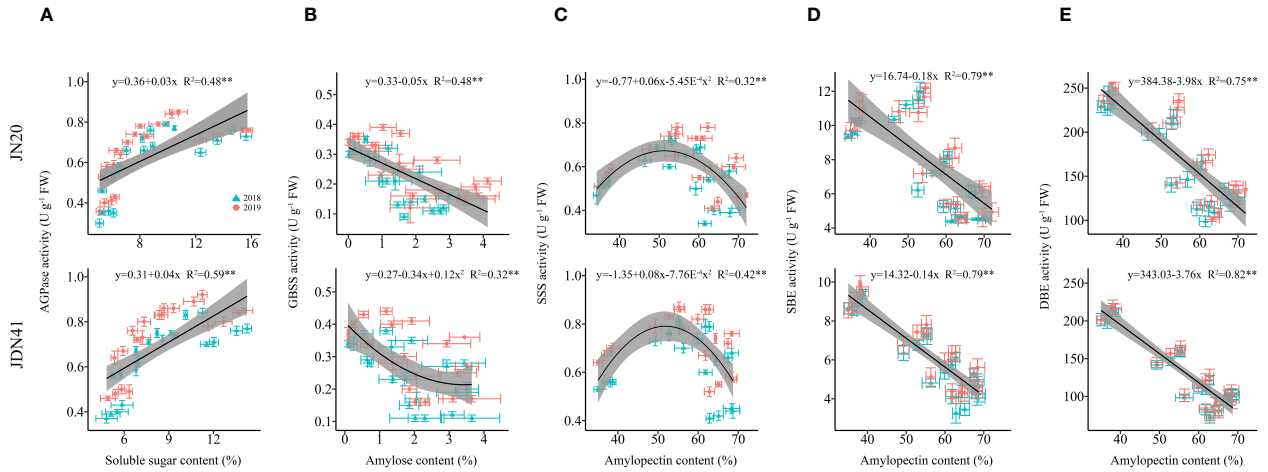

FIGURE 8
Relationship between soluble sugar content and ADP-glucose pyrophosphorylase (AGPase) activity **(A)**, amylose content and granule bound starch synthase (GBSS) activity **(B)**, amylopectin content and soluble starch synthase (SSS) activity **(C)**, amylopectin content and starch branching enzyme (SBE) activity **(D)**, and amylopectin content and starch-debranching enzyme (DBE) activity **(E)** of two waxy maize varieties at different days after pollination. ns indicates no significant differences, and * and ** indicate significant differences at $P < 0.05$, and $P < 0.01$ level, respectively.

enhance protein levels within the grain. Interestingly, the starch content demonstrated a pronounced positive correlation with the carbon/nitrogen (C/N) ratio within the grain, whereas the concentrations of soluble sugars and proteins exhibited a notably adverse effect on this ratio. The C/N ratio, in turn, was significantly allied with an increase in grain dry weight. Therefore, we posit that the application of nitrogen serves as a catalyst in elevating grain dry weight through its nuanced modulation of the metabolic pathways governing carbon and nitrogen in waxy corn grains, underpinning a multifaceted influence on the intricate dynamics of grain composition and weight augmentation.

4 Discussion

4.1 The appropriate nitrogen application rate promotes nitrogen metabolism in waxy maize kernels

Nitrogen (N) is a fundamental nutrient that plays pivotal roles in the synthesis of proteins, amino acids, and other vital compounds in plants (Yue et al., 2021). The appropriate N application is crucial for optimizing maize yield, kernel quality and nutritional value (Wei et al., 2017). The quantity of N present in kernels is mainly

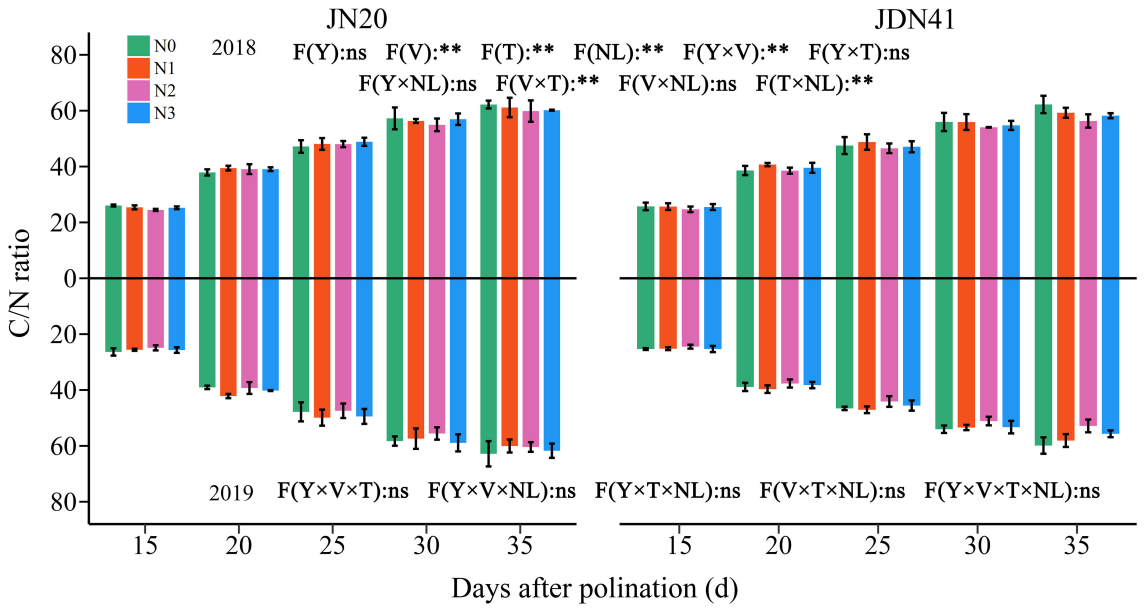

FIGURE 9
Effects of nitrogen rate on grain C/N ratio of two waxy maize varieties at different days after pollination. ns indicates no significant differences, and * and ** indicate significant differences at $P < 0.05$, and $P < 0.01$ level, respectively. The error bar indicates standard error based on 3 data.

10.3389/fpls.2024.1416397

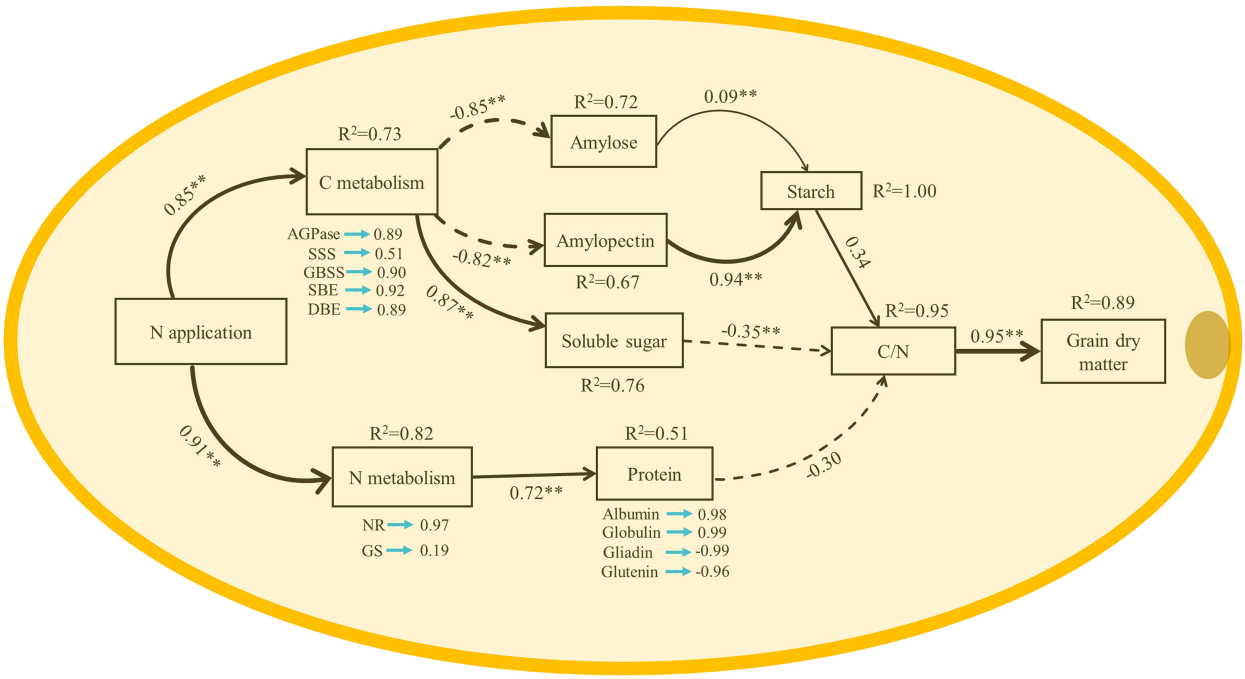

$\chi^2 = 124.748$ Fisher's C = 161.385 $P<0.01$ AIC=1045.642 GFI=0.672

FIGURE 10
Structural equation model analysis (SEM) shows N fertilizer supply increased waxy maize grain dry matter–Effects of nitrogen fertilizer on enzyme activities of carbon and nitrogen metabolism, starch, soluble sugar and protein contents, C/N, dry matter in waxy maize grains. NR, nitrate reductase; GS, glutamine synthetase; AGPase, ADP-glucose pyrophosphorylase; SSS, soluble starch synthase; GBSS, granules bound starch synthase; SBE, starch branching enzyme; DBE, starch-debranching enzyme. The R^2 values denote the proportions of variance explained by relationships with other variables in SEM. Single-headed arrows indicate the hypothesized direction of causation. Indicated values denote the standardized path coefficients of a positive (positive values) or negative (negative values) effect. Solid and dashed lines represent positive and negative paths, respectively. The width of the black arrows indicates the strength of the causal relationship. * and ** represent $P < 0.05$ and $P < 0.01$, respectively.

conditioned by amounts of N remobilization from reserves accumulated in the leaves and stems (Dordas, 2009; Masclaux-Daubresse et al., 2010). A recent study reported that maize kernel N accumulation dynamics were highly positive regulated under 84, 168 and 224 kg N ha^{-1} compared to none N application, and the effects increased with the increasing rate of N application (Olmedo Pico and Vyn, 2021). Similarly, a study in rice and maize indicated that the grain N content increased with N increment, which were conducted under 0 to 240 kg N ha^{-1} with a 40 kg N ha^{-1} frequency (Mondal et al., 2023). In contrast, several studies have demonstrated that the effects of N application on grain quality are highly dose-dependent, reasonable fertilization is one of the most effective measures to improve maize quality, but excessive N deteriorated the grain quality (Rossini et al., 2011; Zhou et al., 2020; Wu et al., 2023). In present study, we found that N dose had significantly positive effects on kernel N content in two waxy maize genotypes (JN20 and JDN41), and N2 (240 kg ha^{-1} N) achieved the highest kernel N content with an increase range of 5.92-19.48% compared to N0 over 15-35 DAP within two years, indicating that reasonable N application was necessary to stabilize kernel N content in waxy corn (Figure 2). At the same time, the kernel N content in JN20 and JDN41 decreased constantly with averages of 1.49% and 1.56% to 1.21% and 1.29% from 15 DAP to 35 DAP, respectively, based on four N treatments within two years (Figure 2), it means that translocation and accumulation of N in grains should take priority over the carbohydrate (C) accumulation.

The grain protein content (GPC), comprised of gliadins and glutenins (storage proteins), as well as albumins and globulins (metabolic proteins), is an important determinant of grain quality in maize. In wheat, increasing nitrogen application resulted in higher concentrations of total protein in the grains (Monostori et al., 2017), which largely relying on the accumulation of gliadins and glutenins (Fuertes-Mendizábal et al., 2013). However, another study demonstrated that a N rate of 240 kg ha^{-1} was sufficient to satisfy N uptake requirements from soil, and maintain protein accumulation in wheat grains (Zhang et al., 2017). In this study, we detected that the albumin content and globulin content in the grains of two waxy maize varieties under four N levels all decreased gradually from 15 to 35 DAP, while that of gliadin content and glutelin content showed a continuously increasing trend, and the gliadin and glutelin content of both genotypes almost reached the highest values under N2 treatment, especially at the later grain filling stage (Figure 5).

Nitrate reductase (NR) and glutamine synthetase (GS) are the major enzymes participating in the process of N assimilation (Liu et al., 2022). NR is the first enzyme in the system of transforming

inorganic nitrogen into organic nitrogen that would limit the overall nitrogen assimilation in plants (Hageman et al., 1962), and re-assimilation of ammonium derived from protein degradation is determined by GS (Bernard et al., 2008). In this study, the impacts of N dose on NR and GS activities were similar as that on kernel N content, and an appropriate N application rate play important roles in resisting the decrease of the activities of NR and GS during grain filling stage to ensure the N metabolism (Figures 3, 4). The regression analysis indicated that grain N content was significantly positively correlated with the NR and GS activity, total protein content, gliadin content and glutelin content, but was negatively correlated with albumin content and globulin content (Supplementary Figures 5, 6). Thus, we propose that appropriate applying N can promote activities of nitrogen metabolism enzymes to induce gliadin and glutelin biosynthesis the in waxy maize kernels.

4.2 The reasonable application of N induces C biosynthesis

N is also the main component of chlorophyll, which affects the accumulation of leaf biomass and the efficiency of photosynthesis (Wani et al., 2021), and almost C is synthesized in plants through photosynthesis. Therefore, N is crucial for carbohydrate metabolism. Hence, N is crucial for carbohydrate metabolism. Numerous studies have investigated the effects of N fertilization on carbohydrate accumulation in maize kernels and have shown that increasing N application during the grain filling phase stimulates the accumulation of starch and soluble sugars in maize kernels. Nitrogen can promote the transport of C to grains (Vijayalakshmi et al., 2013; Ma et al., 2023). It was reported that N fertilizer could promote starch accumulation in wheat, and higher amylopectin and total starch contents were obtained when N level was 240 kg ha^{-1} (Li et al., 2013). However, another study showed that the amylose, amylopectin and total starch contents in wheat gradually decreased with increasing N content, while the starch accumulation rate increased significantly (Lv et al., 2021). As *waxy* gene mutation (*Wx*), waxy corn kernels contain approximately 95–100% amylopectin (Zhou et al., 2016). In this study, amylose was also detected in the grains of two selected waxy maize varieties, and its content ranged from 0.03% to 4.13% over four N levels and five grain filling stages within two years (Figure 6). At the same time, the effects of N level on soluble sugar, amylose and amylopectin contents of both genotypes at any grain filling stage within two years were almost similar, all showing N2≥N3>N1>N0 (Figure 6). The soluble sugar content in the grains of JN20 and JDN41 under N2 increased by an average of 23.74% and 26.42%, compared to N0, respectively, over the five grain filling stages within the two years, and that of the amylopectin content increased by an average of 13.00% and 10.30%, respectively, but that of the amylose content decreased by an average of 59.26% and 61.39%.

In general, ADP-glucose pyrophosphorylase (AGPase), granule bound starch synthase (GBSS), starch debranching enzyme (DBE), soluble starch synthase (SSS) and starch branching enzyme (SBE) are considered to be the five key enzymes involved in starch synthesis and metabolism, regulating the process of starch synthesis and accumulation (Yi et al., 2014). Studies have shown that N availability directly influences the activity of enzymes involved in C metabolism, thereby affecting C accumulation in plant tissues (Krapp et al., 2011). In rice, the application of nitrogen fertilizer at the appropriate rate enhanced C biosynthesis by promoting the activity of key enzymes in the glycolysis and starch synthesis pathways (Xu et al., 2012). N fertilization can affect grain growth mainly by regulating starch synthesis in endosperm, and one of these effects is achieved through altering enzyme activity (Singletary et al., 1990). There have been many studies about the key enzyme activity in wheat, rice and potato as affected by applying N fertilizer. In wheat, N application significantly increased the activities of the GBSS and SSS in wheat, and the starch accumulation rate was higher under higher N level (Wang et al., 2014). In rice, the activities of AGPase, SSS, GBSS and SBE were significantly increased after given N supply (Li et al., 2008). In contrast, the activities of the AGPase and SSS in potato significantly increased under low N level and then decreased with increasing N level, while the activities of the GBSS and SBE did not respond significantly to N fertilization (Whiley et al., 1989). In this study, we detected dynamic changes of the activities of AGPase, SSS, GBSS, SBE and SDBE in grains of two waxy maize varieties after applying different N rates. We found that applying N could enhance the AGP and SSS activity, but had an inhibitory effect on the activities of GBSS and SBE. The correlation analysis results indicated that grain N content was significantly positively correlated with the soluble sugar content, but negatively correlated with the amylose content and amylopectin content (Supplementary Figure 7). In addition, AGPase activity and soluble sugar had a highly positive correlation, and SBE and DBE activity had significant negative correlation with amylopectin content (Figure 8). Above all, we propose that appropriate applying N can regulate the activities of related C metabolism enzymes to induce C biosynthesis the in waxy maize kernels.

4.3 Coordination of N and C improves dry matter accumulation of waxy maize kernels

C metabolism provides the necessary energy and C skeletons for reduction of NO_3^- and synthesis of amino acids and, therefore, improving C metabolism increases N metabolism enzyme activities, assimilation of NH_4^+, and efficiency of N metabolism in crops (Zhang et al., 2023). Improving the intensity and coordination of C and N metabolism in maize is particularly important for improving yield. This study showed that applying N had no effect on the C/N ratio in waxy maize grains at the early grain filling stages, but it caused a decrease in the C/N ratio at the later grain filling stages. Structural equation model (SEM) analysis showed that N application rate could positively affect the enzyme activities related to C and N metabolism to regulate the carbohydrate and protein content in waxy maize grains, resulting in coordinating the C/N ratio, to determine the grain dry matter accumulation (Figure 10). Similarly, a recent study found that optimal N application rate and nitrate-to-ammonium N ratio treatment enhanced key enzyme activities of C and N metabolic pathways,

led to increase nonstructural carbohydrate accumulation, insufficient N supply reduced grain weight, and excessive N supply caused a reduction in the C/N ratio, reducing the export of photosynthesis products and negatively affecting seed formation. These results indicated that applying N promoted the grain dry weight by affecting the processes of waxy corn grain C and N metabolism.

4.4 Reasonable nitrogen application rate ensures the formation of maize yield

As the waxy corn is mainly consumed as fresh food, so the effects of N application rate on its quality and yield seem like the hot research projects. Applying N fertilizer at an optimal rate is essential for ensuring the formation of maize yield. Insufficient N application negatively impacts N reactivation and recycling, injures the leaves, reduces in chlorophyll content and photosynthesis activity (Bassi et al., 2018; Mu et al., 2018; Mu and Chen, 2021), ultimately significantly affects grain formation and weight (Nasielski et al., 2019; Santos et al., 2023). Conversely, excessive N results in early-stage overgrowth, increases the risk of lodging, and reduces NUE, ultimately affects yield formation (Hammad et al., 2022; Shao et al., 2024). In present study, we found that N dose had significantly positive effects on kernel dry matter accumulation in two waxy maize genotypes, and N2 achieved the highest grain dry weight (GDW) with an increase range of 9.88-34.20% compared to N0 over 15-35 DAP within two years (Figure 1), indicating that reasonable N application was necessary to stabilize GDW in waxy corn. As discussed above, the carbon and nitrogen metabolism in waxy maize kernels were enhanced under N2 treatment compared to low N level (N0 and N1) and high N level (N3), leading to the highest accumulation of kernel dry matter. Therefore, for waxy corn, N2 may be a reasonable N application amount.

5 Conclusions

In this study, we found that appropriate application of N promoted the activity of NR and GS to regulate kernel N remobilization, and induced the activities of the enzyme activities related to C metabolism (AGPase, SSS, GBSS, SBE and DBE) to enhance C and N accumulation in the grains of JN20 and JDN41, and to obtain more dry matter at accurate harvest period under N2 treatment. It is worth noting that grain dry matter was significantly positively correlated with C/N ratio, suggesting that the increase of starch content induced grain dry matter. Therefore, reasonable applying N could coordinate the metabolism of C and N in grain during the grain filling stages, which was important to regulate the formation of grain dry weight. Our results highlight the great potential of N fertilizer dose in influencing the C and N accumulation in the grains of waxy maize, which provides a reference for the appropriate application of nitrogen fertilizer and the selection of cultivation management practices for waxy corn production.

Data availability statement

The original contributions presented in the study are included in the article/Supplementary material. Further inquiries can be directed to the corresponding authors.

Author contributions

WF: Data curation, Formal analysis, Funding acquisition, Investigation, Methodology, Project administration, Visualization, Writing – original draft, Writing – review & editing. WX: Formal analysis, Software, Visualization, Writing – original draft. ZZ: Data curation, Formal analysis, Resources, Visualization, Writing – review & editing. ZS: Conceptualization, Investigation, Writing – review & editing. WW: Conceptualization, Investigation, Writing – review & editing. YB: Writing – original draft. HW: Writing – original draft. PQ: Investigation, Writing – review & editing. JX: Funding acquisition, Supervision, Validation, Writing – review & editing. BC: Conceptualization, Supervision, Validation, Writing – original draft.

Funding

The author(s) declare financial support was received for the research, authorship, and/or publication of this article. The authors are greatly thankful to Research Program Sponsored by Ministerial and Provincial Co-Innovation Centre for Endemic Crops Production with High-quality and Efficiency in Loess Plateau (SBGJXTZX), the National Natural Science Foundation of Shanxi (20210302123372) and Graduate Practice Innovation Project of Shanxi Province (2023KY329) for financial support.

Conflict of interest

The authors declare that the research was conducted in the absence of any commercial or financial relationships that could be construed as a potential conflict of interest.

Publisher's note

Supplementary material

The Supplementary Material for this article can be found online at: https://www.frontiersin.org/articles/10.3389/fpls.2024.1416397/full#supplementary-material

References

Adney, B., and Baker, J. (1996). *Measurement of cellulase activities*. 59 (2), 257–268. doi: 10.1351/pac198759020257

Bassi, D., Menossi, M., and Mattiello, L. (2018). Nitrogen supply influences photosynthesis establishment along the sugarcane leaf. *Sci. Rep.* 8, 2327. doi: 10.1038/s41598-018-20653-1

Bernard, S. M., Møller, A. L., Dionisio, G., Kichey, T., Jahn, T. P., Dubois, F., et al. (2008). Gene expression, cellular localisation and function of glutamine synthetase isozymes in wheat (Triticum aestivum L.). *Plant Mol. Biol.* 67, 89–105. doi: 10.1007/s11103-008-9303-y

Chen, Y., Xiao, C., Wu, D., Xia, T., Chen, Q., Chen, F., et al. (2015). Effects of nitrogen application rate on grain yield and grain nitrogen concentration in two maize hybrids with contrasting nitrogen remobilization efficiency. *Eur. J. Agron.* 62, 79–89. doi: 10.1016/j.eja.2014.09.008

Collins, G. N. (1909). A new type of Indian corn from China. *Bur. Plant Ind.* 161, 130. doi: 10.5962/bhl.title.37128

Cui, Z., Chen, X., and Zhang, F. (2010). Current nitrogen management status and measures to improve the intensive wheat-maize system in China. *Ambio* 39, 376–384. doi: 10.1007/s13280-010-0076-6

Dordas, C. (2009). Dry matter, nitrogen and phosphorus accumulation, partitioning and remobilization as affected by N and P fertilization and source-sink relations. *Eur. J. Agron.* 30, 129–139. doi: 10.1016/j.eja.2008.09.001

Foley, J. A., Ramankutty, N., Brauman, K. A., Cassidy, E. S., Gerber, J. S., Johnston, M., et al. (2011). Solutions for a cultivated planet. *Nature* 478, 337–342. doi: 10.1038/nature10452

Fuertes-Mendizábal, T., González-Torralba, J., Arregui, L. M., González-Murua, C., González-Moro, M. B., and Estavillo, J. M. (2013). Ammonium as sole N source improves grain quality in wheat. *J. Sci. Food Agric.* 93, 2162–2171. doi: 10.1002/jsfa.6022

Guo, J. H., Liu, X. J., Zhang, Y., Shen, J. L., Han, W. X., Zhang, W. F., et al. (2010). Significant acidification in major Chinese croplands. *Science* 327, 1008–1010. doi: 10.1126/science.1182570

Hageman, R. H., Cresswell, C. F., and Hewitt, E. J. (1962). Reduction of nitrate, nitrite and hydroxylamine to ammonia by enzymes extracted from higher plants. *Nature* 193, 247–250. doi: 10.1038/193247a0

Hammad, H. M., Chawla, M. S., Jawad, R., Alhuqail, A., Bakhat, H. F., Farhad, W., et al. (2022). Evaluating the impact of nitrogen application on growth and productivity of maize under control conditions. *Front. Plant Sci.* 13, 885479. doi: 10.3389/fpls.2022.885479

He, P., Zhou, W., and Jin, J. (2004). Carbon and nitrogen metabolism related to grain formation in two different senescent types of maize. *J. Plant Nutr.* 27, 295–311. doi: 10.1081/PLN-120027655

Jiang, D., Cao, W., DaiQi, T., and Jing, Q. (2003). Activities of key enzymes for starch synthesis in relation to growth of superior and inferior grains on winter wheat (Triticum aestivum L.) spike. *Plant Growth Regulation*. 41 (3), 247–257. doi: 10.1023/B:GROW.0000007500.90240.7d

Ju, Z. Y., Hettiarachchy, N. S., and Rath, N. (2001). Extraction, denaturation and hydrophobic Properties of Rice Flour Proteins. *J. Food Sci.* 66 (2), 229–232. doi: 10.1111/j.1365-2621.2001.tb11322.x

Kant, S. (2018). Understanding nitrate uptake, signaling and remobilisation for improving plant nitrogen use efficiency. *Semin. Cell Dev. Biol.* 74, 89–96. doi: 10.1016/j.semcdb.2017.08.034

Klimek-Kopyra, A., Szmigiel, A., Zając, T., and Kidacka, A. J. A. A. (2012). Some aspects of cultivation and utilization of waxy maize (Zea mays L. ssp. ceratina). *Acta Agrobotanica*. 65, 3–12. doi: 10.5586/aa.2012.001

Krapp, A., Berthomé, R., Orsel, M., Mercey-Boutet, S., Yu, A., Castaings, L., et al. (2011). Arabidopsis roots and shoots show distinct temporal adaptation patterns toward nitrogen starvation. *Plant Physiol.* 157, 1255–1282. doi: 10.1104/pp.111.179838%

Ladha, J. K., Tirol-Padre, A., Reddy, C. K., Cassman, K. G., Verma, S., Powlson, D. S., et al. (2016). Global nitrogen budgets in cereals: A 50-year assessment for maize, rice, and wheat production systems. *Sci. Rep.* 6, 19355. doi: 10.1038/srep19355

Li, H., and Li, H. (2000). *Principles and experimental techniques of plant physiology and biochemistry*. (Beijing: Higher Education Press).

Li, H., Liang, X., Chen, Y., Lian, Y., Tian, G., and Ni, W. (2008). Effect of nitrification inhibitor DMPP on nitrogen leaching, nitrifying organisms, and enzyme activities in a rice-oilseed rape cropping system. *J. Environ. Sci.* 20, 149–155. doi: 10.1016/S1001-0742(08)60023-6

Li, Q., Ren, Y., Fu, H., Li, Z., Kong, F., and Yuan, J. (2022). Cultivar differences in carbon and nitrogen accumulation, balance, and grain yield in maize. *Front. Plant Sci.* 13, 992041. doi: 10.3389/fpls.2022.992041

Li, W., Shan, Y., Xiao, X., Zheng, J., Luo, Q., Ouyang, S., et al. (2013). Effect of nitrogen and sulfur fertilization on accumulation characteristics and physicochemical properties of A- and B-wheat starch. *J. Agricultural Food Chem.* 61 (10), 2418–2425. doi: 10.1021/jf400107b

Liu, C., Hou, H., Lu, X., Chen, X., Fang, D., Hu, Q., et al. (2021). Production of an innovative mixed Qu (fermentation starter) for waxy maize brewing and comparison of the quality of different waxy maize wines. *J. Sci. Food Agric.* 101, 2328–2336. doi: 10.1002/jsfa.10854

Liu, L., Zhang, X., Xu, W., Liu, X., Li, Y., Wei, J., et al. (2020). Challenges for global sustainable nitrogen management in agricultural systems. *J. Agric. Food Chem.* 68, 3354–3361. doi: 10.1021/acs.jafc.0c00273

Liu, X., Hu, B., and Chu, C. (2022). Nitrogen assimilation in plants: current status and future prospects. *J. Genet. Genomics* 49, 394–404. doi: 10.1016/j.jgg.2021.12.006

Lu, D., Cai, X., Yan, F., Sun, X., Wang, X., and Lu, W. (2014). Effects of high temperature after pollination on physicochemical properties of waxy maize flour during grain development. *J. Sci. Food Agric.* 94, 1416–1421. doi: 10.1002/jsfa.2014.94.issue-7

Lv, X., Ding, Y., Long, M., Liang, W., Gu, X., Liu, Y., et al. (2021). Effect of foliar application of various nitrogen forms on starch accumulation and grain filling of wheat (Triticum aestivum L.) under drought stress. *Front. Plant Sci.* 12. doi: 10.3389/fpls.2021.645379

Ma, R., Jiang, C., Shou, N., Gao, W., and Yang, X.-l. (2023). An optimized nitrogen application rate and basal topdressing ratio improves yield, quality, and water- and N-use efficiencies for forage maize (Zea mays L.). *Agronomy*. 13 (1), 181. doi: 10.3390/agronomy13010181

Marion, M. (1976). A rapid and sensitive method for the quantitation of microgram quantities of protein utilizing the principle of protein-dye binding. *Biochem. B.J.A* 72, 248–254. doi: 10.1016/0003-2697(76)90527-3

Masclaux-Daubresse, C., Daniel-Vedele, F., Dechorgnat, J., Chardon, F., Gaufichon, L., and Suzuki, A. (2010). Nitrogen uptake, assimilation and remobilization in plants: challenges for sustainable and productive agriculture. *Ann. Bot.* 105, 1141–1157. doi: 10.1093/aob/mcq028

Mondal, S., Kumar, R., Mishra, J. S., Dass, A., Kumar, S., Vijay, K. V., et al. (2023). Grain nitrogen content and productivity of rice and maize under variable doses of fertilizer nitrogen. *Heliyon* 9, e17321. doi: 10.1016/j.heliyon.2023.e17321

Monostori, I., Szira, F., Tondelli, A., Árendás, T., Gierczik, K., Cattivelli, L., et al. (2017). Genome-wide association study and genetic diversity analysis on nitrogen use efficiency in a Central European winter wheat (Triticum aestivum L.) collection. *PloS One* 12, e0189265. doi: 10.1371/journal.pone.0189265

Morris, T. F., Murrell, T. S., Beegle, D. B., Camberato, J. J., Ferguson, R. B., Grove, J., et al. (2018). Strengths and limitations of nitrogen rate recommendations for corn and opportunities for improvement. *Agronomy J.* 110 (1), 1–37. doi: 10.2134/agronj2017.02.0112

Mu, X., and Chen, Y. (2021). The physiological response of photosynthesis to nitrogen deficiency. *Plant Physiol. Biochem.* 158, 76–82. doi: 10.1016/j.plaphy.2020.11.019

Mu, X., Chen, Q., Chen, F., Yuan, L., and Mi, G. (2018). Dynamic remobilization of leaf nitrogen components in relation to photosynthetic rate during grain filling in maize. *Plant Physiol. Biochem.* 129, 27–34. doi: 10.1016/j.plaphy.2018.05.020

Mueller, N. D., Gerber, J. S., Johnston, M., Ray, D. K., Ramankutty, N., and Foley, J. A. (2012). Closing yield gaps through nutrient and water management. *Nature* 490, 254–257. doi: 10.1038/nature11420

Mueller, S. M., and Vyn, T. J. (2016). Maize plant resilience to N stress and post-silking N capacity changes over time: A review. *Front. Plant Sci.* 7. doi: 10.3389/fpls.2016.00053

Nakamura, Y., Yuki, K., Park, S.-Y., and Ohya, T. (1989). Carbohydrate metabolism in the developing endosperm of rice grains. *Plant Cell Physiol.* 30, 833–839. doi: 10.1093/oxfordjournals.pcp.a077813%

Nasielski, J., Earl, H., and Deen, B. (2019). Luxury vegetative nitrogen uptake in maize buffers grain yield under post-silking water and nitrogen stress: A mechanistic understanding. *Front. Plant Sci.* 10, 318. doi: 10.3389/fpls.2019.00318

Nelson, D. W., and Sommers, L. E. (1962). Determination of total nitrogen in plant material. *Agron. J.* 65 (1), 109–112. doi: 10.2134/agronj1973.00021962006500010033x

Olmedo Pico, L. B., and Vyn, T. J. (2021). Dry matter gains in maize kernels are dependent on their nitrogen accumulation rates and duration during grain filling. *Plants (Basel)* 10 (6), 1222. doi: 10.3390/plants10061222

Qi, J. C., Zhang, G. P., and Zhou, M. X. (2006). Protein and hordein content in barley seeds as affected by nitrogen level and their relationship to beta-amylase activity. *J. Cereal Sci.* 43, 102–107. doi: 10.1016/j.jcs.2005.08.005

Ran, L., Yu, X., Li, Y., Zou, J., Deng, J., Pan, J., et al. (2020). Analysis of development, accumulation and structural characteristics of starch granule in wheat grain under nitrogen application. *Int. J. Biol. Macromol* 164, 3739–3750. doi: 10.1016/j.ijbiomac.2020.08.192

Rossini, M. A., Maddonni, G. A., and Otegui, M. E. (2011). Inter-plant competition for resources in maize crops grown under contrasting nitrogen supply and density: Variability in plant and ear growth. *Field Crops Res.* 121, 373–380. doi: 10.1016/j.fcr.2011.01.003

Santos, T. D., Amaral Junior, A. T., and Moulin, M. M. (2023). Maize breeding for low nitrogen inputs in agriculture: mechanisms underlying the tolerance to the abiotic stress. *Stresses*. 3 (1), 136–152. doi: 10.3390/stresses3010011

Schwartz, D., and Whistler, R. L. (2009). "Chapter 1 - History and Future of Starch," in *Starch (Third Edition)*. eds. J. BeMiller & R. Whistler. (San Diego: Academic Press). pp. 1-10. doi: 10.1016/B978-0-12-746275-2.00001-X

Shao, H., Wu, X., Chi, H., Zhu, F., Liu, J., Duan, J., et al. (2024). How does increasing planting density affect nitrogen use efficiency of maize: A global meta-analysis. *Field Crops Res.* 311, 109369. doi: 10.1016/j.fcr.2024.109369

Singletary, G. W., Doehlert, D. C., Wilson, C. M., Muhitch, M. J., and Below, F. E. (1990). Response of enzymes and storage proteins of maize endosperm to nitrogen supply 1. *Plant Physiol.* 94, 858–864. doi: 10.1104/pp.94.3.858%

Smith, A. M., and Zeeman, S. C. (2020). Starch: A flexible, adaptable carbon store coupled to plant growth. *Annu. Rev. Plant Biol.* 71, 217–245. doi: 10.1146/annurev-arplant-050718-100241

Swank, J. C., Below, F. E., Lambert, R. J., and Hageman, R. H. (1982). Interaction of carbon and nitrogen metabolism in the productivity of maize 1. *Plant Physiol.* 70, 1185–1190. doi: 10.1104/pp.70.4.1185%

Vijayalakshmi, P., Kiran, T. V., Rao, Y. V., Srikanth, B., Rao, I. S., Sailaja, B., et al. (2013). Physiological approaches for increasing nitrogen use efficiency in rice. *Indian J. Plant Physiol.* 18 (3), 208–222. doi: 10.1007/s40502-013-0042-y

Wang, Z., Li, W., Qi, J., Shi, P., and Yin, Y. (2014). Starch accumulation, activities of key enzyme and gene expression in starch synthesis of wheat endosperm with different starch contents. *J. Food Sci. Technol.* 51, 419–429. doi: 10.1007/s13197-011-0520-z

Wani, S. H., Vijayan, R., Choudhary, M., Kumar, A., Zaid, A., Singh, V., et al. (2021). Nitrogen use efficiency (NUE): elucidated mechanisms, mapped genes and gene networks in maize (Zea mays L.). *Physiol. Mol. Biol. Plants* 27, 2875–2891. doi: 10.1007/s12298-021-01113-z

Wei, S., Wang, X., Zhu, Q., Jiang, D., and Dong, S. (2017). Optimising yield and resource utilisation of summer maize under the conditions of increasing density and reducing nitrogen fertilization. *Sci. Nat.* 104, 86. doi: 10.1007/s00114-017-1509-x

Whiley, A. W., Rasmussen, T. S., Saranah, J. B., and Wolstenholme, B. N. (1989). Effect of temperature on growth, dry matter production and starch accumulation in ten mango (Mangifera indica L.) cultivars. *J. Horticultural Sci.* 64 (6), 753–765. doi: 10.1080/14620316.1989.11516018

Wu, X., Tong, L., Kang, S., Du, T., Ding, R., Li, S., et al. (2023). Combination of suitable planting density and nitrogen rate for high yield maize and their source-sink relationship in Northwest China. *J. Sci. Food Agric.* 103, 5300–5311. doi: 10.1002/jsfa.12602

Xu, G., Fan, X., and Miller, A. J. (2012). Plant nitrogen assimilation and use efficiency. *Annu. Rev. Plant Biol.* 63, 153–182. doi: 10.1146/annurev-arplant-042811-105532

Yang, L., Chi, Y. X., Wang, Y. F., Zeeshan, M., and Zhou, X. B. (2021). Gradual application of potassium fertilizer elevated the sugar conversion mechanism and yield of waxy and sweet fresh-eaten maize in the semiarid cold region. *J. Food Qual.* 2021 (1), 6611124. doi: 10.1155/2021/6611124

Yi, B., Zhou, Y., Gao, M., Zhang, Z., Han, Y., Yang, G.-d., et al. (2014). Effect of drought stress during flowering stage on starch accumulation and starch synthesis enzymes in sorghum grains. *J. Integrative Agriculture* 13 (11), 2399–2406. doi: 10.1016/S2095-3119(13)60694-2

Yue, K., Li, L., Xie, J., Liu, Y., Xie, J., Anwar, S., et al. (2021). Nitrogen supply affects yield and grain filling of maize by regulating starch metabolizing enzyme activities and endogenous hormone contents. *Front. Plant Sci.* 12, 798119. doi: 10.3389/fpls.2021.798119

Zhang, X., Davidson, E. A., Mauzerall, D. L., Searchinger, T. D., Dumas, P., and Shen, Y. (2015). Managing nitrogen for sustainable development. *Nature* 528, 51–59. doi: 10.1038/nature15743

Zhang, Z. Q., Hu, Y. X., Tung, S. A., Yang, L., Wang, Y., and Zhou, X. B. (2023). Evaluating the effects of water-nitrogen interactions on carbon and nitrogen accumulation as well as related metabolic enzymes activity in autumn maize. *J. Soil Sci. Plant Nutr.* 23, 5245–5256. doi: 10.1007/s42729-023-01398-x

Zhang, P., Ma, G., Wang, C., Lu, H., Li, S., Xie, Y., et al. (2017). Effect of irrigation and nitrogen application on grain amino acid composition and protein quality in winter wheat. *PloS One* 12, e0178494. doi: 10.1371/journal.pone.0178494

Zhang, W., Zhao, Y., Li, L., Xu, X., Yang, L., Luo, Z., et al. (2021). The effects of short-term exposure to low temperatures during the booting stage on starch synthesis and yields in wheat grain. *Front. Plant Sci.* 12. doi: 10.3389/fpls.2021.684784

Zhou, Z., Song, L., Zhang, X., Li, X., Yan, N., Xia, R., et al. (2016). Introgression of opaque2 into Waxy Maize Causes Extensive Biochemical and Proteomic Changes in Endosperm. *PloS One* 11, e0158971. doi: 10.1371/journal.pone.0158971

Zhou, T., Zhou, Q., Li, E., Yuan, L., Wang, W., Zhang, H., et al. (2020). Effects of nitrogen fertilizer on structure and physicochemical properties of 'super' rice starch. *Carbohydr Polym.* 239, 116237. doi: 10.1016/j.carbpol.2020.116237

frontiers | Frontiers in Plant Science

TYPE Original Research
PUBLISHED 23 August 2024
DOI 10.3389/fpls.2024.1343073

OPEN ACCESS

EDITED BY
Enrique Ostria-Gallardo,
University of Concepcion, Chile

REVIEWED BY
Jian Fu Zhang,
Fujian Academy of Agricultural Sciences, China
Satoru Naganawa Kinoshita,
University of Münster, Germany

*CORRESPONDENCE
Tom Beeckman
tom.beeckman@psb.ugent.be
Hans Motte
hans.motte@psb.ugent.be

RECEIVED 22 November 2023
ACCEPTED 29 July 2024
PUBLISHED 23 August 2024

CITATION
Pélissier P-M, Parizot B, Jia L, De Knijf A, Goossens V, Gantet P, Champion A, Audenaert D, Xuan W, Beeckman T and Motte H (2024) Nitrate and ammonium, the yin and yang of nitrogen uptake: a time-course transcriptomic study in rice.
Front. Plant Sci. 15:1343073.
doi: 10.3389/fpls.2024.1343073

Nitrate and ammonium, the yin and yang of nitrogen uptake: a time-course transcriptomic study in rice

Pierre-Mathieu Pélissier[1,2], Boris Parizot[1,2], Letian Jia[3], Alexa De Knijf[1,2], Vera Goossens[4,5], Pascal Gantet[6], Antony Champion[6], Dominique Audenaert[4,5], Wei Xuan[3], Tom Beeckman[1,2]* and Hans Motte[1,2]*

[1]Department of Plant Biotechnology and Bioinformatics, Ghent University, Ghent, Belgium, [2]VIB Center for Plant Systems Biology, Ghent, Belgium, [3]State Key Laboratory of Crop Genetics & Germplasm Enhancement and MOA Key Laboratory of Plant Nutrition and Fertilization in Lower Middle Reaches of the Yangtze River, Nanjing Agricultural University, Nanjing, China, [4]Center for Bioassay Development and Screening (C-BIOS), Ghent University, Ghent, Belgium, [5]VIB Screening Core, Ghent, Belgium, [6]UMR DIADE, Université de Montpellier, IRD, CIRAD, Montpellier, France

Nitrogen is an essential nutrient for plants and a major determinant of plant growth and crop yield. Plants acquire nitrogen mainly in the form of nitrate and ammonium. Both nitrogen sources affect plant responses and signaling pathways in a different way, but these signaling pathways interact, complicating the study of nitrogen responses. Extensive transcriptome analyses and the construction of gene regulatory networks, mainly in response to nitrate, have significantly advanced our understanding of nitrogen signaling and responses in model plants and crops. In this study, we aimed to generate a more comprehensive gene regulatory network for the major crop, rice, by incorporating the interactions between ammonium and nitrate. To achieve this, we assessed transcriptome changes in rice roots and shoots over an extensive time course under single or combined applications of the two nitrogen sources. This dataset enabled us to construct a holistic co-expression network and identify potential key regulators of nitrogen responses. Next to known transcription factors, we identified multiple new candidates, including the transcription factors OsRLI and OsEIL1, which we demonstrated to induce the primary nitrate-responsive genes *OsNRT1.1b* and *OsNIR1*. Our network thus serves as a valuable resource to obtain novel insights in nitrogen signaling.

KEYWORDS

transcriptome, rice, co-expression network, nitrogen, OsRLI1, OsEIL1

Introduction

Nitrogen, mainly in the form of nitrate (NO_3^-) or ammonium (NH_4^+), is a key nutrient for plant development and a limiting factor for crop yield and grain quality (Makino, 2011). Nitrogen application soared with the green revolution and is expected to keep growing (Good et al., 2004; Food and Agriculture Organization of the United Nations [FAO], 2017). However, major staple crops use less than half of the nitrogen applied through fertilizers, the rest being lost by leaching or volatilization, causing economic losses and ecological damages such as eutrophication and greenhouse gas emissions (Raun and Johnson, 1999; Bouwman et al., 2002; Robertson and Vitousek, 2009; Sutton et al., 2011; Coskun et al., 2017; Beeckman et al., 2018, Beeckman et al., 2024). Therefore, a better understanding of how plants respond and assimilate nitrogen is of great interest to improve their nitrogen use efficiency (NUE). Attempts to improve NUE have often targeted single genes involved in nitrogen metabolism or transport (McAllister et al., 2012). In contrast, transcription-factor-centered approaches yielded promising results, as one transcription factor can potentially regulate several genes Past research has elucidated complex nitrogen-related pathways governed by transcription factors. However, further exploration is warranted to advance our understanding of regulatory networks involved in NUE, particularly in crops (Ueda and Yanagisawa, 2018).

NUE is a complex trait not only because of complex signaling, but also because plants react differently to nitrate and ammonium. Most plants prefer nitrate over ammonium and are stressed when ammonium is provided alone or in high quantities (Kronzucker et al., 2001; Britto and Kronzucker, 2013; Bittsanszky et al., 2015; Hachiya and Sakakibara, 2016), but rice is tolerating ammonium reasonably well (Sasakawa and Yamamoto, 1978). Besides fulfilling its role as a nutrient, nitrate also acts as a signaling molecule at the local and the systemic level (Crawford, 1995; Krouk et al., 2010; Xuan et al., 2017; Pélissier et al., 2021), inducing responses in Arabidopsis as early as 3 minutes after treatment (Krouk et al., 2010) while this appears to not be the case for ammonium. At least in Arabidopsis, and to some extent in rice, knowledge on nitrate response regulation increased considerably due to systems biology approaches aiming at characterizing transcriptional networks (Gaudinier et al., 2018; Varala et al., 2018; Ueda et al., 2020). Both in rice and Arabidopsis, nitrate binds to NITRATE TRANSPORTER (NRT) transceptors (OsNRT1.1b or AtNRT1.1 in rice or Arabidopsis, respectively), which trigger Ca^{2+} signaling and activate different Ca^{2+}-sensor protein kinases (CPKs) that phosphorylate NIN-LIKE PROTEIN (NLP) transcription factors: AtNLP6 and AtNLP7 in Arabidopsis or OsNLP3 in rice. As a result, NLPs are retained in the nucleus and regulate hundreds of nitrate responsive genes triggering a complex cascade of systemic signaling and feedback loops (Marchive et al., 2013; Guan et al., 2017; Liu et al., 2017; Hu et al., 2019; Alvarez et al., 2020). Nitrate is also perceived directly by AtNLP7, which leads to a de-repression of this transcription factor (Liu et al., 2022).

In contrast to nitrate, no ammonium signaling mechanism has been discovered, at least not in plants. Ammonium-induced changes in the root system architecture or other responses seemed to be primarily caused by changes in internal cellular pH and auxin mobility rather than changes induced by a biochemical signaling pathway (Jia et al., 2020; Meier et al., 2020; Hachiya et al., 2021). These results argue that ammonium, in contrast to nitrate, does not directly affect a transcriptional pathway. Notably, nitrate and nitrate signaling affect ammonium responses and NRT1.1-dependent signaling plays crucial roles in controlling ammonium uptake and assimilation (Jian et al., 2018; Wu et al., 2019; Fang et al., 2021; Yan et al., 2023), while nitrate is reduced to ammonium during assimilation and partially elicits an ammonium response (Wang et al., 2004). Conversely ammonium affect nitrate uptakes and other responses (Wang et al., 2009b; Hachiya and Sakakibara, 2016). Hence, there is a clear interaction between these two nitrogen sources and variations in one will inevitably affect the overall response. This interplay is important to consider in network analysis, and could help to uncover regulatory mechanisms that might be overlooked if only one nitrogen source is considered. Genes that respond to both nitrogen sources, for example, can complicate the identification of specific responses to one nitrogen source. Considering both allows for distinguishing between the different responses, can refine network analysis and is potentially instrumental in elucidating otherwise overlooked regulatory mechanisms. Although several studies investigated the responses to nitrate, ammonium and their co-application in Arabidopsis (Patterson et al., 2010; Ristova et al., 2016) and rice (Obertello et al., 2015; Chandran et al., 2016; Yang et al., 2017; Fu et al., 2023), they often lack an extensive time-course necessary for construction of gene regulatory networks.

Here, to enable a better view on the nitrogen response and its regulatory network in rice, we conducted an extensive time-course and genome-wide transcriptional analysis both in roots and shoots and in responses to ammonium, nitrate, or the combination of both. We used this dataset to construct a gene co-expression network which allowed us to reveal several transcription factors with a possible role in nitrogen signaling, and showed that the transcription factors OsRLI1 and OsEIL1 are sufficient to activate a nitrate response. As such, our dataset does not only provide a new resource to retrieve the genome-wide gene expression in response to different nitrogen sources, but is also valuable to get insights into nitrogen signaling in rice, and by extension, in crops.

Results

Phenotypic responses of rice to different nitrogen forms

To investigate the response of rice to different nitrogen forms, we used a hydroponic system in which ammonium and/or nitrate could be supplemented to the medium. 5mM of nitrate (NO_3^- as KNO_3), 5mM of ammonium (NH_4^+ as $(NH_4)_2SO_4$), an equimolar combination of both nitrogen forms (2.5mM of NH_4NO_3) or a control (5mM K^+ as K_2SO_4) with potassium (K^+) balanced at 5mM among all treatments as K_2SO_4, were supplemented into the nitrogen-free growing media of the rice seedlings 5 days after germination and the seedlings were let grown for 10 more days before phenotyping (see Materials & Methods for details on the

10.3389/fpls.2024.1343073

procedure). In our set-up, supplementation with ammonium and nitrate had a similar positive effect on shoot biomass, while co-application of both forms showed a synergistic positive effect (Figure 1A). The lateral root density positively correlated with the shoot biomass and showed a similar synergistic response to the combined treatment. The root system treated with nitrate had a long primary root with long lateral roots close to the root-hypocotyl junction, while the ammonium-supplemented root system had a dense network of small lateral roots evenly spread over the primary root (Figures 1B–E). Co-application seemed to result in a combination of the two phenotypes. Finally, we observed an increase in leaf chlorophyll content upon treatment by ammonium or ammonium-nitrate but not by nitrate alone (Figure 1F).

Dynamic rice nitrogen transcriptome

We used the same hydroponic system as described above to collect samples for the transcriptomic analysis, but rice tissues were harvested soon after the nitrogen supplementation (see Material and Methods for details). In Arabidopsis, early response genes are induced as early as 12 minutes (*NITRITE REDUCTASE1 (NIR1)*), 15 minutes (*NRT2.1* and *NITRATE REDUCTASE1* (*NIA1*)) or 20 minutes (*NITRATE TRANSPORTER1.1 (NRT1.1)*) after nitrate treatment (Krouk et al., 2010). Therefore, to capture relevant transcriptional profiles, we sampled root and shoot tissue separately immediately (0h), 15 minutes, 1h, 2h, 4h, 12h, 24h and 48h after treatment and used these samples for RNA sequencing (RNA-seq) thereby generating an extensive dataset covering the nitrogen transcriptional responses in rice (Figure 2).

We performed a pair-wise differential analysis to assess differential expression for each time point and treatment (Supplementary Dataset S1, Supplementary Dataset S2). Considering an absolute fold-change >2, and an adjusted p.value (FDR) < 0.05, a significant number of genes were differentially expressed by the treatments in the shoot or root and over the time-course (Supplementary Figures S1–S3; Supplementary Dataset S1, Supplementary Dataset S2). Nitrate, alone or in combination with ammonium, rapidly induced over 250 genes in the roots within 15 minutes (Supplementary Figures S1). This list includes homologues of Arabidopsis primary nitrate response genes such as *LOB DOMAIN-CONTAINING PROTEIN37/38/39 (LBD37/38/39), NITRATE-INDUCIBLE GARP-TYPE TRANSCRIPTIONAL REPRESSOR1 (NIGT1), NRT1.1*, nitrate and nitrite reductases,

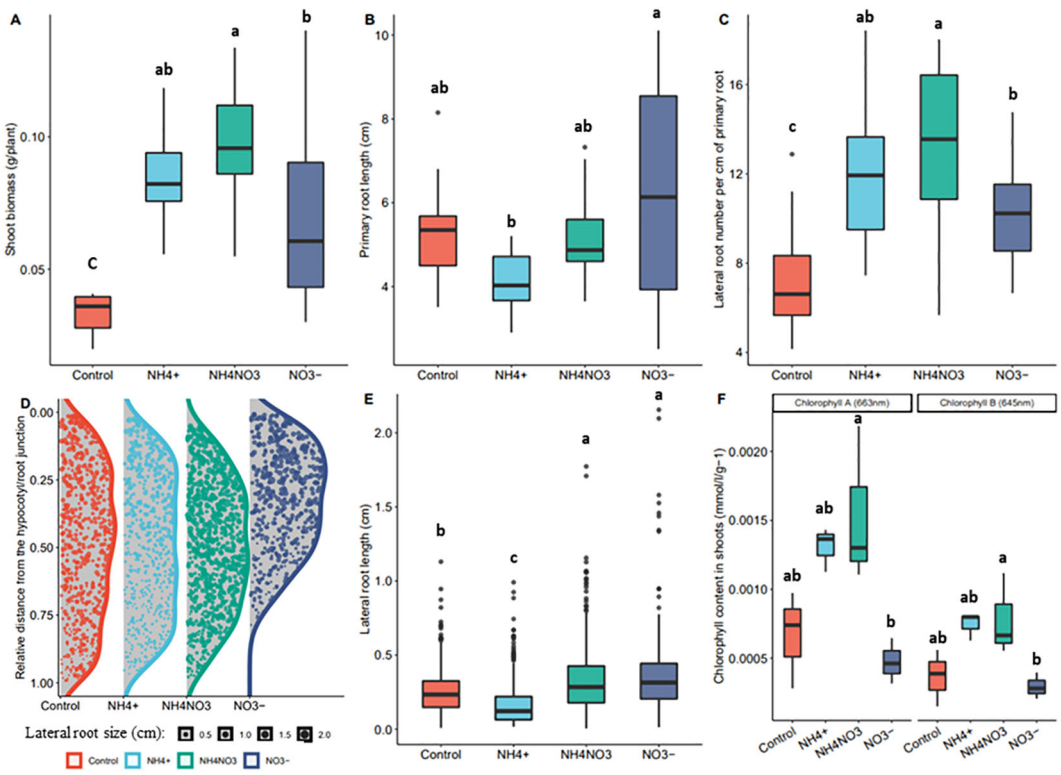

FIGURE 1
Rice phenotype in response to different nitrogen forms. Effects of nitrate (NO_3^-), ammonium (NH_4^+) and equimolar combination of both forms (NH_4NO_3) on rice seedlings grown for 5 days on nitrogen free medium and supplemented with the different treatments for 10 days. Boxplots lower side, middle line and upper side represent the median, the 25th and 75th percentiles, respectively (interquartile range or IQR). Boxplots whiskers represent data falling within a 1.5xIQR distance, measurements beyond this distance are plotted as single points. **(A)** fresh shoot biomass per plant (n=15). **(B)** Primary root length (n=15) **(C)** Emerged lateral root density (n=15) **(D)** Density plot of the distribution of lateral roots over the primary root. On the Y axis, 0.00 represents the root-hypocotyl junction, and 1.00 represents the root tip. The data is normalized on the primary root length. The length of each lateral root is represented by the size of the dots. **(E)** Average lateral root length (n=15) **(F)** Leaf blade chlorophyll content (samples (n) are 5 seedlings pooled together, n=3). Different letters correspond to the post-hoc Tuckey's test significance (p.value=0.05), performed after an ANOVA test, and showing significant differences between the samples.

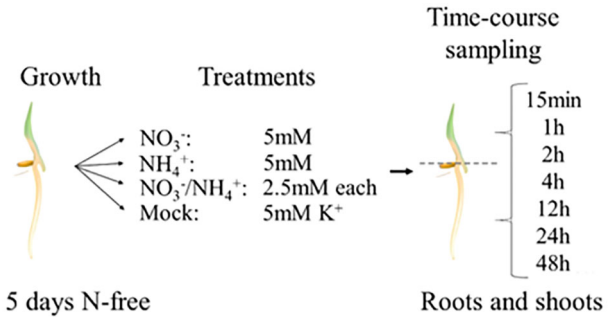

FIGURE 2
Experimental set-up of the RNA-seq.

GLUCOSE-6-PHOSPHATE DEHYDROGENASE3 (G6PDH3) and *ARABIDOPSIS NAC DOMAIN-CONTAINING protein 4 (NAC4)* (Supplementary Dataset S1). In contrast, the response to ammonium was very weak at the 15 minutes-timepoint but a high number of differentially expressed genes was observed after 1h (Supplementary Figures S1, S3; Supplementary Dataset S1), including the transporter-encoding *AMMONIUM TRANSPORTER1.2* (*OsAMT1.2*) and *OsAMT2.2* or the amino acid assimilation enzyme-encoding *ALANINE AMINOTRANSFERASE1* (*OsAlaAT1*), *OsAlaAT2*, *ASPARAGINE SYNTHETASE1* (*OsASN1*), *PHOSPHOENOL PYRUVATE CARBOXYKINASE1* (*OsPPCK1*), and *GLUTAMATESYNTHASE1* (*OsGLT1*). The highest number of differentially expressed genes was in general observed with the combined treatment of ammonium and nitrate. The majority of these genes were also affected by either the ammonium or nitrate treatment (Supplementary Figure S1). Hence, the combined ammonium-nitrate response seems to largely reflect the sum of the individual responses.

In the shoot, a strong response only occurred from 4h onwards, primarily attributable to the nitrate treatment. The ammonium treatment resulted in a slower response, but from 12h onwards, large transcriptomic changes were observed as well (Supplementary Dataset S2, Supplementary Figure S2).

Co-expression network analysis identifies unique gene clusters responsive to nitrate and ammonium treatments in roots and shoots

To analyze the gene response profiles towards the different treatments, we built a co-expression network using the R package WGCNA (Langfelder and Horvath, 2008) for the most varying genes in the roots (18457) and shoots (18343). The network revealed 54 co-expression clusters in the roots and 55 in the shoots (Supplementary Figures S4, S5; Supplementary Datasets S1, S2). The accompanying edge and node tables, compatible with network visualization tools such as Cytoscape or Gephi can be downloaded at https://osf.io/2uzd3/. To provide access to these resources, we generated a Shiny app Supplementary Figure S6), https://www.psb.ugent.be/shiny/rice-response-to-nitrogen/). The user can query any of the 42189 rice genes to display the expression profile in response to the different nitrogen treatments. If the gene is also included in the 18457 genes or 18343 genes used for the co-expression network, the Eigengene of its WGNCA cluster and a correlation coefficient with highly correlated genes (biweight midcorrelation, computed during the gene co-expression network creation) is also displayed. The latter is also shown in Supplementary Datasets S3 and Supplementary Dataset S4, which facilitate the identification of highly co-expressed gene pairs. The cluster membership and associated p values indicating the contribution to the cluster profile for each gene as well as the number of connections to other genes within the same cluster are indicated in Supplementary Datasets S1, S2.

In the roots, we identified clusters specifically and early induced by nitrate (nitrate and ammonium-nitrate treatments only) containing transiently ('green3') or constitutively induced genes ('thistle3') (Figure 3; Supplementary Figure S4). We identified two clusters specifically induced by ammonium ('darkslateblue' and 'deeppink1'). Two clusters of genes were induced by ammonium and with an approximately 4h delay by nitrate or weaker induction by nitrate, possibly due to the nitrate to ammonium reduction ('mediumorchid', 'thistle4'). We identified small clusters with a specific response to ammonium ('yellow3') or nitrate ('indianred3'), but no or very weak response to the combination of the two nitrogen forms, indicative for a countereffect of the other nitrogen form on these genes. Vice versa, we did not identify clusters of genes induced by the ammonium-nitrate treatment only. Some other clusters show a similar response to all nitrogen forms, and are likely related to the nitrogen nutrition. Most other clusters showed a high response in the mock as well or show irregular or variable expression profiles (Supplementary Figure S4).

In the shoots, we identified early responsive and nitrate-specific clusters that are similar to the nitrate-specific clusters in the roots, including a transient ('pink2', similar to 'green3') and a constitutive cluster of upregulated genes ('lightcyan1', similar to 'thistle3'). Also a cluster of genes exclusively induced by nitrate could be observed ('plum4'), similar as the 'indianred3' cluster in the roots. Contrary to the roots, we did not identify an ammonium-specific cluster in the shoots. Moreover, many more shoot clusters exhibit irregular patterns or show similar responses in the mock as in the treatments, making them of less interest. Overall, our co-expression networks revealed clusters of genes illustrating strong temporal and differential biological responses to the different forms of nitrogen provided.

To further investigate the clusters nature, we conducted a gene-ontology enrichment analysis (Supplementary Datasets S5, S6). We first compared the nitrate-specific clusters in the roots ('green3', 'thistle3') and the shoots ('pink2', 'lightcyan1'). The genes ontologies enriched in both roots and shoots nitrate-specific clusters are highly similar and many genes are retrieved in both clusters: 72.8% of the 125 genes composing the nitrate-specific shoot clusters are retrieved in the 414 genes composing the nitrate-specific root clusters. The genes present in all these clusters are primarily related to nitrate assimilation and nitrate transport.

Highly enriched terms for the ammonium-specific clusters in the roots 'darkslateblue' and 'deeppink1' are mainly related to ammonium or amino acid assimilation and cellular respiration or

10.3389/fpls.2024.1343073

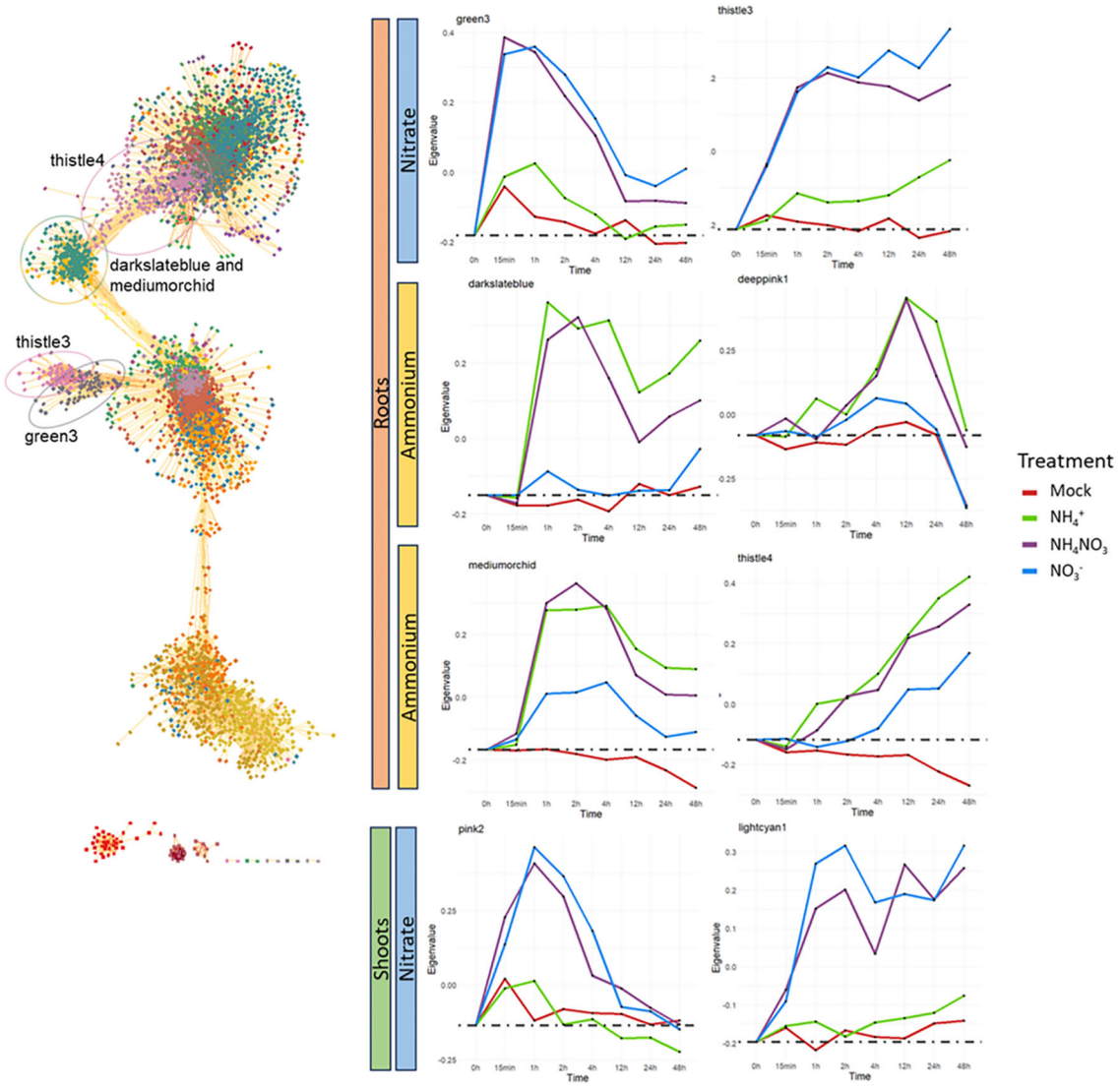

FIGURE 3
WGNCA co-expression network in the root and examples of WGNCA clusters in roots and shoots with a specific response to nitrate or ammonium. The expression profile of the clusters is shown by the eigengene, a representative for the overall expression and calculated as the first principal component of the gene expression data in the respective cluster. Root-specific clusters are indicated in the network. The cluster deeppink1, which is a relative small cluster, is not indicated.

ATP production. The 'indianred3' root cluster and the 'plum4' shoot cluster, containing genes that are exclusively induced by nitrate alone, are both highly enriched in iron-related terms. The root cluster 'yellow3' showing an exclusive response to ammonium alone, mainly concerns genes related to oxidative stress (Supplementary Datasets S3, S4).

Nitrogen network highlight known and novel transcription factors involved in the nitrate specific response

For further analysis of the co-expression network, we zoomed in on the two main nitrate-specific clusters in the root network ('green3' and 'thistle3') containing genes that were rapidly induced upon nitrate (Figure 4; Supplementary Table S1). With for example *OsNRT1.1B* (Os10g40600) and *NITRATE REDUCTASE1* (*OsNR1*) (Os08g36480), this group contains typical nitrate sentinel genes. In the same group, we identified 38 transcription factors based on PlantTFDB v5.0 (https://planttfdb.gao-lab.org/) (Tian et al., 2019) (Supplementary Dataset S1). Several of these transcription factors have a high module membership and a high number of connections within one of the two clusters and could be designated as 'hub' genes with potentially an important role in the nitrate response or signaling (Figure 4, Table 1). A highly connected transcription factor in 'green3' is *OsLBD38* (Os03g41330) which homologues were shown to be involved in nitrogen signaling in Arabidopsis or other species (Rubin et al., 2009; Teng et al., 2022), while *OsLBD38* seems to be part of a conserved regulatory cluster between Arabidopsis and rice (Obertello et al., 2015). OsLBD38 is also the

10.3389/fpls.2024.1343073

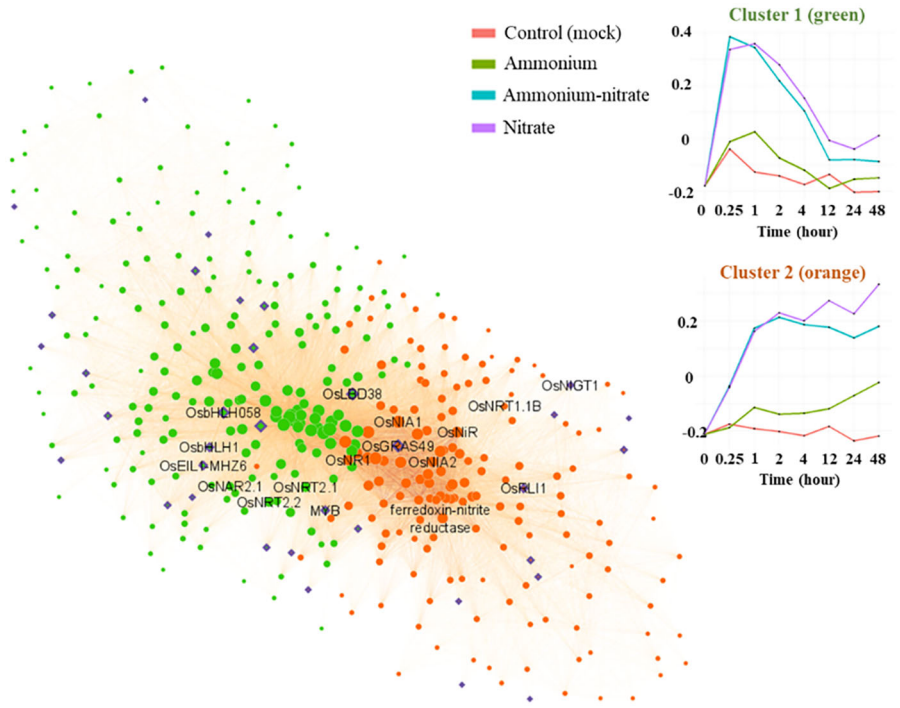

FIGURE 4
Co-expression network for the two main nitrate specific clusters. The green genes belong to the cluster 'green3", the orange ones to 'thistle3'. The purple genes correspond to transcription factors. The transcription factors present in these clusters, together with their number of connections to other genes, are available in Table 1.

TABLE 1 Transcription factors with at least one connection in the clusters green3 or thistle3 as presented in Figure 4.

Cluster	LOCUS ID	Gene name	Transcription factor family (PlantTFDB v5.0)	MM WGNCA cluster	p.MM WGNCA cluster	number of connections
Cluster 1 (green3)	LOC_Os05g38140.1	OsbHLH058	bHLH	0.949189	4.43E-15	154
	LOC_Os03g62230.1		C2H2	0.930715	2.61E-13	144
	LOC_Os03g41330.1	OsLBD38	LBD	0.839871	1.22E-08	112
	LOC_Os07g43530.1	OsbHLH1	bHLH	0.924495	8.03E-13	106
	LOC_Os11g06010.1	OsbHLH151	bHLH	0.924182	8.48E-13	105
	LOC_Os05g37730.1		MYB	0.869067	9.67E-10	92
	LOC_Os03g20790.1	OsEIL1	EIL	0.853357	4.05E-09	91
	LOC_Os08g43090.1	OsbZIP68	bZIP	0.805793	1.33E-07	81
	LOC_Os05g45020.1	OsC3H37	C3H	0.795072	2.57E-07	76
	LOC_Os01g04930.1		MYB	0.769732	1.05E-06	67
	LOC_Os01g43550.2	OsWRKY12	WRKY	0.836758	1.55E-08	58
	LOC_Os06g05890.1	OsBBX16	DBB	0.78879	3.71E-07	57
	LOC_Os09g31400.1	OsEIL3	EIL	0.791398	3.19E-07	56
	LOC_Os03g20780.1	OsEIN3	EIL	0.771365	9.68E-07	51
	LOC_Os12g21700.1	OsC3H66	C3H	0.778115	6.75E-07	44
	LOC_Os03g50920.1	OsZHD11	ZF-HD	0.860267	2.2E-09	42

(Continued)

10.3389/fpls.2024.1343073

TABLE 1 Continued

Cluster	LOCUS ID	Gene name	Transcription factor family (PlantTFDB v5.0)	MM WGNCA cluster	p.MM WGNCA cluster	number of connections
	LOC_Os01g43590.2	OsHsfC1a	HSF	0.797629	2.21E-07	38
	LOC_Os03g13400.1	OsIDD14	C2H2	0.804705	1.43E-07	37
	LOC_Os08g38220.1	OsDof24	Dof	0.823533	4.09E-08	24
	LOC_Os04g32590.1		Trihelix	0.718961	1.11E-05	23
	LOC_Os01g45090.1	OsMYB8	MYB	0.777949	6.81E-07	7
	LOC_Os02g52670.1	OsDERF5	ERF	0.639761	0.000186	2
Cluster 2 (thistle3)	LOC_Os11g47890.1	OsGRAS49	GRAS	0.942288	2.37E-14	112
	LOC_Os04g56990.1	OsRLI1	G2-like	0.937522	6.73E-14	107
	LOC_Os09g21180.1	OsHox25	HD-ZIP	0.815732	6.99E-08	64
	LOC_Os10g18099.1		WRKY	0.865895	1.31E-09	60
	LOC_Os02g22020.1	OsNIGT1	G2-like	0.881506	2.71E-10	59
	LOC_Os01g64020.1	OsbZIP11	bZIP	0.905257	1.53E-11	46
	LOC_Os03g46790.1	OsbHLH022	bHLH	0.841582	1.07E-08	38
	LOC_Os02g06910.1	OsARF6a	ARF	0.831721	2.27E-08	27
	LOC_Os07g25710.3	OsPHR2	G2-like	0.714212	1.35E-05	21
	LOC_Os07g02800.2		G2-like	0.705864	1.89E-05	16
	LOC_Os11g47870.1		GRAS	0.816776	6.51E-08	8
	LOC_Os03g52450.1	OsTIFY1b	GATA	0.76735	1.19E-06	7
	LOC_Os12g06640.1		Trihelix	0.656455	0.00011	3

The module membership (MM) and the associated p.value (p.MM) indicates how strongly a gene is associated with the cluster and is calculated based on the gene's connectivity within the cluster, reflecting its contribution to the overall. The number of connections shows the number of other genes within the same WGNCA cluster that show a co-expression coefficient of at least 0.1 with the gene.

most connected transcription factor in the shoot cluster 'lightcyan1' (Supplementary Dataset S2). *OsNIGT1* (Os02g22020), known to be an important transcriptional regulator of the nitrate signaling as well, is also present in 'thistle3' (Figure 4, Table 1; Supplementary Dataset S1) (Maeda et al., 2018). Several transcription factors have come forward that have not been previously related to nitrate response. *OsGRAS49* (Os11g47890) for instance, which is to our knowledge not reported to have a role in the nitrate response, is a potential 'hub' transcription factor in the nitrate specific clusters in both roots and shoots (Supplementary Dataset S1, S2).

OsEIL1 and OsRLI1 affect the expression of core nitrate responsive genes

To assess these transcription factors possible role in nitrate signaling, we selected the top hub transcription factors in 'green3' and 'thistle3' (Figure 4; Supplementary Dataset S1) and tested whether they could induce the expression of the nitrate sentinel genes *OsNRT1.1B* and *OsNR1*. We used a rice protoplast transactivation assay to perform *in vivo* validation of the inferred regulatory relationships (Figure 5; Supplementary Figure S4): a reporter plasmid harboring the mEGFP gene under the control of the promoter of a putative target gene was co-transfected with an expression vector harboring the coding sequence of one of the selected transcription factor downstream of a constitutive promoter (p35s).

We found two transcription factors that strongly induced the expression of *OsNR1* and *OsNRT1.1B*: ETHYLENE INSENSITIVE3 (EIN3)-LIKE1 (OsEIL1)/MAHOHUZI6 (MHZ6) (Os03g20790) and REGULATOR OF LEAF INCLINATION1 (OsRLI1)/ HIGHLY INDUCED BY NITRATE GENE1 (HINGE1) (Os04g56990) (Figure 5; Supplementary Figure S4).

To further investigate the role of OsRLI1 and OsEIL1 in rice nitrate response, we generated or acquired the mutant rice lines of *oseil1* and *osrli1*. Both mutants showed a small increase in lateral root number and primary root length, but this phenotype was independent of the different nitrogen treatments (Supplementary Figure S5). To assess the importance of the transcription factors for the nitrate response, we treated the mutants with nitrate and tracked *OsNRT1.1B* and *OsNR1* expression over time (Figure 6). The expression of *OsNRT1.1B* and *OsNR1* was less induced by nitrate in the *oseil1* mutant background than in the wild-type line (Figure 6A), which further supports a role of *OsEIL1* for the induction of nitrate responsive genes and hence in the nitrate regulatory pathway. In contrast, we did not detect a significant difference of the nitrate responsive genes in the *osrli1* background (Figure 6B).

10.3389/fpls.2024.1343073

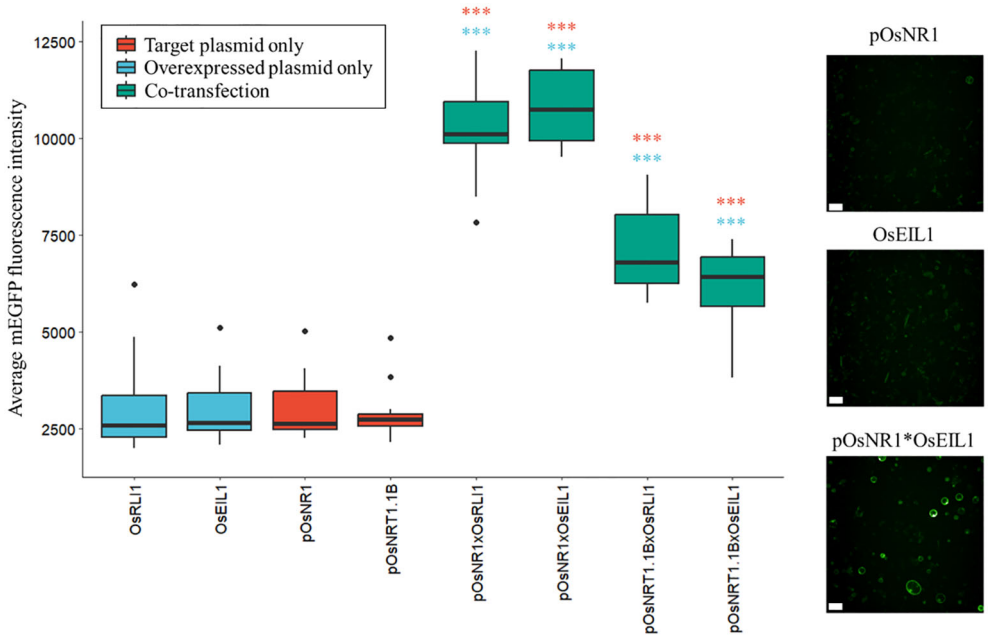

FIGURE 5
Protoplast transactivation assay. Induction of nitrate response genes by the two selected transcription factors in a rice protoplast transactivation assay. The boxplots show the average mEGFP fluorescence intensity per transfected protoplast (min. 118 protoplasts per condition, average 408) in one well (n=16). Samples (green) are co-transfected with the indicated combinations of inducer and target plasmids. The negative controls are only transfected with the inducer plasmid (blue) or with the target plasmids (red). Significance was determined by a one-way ANOVA followed by a Tukey's post-hoc test (***$p < 1.10^{-6}$, blue: sample versus the transcription factor control, red: versus the promoter of the reporter control). Confocal images show negative controls (pOsNR1 and pOsEIL1) and activation of OsNR1 by OsEIL1 (pOsNR1*OsEIL1) in the mEGFP channel (emission: 522nm, excitation: 488nm). Scale bars: 50µm.

Discussion

Co-expression network identifies novel candidates in nitrogen signaling

In this study, we provided a detailed overview of the transcriptional response of rice in roots and shoots to different nitrogen forms and generated a resource with the expression profile of any rice gene of interest in response to nitrate, ammonium, or the combination of both (all expressions profiles are available on https://www.psb.ugent.be/shiny/rice-response-to-nitrogen/). We used this dataset to generate a co-expression network, and identified clusters with a specific response to nitrogen in both roots and shoots. Furthermore, the co-expression network created the possibility to infer putative transcription factors/target genes relationships. As the different nitrogen treatments lead to distinct variations due to unique interactions, we anticipated uncovering otherwise overlooked regulatory relationships. We illustrated this by identifying new transcription factors with a role in nitrate signaling and showing the potential effect of two transcription factors, OsRLI1 and OsEIL1, on the induction of nitrate response.

OsRLI1 is a transcription factor involved in phosphate starvation signaling (Zhang et al., 2021). As a matter of fact, nitrate is known to affect the phosphate signaling pathway

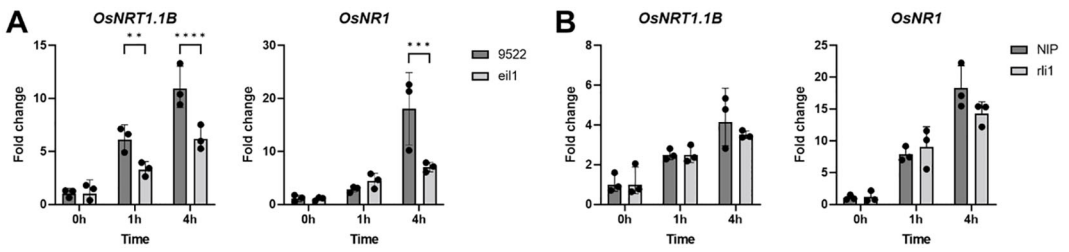

FIGURE 6
Gene expression of OsNRT1.1B and OsNR1 in osrli1 **(A)** or oseil1 **(B)** mutants or their respective wild-type background in roots of rice supplemented with NO_3 in the form of KNO_3. Significance was determined by a one-way ANOVA followed by a Tukey's post-hoc test (**$p < 0.01$; ***$p < 0.001$; ****$p < 0.0001$).

(Hu et al., 2019). Supporting this, our co-expression network revealed that *OsRLI1* expression is correlated with the expression of several phosphate-starvation signature induced genes: *INOSITOL-3-PHOSPHATE SYNTHASE ISOZYME1* (*OsIPS1*) (often used as a phosphate starvation reporter (Hou et al., 2005; Wang et al., 2009a; Dai et al., 2012)), *1-AMINOCYCLOPROPANE-1-CARBOXYLIC ACID SYNTHASE* (*OsACS*) [involved in tolerance to phosphate starvation in rice (Lee et al., 2019)], *SPX-MAJOR FACILITY SUPERFAMILY2* (*OsSPX-MSF2*) (involved in phosphate signaling/transport and induced by phosphate starvation (Wang et al., 2012)), and finally *PHOSPHATE STARVATION RESPONSE2* (*OsPHR2*) which is the main regulator of phosphate starvation responses (Zhou et al., 2008) and inducer of *OsRLI1* (Zhou et al., 2008; Wu and Wang, 2011; Zhang et al., 2021). *OsRLI1* is moreover a close homologue of *OsPHR2* and *AtPHR1* and interacts just as these with SPX-domain containing proteins (Puga et al., 2014; Wang et al., 2014; Ruan et al., 2018; Zhang et al., 2021). OsPHR2 binds to OsSPX1/2/4 upon high phosphate. A low cellular inositol phosphate level, which depends on the phosphate level of the cell, disrupts the SPX retention of OsPHR2 which then is free to migrate to the nucleus where it binds to phosphate starvation inducible genes promoters (Wild et al., 2016; Crombez et al., 2019; Hu et al., 2019). At least the interaction with OsSPX4 depends also on nitrate levels: the transceptor OsNRT1.1B can promote OsSPX4 protein degradation in a nitrate-dependent manner, impacting directly the phosphate signaling pathway (Hu et al., 2019). OsRLI1 was shown to be induced by nitrate to induce the phosphate starvation response and finetune the N-P balance (Zhang et al., 2021). Our results show that it may also induce nitrate responsive genes, further complicating the phosphate-nitrate crosstalk.

OsEIL1 is a transcription factor involved in ethylene signaling (Yang et al., 2015a, Yang et al., 2015b) and regulates various genes such as transcription factors and metabolic genes (Dolgikh et al., 2019) and hormonal pathways (Chang et al., 2013). Here, we showed that *OsEIL1* upregulation by nitrate correlates with *OsNRT1.1B* induction in rice. In Arabidopsis, nitrate induces ethylene production via induction of 1-aminocyclopropane-1-carboxylic acid (ACC) synthases (ACS) and ACC oxidases (ACO), key enzymes in the ethylene biosynthesis pathway (Kende, 1993; Khan et al., 2015). Moreover, nitrate-induced expression of *NRT1.1* requires ethylene signaling (Tian et al., 2009), but it is not known how these pathways exactly connect to each other. Additionally, certain nitrate transporters were shown to be directly controlled by ethylene (Zheng et al., 2013; Zhang et al., 2014). As in Arabidopsis, multiple *ACS* genes are in our dataset induced upon nitrate in our rice dataset, including *OsACS2*, *OsACS5* and *OsACS6*, supporting a comparable pathway in rice and Arabidopsis. However, the absence of binding motifs for the OsEIL1 transcription factor (Hiraga et al., 2009) or ethylene response factors ERFs (Ohme-Takagi and Shinshi, 1995) in the promoters of *OsNRT1.1B* and *OsNR1* argue for an indirect impact on these genes by OsEIL1. Still, our results show that *OsEIL1* is not only able to – possibly indirectly – induce *OsNRT1.1B* and *OsNR1*, but also that *OsEIL1* is important for the nitrate-induced expression of those genes, featuring OsEIL1 as a central transcription factor in the ethylene signaling-dependent nitrate response in rice.

Ammonium as a signal?

While we focused on the nitrate-specific clusters to investigate new candidate regulators, other parts of the co-expression network can be explored as well. For instance, the ammonium-specific cluster may provide valuable insights into ammonium signaling, although this could be more challenging due to the generally slower transcriptional response compared to nitrate. This slow transcriptional response indicates that ammonium does not directly activate a transcriptionally regulated signaling pathway. Still, ammonium is suggested to be signaling molecule (Liu and von Wirén, 2017). Bacteria have even been shown to possess an ammonium-sensing histidine kinase (Pflüger et al., 2018, Pflüger et al., 2024), but similar mechanisms have not yet been demonstrated in plants. Interestingly, the bacterial sensor is part of the ammonium transporter/methylamine permease/Rhesus family, which also includes plant AMT proteins that have been proposed to function as ammonium receptors (Liu and von Wirén, 2017). The fact that ammonium does not induce rapid transcriptional changes in rice does not exclude that ammonium can act as a potential signaling molecule via another biochemical pathway and indirectly trigger a transcriptional response. In this respect, it is important to note that we observed a strong transcriptional response starting 1 hour after treatment, with a considerable number of transcription factors identified in the ammonium-specific clusters, including for example *MONOCULM1* (*OsMOC1*, *Os04g35250), OsNAC5* (*Os11g08210*) and *OsNLP6 (Os02g04340)* that showed high expression levels (FC > 8) after 1 hour of treatment. Interestingly, *OsNLP6* is a homolog of *OsNLP1*, *OsNLP3*, and *OsNLP4* which are all known for their implication in nitrate and ammonium responses or in nitrogen use efficiency (Hu et al., 2019; Alfatih et al., 2020; Wang et al., 2021; Wu et al., 2021). *OsNLP6* is only known for having a very low basal expression and not responding to various stress tested in previous studies, but was never characterized further (Jagadhesan et al., 2020; Wu et al., 2021). The high expression of *OsMOC1* is somewhat surprising as it is mainly known for its critical role in regulating tiller number and plant architecture (Liao et al., 2019). Finally, *OsNAC5* is an abiotic stress-responsive gene (Takasaki et al., 2010), which might indicate that a stress induce the transcriptional response. Ammonium is known to affect rapidly the internal and external pH of roots, which may be the chemical cue resulting in this response (Jia et al., 2020; Motte and Beeckman, 2020). We also observed that ammonium upregulated alanine aminotransferases expression, indicating an accumulation of alanine in planta. Such responses are usually observed in stress conditions to store nitrogen and to provide energy and reductants under for instance anoxia situations in the cell (Vanlerberghe et al., 1991; Miyashita et al., 2007). Alanine biosynthesis is a known ammonium detoxification process with alanine serving as a nitrogen store (Esteban et al., 2016). In Arabidopsis roots, hypoxia induces *AlaAT1* and *AlaAT2* as early as 2h after stress application with a peak at 8h, followed by a decrease after 24h, which corresponds to what we and others observed in rice upon ammonium treatment (Miyashita et al., 2007) and was also observed in maize (Muench et al., 1998). Gene ontology enrichment for the ammonium-specific cluster ('darkslateblue') revealed an increase in proton related ATPase activity terms potentially indicating a response to counteract cytoplasmic

acidification caused by ammonium uptake, thereby contributing to ammonium tolerance in rice. The enrichment of the pyruvate metabolic process term suggests a higher demand for energy production or amino acid biosynthesis, as pyruvate is a central metabolite connecting glycolysis, the TCA cycle, and the amino acid synthesis pathways. Overall, this suggests that the response is more likely related to acidification or stress rather than ammonium acting as a signaling molecule. In any case, the poor overlap in response to ammonium in the shoot and root supports a local effect.

Synergistic effects: dual action or mitigation of stress?

Both in our and previous studies, co-application of ammonium-nitrate resulted in more growth compared to both forms individually (Figure 1) (Kronzucker et al., 1999). Our data showed a broader transcriptional response to the combined nitrogen treatment, encompassing responses that are otherwise only elicited by either ammonium or nitrate alone. This is particularly clear in the cluster analysis, where the ammonium-nitrate profile closely follows either the ammonium or nitrate expression patterns, but rarely exhibits a distinct profile. Hence, the combined provision may elicit a dual action that translate into improved growth. This was specifically observed in lateral root density, where the spatial distribution resulting from the combined treatment resembled the cumulative distribution patterns observed under each individual nitrogen form. Additionally, the ammonium treatment resulted in higher leaf chlorophyll content, which is in line with the positive effect of ammonium on photosynthesis activity as reported in Arabidopsis (Sanchez-Zabala et al., 2015). This effect was also observed with the ammonium-nitrate combination, but not with nitrate alone, further illustrating that the action of one of the forms is preserved within the combined treatment.

An alternative explanation for the differences in growth between co-application and single application is that the provision of only one nitrogen form could trigger a stress response, which is absent when both forms are present. Indeed, despite rice being considered as an ammonium-tolerant plant, we observed that ammonium supplementation alone reduces the size of the rice root system, a phenotype typically associated with ammonium toxicity (Liu and von Wirén, 2017). Accumulation of chlorophyll is in Arabidopsis associated with a mild ammonium stress (Sanchez-Zabala et al., 2015). Likewise, the 'yellow3' co-expression cluster that group genes induced by ammonium but not by ammonium-nitrate shows an oxidative stress signature, while a number of stress-related genes are induced upon ammonium treatment (see above). Hence, while considered to be ammonium tolerant, rice clearly displays toxicity-related phenotypes, as also observed in other recent studies (Jia et al., 2020; Xie et al., 2023; Yan et al., 2023). The presumed ammonium tolerance likely originates from observations of paddy field-grown rice, where ammonium is partially converted to nitrate, and rice at the end perceives both ammonium and nitrate. Furthermore, genes in the 'indianred3' and 'plum4' clusters that are exclusively induced by nitrate only and by none of the other treatments are primarily linked to iron homeostasis and transport as illustrated by the GO enrichment. Such genes, including *OsIRO2*, *OsIRO3*, *OsNRAMP1*, *OsPOT*, *OsOPT7* and *OsMIR* are typically upregulated upon iron starvation (Zheng et al., 2009; Zhang et al., 2017), which is known to occur when nitrate is the sole nitrogen form provided (Chen et al., 2018). Hence, the observed improvement in growth with the combined treatment may be attributed to the mitigation of stress effects that are typically induced by the individual nitrogen forms.

Nitrogen network for data mining

By focusing on a few nitrate-specific clusters, we demonstrated that our dataset, which includes responses to both ammonium and nitrate, can be utilized to identify candidate transcription factors involved in nitrogen signaling. Other clusters with different nitrogen response profiles presented in this study can be investigated as well, either to identify novel regulators or to predict functions for unknown genes. For instance, uncharacterized putative transporter encoding genes that were identified as strongly co-expressed with nitrate transporters in our network might encode transporters with a role in nitrate transport. Overall, our present study provides the research community with an extensive dataset describing how rice, a major staple crop, responds at the transcriptional level to two main nitrogen feedstocks. A better understanding of how plants sense, take up and process the two main forms of nitrogen provided by fertilization is an important field of study within the contemporary context of the increasing need to breed crop plants with enhanced nitrogen use efficiency.

Material and methods

Root and shoot treatment and sampling for transcriptomics

Rice seedlings [Oryza sativa Nipponbare cultivar (#GSOR100, USDA-ARS)] were dehulled and sterilized with ethanol 70% for 5 minutes, followed by immersion in bleach 6% with Tween-20 for 30 minutes. Seedlings were imbibed by immersion in sterile water for 12h to synchronize germination at 30 degrees. Germinating seeds were transferred on a hydroponic system, and roots were immersed in a nitrogen-free basal salt medium composed of K_2SO_4 0.7mM, KH_2PO_4 0.3mM, $CaCl_2.2H_2O$ 1mM, $MgSO_4.7H_2O$ 1mM, $Na_2SiO_3.9H_2O$, Na_2-Fe-EDTA 20µM for macronutrients, and $MnCl_2.4H_2O$ 9µM, $Na_2MoO_4.2H_2O$ 0.39µM, H_3BO_3 20µM, $ZnSO_4.7H_2O$ 0.77µM, $CuSO_4.5H_2O$ 0.32µM for micronutrients (pH 5.8). Seedlings were then transferred to a growth cabinet in the dark at 30 degrees for 3 days in a randomized block design. The light was then turned on after 72h and let on for 48h before treatment occurred. Nitrogen treatments consisted of injection with 5mM KNO_3 (5mM NO_3^- treatment), 2.5mM $(NH_4)_2SO_4$ + 2.5mM K_2SO_4 (5mM NH_4^+ treatment), 2.5mM KNO_3 + 1.25mM $(NH_4)_2SO_4$ + 1.25mM K_2SO_4 (2.5mM NH_4^+ and 2.5mM NO_3^- treatment) or 2.5mM K_2SO_4 (mock treatment) in this basal medium. K_2SO_4 was used to balance potassium (K^+) equimolarly to 5mM in each of the treatments. Rice seedlings were extracted

15min, 1h, 2h, 4h, 12h, 24h and 48h after nitrogen treatments. A supplemental control without treatment was extracted at the 0h time point in 3 biological replicates for roots and shoots, to estimate the impact of the manipulation of the samples (referred to as "Control 0h"). At the extraction time-point, shoots and roots were cut with a razor blade and frozen in liquid nitrogen. The remaining seeds were discarded. Three different boxes were used for each treatment and for each time-point, for a total of 87 boxes. At least 10 germinated seedlings were sampled per box.

Root and shoot phenotyping

For the phenotyping experiments, the same procedure as described above was followed but seedlings were let grown in the hydroponic media for 10 days after treatment and the medium was refreshed daily. Chlorophyll was extracted with DMSO and measured by absorbance at 663nm (Chlorophyll A) and 645nm (Chlorophyll B). Chlorophyll content was measured as:

$$\text{Chlorophyll A}(\text{mmol} = \text{l} = \text{g}) = (\S\,\text{Abs at } 663\text{nm} = \S\,75:05{*}1) = \text{g of fresh leaves}$$

$$\text{Chlorophyll B}(\text{mmol} = \text{l} = \text{g}) = (\S\,\text{Abs at } 645\text{nm} = \S\,47:0{*}1) = \text{g of fresh leaves}$$

RNA extraction

Frozen roots and shoot samples were grinded with one 3mm metal bead into Eppendorf tubes. RNA was extracted with Trizol (Life Technologies) and the RNeasy Mini Kit (Qiagen) following the manufacturer instructions. An extra DNase step was performed with RNase-Free DNase Set (Qiagen). RNA samples were resuspended in RNAse free water. RNA concentration and purity were determined spectrophotometrically using the Nanodrop ND-1000 (Nanodrop Technologies) and RNA integrity was assessed using a Bioanalyzer 2100 (Agilent).

RNA-seq library preparation

The sequencing and library preparation was performed by the VIB Nucleomics Core Facility (Leuven, Belgium; www.nucleomics.be). Per sample, 500ng of total RNA was used as input. Using the Illumina TruSeq® Stranded mRNA Sample Prep Kit (protocol version: Part # 15031047 Rev. E - October 2013), poly-A containing mRNA molecules were purified from the total RNA input using poly-T oligo-attached magnetic beads. In a reverse transcription reaction using random primers, RNA was converted into first strand cDNA and subsequently converted into double-stranded cDNA in a second strand cDNA synthesis reaction using DNA PolymeraseI and RNAse H. The cDNA fragments were extended with a single 'A' base to the 3' ends of the blunt-ended cDNA fragments after which multiple indexing adapters were ligated introducing different barcodes for each sample. Finally, PCR enrichment was conducted to enrich those DNA fragments that have adapter molecules on both ends and to amplify the amount of DNA in the library. Sequence-libraries of each sample were equimolarly pooled and sequenced on Illumina NextSeq 500 (High Output, 75 bp, Single Reads, v2). The raw transcriptomic data (*fastq* files) have been deposited in the functional genomics data collection ArrayExpress under the accession number E-MTAB-13146.

Sequence mapping

All analyses were done on the VIB-UGent Plant System Biology Galaxy platform (Afgan et al., 2018). The Trimmomatic tool (Bolger et al., 2014) was used to trim the reads for low-quality read-ends with the following options: raw fastq file, type TrueSeq3 adapter sequences. Data quality was assessed with the FastQC tool before and after trimming with the Trimmomatic tool. The output of Trimmomatic was processed by the Salmon tool (Patro et al., 2017). Salmon was used for transcript-level quantification estimates of RNAseq data. The reads were mapped on the coding sequences of release 7 of the MSU Rice Genome Annotation Project (Kawahara et al., 2013) with the following options: stranded reads and reads derived from the reverse strand, with an Incompatible Prior setting of $1x10^{-20}$. Salmon acts in two steps: the indexation of the reference genome (Oryza sativa japonica v7JGI) and the mapping of the reads trimmed by Trimmomatic to this reference genome, followed by their quantification. The output is an estimated number of reads in transcript per millions. The package txtimport 1.14.0 (Soneson et al., 2015) in the R Statistical software version 3.4.3 was used to process the Salmon output data (transcript-level abundance) and summarize it into matrices of counts of reads/fragments (gene-level abundance).

Differential expression analysis

DESeq2 data preparation and cleaning

The txtimport output was then processed with the DESeq2 version 1.26.0 package for differential analysis (Love et al., 2014). A DESeqDataSet was created using the function 'DESeqDataSetFrom Tximport' with a design (~time + treatment + time:treatment), with time and treatment as categorical variables. We then used the DESeq() function to estimate size factors and dispersion values, fit a negative binomial model to the count data, and perform differential gene expression analysis. The resulting DESeqDataset was normalized using the varianceStabilizingTransfomation() (VSD) function. A heatmap of sample-to-sample distance comparison was built for roots and shoots independently to identify outliers samples, using the VSD-transformed data as recommended by the WGCNA developers. Two outliers were detected with the heatmap: one outlier in the roots (2h after NH_4^+ treatment, replicate 3) and one in the shoots (1h after NO_3^- treatment, replicate 2). These samples were discarded for further analysis. The samples correlation was assessed by PCA analysis once outliers were removed (Supplementary Figures S6, S7) and illustrate a good clustering of the samples.

Pair-wise differential analysis

For the pair-wise differential analysis, the same DESeqDataSet was used as input; the DESeq() function was used repeatedly with contrasts set manually between each treatment and the control for each time points independently. Genes with an absolute fold-change > 2 and an FDR < 0.05 were considered as differentially expressed.

Gene co-expression construction

The gene co-expression network and clusters were built using the WGCNA package (Langfelder and Horvath, 2008). We used the varianceStabilizingTransformation() (VSD) function of the package DESeq2 to transform and normalize the DESeqDataSet data described above without the outliers, as recommended for big experiments containing more than 100 samples, and averaged the 3 biological samples per treatment, per time-point. Only genes with more than 5 counts in at least 2 repetitions per treatment per time point were kept, removing non or very lowly expressed genes. This first threshold reduced the total number of genes to around 26000 for roots and shoots. For computational reasons and to remove noise background, a second threshold removing the 30% least-varying genes based on their expression variance between the treatments as recommended by the WGCNA developers was applied. The final input for the gene co-expression network construction was 18343 genes for the shoots and 18457 genes for the roots. DatasetGene connectivity was determined with a power β (soft thresholding) of 7 for the roots and to 8 for the shoots, chosen with the function pickSoftThreshold() with the following options: networkType = "signed hybrid", corFnc = "bicor", maxPOutliers = 0.02. The function 'adjacency()' was used with the same options. The options used to design the network with the function cutreeDynamic were deepSplit = 3, and minModuleSize = 20. For every cluster generated, a cluster eigengene is computed; this eigengene (first principal component of a cluster) can be seen as representative of all the genes that compose the cluster. Eigengenes with a correlation with another eigengene higher than 80% (R2 = 0.8) were merged into one cluster. Network visualization was done with Cytoscape 3.7.2 (Shannon et al., 2003)

Gene ontology enrichment analysis

To identify enriched biological processes, molecular functions, and cellular components within co-expression clusters, a Gene Ontology (GO) enrichment analysis was performed using the GO enrichment tool of the Plaza Monocots 4.0 Platform (Van Bel et al., 2018) using the Locus ID and the publicly available Rice v7.0JGI database with the whole annotated genome as the reference set. The significance threshold for enriched GO terms was set at a p-value of 0.01.

Plasmid construction

Transcription factor coding sequences were isolated by PCR from rice shoots or root cDNA and used to generate the 'inducers plasmids'. Promoter sequences of the target genes were isolated from genomic DNA and correspond to the -2000bp sequence upstream of the start codon of the target gene or were limited by the presence of another gene downstream and used to generate the 'target plasmids'. The plasmids were constructed with the Golden Gateway assembly system: in the inducer plasmids, the coding sequences of the transcription factors were combined with a constitutive promoter (p35s) followed by a nuclear localization sequence. A NOST terminator was placed downstream of the gene coding sequence. In the target plasmids, the genes promoters were cloned upstream of a nuclear localization sequence followed by the fluorescent protein mEGFP coding sequence and a NOST terminator. The inducers plasmids structure can be summarized as "p35s::NLS::transcription-factor-CDS::NOST". The target plasmids structure can be summarized as "gene-promoter:: NLS::mEGFP::NOST". Sequences were validated by sequencing (Eurofins Genomics, Belgium) and reference sequences were extracted from the Plaza Monocots 4.0 Platform (Van Bel et al., 2018). The list of primers used for the genes coding sequences and promoter isolation is available in Supplementary Table S1.

Extraction and transformation of rice protoplasts

14-days old rice seedlings (#GSOR100 USDA-ARS) grown in the dark in sterile vitro-vent boxes on a solid media containing 0.305g/l Murashige & Skoog Modified Basal Salt Mixture Nitrogen-free salts (Phytotech Labs #M407), 0.6mM KH_2PO_4, 9.4mM K_2SO_4, 1mM NH_4NO_3, 1.6mM $Na_2SiO_3.9H_2O$, 8g/l agar and 0.025g/l MES at pH 5.7, were harvested by cutting the stem above the seed and the aerial part kept for protoplast isolation. The protoplasts extraction and transformation followed the protocol described in other studies with few adaptations (Abel and Theologis, 1994; Yoo et al., 2007; Zhang et al., 2011). Briefly, once extracted, the protoplasts were mixed with different combinations of one inducer plasmid and one target plasmid. Addition of PEG-4000 to the mix induced the transient transformation of the protoplasts which assimilated the different combinations of the two types of plasmids, and transformation was stopped after 15 minutes. After incubation overnight, the protoplasts in solution were distributed in a 90-well plate and mEGFP fluorescence intensity (excitation: 488nm, emission: 522nm) was measured by confocal microscopy.

Generation of the oseil1 and osrli1 mutants

The OsEIL1 knock-out mutant was generated in a *Japonica* variety Wuyunjing-7 (9522) using the CRISPR-Cas9 technique, while OsRLI1 knock-out mutant is *Japonica* variety Nipponbare background and was generated in a previous study (Ruan et al., 2018). Homozygous mutant lines were used for subsequent analysis.

Phenotyping and RT-qPCR of the oseil1 and osrli1 mutants

Rice seeds of wild-type and mutant lines were sterilized with 70% (v/v) ethanol for 1 min, followed by 30% (v/v) sodium hypochlorite

solution for 30 min. Seedlings were imbibed by immersion in sterile water for 12h to synchronize their germination and let grown in the dark on nitrogen free solution for 3 days, and then transferred to the growth chamber (30 degrees, continuous light) for another 3 days. Seedlings with ~2 cm seminal root were selected for different nitrogen treatments with modified Kimura B solution: high nitrogen (1.5 mM $(NH_4^+)_2SO_4$, or 3 mM KNO_3^-, HN) and nitrogen free (- N or N-free). The time course started at the moment of the transfer. 20 seedlings roots per technical replicate where harvested, and samples were processed as described above for the transcriptome experiment. The RNA was synthetized into cDNA, and the primers presented in Supplementary Table S1 were used for the RT-qPCR as previously described (Xie et al., 2023)

Phenotyping of the oseil1 and osrli1 mutants

Geminated rice seedlings were first grown in water for 3 days in a growth chamber under a photoperiod of 14 h light (200µmol m^{-2} s^{-2} light density and 70% humidity) and a temperature of 28 degrees, and rice seedlings with ~2 cm long seminal root were then transferred to the hydroponic culture supplied with modified Kimura B solution (500 mL volume for each cup with 10 seedlings) for different nitrogen treatments. For nitrogen -free treatment, nitrogen sources $(NH_4)_2SO_4$ and KNO_3 was replaced with K_2SO_4 at a concentration of 1.5 mM; for NH_4^+ treatment alone, KNO_3 was replaced with K_2SO_4 at the same concentration; for NO_3^- treatment alone, $(NH_4)_2SO_4$ was replaced with 3 mM KNO_3. The 2-[morpholino]ethane sulfonic acid (MES) was supplied to hydroponic cultures to buffer pH of the medium when mentioned. The rice seedlings were treated for 4 days, and the nutrient solution was renewed every two days.

Data availability statement

The datasets presented in this study can be found in online repositories. The names of the repository/repositories and accession number(s) can be found in the article/Supplementary Material.

Author contributions

P-MP: Conceptualization, Data curation, Formal analysis, Investigation, Methodology, Project administration, Visualization, Writing – original draft, Writing – review & editing. BP: Conceptualization, Data curation, Formal analysis, Investigation, Methodology, Supervision, Writing – original draft, Writing – review & editing. LJ: Formal analysis, Resources, Writing – original draft. AD: Investigation, Methodology, Resources, Writing – original draft. VG: Formal analysis, Resources, Visualization, Writing – original draft. PG: Methodology, Resources, Writing – original draft. AC: Methodology, Resources, Writing – original draft. DA: Conceptualization, Resources, Writing – original draft. WX: Investigation, Resources, Writing – original draft. TB: Conceptualization, Funding acquisition, Investigation, Project administration, Resources, Supervision, Writing – original draft, Writing – review & editing. HM: Investigation, Project administration, Resources, Supervision, Writing – original draft, Writing – review & editing, Conceptualization.

Funding

The author(s) declare financial support was received for the research, authorship, and/or publication of this article. Funding for this study was provided by EuroChem Agro, the China National Key Program for Research and Development, the Chinese Ministry of Science and Technology, and the Research Foundation-Flanders (FWO). The funders had no role in the execution of the study or the decision to publish the findings.

Acknowledgments

The authors thank Wouter Smet for critical reading and discussions on the manuscript. We would also like to thank Ignacio Eguinoa, Lieven Sterck and Frederik Coppens for their help and support for the use of bioinformatic tools. We also thank Keke Yi for sharing rice osrli1 seeds.

Conflict of interest

The authors declare that the research was conducted in the absence of any commercial or financial relationships that could be construed as a potential conflict of interest.

Publisher's note

Supplementary material

The Supplementary Material for this article can be found online at: https://www.frontiersin.org/articles/10.3389/fpls.2024.1343073/full#supplementary-material

SUPPLEMENTARY FIGURE 1
Number of differentially expressed genes (FDR < 0.05, absolute fold-change > 2), for each time point in the roots. The bar represents the number of genes present at the intersection indicated by the dot in the bottom of the graph. The Gene/Treatments graph represent the total number of genes differentially regulated per treatment. Brown: genes differentially expressed by NH_4NO_3 only. Yellow: genes differentially expressed by NH_4^+ only. Red:

genes differentially expressed by NO_3^- only. Grey: other combinations as presented below the graph.

SUPPLEMENTARY FIGURE 2
Number of differentially expressed genes (FDR < 0.05, absolute fold-change > 2), for each time point in the shoots. The bar represents the number of genes present at the intersection indicated by the dot in the bottom of the graph. The Gene/Treatments graph represent the total number of genes differentially regulated per treatment. Brown: genes differentially expressed by NH_4NO_3 only. Yellow: genes differentially expressed by NH_4^+ only. Red: genes differentially expressed by NO_3^- only. Grey: other combinations as presented below the graph.

SUPPLEMENTARY FIGURE 3
Number of differentially expressed genes (FDR < 0.05, absolute fold-change > 2), for each time point in the roots **(A)** and shoots **(B)**. The histogram plot represents the number of genes present at the intersection indicated by the dot in the bottom of the graph. The Gene/Time points graph represent the total number of genes differentially regulated per treatment. Blue: genes that are differentially regulated from the first time point (15 minutes after treatment) after treatment and that remain differentially regulated at each time point until the end of the time course (48h after treatment). Yellow: genes that are differentially regulated from 1h after treatment and that remain differentially regulated at each time point until the end of the time course (48h after treatment).

SUPPLEMENTARY FIGURE 4
WGNCA co-expression clusters in the root. Overview of the expression profile of all clusters. The average expression of all the genes composing the cluster is presented in red, individual gene expression is shown in black. Within each plot, the profile of mock, ammonium (NH4), ammonium-nitrate (NN) and nitrate (NO3) is shown from left to right. The name and number of genes per cluster is indicated at the top of each plot.

SUPPLEMENTARY FIGURE 5
WGNCA co-expression clusters in the shoot. Overview of the expression profile of all clusters. The average expression of all the genes composing the cluster is presented in red, individual gene expression is shown in black. Within each plot, the profile of mock, ammonium (NH4), ammonium-nitrate (NN) and nitrate (NO3) is shown from left to right. The name and number of genes per cluster is indicated at the top of each plot.

SUPPLEMENTARY FIGURE 6
Screenshot of Shiny app enabling access to the rice gene expression profiles in response to different nitrogen treatments and the co-expression analysis. 1: User selected gene of interest. 2: Option to select a threshold for the co-expression coefficient in the table 5 and 6. 3: Gene expression profile in response to different forms of nitrogen over a time-course in the roots or the shoots. 4: Eigengene of the WGCNA cluster of the selected gene in the roots or the shoots. 5,6: List of genes co-expressed with the gene of interest in the roots or the shoots. The co-expression coefficient corresponds to the adjacency table (biweight midcorrelation) constructed with WGCNA. Available at https://www.psb.ugent.be/shiny/rice-response-to-nitrogen/.

SUPPLEMENTARY FIGURE 7
Complete protoplast transactivation assay. Induction of nitrate response genes by the different transcription factors in a rice protoplast transactivation assay. The boxplots show the average mEGFP fluorescence intensity per transfected protoplast (min. 118 protoplasts per condition, average 408) in one well (n=16). Samples (green) are co-transfected with the indicated combinations of inducer and target plasmids. The negative controls are only transfected with the inducer plasmid (blue) or with the target plasmids (red). Significance was determined by a one-way ANOVA followed by a Tukey's post-hoc test (*** p < 1.10-6, blue: sample versus the transcription factor control, red: versus the promoter of the reporter control).

SUPPLEMENTARY FIGURE 8
Phenotypes under different nitrogen treatments of oseil1 mutants and osrli1 mutants. (A): Images of the oseil1 mutant and its 9522 background, with measurements of the seminal and lateral roots number. 9522 is the genetic background in which the oseil1 mutant has been constructed. **(B)**: Images of the osrli1 mutant and its NIP background, with measurements of the seminal and lateral roots number. NIP is the genetic background in which the osrli1 mutant has been constructed. The orange dotted line indicates the position of the root tip when the seedlings were transferred to medium supplied with different N. The white dotted line indicates the position of the root tip when the seedlings were treated for 4 days. Different letters correspond to the post-hoc Tuckey's test significance (p.value=0.05), performed after a two-way ANOVA test, and show significant differences between the samples.

SUPPLEMENTARY FIGURE 9
Principal component analysis of the roots RNA-seq samples. Principal component analysis of the of the DESeq2 output normalized with the varianceStabilizingtransFormation() function in roots.

SUPPLEMENTARY FIGURE 10
Principal component analysis of the shoots RNA-seq samples. Principal component analysis of the of the DESeq2 output normalized with the varianceStabilizingTransformation() function in shoots.

SUPPLEMENTARY TABLE 1
Primers used in this study

SUPPLEMENTARY DATA SHEET 1
Genome-wide differential gene expression analysis upon different nitrogen treatments in rice roots

SUPPLEMENTARY DATA SHEET 2
Genome-wide differential gene expression analysis upon different nitrogen treatments in rice shoots.

SUPPLEMENTARY DATA SHEET 3
Co-expression coefficients between gene pairs corresponding to the adjacency table (biweight midcorrelation) of the roots co-expression network constructed with the WGCNA tool.

SUPPLEMENTARY DATA SHEET 4
Co-expression coefficients between gene pairs corresponding to the adjacency table (biweight midcorrelation) of the shoots co-expression network constructed with the WGCNA tool.

SUPPLEMENTARY DATA SHEET 5
Gene ontology enrichment of the WGNCA root co-expression clusters.

SUPPLEMENTARY DATA SHEET 6
Gene ontology enrichment of the WGNCA shoot co-expression clusters.

References

Abel, S., and Theologis, A. (1994). Transient transformation of Arabidopsis leaf protoplasts: a versatile experimental system to study gene expression. *Plant J.* 5, 421–427. doi: 10.1111/j.1365-313X.1994.00421.x

Afgan, E., Baker, D., Batut, B., van den Beek, M., Bouvier, D., Cech, M., et al. (2018). The Galaxy platform for accessible, reproducible and collaborative biomedical analyses: 2018 update. *Nucleic Acids Res.* 46, W537–W544. doi: 10.1093/nar/gky379

Alfatih, A., Wu, J., Zhang, Z.-S., Xia, J.-Q., Jan, S. U., Yu, L.-H., et al. (2020). Rice NIN-LIKE PROTEIN 1 rapidly responds to nitrogen deficiency and improves yield and nitrogen use efficiency. *J. Exp. Bot.* 71, 6032–6042. doi: 10.1093/jxb/eraa292

Alvarez, J. M., Schinke, A. L., Brooks, M. D., Pasquino, A., Leonelli, L., Varala, K., et al. (2020). Transient genome-wide interactions of the master transcription factor NLP7 initiate a rapid nitrogen-response cascade. *Nat. Commun.* 11, 1157. doi: 10.1038/s41467-020-14979-6

Beeckman, F., Annetta, L., Corrochano-Monsalve, M., Beeckman, T., and Motte, H. (2024). Enhancing agroecosystem nitrogen management: microbial insights for improved nitrification inhibition. *Trends Microbiol.* 32, 590–601. doi: 10.1016/j.tim.2023.10.009

Beeckman, F., Motte, H., and Beeckman, T. (2018). Nitrification in agricultural soils: impact, actors and mitigation. *Curr. Opin. Biotechnol.* 50, 166–173. doi: 10.1016/j.copbio.2018.01.014

Bittsanszky, A., Pilinszky, K., Gyulai, G., and Komives, T. (2015). Overcoming ammonium toxicity. *Plant Sci.* 231, 184–190. doi: 10.1016/j.plantsci.2014.12.005

Bolger, A. M., Lohse, M., and Usadel, B. (2014). Trimmomatic: a flexible trimmer for Illumina sequence data. *Bioinformatics* 30, 2114–2120. doi: 10.1093/bioinformatics/btu170

Bouwman, A. F., Boumans, L. J. M., and Batjes, N. H. (2002). Emissions of N2O and NO from fertilized fields: Summary of available measurement data. *Global Biogeochemical Cycles* 16, 6–1-6-13. doi: 10.1029/2001GB001811

Britto, D. T., and Kronzucker, H. J. (2013). Ecological significance and complexity of N-source preference in plants. *Ann. Bot.* 112, 957–963. doi: 10.1093/aob/mct157

Chandran, A. K., Priatama, R. A., Kumar, V., Xuan, Y., Je, B. I., Kim, C. M., et al. (2016). Genome-wide transcriptome analysis of expression in rice seedling roots in response to supplemental nitrogen. *J. Plant Physiol.* 200, 62–75. doi: 10.1016/j.jplph.2016.06.005

Chang, K. N., Zhong, S., Weirauch, M. T., Hon, G., Pelizzola, M., Li, H., et al. (2013). Temporal transcriptional response to ethylene gas drives growth hormone cross-regulation in Arabidopsis. *Elife* 2, e0, 0675. doi: 10.7554/eLife.00675

Chen, H., Zhang, Q., Cai, H., Zhou, W., and Xu, F. (2018). H2 O2 mediates nitrate-induced iron chlorosis by regulating iron homeostasis in rice. *Plant Cell Environ.* 41, 767–781. doi: 10.1111/pce.13145

Coskun, D., Britto, D. T., Shi, W., and Kronzucker, H. J. (2017). Nitrogen transformations in modern agriculture and the role of biological nitrification inhibition. *Nat. Plants* 3, 17074. doi: 10.1038/nplants.2017.74

Crawford, N. M. (1995). Nitrate: nutrient and signal for plant growth. *Plant Cell* 7, 859–868. doi: 10.1105/tpc.7.7.859

Crombez, H., Motte, H., and Beeckman, T. (2019). Tackling plant phosphate starvation by the roots. *Dev. Cell* 48, 599–615. doi: 10.1016/j.devcel.2019.01.002

Dai, X., Wang, Y., Yang, A., and Zhang, W. H. (2012). OsMYB2P-1, an R2R3 MYB transcription factor, is involved in the regulation of phosphate-starvation responses and root architecture in rice. *Plant Physiol.* 159, 169–183. doi: 10.1104/pp.112.194217

Dolgikh, V. A., Pukhovaya, E. M., and Zemlyanskaya, E. V. (2019). Shaping ethylene response: the role of EIN3/EIL1 transcription factors. *Front. Plant Sci.* 10. doi: 10.3389/fpls.2019.01030

Esteban, R., Ariz, I., Cruz, C., and Moran, J. F. (2016). Review: Mechanisms of ammonium toxicity and the quest for tolerance. *Plant Sci.* 248, 92–101. doi: 10.1016/j.plantsci.2016.04.008

Fang, X. Z., Fang, S. Q., Ye, Z. Q., Liu, D., Zhao, K. L., and Jin, C. W. (2021). NRT1.1 dual-affinity nitrate transport/signalling and its roles in plant abiotic stress resistance. *Front. Plant Sci.* 12. doi: 10.3389/fpls.2021.715694

Food and Agriculture Organization of the United Nations [FAO]. (2017). World fertilizer trends and outlook to 2020. *Summary report*.

Fu, Y., Zhong, X., Lu, C., Liang, K., Pan, J., Hu, X., et al. (2023). Growth, nutrient uptake and transcriptome profiling of rice seedlings in response to mixed provision of ammonium- and nitrate-nitrogen. *J. Plant Physiol.* 284, 153976. doi: 10.1016/j.jplph.2023.153976

Gaudinier, A., Rodriguez-Medina, J., Zhang, L., Olson, A., Liseron-Monfils, C., Bågman, A.-M., et al. (2018). Transcriptional regulation of nitrogen-associated metabolism and growth. *Nature* 563, 259–264. doi: 10.1038/s41586-018-0656-3

Good, A. G., Shrawat, A. K., and Muench, D. G. (2004). Can less yield more? Is reducing nutrient input into the environment compatible with maintaining crop production? *Trends Plant Sci.* 9, 597–605. doi: 10.1016/j.tplants.2004.10.008

Guan, P., Ripoll, J. J., Wang, R., Vuong, L., Bailey-Steinitz, L. J., Ye, D., et al. (2017). Interacting TCP and NLP transcription factors control plant responses to nitrate availability. *Proc. Natl. Acad. Sci. U.S.A.* 114, 2419–2424. doi: 10.1073/pnas.1615676114

Hachiya, T., Inaba, J., Wakazaki, M., Sato, M., Toyooka, K., Miyagi, A., et al. (2021). Excessive ammonium assimilation by plastidic glutamine synthetase causes ammonium toxicity in Arabidopsis thaliana. *Nat. Commun.* 12, 4944. doi: 10.1038/s41467-021-25238-7

Hachiya, T., and Sakakibara, H. (2016). Interactions between nitrate and ammonium in their uptake, allocation, assimilation, and signaling in plants. *J. Exp. Botany.* 68, 2501–2512. doi: 10.1093/jxb/erw449

Hiraga, S., Sasaki, K., Hibi, T., Yoshida, H., Uchida, E., Kosugi, S., et al. (2009). Involvement of two rice ETHYLENE INSENSITIVE3-LIKE genes in wound signaling. *Mol. Genet. Genomics* 282, 517–529. doi: 10.1007/s00438-009-0483-1

Hou, X. L., WU, P., JIAO, F. C., JIA, Q. J., CHEN, H. M., YU, J., et al. (2005). Regulation of the expression of OsIPS1 and OsIPS2 in rice via systemic and local Pi signalling and hormones. *Plant Cell Environ.* 28, 353–364. doi: 10.1111/j.1365-3040.2005.01272.x

Hu, B., Jiang, Z., Wang, W., Qiu, Y., Zhang, Z., Liu, Y., et al. (2019). Nitrate-NRT1.1B-SPX4 cascade integrates nitrogen and phosphorus signalling networks in plants. *Nat. Plants* 5, 401–413. doi: 10.1038/s41477-019-0384-1

Jagadhesan, B., Sathee, L., Meena, H. S., Jha, S. K., Chinnusamy, V., Kumar, A., et al. (2020). Genome wide analysis of NLP transcription factors reveals their role in nitrogen stress tolerance of rice. *Sci. Rep.* 10, 9368. doi: 10.1038/s41598-020-66338-6

Jia, L., Xie, Y., Wang, Z., Luo, L., Zhang, C., Pélissier, P. M., et al. (2020). Rice plants respond to ammonium stress by adopting a helical root growth pattern. *Plant J.* 104, 1023–1037. doi: 10.1111/tpj.14978

Jian, S., Liao, Q., Song, H., Liu, Q., Lepo, J. E., Guan, C., et al. (2018). NRT1.1-related NH4+ Toxicity is associated with a disturbed balance between NH4+ Uptake and assimilation. *Plant Physiol.* 178, 1473–1488. doi: 10.1104/pp.18.00410

Kawahara, Y., de la Bastide, M., Hamilton, J. P., Kanamori, H., McCombie, W. R., Ouyang, S., et al. (2013). Improvement of the Oryza sativa Nipponbare reference genome using next generation sequence and optical map data. *Rice* 6, 4. doi: 10.1186/1939-8433-6-4

Kende, H. (1993). Ethylene biosynthesis. *Annu. Rev. Plant Biol.* 44, 283–307. doi: 10.1146/annurev.pp.44.060193.001435

Khan, M. I., Trivellini, A., Fatma, M., Masood, A., Francini, A., Iqbal, N., et al. (2015). Role of ethylene in responses of plants to nitrogen availability. *Front. Plant Sci.* 6. doi: 10.3389/fpls.2015.00927

Kronzucker, H. J., Britto, D. T., Davenport, R. J., and Tester, M. (2001). Ammonium toxicity and the real cost of transport. *Trends Plant Sci.* 6, 335–337. doi: 10.1016/S1360-1385(01)02022-2

Kronzucker, H. J., Siddiqi, M. Y., Glass, A. D., and Kirk, G. J. (1999). Nitrate-ammonium synergism in rice. A subcellular flux analysis. *Plant Physiol.* 119, 1041–1046. doi: 10.1104/pp.119.3.1041

Krouk, G., Mirowski, P., LeCun, Y., Shasha, D. E., and Coruzzi, G. M. (2010). Predictive network modeling of the high-resolution dynamic plant transcriptome in response to nitrate. *Genome Biol.* 11, R123. doi: 10.1186/gb-2010-11-12-r123

Langfelder, P., and Horvath, S. (2008). WGCNA: an R package for weighted correlation network analysis. *BMC Bioinf.* 9, 559. doi: 10.1186/1471-2105-9-559

Lee, H. Y., Chen, Z., Zhang, C., and Yoon, G. M. (2019). Editing of the OsACS locus alters phosphate deficiency-induced adaptive responses in rice seedlings. *J. Exp. Bot.* 70, 1927–1940. doi: 10.1093/jxb/erz074

Liao, Z., Yu, H., Duan, J., Yuan, K., Yu, C., Meng, X., et al. (2019). SLR1 inhibits MOC1 degradation to coordinate tiller number and plant height in rice. *Nat. Commun.* 10, 2738. doi: 10.1038/s41467-019-10667-2

Liu, K.-H., Liu, M., Lin, Z., Wang, Z.-F., Chen, B., Liu, C., et al. (2022). NIN-like protein 7 transcription factor is a plant nitrate sensor. *Science* 377, 1419–1425. doi: 10.1126/science.add1104

Liu, K.-h., Niu, Y., Konishi, M., Wu, Y., Du, H., Sun Chung, H., et al. (2017). Discovery of nitrate–CPK–NLP signalling in central nutrient–growth networks. *Nature* 545, 311–316. doi: 10.1038/nature22077

Liu, Y., and von Wirén, N. (2017). Ammonium as a signal for physiological and morphological responses in plants. *J. Exp. Bot.* 68, 2581–2592. doi: 10.1093/jxb/erx086

Love, M. I., Huber, W., and Anders, S. (2014). Moderated estimation of fold change and dispersion for RNA-seq data with DESeq2. *Genome Biol.* 15, 550. doi: 10.1186/s13059-014-0550-8

Maeda, Y., Konishi, M., Kiba, T., Sakuraba, Y., Sawaki, N., Kurai, T., et al. (2018). A NIGT1-centred transcriptional cascade regulates nitrate signalling and incorporates phosphorus starvation signals in Arabidopsis. *Nat. Commun.* 9, 1376. doi: 10.1038/s41467-018-03832-6

Makino, A. (2011). Photosynthesis, grain yield, and nitrogen utilization in rice and wheat. *Plant Physiol.* 155, 125–129. doi: 10.1104/pp.110.165076

Marchive, C., Roudier, F., Castaings, L., Brehaut, V., Blondet, E., Colot, V., et al. (2013). Nuclear retention of the transcription factor NLP7 orchestrates the early response to nitrate in plants. *Nat. Commun.* 4, 1713. doi: 10.1038/ncomms2650

McAllister, C. H., Beatty, P. H., and Good, A. G. (2012). Engineering nitrogen use efficient crop plants: the current status. *Plant Biotechnol. J.* 10, 1011–1025. doi: 10.1111/j.1467-7652.2012.00700.x

Meier, M., Liu, Y., Lay-Pruitt, K. S., Takahashi, H., and von Wirén, N. (2020). Auxin-mediated root branching is determined by the form of available nitrogen. *Nat. Plants* 6, 1136–1145. doi: 10.1038/s41477-020-00756-2

Miyashita, Y., Dolferus, R., Ismond, K. P., and Good, A. G. (2007). Alanine aminotransferase catalyses the breakdown of alanine after hypoxia in Arabidopsis thaliana. *Plant J.* 49, 1108–1121. doi: 10.1111/j.1365-313X.2006.03023.x

Motte, H., and Beeckman, T. (2020). A pHantastic ammonium response. *Nat. Plants* 6, 1080–1081. doi: 10.1038/s41477-020-00765-1

Muench, D. G., Christopher, M. E., and Good, A. G. (1998). Cloning and expression of a hypoxic and nitrogen inducible maize alanine aminotransferase gene. *Physiologia Plantarum* 103, 503–512. doi: 10.1034/j.1399-3054.1998.1030409.x

Obertello, M., Shrivastava, S., Katari, M. S., and Coruzzi, G. M. (2015). Cross-species network analysis uncovers conserved nitrogen-regulated network modules in rice. *Plant Physiol.* 168, 1830–1843. doi: 10.1104/pp.114.255877

Ohme-Takagi, M., and Shinshi, H. (1995). Ethylene-inducible DNA binding proteins that interact with an ethylene-responsive element. *Plant Cell* 7, 173–182. doi: 10.1105/tpc.7.2.173

Patro, R., Duggal, G., Love, M. I., Irizarry, R. A., and Kingsford, C. (2017). Salmon provides fast and bias-aware quantification of transcript expression. *Nat. Methods* 14, 417–419. doi: 10.1038/nmeth.4197

Patterson, K., Cakmak, T., Cooper, A., Lager, I., Rasmusson, A. G., and Escobar, M. A. (2010). Distinct signalling pathways and transcriptome response signatures differentiate ammonium- and nitrate-supplied plants. *Plant Cell Environ.* 33, 1486–1501. doi: 10.1111/j.1365-3040.2010.02158.x

Pélissier, P.-M., Motte, H., and Beeckman, T. (2021). Lateral root formation and nutrients: nitrogen in the spotlight. *Plant Physiol.* 187, 1104–1116. doi: 10.1093/plphys/kiab145

Pflüger, T., Gschell, M., Zhang, L., Shnitsar, V., Zabadné, A. J., Zierep, P., et al. (2024). How sensor Amt-like proteins integrate ammonium signals. *Sci. Adv.* 10, eadm9441. doi: 10.1126/sciadv.adm9441

Pflüger, T., Hernández, C. F., Lewe, P., Frank, F., Mertens, H., Svergun, D., et al. (2018). Signaling ammonium across membranes through an ammonium sensor histidine kinase. *Nat. Commun.* 9, 164. doi: 10.1038/s41467-017-02637-3

Puga, M. I., Mateos, I., Charukesi, R., Wang, Z., Franco-Zorrilla, J. M., de Lorenzo, L., et al. (2014). SPX1 is a phosphate-dependent inhibitor of Phosphate Starvation Response 1 in Arabidopsis. *Proc. Natl. Acad. Sci. U.S.A.* 111, 14947–14952. doi: 10.1073/pnas.1404654111

Raun, W. R., and Johnson, G. V. (1999). Improving nitrogen use efficiency for cereal production. *Agron. J.* 91, 357–363. doi: 10.2134/agronj1999.00021962009100030001x

Ristova, D., Carre, C., Pervent, M., Medici, A., Kim, G. J., Scalia, D., et al. (2016). Combinatorial interaction network of transcriptomic and phenotypic responses to nitrogen and hormones in the Arabidopsis thaliana root. *Sci. Signal* 9, rs13. doi: 10.1126/scisignal.aaf2768

Robertson, G. P., and Vitousek, P. M. (2009). Nitrogen in agriculture: balancing the cost of an essential resource. *Annu. Rev. Environ. Resour.* 34, 97–125. doi: 10.1146/annurev.environ.032108.105046

Ruan, W., Guo, M., Xu, L., Wang, X., Zhao, H., Wang, J., et al. (2018). An SPX-RLI1 module regulates leaf inclination in response to phosphate availability in rice. *Plant Cell* 30, 853–870. doi: 10.1105/tpc.17.00738

Rubin, G., Tohge, T., Matsuda, F., Saito, K., and Scheible, W. R. (2009). Members of the LBD family of transcription factors repress anthocyanin synthesis and affect additional nitrogen responses in Arabidopsis. *Plant Cell* 21, 3567–3584. doi: 10.1105/tpc.109.067041

Sanchez-Zabala, J., Gonzalez-Murua, C., and Marino, D. (2015). Mild ammonium stress increases chlorophyll content in Arabidopsis thaliana. *Plant Signal Behav.* 10, e991596. doi: 10.4161/15592324.2014.991596

Sasakawa, H., and Yamamoto, Y. (1978). Comparison of the uptake of nitrate and ammonium by rice seedlings: influences of light, temperature, oxygen concentration, exogenous sucrose, and metabolic inhibitors. *Plant Physiol.* 62, 665–669. doi: 10.1104/pp.62.4.665

Shannon, P., Markiel, A., Ozier, O., Baliga, N. S., Wang, J. T., Ramage, D., et al. (2003). Cytoscape: a software environment for integrated models of biomolecular interaction networks. *Genome Res.* 13, 2498–2504. doi: 10.1101/gr.1239303

Soneson, C., Love, M. I., and Robinson, M. D. (2015). Differential analyses for RNA-seq: transcript-level estimates improve gene-level inferences. *F1000Res* 4, 1521. doi: 10.12688/f1000research.7563.2

Sutton, M. A., Oenema, O., Erisman, J. W., Leip, A., van Grinsven, H., and Winiwarter, W. (2011). Too much of a good thing. *Nature* 472, 159–161. doi: 10.1038/472159a

Takasaki, H., Maruyama, K., Kidokoro, S., Ito, Y., Fujita, Y., Shinozaki, K., et al. (2010). The abiotic stress-responsive NAC-type transcription factor OsNAC5 regulates stress-inducible genes and stress tolerance in rice. *Mol. Genet. Genomics* 284, 173–183. doi: 10.1007/s00438-010-0557-0

Teng, R. M., Yang, N., Li, J. W., Liu, C. F., Chen, Y., Li, T., et al. (2022). Isolation and characterization of an LBD transcription factor csLBD39 from tea plant (Camellia sinensis) and its roles in modulating nitrate content by regulating nitrate-metabolism-related genes. *Int. J. Mol. Sci.* 23, 9294. doi: 10.3390/ijms23169294

Tian, Q. Y., Sun, P., and Zhang, W. H. (2009). Ethylene is involved in nitrate-dependent root growth and branching in Arabidopsis thaliana. *New Phytol.* 184, 918–931. doi: 10.1111/j.1469-8137.2009.03004.x

Tian, F., Yang, D.-C., Meng, Y.-Q., Jin, J., and Gao, G. (2019). PlantRegMap: charting functional regulatory maps in plants. *Nucleic Acids Res.* 48, D1104–D1113. doi: 10.1093/nar/gkz1020

Ueda, Y., Ohtsuki, N., Kadota, K., Tezuka, A., Nagano, A. J., Kadowaki, T., et al. (2020). Gene regulatory network and its constituent transcription factors that control nitrogen-deficiency responses in rice. *New Phytol.* 227, 1434–1452. doi: 10.1111/nph.16627

Ueda, Y., and Yanagisawa, S. (2018). "Transcription factor-based genetic engineering to increase nitrogen use efficiency," in *Engineering nitrogen utilization in crop plants*. Eds. A. Shrawat, A. Zayed and D. A. Lightfoot (Springer International Publishing, Cham), 37–55.

Van Bel, M., Diels, T., Vancaester, E., Kreft, L., Botzki, A., Van de Peer, Y., et al. (2018). PLAZA 4.0: an integrative resource for functional, evolutionary and comparative plant genomics. *Nucleic Acids Res.* 46, D1190–D1196. doi: 10.1093/nar/gkx1002

Vanlerberghe, G. C., Joy, K. W., and Turpin, D. H. (1991). Anaerobic metabolism in the N-limited green alga selenastrum minutum: III. Alanine is the product of anaerobic ammonium assimilation. *Plant Physiol.* 95, 655–658. doi: 10.1104/pp.95.2.655

Varala, K., Marshall-Colon, A., Cirrone, J., Brooks, M. D., Pasquino, A. V., Leran, S., et al. (2018). Temporal transcriptional logic of dynamic regulatory networks underlying nitrogen signaling and use in plants. *Proc. Natl. Acad. Sci. U.S.A.* 115, 6494–6499. doi: 10.1073/pnas.1721487115

Wang, M., Hasegawa, T., Beier, M., Hayashi, M., Ohmori, Y., Yano, K., et al. (2021). Growth and nitrate reductase activity are impaired in rice osnlp4 mutants supplied with nitrate. *Plant Cell Physiol.* 62, 1156–1167. doi: 10.1093/pcp/pcab035

Wang, C., Huang, W., Ying, Y., Li, S., Secco, D., Tyerman, S., et al. (2012). Functional characterization of the rice SPX-MFS family reveals a key role of OsSPX-MFS1 in controlling phosphate homeostasis in leaves. *New Phytol.* 196, 139–148. doi: 10.1111/j.1469-8137.2012.04227.x

Wang, Z., Ruan, W., Shi, J., Zhang, L., Xiang, D., Yang, C., et al. (2014). Rice SPX1 and SPX2 inhibit phosphate starvation responses through interacting with PHR2 in a phosphate-dependent manner. *Proc. Natl. Acad. Sci. U.S.A.* 111, 14953–14958. doi: 10.1073/pnas.1404680111

Wang, R., Tischner, R., Gutiérrez, R. A., Hoffman, M., Xing, X., Chen, M., et al. (2004). Genomic analysis of the nitrate response using a nitrate reductase-null mutant of arabidopsis. *Plant Physiol.* 136, 2512–2522. doi: 10.1104/pp.104.044610

Wang, R., Xing, X., Wang, Y., Tran, A., and Crawford, N. M. (2009b). A genetic screen for nitrate regulatory mutants captures the nitrate transporter gene NRT1.1. *Plant Physiol.* 151, 472–478. doi: 10.1104/pp.109.140434

Wang, C., Ying, S., Huang, H., Li, K., Wu, P., and Shou, H. (2009a). Involvement of OsSPX1 in phosphate homeostasis in rice. *Plant J.* 57, 895–904. doi: 10.1111/j.1365-313X.2008.03734.x

Wild, R., Gerasimaite, R., Jung, J. Y., Truffault, V., Pavlovic, I., Schmidt, A., et al. (2016). Control of eukaryotic phosphate homeostasis by inositol polyphosphate sensor domains. *Science* 352, 986–990. doi: 10.1126/science.aad9858

Wu, X., Liu, T., Zhang, Y., Duan, F., Neuhäuser, B., Ludewig, U., et al. (2019). Ammonium and nitrate regulate NH4+ uptake activity of Arabidopsis ammonium transporter AtAMT1;3 via phosphorylation at multiple C-terminal sites. *J. Exp. Bot.* 70, 4919–4930. doi: 10.1093/jxb/erz230

Wu, P., and Wang, Z. (2011). Molecular mechanisms regulating Pi-signaling and Pi homeostasis under OsPHR2, a central Pi-signaling regulator, in rice. *Front. Biol.* 6, 242–245. doi: 10.1007/s11515-011-1050-9

Wu, J., Zhang, Z. S., Xia, J. Q., Alfatih, A., Song, Y., Huang, Y. J., et al. (2021). Rice Nin-Like Protein 4 plays a pivotal role in nitrogen use efficiency. *Plant Biotechnol. J.* 19, 448–461. doi: 10.1111/pbi.13475

Xie, Y., Lv, Y., Jia, L., Zheng, L., Li, Y., Zhu, M., et al. (2023). Plastid-localized amino acid metabolism coordinates rice ammonium tolerance and nitrogen use efficiency. *Nat. Plants* 9, 1514–1529. doi: 10.1038/s41477-023-01494-x

Xuan, W., Beeckman, T., and Xu, G. (2017). Plant nitrogen nutrition: sensing and signaling. *Curr. Opin. Plant Biol.* 39, 57–65. doi: 10.1016/j.pbi.2017.05.010

Yan, Y., Zhang, Z., Sun, H., Liu, X., Xie, J., Qiu, Y., et al. (2023). Nitrate confers rice adaptation to high ammonium by suppressing its uptake but promoting its assimilation. *Mol. Plant* 16, 1871–1874. doi: 10.1016/j.molp.2023.11.008

Yang, H. C., Kan, C. C., Hung, T. H., Hsieh, P. H., Wang, S. Y., Hsieh, W. Y., et al. (2017). Identification of early ammonium nitrate-responsive genes in rice roots. *Sci. Rep.* 7, 16885. doi: 10.1038/s41598-017-17173-9

Yang, C., Lu, X., Ma, B., Chen, S. Y., and Zhang, J. S. (2015a). Ethylene signaling in rice and Arabidopsis: conserved and diverged aspects. *Mol. Plant* 8, 495–505. doi: 10.1016/j.molp.2015.01.003

Yang, C., Ma, B., He, S.-J., Xiong, Q., Duan, K.-X., Yin, C.-C., et al. (2015b). Maohuzi6/ethylene insensitive3-like1 and ethylene insensitive3-like2 regulate ethylene response of roots and coleoptiles and negatively affect salt tolerance in rice. *Plant Physiol.* 169, 148–165. doi: 10.1104/pp.15.00353

Yoo, S. D., Cho, Y. H., and Sheen, J. (2007). Arabidopsis mesophyll protoplasts: a versatile cell system for transient gene expression analysis. *Nat. Protoc.* 2, 1565–1572. doi: 10.1038/nprot.2007.199

Zhang, Z., Li, Z., Wang, W., Jiang, Z., Guo, L., Wang, X., et al. (2021). Modulation of nitrate-induced phosphate response by the MYB transcription factor RLI1/HINGE1 in the nucleus. *Mol. Plant* 14, 517–529. doi: 10.1016/j.molp.2020.12.005

Zhang, H., Li, Y., Yao, X., Liang, G., and Yu, D. (2017). Positive regulator of iron homeostasis1, ospri1, facilitates iron homeostasis. *Plant Physiol.* 175, 543–554. doi: 10.1104/pp.17.00794

Zhang, Y., Su, J., Duan, S., Ao, Y., Dai, J., Liu, J., et al. (2011). A highly efficient rice green tissue protoplast system for transient gene expression and studying light/chloroplast-related processes. *Plant Methods* 7, 30. doi: 10.1186/1746-4811-7-30

Zhang, G. B., Yi, H. Y., and Gong, J. M. (2014). The Arabidopsis ethylene/jasmonic acid-NRT signaling module coordinates nitrate reallocation and the trade-off between growth and environmental adaptation. *Plant Cell* 26, 3984–3998. doi: 10.1105/tpc.114.129296

Zheng, D., Han, X., An, Y. I., Guo, H., Xia, X., and Yin, W. (2013). The nitrate transporter NRT2.1 functions in the ethylene response to nitrate deficiency in Arabidopsis. *Plant Cell Environ.* 36, 1328–1337. doi: 10.1111/pce.12062

Zheng, L., Huang, F., Narsai, R., Wu, J., Giraud, E., He, F., et al. (2009). Physiological and transcriptome analysis of iron and phosphorus interaction in rice seedlings. *Plant Physiol.* 151, 262–274. doi: 10.1104/pp.109.141051

Zhou, J., Jiao, F., Wu, Z., Li, Y., Wang, X., He, X., et al. (2008). OsPHR2 is involved in phosphate-starvation signaling and excessive phosphate accumulation in shoots of plants. *Plant Physiol.* 146, 1673–1686. doi: 10.1104/pp.107.111443

frontiers | Frontiers in Plant Science

TYPE Original Research
PUBLISHED 26 August 2024
DOI 10.3389/fpls.2024.1386234

OPEN ACCESS

EDITED BY
Néstor Fernández Del-Saz,
University of the Balearic Islands, Spain

REVIEWED BY
Sangeeta Paul,
Indian Agricultural Research Institute (ICAR), India
Daniel J. Ballhorn,
Portland State University, United States

*CORRESPONDENCE
Marcia González-Teuber
mgonzat@uc.cl
Luisa Bascuñán-Godoy
lubascun@gmail.com

RECEIVED 14 February 2024
ACCEPTED 31 July 2024
PUBLISHED 26 August 2024

CITATION
Alquichire-Rojas S, Escobar E, Bascuñán-Godoy L and González-Teuber M (2024) Root symbiotic fungi improve nitrogen transfer and morpho-physiological performance in *Chenopodium quinoa*. *Front. Plant Sci.* 15:1386234. doi: 10.3389/fpls.2024.1386234

Root symbiotic fungi improve nitrogen transfer and morpho-physiological performance in *Chenopodium quinoa*

Shirley Alquichire-Rojas[1], Elizabeth Escobar[2], Luisa Bascuñán-Godoy[2*] and Marcia González-Teuber[3*]

[1]Facultad de Ciencias, Universidad Católica de la Santísima Concepción, Concepción, Chile, [2]Departamento de Botánica, Facultad de Ciencias Naturales y Oceanográficas, Universidad de Concepción, Concepción, Chile, [3]Facultad de Ciencias Biológicas, Pontificia Universidad Católica de Chile, Santiago, Chile

Root-associated fungal endophytes may facilitate nitrogen (N) absorption in plants, leading to benefits in photosynthesis and growth. Here, we investigated whether endophytic insect pathogenic fungi (EIPF) are capable of transferring soil N to the crop species *Chenopodium quinoa*. We evaluated nutrient uptake, carbon allocation, and morpho-physiological performance in *C. quinoa* in symbiosis with two different EIPF (*Beauveria* and *Metarhizium*) under contrasting soil N supply. A controlled experiment was conducted using two plant groups: (1) plants subjected to low N level (5 mM urea) and (2) plants subjected to high N level (15 mM urea). Plants from each group were then inoculated with different EIPF strains, either *Beauveria* (EIPF1+), *Metarhizium* (EIPF2+) or without fungus (EIPF-). Differences in N and C content, amino acids, proteins, soluble sugars, starch, glutamine synthetase, glutamate dehydrogenase, and physiological (photosynthesis, stomatal conductance, transpiration), and morphological performance between plant groups under each treatment were examined. We found that both *Beauveria* and *Metarhizium* translocated N from the soil to the roots of *C. quinoa*, with positive effects on photosynthesis and plant growth. These effects, however, were differentially affected by fungal strain as well as by N level. Additionally, an improvement in root C and sugar content was observed in presence of EIPF, suggesting translocation of carbohydrates from leaves to roots. Whereas both strains were equally effective in N transfer to roots, *Beauveria* seemed to exert less demand in *C. quinoa* for photosynthesis-derived carbohydrates compared to *Metarhizium*. Our study revealed positive effects of EIPF on N transfer and morpho-physiological performance in crops, highlighting the potential of these fungi as an alternative to chemical fertilizers in agriculture systems.

KEYWORDS

entomopathogenic fungi, nitrogen transfer, photosynthesis, carbon allocation, plant growth, symbiosis, quinoa

1 Introduction

Nitrogen (N) is among the most limiting nutrients for plant growth (Stewart et al., 2005). N has a principal role in the synthesis of nucleic acids, amino acids, and proteins, and is a major contributor to photosynthetic proteins and pigments in plants (Miller and Cramer, 2005; Svennerstam et al., 2008; Guo et al., 2020; Muratore et al., 2021; Llebrés et al., 2022). N is taken up by roots and transformed into organic molecules in both roots and leaves by different enzymes, including glutamate dehydrogenase and glutamine synthetase, which incorporate NH_4^+ into amino acids (de la Peña et al., 2019). About 60% of N in plants is stored in forms such as Rubisco, which is the limiting enzyme in the carbon fixation process. In order to overcome N limitation, plants establish symbiotic relationships with a range of microorganisms, such as rhizobial bacteria and soil fungi, including mycorrhiza and endophytic fungi (Udvardi and Poole, 2013; Bücking and Kafle, 2015; Wang et al., 2017). Besides nitrogen fixing bacteria such as rhizobia, which are responsible for nodulation and N_2-fixation, fungi may play an important role in N transfer from the soil to roots. Thus, root-associated microorganisms facilitate the absorption of N, which may lead to increased photosynthetic efficiency and enhanced plant growth and productivity (Chen et al., 2020; Das et al., 2022).

Root-colonizing fungi, including arbuscular mycorrhiza, ectomycorrhizal as well as endophytic fungi, form symbiosis with lateral roots of plants and create an extraradical mycelium (ERM), which penetrates the intercellular spaces between the cortical root cells, forming the intraradical mycelium (IRM) (Smith and Read, 2008). According to current knowledge, NO_3- and NH_4+ are the primary N sources taken up by fungi. N is converted into arginine in the ERM, which is the main form in which N is transported from the ERM to the IRM. Once in the IRM, arginine is metabolized into ammonium and subsequently released to the symbiotic interface, where it is acquired and assimilated by plants (Behie and Bidochka, 2014a; Wang et al., 2017; Rui et al., 2022). While the mechanisms of N transport are relatively well known for mycorrhiza fungi, the ability of fungal endophytes to transfer N to the roots is a relatively recent finding. Since fungal endophytes are ubiquitous in soils and able to colonize a wide range of plants (from monocots to dicots) (Behie and Bidochka, 2014b), their N transfer capabilities may potentially be applied in agricultural systems as a means to increase productivity in crop species.

Numerous fungal endophyte strains increase nitrogen uptake efficiency in plants (Usuki and Narisawa, 2007; Behie and Bidochka, 2014b; González-Teuber et al., 2019). For example, the dark septate endophyte *Heterconium chaetospira* is able to transfer N obtained from decomposed soil organic material to the roots of *Brassica campestris* (Usuki and Narisawa, 2007). Additionally, endophytic, insect pathogenic fungi (EIPF) such as the genera *Metarhizium* and *Beauveria*, which colonize plant roots, have been shown to translocate soil nitrogen to different host plants (Behie et al., 2012; Behie and Bidochka, 2014a, b). *Beauveria* and *Metarhizium* infect soil-borne insects and have the ability to establish associations with host roots and transfer insect-derived nitrogen, which has been found to increase plant performance on the whole (Behie et al., 2012; Behie and Bidochka, 2014a; González-Pérez et al., 2022). Behie et al. (2012) demonstrated that, in association with *Metarhizium*, haricot bean and switchgrass derive approximately 30% of their N content from soil insects. Interestingly, similarly to mycorrhiza, N transfer to plant roots in this process occurs in exchange for photosynthetically fixed carbon (Kiers et al., 2011; Wang et al., 2017; Balestrini et al., 2020). In a labeling study using CO_2 isotopes, Behie et al. (2015) showed ($^{13}CO_2$) that atmospheric CO_2 was incorporated into plant carbohydrates, and subsequently translocated to *Metarhizium*-specific carbohydrates. This nutrient exchange of both partners appears necessary to maintain the plant-fungus symbiosis; nevertheless, how this exchange varies depending on the soil N level has been little explored (Barelli et al., 2019).

Chenopodium quinoa is a pseudo-cereal crop of the Chenopodiaceae family native to the Andean region of South America. Quinoa is an important crop species due to its high protein content and its resilience to stressful conditions (Bascuñán-Godoy et al., 2016; Lutz and Bascuñán-Godoy, 2017). Previous studies have shown that *C. quinoa* is able to establish symbiotic associations with numerous root endophytic fungi (González-Teuber et al., 2017), which benefit quinoa by improving plant morphological and physiological responses to abiotic stresses such as drought and salinity (González-Teuber et al., 2018; 2022). The role, however, of EIPF on the morpho-physiological performance of *C. quinoa* has not been addressed. Since EIPF genera *Beauveria* and *Metarhizium* are ubiquitous soil fungi able to transfer N from soil into roots (Behie et al., 2012), they have the potential to be applied in crop species as a means to increase their productivity. Here, we explored the question of whether EIPF are able to transfer N to *C. quinoa* from the soil without the need to infect insects. To do this, we evaluated nutrient uptake, carbon allocation, and morpho-physiological performance in *C. quinoa* in symbiosis with two different EIPF (*Beauveria* and *Metarhizium*) under contrasting soil N supply. We also discuss potential plant-fungus nutrient exchanges linked to soil N level.

2 Materials and methods

2.1 Study system

The Quinoa lowland genotype UdeC9 (latitude 35.73° S; longitude 72.53° W) was used for this study because it is highly susceptible to low nitrogen availability (Bascuñán-Godoy et al., 2018). UdeC9 seeds were provided by the National Seed Bank collection at Vicuña, Chile (INIA-Intihuasi). EIPF *Beauveria* were obtained from soils under vine crops in Viña Casanueva (Maule), Chile (36° 42′ 36′′ S; 72° 20′ 59′′ W) and *Metarhizium* in Viña Santa Rita (Alto Jahuel), Chile (33° 43′ 12′′ S; 70° 40′ 12′′ W). Specimens were isolated from soil samples using the *Tenebrio molitor* larval baiting technique (Meyling, 2007). One strain each of *Beauveria bassiana* and *Metarhizium* were selected for inoculation experiments. Identified morphologically, *Beauveria*

showed hyaline and subglobose conidia, whereas *Metarhizium* showed cylindrical conidia with olive-green coloration, which is characteristic of the species (Aguilera-Sammaritano et al., 2021; Wang et al., 2020a). Both fungal genera were only identified through microscopical analysis. Nevertheless, DNA amplification with specific primers designed for both *Beauveria* and *Metarhizium* genera (see below) helped us to validate our original taxonomical identification. Both EIPF were grown in potato dextrose agar (PDA) for 15 days at 25°C. Fungal spores were then collected by repeatedly flooding the agar plates with sterile distilled water plus Tween 80 (0.01% v/v) and rubbing the surface with a sterile scraper. The samples were transferred to sterile bottles for storage. The spore concentration was adjusted to 1×10^7 spores mL^{-1} by counting spores using a Neubauer chamber cell counting (HBG), and then used to inoculate the substrate directly by drenching.

2.2 Experimental design

The experiment was performed in a completed randomized design with a total of six treatments each containing 27–30 experimental units. The plants were divided into two groups: the first was fertilized with a single dose of a low-level N-urea solution (5 mM) while the second was fertilized with a high-level N-urea solution (15 mM). Both doses have previously been determined in *C. quinoa* through biomass curves under the supply of different amounts of N (Bascuñán-Godoy et al., 2018; Pinto-Irish et al., 2020; Jerez et al., 2023). After 15 days of vegetative growth, plants from each N level treatment were separated into three groups: (1) non-inoculated plants (EIPF-), (2) plants inoculated with *Beauveria* (EIPF1+), and (3) plants inoculated with *Metarhizium* (EIPF2+).

2.3 Plant growth conditions

Chenopodium quinoa seeds were surface-sterilized in 0.5% sodium hypochlorite for 3 minutes, triple-rinsed in sterile distilled water and then germinated on sterilized paper in petri dishes over a period of 24 hours in darkness before being sown on sterilized sand. Germinated seeds were transplanted individually in 0.52 L pots with sterile coarse sand that had previously been autoclaved at 120°C for 40 minutes. Plants were supplied once on planting day with MS solution nutrient medium, described by Murashige and Skoog (1962), consisting of 0.30 mM $MgSO_4.7H_2O$, 0.22 mM $CaCl_2$, 0.62 mM KH_2PO_4, 12.7 mM KCl, 0.05 µM KI, 1.00 µM H_3BO_3, 1.32 µM $MnSO_4.4H_2O$, 0.30 µM $ZnSO_4.7H_2$ O, 0.01 µM $Na_2MoO_4.2H_2O$, 0.001 µM $CuSO_4.5H_2O$, 0.001 µM $CoCl_2.6H_2O$, 0.51 µM Na_2-EDTA, 0.50 µM $FeSO_4.7H_2O$. N-urea varied according to treatment. pH was set at 5.8. All plants in all treatments were then watered with additional distilled water as required. To avoid effects of microclimatic variations due to pot position, plants were randomly rearranged once a week. Plants were grown in a chamber at 20–25°C with a light/dark cycle of 12 h:12 h at a relative humidity of ~70% for 33 days. The photosynthetically active photon flux density (PPFD) ranged from 700 to 800 µmol m^{-2} s^{-1}. After 15 days of vegetative growth, plants were watered with 30 mL spore solution of either *Beauveria* or *Metarhizium*. Non-inoculated plants at each N level were irrigated with sterile spore-free water. Morphological and physiological traits were measured after 15 days of applied treatments, including above- and below-ground biomass, photosynthesis, stomatal conductance, and transpiration. Additionally, leaf and root material from remaining plants were collected, and immediately frozen in liquid nitrogen and stored at -80°C for further measurements of biochemical parameters. Root frozen material was also used for DNA extraction and further fungal DNA amplification.

2.4 Carbon and nitrogen measurements

Carbon and nitrogen content was determined in leaves and roots (1 mg) by dry combustion with a Perkin Elmer Elemental Analyzer (EA 2400 Series II CHNS/O Analyzer) and expressed as the % of element in dried leaf and root material.

2.5 Amino acid and protein measurements

Amino acid concentration in above-ground biomass was determined by HPLC-DAD for each treatment. 100 mg of leaf material was homogenized and used for amino acid extraction as described in González-Teuber et al. (2023). Protein concentration in leaves and roots was measured using Bradford's reagent (Bradford, 1976), with bovine serum albumin used as a standard.

2.6 Carbohydrate measurements

100 mg of leaf and root material was homogenized and extracted with methanol/chloroform/water (12:5:3 v/v/v). Supernatant was used for analysis of total soluble sugars (TSS) and remaining residues were kept at -20°C for starch determination. TSS were determined using 2% phenol and sulfuric acid (Dickson, 1979; Chow and Landhäusser, 2004). Starch was hydrolyzed to glucose using a sodium acetate buffer and amyloglucosidase (Sigma-Aldrich 10115, St. Louis, MO, USA) at 45°C and measured with a phenol-sulfuric acid reaction (Marquis et al., 1997). Both TSS and starch concentrations were determined spectrophotometrically at 490 nm with an Infinite 200 PRO (Tecan) using sucrose and glucose, respectively, as standards. Non-structural carbohydrates (NSC) were calculated by adding TSS and starch concentrations.

2.7 Measurements of Glutamine Synthetase (GS) and Glutamate Dehydrogenase (GDH) activities

To explore mechanisms of nitrogen assimilation in leaves, GS and GDH have been measured. Both are key enzymes in plant nitrogen metabolism, responding adaptively to low nitrogen availability in diverse crop species, including *C quinoa* (Bascuñán-Godoy et al., 2018). The primary pathway is constituted by GS enzyme, and

alternate pathway followed by GDH enzyme (Miflin and Habash, 2002; Song et al., 2022). GS activity (EC 6.3.1.2) was measured by the formation of γ-glutamyl hydroxamate using the transferase assay (Lea et al., 1990). 100 mg of fresh Quinoa leaves were ground into a powder in an ice-chilled mortar with liquid N_2 and suspended in a 500 µL of homogenization buffer (100 mM Tris-HCl buffer, pH 7.8, containing 3.3 mM $MgCl_2$, 10 mM β-mercaptoethanol, 1 mM dithiothreitol, 15% v/v ethylene glycol). The mixture for the GS essay contained 500 µL of reaction buffer (80 mM glutamic acid, 20 mm $MgSO_4$, 8 mM ATP, 6 mM hydroxyamide, 1 mM ethylenediaminetetraacetic acid, 0.1 mM Tricine, pH 7.8). The reaction was initiated by the addition of 200 µL of enzyme extract, incubated at 30°C per 15 min, and then terminated by the addition of 700 µL of ferric chloride reagent (0.67 mM $FeCl_3$, 0.37 M HCl and 20% v/v trichloroacetic acid). Finally, the optical density of the supernatant was determined spectrophotometrically at 540 nm.

Glutamate dehydrogenase (GDH) activity (EC 1.4.1.4) was determined according to the procedure outlined by Kumar et al. (2000). Leaf enzyme extract was used for the determination of GDH. The mixture for the GDH-NADH assay contained 1400 µL of reaction buffer (100 mM Tris-HCl, 20 mM ketoglutarate, 150 mM $(NH_4)_2SO_4$, 0.2 mM NADH and 1 mM $MgCl_2$) or GDH-NAD^+ essay contains 1400 µL of reaction buffer (100 mM Tris-HCl, 50 mM L-glutamate, 0.6 mM NAD^+). The reaction was initiated by the addition of 100 µL of enzyme extract and absorbance determined spectrophotometrically at 340 nm. GDH activity was expressed as one unit of enzyme activity in terms of the amount of enzyme required to oxidize or reduce 1 nmol of NADH or NAD^+ min^{-1} mg^{-1} protein.

2.8 Plant photosynthetic and morphological parameters

Gas exchange measurements of net photosynthesis (A_N) (µmol CO_2 m^{-2} s^{-1}), stomatal conductance (g_s) (nmol H_2O m^{-2} s^{-1}), and transpiration (T) (mmol H_2O m^{-2} s^{-1}) were performed for fully expanded leaves (third leaf from the top) using a portable open gas exchange system (CIRAS-2, PP Systems Amesbury, MA, USA). A_N, g_s, and T rates were measured at mid-morning (between 9 a.m. and 2 p.m.) after gas exchange had stabilized. Conditions in the leaf chamber were as follows: temperature at 25°C, 50% relative humidity, CO_2 concentration 400 mol mol^{-1} and 1,000 µmol photon m^{-2} s^{-1}. Leaves were first equilibrated for at least 5 min in 400 µmol mol^{-1} of external CO_2 in a leaf cuvette. At the end of the experiment, half of the plants of each treatment were divided into above- (shoots) and below-ground (roots) tissues for weighing. Roots were first washed with tap water, and then roots and shoots were oven-dried separately at 60°C for 72 h. Fresh and dry weights of each were derived pre and post drying, respectively.

2.9 Fungal DNA amplification in roots

Beauveria and *Metarhizium* DNA was extracted from fresh mycelium pure culture and roots of three plants (50 - 200 mg of fresh tissue) using NucleoSpin® Plant II MACHEREY-NAGEL Kit according to the manufacturer's protocol. The extracted DNA was stored at -20°C for subsequent detection and specific primer amplification analyses. Primer for *Beauveria* spp. and *Metarhizium* spp. detections are listed in Supplementary Material Table S1. qPCR analysis was performed on an Agilent Mx3000P QPCR system (Agilent Technologies, USA) using Brilliant II SYBR Green qPCR Master Mix (Agilent Technologies, USA). Each qPCR reaction contained 7.5 of II SYBR Green qPCR Master Mix (Agilent Technologies, USA), 5 µl of gDNA, and 10 ng/µl of each primer in a final volume of 15 µL. The thermocycling program was set as: *Beauveria* spp., 95°C for 10 min, followed by 40 cycles of 95°C for 30 s, 54°C for 30s, 72°C for 40 s, and *Metarhizium* spp., 95°C for 10 min, followed by 40 cycles of 90°C for 15 s, 60°C for 15 s, and 72°C for 25 s. qPCR amplification were performed in triplicate for each template dilution. The threshold line and the sample specific threshold cycle numbers (C_T) were determined with the default parameters of the software Agilent Aria Real-Time PCR system (Agilent Technologies, USA). Standard quantification curves consisted of the C_T diluted values plotted against the logarithm of the number of gDNA amount that were calculated for each standard quantification curve from *Beauveria* spp. or *Metarhizium* spp. pure culture between 2.5 to 2,500 pg and relate C_T values according to Smith and Osborn (2009). The validation analysis was performed with three independent biological replicates. The specificity of each primer pair was verified by determining the melting curves at the end of each run. The quality of primers product was confirmed by gel electrophoresis (Supplementary Figure S1).

2.10 Statistical analysis

Before any statistical analysis, the data were transformed as necessary to achieve normality and homogeneity of residuals. Considering the high dispersion in the data, outliers were discarded using the criteria of the Rosner (Rosner, 1975) and Dixon tests (Barnett and Lewis, 1995). A two-way analysis of variance (ANOVA) was conducted to assess the effects of the presence/absence of EIPF and N level on morphological, physiological, and biochemical responses in *C. quinoa*. A *post hoc* Fisher's LSD test was performed to analyze differences among treatments. All analyses were conducted in R Studio (R Core Team, 2024).

3 Results

3.1 Effects of N level and EIPF on N content, proteins and amino acids

While foliar N content was significantly affected by N level, but not by EIPF (Table 1; Figure 1A), root N content was significantly affected by both N level and EIPF (Table 1). At both N levels root N content was significantly higher in EIPF-treated plants than in EIPF- plants (Figure 1B). For proteins, both foliar and root protein concentrations were significantly affected by N level as well as by EIPF inoculation (Table 1). For foliar proteins, under both N levels no positive effects of EIPF were observed relative to EIPF- plants

10.3389/fpls.2024.1386234

TABLE 1 Two-way ANOVA of the effects of nitrogen (N) level and EIPF inoculation on physiological and morphological traits in *Chenopodium quinoa*.

	F-value			
	N	EIPF	N × EIPF	Replicates
Foliar N (mg N per plant)	**1012.70** **	1.12 NS	0.89 NS	8–9
Root N (mg N per plant)	**382.61** **	**8.88** **	0.12 NS	6–8
Foliar proteins (mg proteins g^{-1} dry weight)	**223.12** **	**4.50** **	1.56 NS	7–8
Root proteins (mg proteins g^{-1} dry weight)	**16.63** **	**15.71** **	0.02 NS	5–6
Foliar C (mg C per plant)	**723.39** **	**6.67** **	2.43 NS	8–9
Root C (mg C per plant)	**154.61** **	**4.02** *	0.56 NS	6–8
Foliar NSC (mg g^{-1} dry weight)	0.96 NS	**7.49** **	1.24 NS	5–9
Root NSC (mg g^{-1} dry weight)	**21.62** **	0.35 NS	**3.95** **	5–10
GS (nmol Glu min^{-1} mg^{-1} proteins)	**5.81** *	**8.49** **	**7.37** **	4–6
GDH-NADH (nmol NADH min^{-1} mg^{-1} proteins)	**13.55** **	2.02 NS	0.13 NS	4
GDH-NAD^+ (nmol NAD^+ min^{-1} mg^{-1} proteins)	**23.02** **	0.28 NS	0.06 NS	4
Net photosynthesis (μmol CO_2 m^{-2} s^{-1})	**49.02** **	**5.59** **	2.49 NS	4–6
Stomatal conductance (nmol H_2O m^{-2} s^{-1})	**11.36** **	**17.73** **	1.48 NS	4–6
Transpiration (mmol H_2O m^{-2} s^{-1})	**7.38** *	**18.57** **	2.24 NS	4–6
Above-ground biomass (g dry weight)	**508.23** **	**9.43** **	1.51 NS	11–15
Below-ground biomass (g dry weight)	**184.37** **	2.34 NS	0.23 NS	11–15
Total biomass (g dry weight)	**449.65** ***	**6.48** **	1.06 NS	11–15

Nitrogen (N) level - LN, low nitrogen: 5 mM and HN, high nitrogen: 15 mM. EIPF-, non-inoculated plants; EIPF1+, inoculated with *Beauveria*; EIPF2+, inoculated with *Metarhizium*). F values are shown; * indicates significance at the 0.05 level, ** indicates significance at the 0.01 level, whereas *** indicates significance at the 0.001 level. NS indicates no significant difference. Bold values denote statistical significance at the $p < 0.05$ level.

(Figure 1C). In contrast, root proteins under both N levels were considerably higher in EIPF-inoculated plants (an increase higher than 30% for both EIPF1+ and EIPF2+ plant groups) compared to EIPF- plants (Figure 1D). Foliar total and single amino acid concentrations were significantly affected by N level; nevertheless, no significant effects of EIPF were observed on them (Supplementary Table S2). Not surprisingly, amino acids increased under high N levels compared to low N conditions (Supplementary Table S2).

3.2 Effects of N and EIPF on carbon content and carbohydrates

Both foliar and root C content were significantly affected by N level and EIPF inoculation (Table 1). Foliar C content was only improved under low N levels by EIPF1+; at high N levels no effects by EIPF were observed on this trait (Figure 2A). For root C content, positive effects of both EIPF were only observed under low N levels; no effects were evident under high N conditions (Figure 2B). Whereas leaf NSC was significantly affected by EIPF1+ under both N levels, no effects of EIPF2+ was observed on this trait regardless of N level (Figure 2C). Contrary, root NSC was only significantly affected by EIPF2+ under low N levels; no effects of EIPF were evident under high N levels (Figure 2D). Effects of N level and EIPF on TSS and starch concentration are shown in Table 2. Under low N levels no significant differences in foliar TSS were observed among EIPF+ and EIPF- plants; nevertheless, under high N levels only EIPF1+ positively affected foliar TSS in plants (Table 2). For root TSS, under low N levels, there was a tendency that both EIPF improved this trait in *C. quinoa* plants relative to EIPF-; nevertheless, significant differences were observed only for EIPF2+. In contrast, under high N levels no significant differences in root TSS were observed between EIPF- and EIPF+ plants (Table 2). For foliar starch, under low N levels, no significant differences were observed between EIPF- and EIPF+ plants; nevertheless, under low N levels foliar starch was considerably improved by EIPF1+ colonization (Table 2). For root starch, no significant effects by EIPF were observed neither under low nor under high N levels (Table 2).

3.3 Effects of N level and EIPF on enzyme activities

There was a significant effect of N level and EIPF inoculation on GS activity (Table 1). Under low N levels no differences were observed in GS activity inoculated and non-inoculated plants (Figure 3A). In contrast, under high N levels GS activity was considerably improved by EIPF1+ and EIPF2+ inoculation (Figure 3A). For GDH-NADH and GDH-NAD^+ activities only a significant effect of N level was observed (Table 1). Both activities were higher under low N levels than under high N levels (Figures 3B, C). Nevertheless, for both enzymes no differences were detected between inoculated and non-inoculated plants regardless of N level (Figures 3B, C).

3.4 Effects of N level and EIPF on photosynthetic traits

Net photosynthesis (A_N), stomatal conductance (g_s), and transpiration were significantly affected by N level and EIPFs

10.3389/fpls.2024.1386234

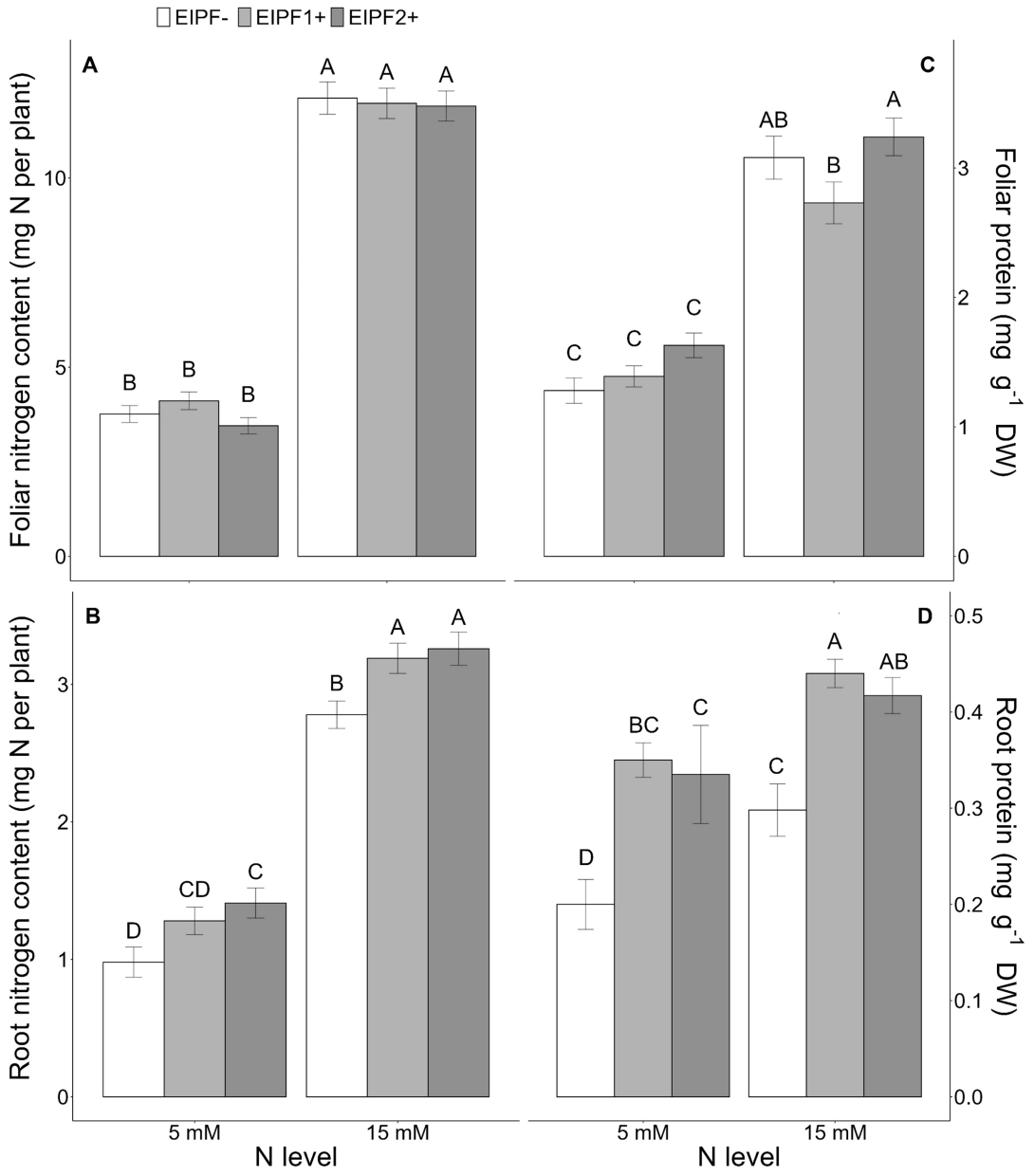

FIGURE 1
Effects of nitrogen (N) level and EIPF inoculation on foliar and root N and protein contents in *C. quinoa*. **(A)** foliar N content (n = 8-9), **(B)** root N content (n = 6-8), **(C)** foliar protein content (n = 7-8), and **(D)** root protein content (n = 5-6). Error bar labels with different letters indicate significant differences ($P < 0.05$) among treatments. 5 mM, low nitrogen level; 15 mM, high nitrogen level; EIPF-, non-inoculated plants; EIPF1+, inoculated with *Beauveria*; EIPF2+, inoculated with *Metarhizium*.

(Table 1). Photosynthesis, but neither stomatal conductance nor transpiration, increased significantly at high N level. At low N levels, photosynthesis increased 127% and 75% by EIPF1+ and EIPF2+, respectively, relative to EIPF- (Figure 4A). No changes in photosynthesis were observed in response to EIPF inoculation at high N levels (Figure 4A). For stomatal conductance and transpiration, at low N levels only EIPF1+ triggered an increase in both traits. At high N levels both EIPF1+ and EIPF2+ increased stomatal conductance and transpiration (Figures 4B, C).

3.5 Effects of N levels and EIPF on plant growth

Above-ground and total biomass were significantly affected by N level and EIPF, whereas below-ground biomass was only affected by N level (Table 1). Plants under low N levels displayed 50% lower above-ground, below-ground and total biomass relative to high N level plants (Figures 5A–C). EIPF1+ significantly increased above-ground and total biomass at both N levels (Figures 5A, C).

10.3389/fpls.2024.1386234

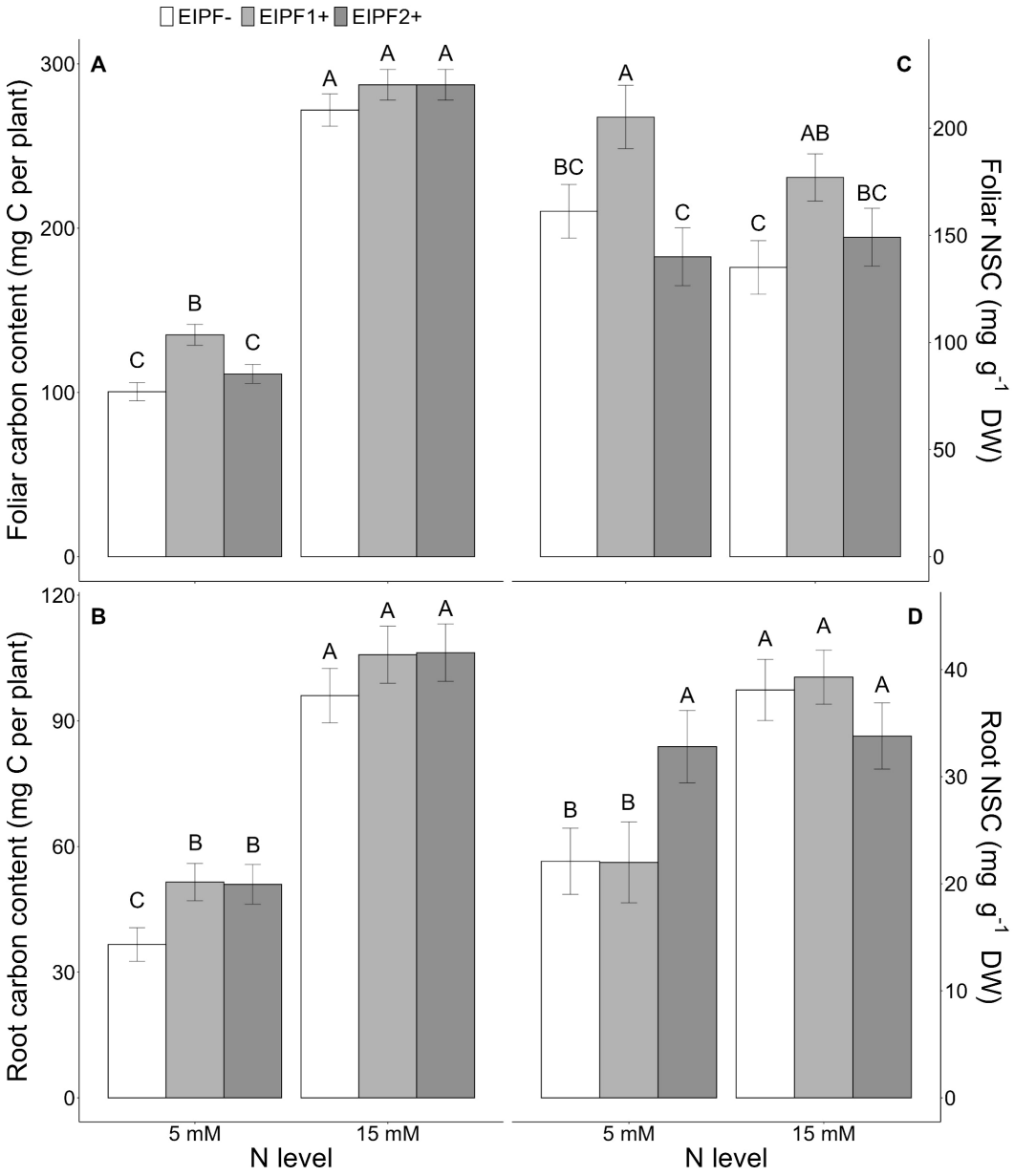

FIGURE 2
Effects of nitrogen (N) level and EIPF inoculation on foliar and root C and non-structural carbon (NSC) contents in *C. quinoa*. **(A)** foliar carbon content (n = 8-9), **(B)** root carbon content (n = 6-8), **(C)** foliar NSC content (n = 5-9), and **(D)** root NSC content (n = 5-10). Error bar labels with different letters indicate significant differences (P < 0.05) among treatments. 5 mM, low nitrogen level; 15 mM, high nitrogen level; EIPF-, non-inoculated plants; EIPF1+, inoculated with *Beauveria*; EIPF2+, inoculated with *Metarhizium*.

In contrast, EIPF2+ did not affect any biomass trait regardless of N level (Figure 5A).

3.6 Fungal DNA amplification in roots

Primers designed for each fungus were specific, generating only one PCR product whose size was consistent with the observed weight (465 kb for *Beauveria* and 337 kb for *Metarhizium*) (Supplementary Figure S1). Based on qPCR analysis, presence of *Beauveria* and *Metarhizium* DNA in roots was confirmed in all inoculated plants, except for uninoculated plants (EIPF-) (Supplementary Figure S2A). Fungal DNA obtained from *Beauveria* roots (EIPF1+) tended to be higher than in control roots at both N levels (LN, control vs *Beauveria*: F = 6.09, P = 0.069; HN, control vs *Beauveria*: F = 6.22, P = 0.061). Similarly, fungal DNA from *Metarhizium* roots (EIPF2+) was significantly higher than in control roots at both N levels (LN, control vs *Metarhizium*: F = 79.86, P = < 0.0001; HN, control vs *Beauveria*: F = 25.71, P = 0.007) (Supplementary Figure S2B).

4 Discussion

We showed that EIPF strains *Beauveria* and *Metarhizium* isolated from southern Chilean vineyards were able to translocate

10.3389/fpls.2024.1386234

TABLE 2 Effects of nitrogen (N) level and EIPF inoculation on foliar and root total soluble sugars and starch in *Chenopodium quinoa*.

	EIPF-		EIPF1+		EIPF2+		F-*value*		
	LN	HN	LN	HN	LN	HN	N	EIPF	N × EIPF
Foliar TSS (mg g^{-1} DW)	6.2 ± (0.40) CD	7.18 ± (0.46) BC	5.85 ± (0.49) CD	9.46 ± (0.47) A	5.8 ± (0.45) D	7.98 ± (0.53) B	**35.89** **	2.64 NS	**3.49** *
Root TSS (mg g^{-1} DW)	6.7 ± (0.70) C	11.0 ± (0.65) A	8.47 ± (0.77) BC	10.5 ± (0.54) A	9.51 ± (0.70) AB	10.3 ± (0.65) AB	**19.45** **	0.89 NS	**3.46** *
Foliar starch (mg g^{-1} DW)	167 ± (11) AB	134 ± (10.1) C	177 ± (12) A	170 ± (8.21) A	139 ± (11) BC	138 ± (10.1) BC	1.64 NS	**6.14** **	1.31 NS
Root starch (mg g^{-1} DW)	17.8 ± (2.91) BC	28.9 ± (2.44) A	12.5 ± (3.45) C	26.6 ± (2.72) A	24.2 ± (2.91) AB	23.8 ± (3.15) AB	**11.95** **	0.97 NS	**3.33** *

Total soluble sugars (TSS) (n = 5–9); starch (n = 5–10). Data represent means ± (standard error). Different letters represent significant differences between N levels (LN, low nitrogen: 5 mM and HN, high nitrogen: 15 mM) and EIPF (without inoculation EIPF-; with *Beauveria*, EIPF1+; with *Metarhizium*, EIPF2+). F values are shown; * indicates significance at the 0.05 level, ** indicates significance at the 0.01 level, whereas *** indicates significance at the 0.001 level. NS indicates no significant difference. Bold values denote statistical significance at the $p < 0.05$ level.

N from soil to roots of *C. quinoa*, with positive effects on N and C storage, photosynthesis, and plant growth. Our results are consistent with previous studies demonstrating that EIPF are able to transfer insect-derived N from soils to plants (Behie et al., 2012; Behie and Bidochka, 2014a, b; Barelli et al., 2019). Here, we showed evidence that this translocation phenomenon is also possible in the absence of soil insects.

Enhanced root N and protein content, triggered by EIPF, was observed in *C. quinoa* at both low and high N levels. Barelli et al. (2019) showed that insect-derived N transfer by the strain *Metarhizium robertsii* to *Phaseolus vulgaris* was only evident under nutrient-poor soil conditions (i.e., low carbon and nitrogen content), suggesting that nutrient supply from the host plant to the fungus is essential for maintaining the symbiosis. A similar situation occurs in plant-mycorrhizal interactions (González-González et al., 2020; Wang et al., 2020b). For example, Fellbaum et al. (2012) showed that C flux from the root to the fungus triggers the uptake and transport of N in symbiosis. Moreover, N transport is stimulated only when C is delivered by the host across the mycorrhizal interface, not when C is supplied directly to the fungal extraradical mycelium (Fellbaum et al., 2012). In our system, an improvement in root C as well as carbohydrate content was observed in the presence of EIPF, which suggests greater leaf to root translocation. This was particularly evident at low N levels, suggesting nutrient exchange between *C. quinoa* and both *Beauveria* and *Metarhizium*. Mechanisms involved in plant to fungus and fungus to plant C and N translocation have yet to be investigated for EIPF. Regarding N metabolism, our results indicate that GS and GDH increase at high foliar N levels, but not at low N levels. The foliar N recycling level is likely not high enough to induce an activation of the enzyme related with amination at LN. In contrast to that observed in roots, no differences in foliar N content between EIPF- and EIPF+ plants were observed. We cannot rule out the possibility that enhanced root N content in inoculated plants was likely incorporated into roots in other forms, such amino acids or other organic molecules. The latter is consistent with our observations of improved root protein content (Yang et al., 2020; Guo et al., 2021). In symbiosis, the role of root enzymes and N and sugar transporters are key in the exchange of these nutrients (Doidy et al., 2012; Fellbaum et al., 2012; Sun et al., 2020). Still little is known about plant carbohydrates obtained by EIPF and how they are transported into the fungus, however (Fang and St. Leger, 2010; Barelli et al., 2019). Further research is needed to understand plant-EIPF chemical communication during the establishment of the symbiosis.

Improved N transfer triggered by fungi usually relates to improved plant growth in either above- or below-ground biomass (Zhou et al., 2018; Barelli et al., 2019). This phenomenon seems to be context dependent, however, and may rely on a range of factors, such as soil nutrient availability. For example, growth benefits promoted by *Beauveria bassiana* in maize plants were only evident under high soil nutrient availability (NPK fertilizer) (Tall and Meyling, 2018). In contrast, Zhou et al. (2018) found that low N-fertilizer application promoted growth in rice and *Arabidopsis*, triggered by the fungal endophyte *Phomopsis liquidambaris*. Here, we showed that benefits on plant growth were only evident in presence of EIPF1+ (*Beauveria* strain) regardless the N level. Contrary, EIPF2+ (*Metarhizium* strain) showed positive effects in terms of photosynthesis under low N levels; nevertheless, these effects were not reflected in better plant growth. Enhanced plant biomass triggered by EIPF1+ was, however, not related to improved N transfer from below-ground to above-ground biomass, suggesting that other mechanisms are likely involved. Stomatal conductance was positively affected by EIPF, particularly by *Beauveria*, which has been associated with increases in photosynthesis and plant growth in *C. quinoa* (Bascuñán-Godoy et al., 2018). Additionally, *Beauveria* strain used in this study is able to synthesize phytohormones *in vitro*, including auxin and gibberellin (unpublished data), which may relate to plant growth promotion (Bader et al., 2020; García-Latorre et al., 2023).

In general, *Beauveria* was more beneficial in terms of plant morpho-physiological performance than *Metarhizium*. While both fungal strains improved root N transfer, benefits in terms of foliar non-structural carbohydrates (NSC) and above-ground biomass were only evident in the presence of *Beauveria*. In contrast, greater accumulation of NSC and starch was observed in below-ground biomass in the presence of *Metarhizium*. These findings suggest that symbiosis with *Metarhizium* enhanced leaf to root C allocation in *C. quinoa*, which relates to the fact that *Metarhizium* root colonization (fungal DNA abundance) was considerably higher than *Beauveria* colonization under low N levels. Thus, *Metarhizium* plants effectively trade photosynthates for nitrogen, which is

10.3389/fpls.2024.1386234

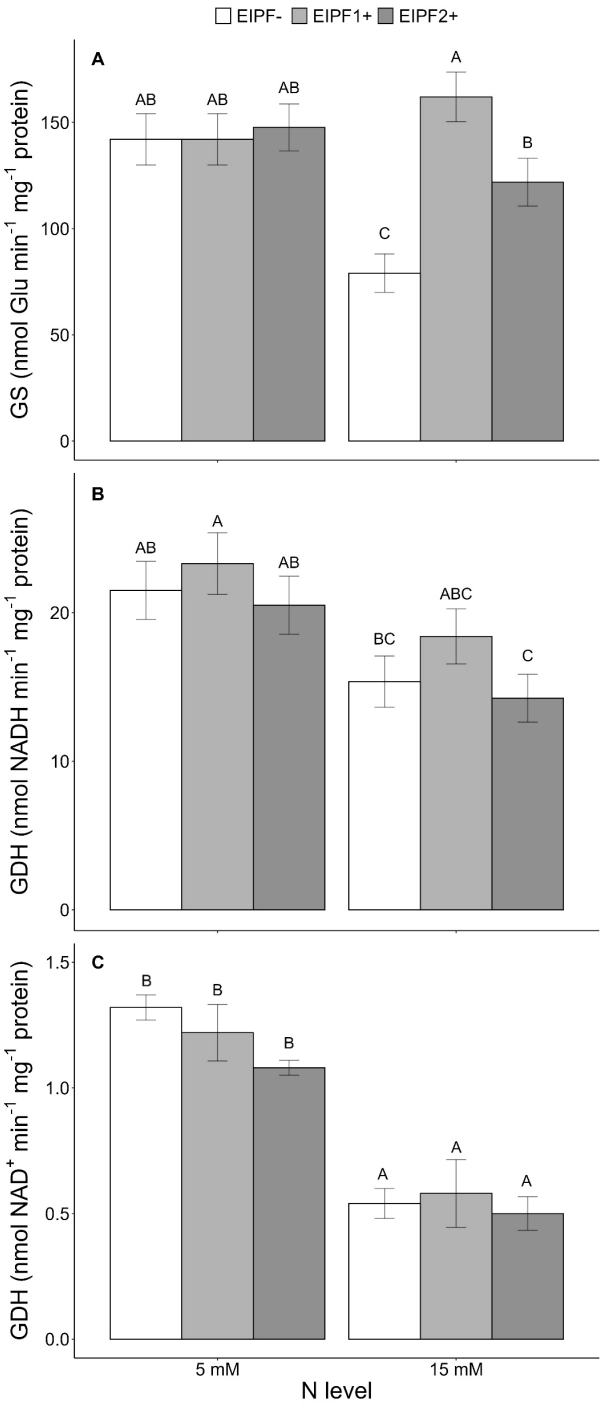

FIGURE 3
Effects of nitrogen (N) level and EIPF inoculation on foliar enzyme activities in *C. quinoa*. **(A)** glutamine synthetase (GS) (n = 4-6), **(B)** glutamate dehydrogenase (GDH-NADH) (n = 4), and **(C)** glutamate dehydrogenase (GDH-NAD+) (n = 4). Error bar labels with different letters indicate significant differences (P < 0.05) among treatments. 5 mM, low nitrogen level; 15 mM, high nitrogen level; EIPF-, non-inoculated plants; EIPF1+, inoculated with *Beauveria*; EIPF2+, inoculated with *Metarhizium*.

translocated to the roots, possibly for maintenance and functioning of the symbiosis. In our system, *Beauveria* is likely a better partner for *C. quinoa* than *Metarhizium*. Both strains seem to be equally effective in transferring N to roots, but *Beauveria* triggered lower C allocation to roots, exerting less demand for photosynthetically derived carbohydrates relative to *Metarhizium*. Importantly, *Beauveria*, even at low root colonization, established more beneficial interactions with *C. quinoa* in terms of photosynthetic parameters and plant growth. How the plant senses and differentially rewards different EIPF partners is still unknown. Recent studies indicate that plants under stress conditions have evolved a 'crying-for-help' strategy, which would enable them to

10.3389/fpls.2024.1386234

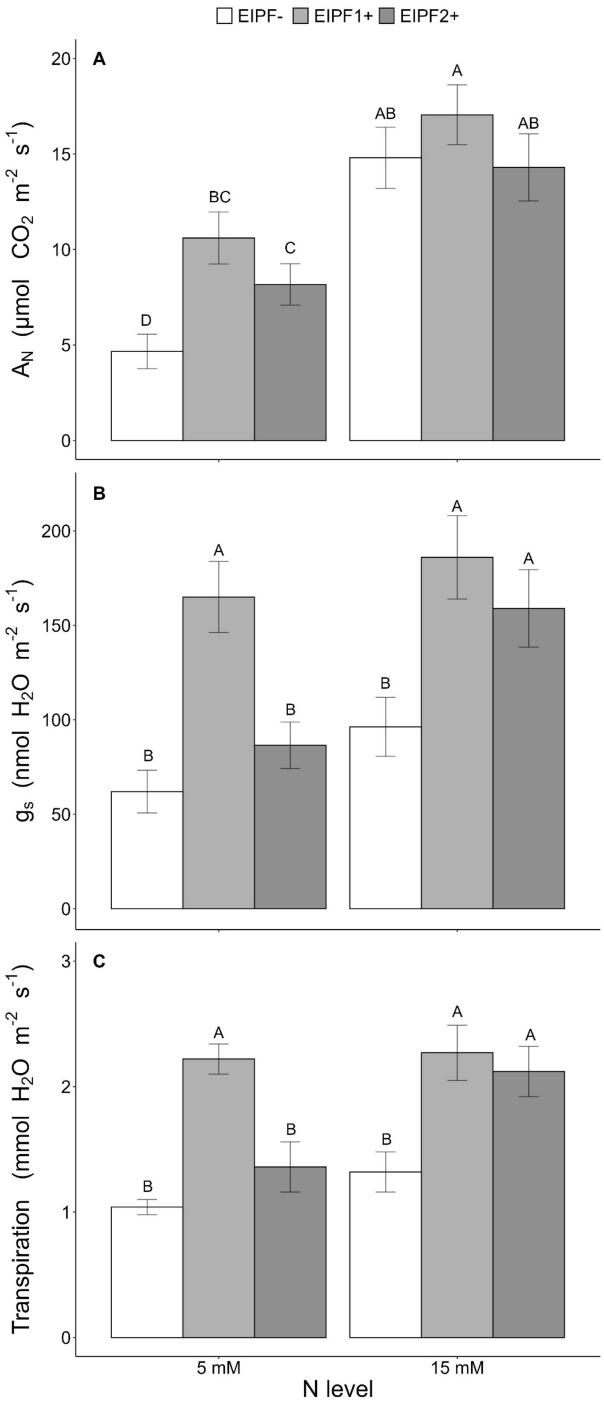

FIGURE 4
Effects of nitrogen (N) level and EIPF inoculation on photosynthetic parameters in *C. quinoa* **(A)** net photosynthetic rate (µmol CO2 m^{-2} s^{-1}) (n = 4-6), **(B)** stomatal conductance rate (mmol H2O m-2 s-1) (n = 4-6), and **(C)** transpiration (mmol H2O m-2 s-1) (n = 4-6). Error bar labels with different letters indicate significant differences (P < 0.05) among treatments. 5 mM, low nitrogen level; 15 mM, high nitrogen level; EIPF-, non-inoculated plants; EIPF1+, inoculated with Beauveria; EIPF2+, inoculated with Metarhizium.

recruit beneficial microbial partners mediated by changes in the root exudate composition (Rizaludin et al., 2021). The outcome of the interaction, however, is difficult to generalize; it often relies on diverse factors such as abiotic factors, host plant physiology, infection intensity and genotypes of both host plant and fungal strain (González-Teuber et al., 2021).

Our study showed that symbiotic associations between *C. quinoa* and *Metarhizium* and *Beauveria* help plants to improve N transfer, even in absence of insects, with positive effects on N and C storage, photosynthesis, and plant growth. Moreover, N availability seems to be key in regulating these benefits. A better understanding of the biochemical mechanisms and underlying molecular basis is

10.3389/fpls.2024.1386234

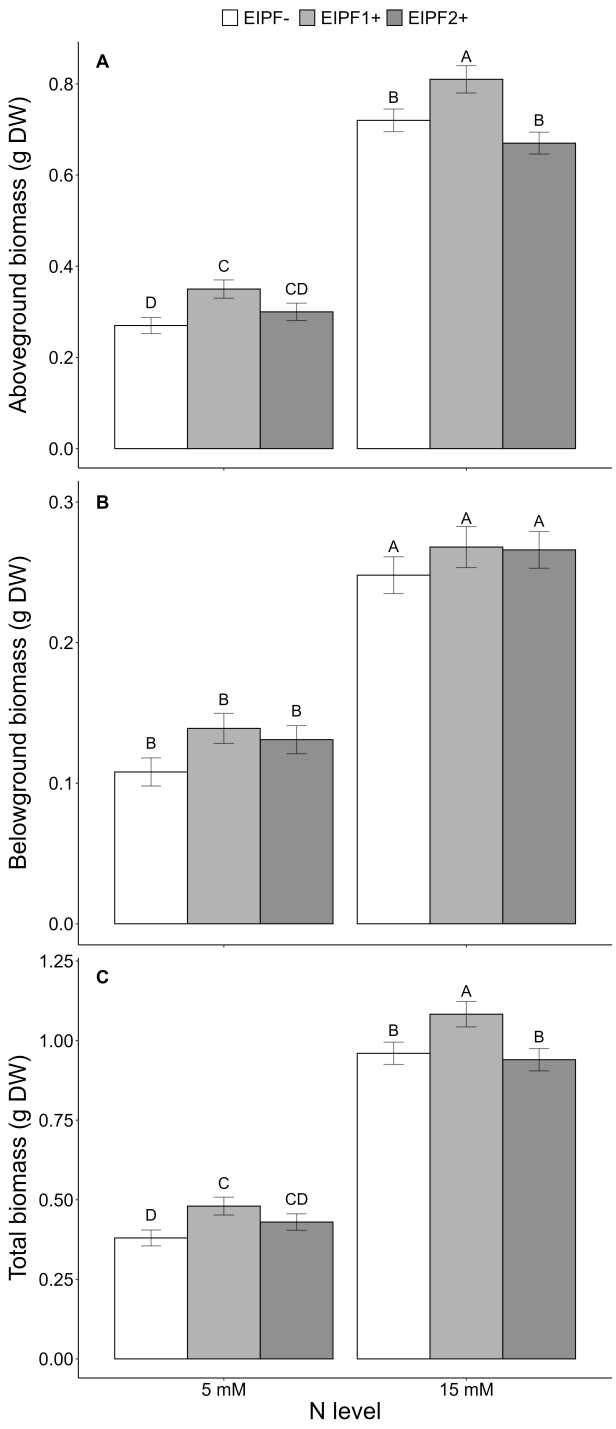

FIGURE 5
Effects of nitrogen (N) level and EIPF on plant growth (g dry weight) in *C. quinoa*. **(A)** above-ground biomass (n = 11-15), **(B)** below-ground biomass (n = 11-15), **(C)** total biomass (n = 11-15). Error bar labels with different letters indicate significant differences (P < 0.05) among treatments. 5 mM, low nitrogen level; 15 mM, high nitrogen level; EIPF-, non-inoculated plants; EIPF1+, inoculated with *Beauveria*; EIPF2+, inoculated with *Metarhizium*.

required to explain how plant and fungal partners regulate nutrient exchange in this system. Since *Beauveria* and *Metarhizium* are ubiquitous in soil ecosystems (Behie and Bidochka, 2014b) and establish associations with a wide range of plants, these EIPF have the potential to provide a sustainable alternative to chemical fertilizers in agricultural systems. Since multiple microbial symbionts may act in tandem to increase host benefits (González-Teuber et al., 2022), future research should consider testing simultaneous effects of both EIPF *Beauveria* and *Metarhizium* on plant growth promotion and nutrient exchange.

Data availability statement

The raw data supporting the conclusions of this article will be made available by the authors, without undue reservation.

Author contributions

SA-R: Writing – original draft, Formal analysis. EE: Formal analysis, Writing – original draft. LB-G: Writing – review & editing, Funding acquisition. MG-T: Writing – review & editing, Funding acquisition.

Funding

The author(s) declare that financial support was received for the research, authorship, and/or publication of this article. This work was supported by grants ANID Fondecyt Regular N° 1230282 (MG-T) and ANID Fondecyt Regular N° 1211473 (LB-G).

Acknowledgments

We are grateful to José Ortiz and Teodoro Coba for their valuable help in the lab. SA-R is grateful to PhD-ANID grant N° 21210677.

Conflict of interest

The authors declare that the research was conducted in the absence of any commercial or financial relationships that could be construed as a potential conflict of interest.

Publisher's note

Supplementary material

The Supplementary Material for this article can be found online at: https://www.frontiersin.org/articles/10.3389/fpls.2024.1386234/full#supplementary-material

References

Aguilera-Sammaritano, J., Caballero, J., Deymié, M., Rosa, M., Vazquez, F., Pappano, D., et al. (2021). Dual effects of entomopathogenic fungi on control of the pest *Lobesia botrana* and the pathogenic fungus *Eutypella microtheca* on grapevine. *Biol. Res.* 54, 44. doi: 10.1186/s40659–021–00367–x

Bader, A. N., Salerno, G. L., Covacevich, F., and Consolo, V. F. (2020). Native *Trichoderma harzianum* strains from Argentina produce indole-3 acetic acid and phosphorus solubilization, promote growth and control wilt disease on tomato (*Solanum lycopersicum* L.). *J. King Saud. Univ. Sci.* 32, 867–873. doi: 10.1016/j.jksus.2019.04.002

Balestrini, R., Brunetti, C., Chitarra, W., and Nerva, L. (2020). Photosynthetic traits and nitrogen uptake in crops: which is the role of arbuscular mycorrhizal fungi? *Plants* 9, 1105. doi: 10.3390/plants9091105

Barelli, L., Behie, S. W., and Bidochka, M. J. (2019). Availability of carbon and nitrogen in soil affects *Metarhizium robertsii* root colonization and transfer of insect-derived nitrogen. *FEMS Microbiol. Ecol.* 95, fiz144. doi: 10.1093/femsec/fiz144

Barnett, V., and Lewis, T. (1995). *Outliers in Statistical Data. Third Edition* (Chichester, UK: John Wiley and Sons), 235–236.

Bascuñán-Godoy, L., Reguera, M., Abdel-Tawab, Y. M., and Blumwald, E. (2016). Water deficit stress-induced changes in carbon and nitrogen partitioning in *Chenopodium quinoa* Willd. *Planta* 243, 591–603. doi: 10.1007/s00425-015-2424-z

Bascuñán-Godoy, L., Sanhueza, C., Pinto, K., Cifuentes, L., Reguera, M., Briones, V., et al. (2018). Nitrogen physiology of contrasting genotypes of *Chenopodium quinoa* Willd. (*Amaranthaceae*). *Sci. Rep.* 8, 17524. doi: 10.1038/s41598-018-34656-5

Behie, S. W., and Bidochka, M. J. (2014a). Nutrient transfer in plant–fungal symbioses. *Trends Plant Sci.* 19, 734–740. doi: 10.1016/j.tplants.2014.06.007

Behie, S. W., and Bidochka, M. J. (2014b). Ubiquity of insect-derived nitrogen transfer to plants by endophytic insect-pathogenic fungi: an additional branch of the soil nitrogen cycle. *Appl. Environ. Microbiol.* 80, 1553–1560. doi: 10.1128/AEM.03338-13

Behie, S. W., Jones, S. J., and Bidochka, M. J. (2015). Plant tissue localization of the endophytic insect pathogenic fungi *Metarhizium* and *Beauveria*. *Fungal Ecol.* 13, 112–119. doi: 10.1016/j.funeco.2014.08.001

Behie, S. W., Zelisko, P. M., and Bidochka, M. (2012). Endophytic insect-parasitic fungi translocate nitrogen directly from insects to plants. *Science* 336, 1576–1577. doi: 10.1126/science.1222289

Bradford, M. M. (1976). A rapid and sensitive method for the quantitation of microgram quantities of protein utilizing the principle of protein-dye binding. *Anal. Biochem.* 72, 248–254. doi: 10.1016/0003-2697(76)90527-3

Bücking, H., and Kafle, A. (2015). Role of arbuscular mycorrhizal fungi in the nitrogen uptake of plants: current knowledge and research gaps. *Agron. J.* 5, 587–612. doi: 10.3390/agronomy5040587

Chen, Z., Jin, Y., Yao, X., Chen, T., Wei, X., Li, C., et al. (2020). Fungal endophyte improves survival of *Lolium perenne* in low fertility soils by increasing root growth, metabolic activity and absorption of nutrients. *Plant Soil* 452, 185–206. doi: 10.1007/s11104-020-04556-7

Chow, P. S., and Landhäusser, S. M. (2004). A method for routine measurements of total sugar and starch content in woody plant tissues. *Tree Physiol.* 24, 1129–1136. doi: 10.1093/treephys/24.10.1129

Das, P. P., Singh, K. R., Nagpure, G., Mansoori, A., Singh, R. P., Ghazi, I. A., et al. (2022). Plant-soil-microbes: A tripartite interaction for nutrient acquisition and better plant growth for sustainable agricultural practices. *Environ. Res.* 214, 113821. doi: 10.1016/j.envres.2022.113821

de la Peña, M., González-Moro, M. B., and Marino, D. (2019). Providing carbon skeletons to sustain amide synthesis in roots underlines the suitability of *Brachypodium distachyon* for the study of ammonium stress in cereals. *AoB Plants* 11, plz029. doi: 10.1093/aobpla/plz029

Dickson, R. E. (1979). Analytical procedures for the sequential extraction of ^{14}C-labeled constituents from leaves, bark and wood of cottonwood plants. *Physiol. Plant* 45, 480–488. doi: 10.1111/j.1399-3054.1979.tb02618.x

Doidy, J., Grace, E., Kühn, C., Simon-Plas, F., Casieri, L., and Wipf, D. (2012). Sugar transporters in plants and in their interactions with fungi. *Trends Plant Sci.* 17, 413–422. doi: 10.1016/j.tplants.2012.03.009

Fang, W., and St. Leger, R. J. (2010). Mrt, a gene unique to fungi, encodes an oligosaccharide transporter and facilitates rhizosphere competency in *Metarhizium robertsii*. *Plant Physiol.* 154, 1549–1557. doi: 10.1104/pp.110.163014

Fellbaum, C. R., Gachomo, E. W., Beesetty, Y., Choudhari, S., Strahan, G. D., Pfeffer, P. E., et al. (2012). Carbon availability triggers fungal nitrogen uptake and transport in arbuscular mycorrhizal symbiosis. *Proc. Natl. Acad. Sci.* 109, 2666–2671. doi: 10.1073/pnas.1118650109

García-Latorre, C., Rodrigo, S., Marin-Felix, Y., Stadler, M., and Santamaria, O. (2023). Plant-growth promoting activity of three fungal endophytes isolated from plants living in dehesas and their effect on *Lolium multiflorum*. *Sci. Rep.* 13, 7354. doi: 10.1038/s41598-023-34036-8

González-González, M. F., Ocampo-Alvarez, H., Santacruz-Ruvalcaba, F., Sánchez-Hernández, C. V., Casarrubias-Castillo, K., Becerril-Espinosa, A., et al. (2020). Physiological, ecological, and biochemical implications in tomato plants of two plant

biostimulants: arbuscular mycorrhizal fungi and seaweed extract. *Front. Plant Sci.* 11. doi: 10.3389/fpls.2020.00999

González-Pérez, E., Ortega-Amaro, M. A., Bautista, E., Delgado-Sánchez, P., and Jiménez-Bremont, J. F. (2022). The entomopathogenic fungus *Metarhizium anisopliae* enhances *Arabidopsis*, tomato, and maize plant growth. *Plant Physiol. Biochem.* 176, 34–43. doi: 10.1016/j.plaphy.2022.02.008

González-Teuber, M., Palma-Onetto, O., Aguilera-Sammaritano, J., and Mithöfer, A. (2021). Roles of leaf functional traits in fungal endophyte colonization: potential implications for host–pathogen interactions. *J. Ecol.* 109, 3972–3987. doi: 10.1111/1365-2745.13678

González-Teuber, M., Contreras, R. A., Zúñiga, G. E., Barrera, D., and Bascuñán-Godoy, L. (2022). Synergistic association with root endophytic fungi improves morpho-physiological and biochemical responses of *Chenopodium quinoa* to salt stress. *Front. Ecol. Evol.* 9. doi: 10.3389/fevo.2021.787318

González-Teuber, M., Palma-Onetto, V., Aguirre, C., Ibáñez, A. J., and Mithöfer, A. (2023). Climate change-related warming-induced shifts in leaf chemical traits favor nutrition of the specialist herbivore *Battus polydamas archidamas*. Front. *Ecol. Evol.* 11. doi: 10.3389/fevo.2023.1152489

González-Teuber, M., Urzúa, A., Morales, A., Ibáñez, C., and Bascuñán-Godoy, L. (2019). Benefits of a root fungal endophyte on physiological processes and growth of the vulnerable legume tree *Prosopis Chilensis* (Fabaceae). *J. Plant Ecol.* 12, 264–271. doi: 10.1093/jpe/rty019

González-Teuber, M., Urzúa, A., Plaza, P., and Bascuñán-Godoy, L. (2018). Effects of root endophytic fungi on response of *Chenopodium quinoa* to drought stress. *Plant Ecol.* 219, 231–240. doi: 10.1007/s11258-017-0791-1

González-Teuber, M., Vilo, C., and Bascuñán-Godoy, L. (2017). Molecular characterization of endophytic fungi associated with the roots of *Chenopodium quinoa* inhabiting the Atacama Desert, Chile. *Genomics Data* 11, 109–112. doi: 10.1016/j.gdata.2016.12.015

Guo, N., Hu, J., Yan, M., Qu, H., Luo, L., Tegeder, M., et al. (2020). *Oryza sativa* Lysine-Histidine-type Transporter 1 functions in root uptake and root-to-shoot allocation of amino acids in rice. *Plant J.* 103, 395–411. doi: 10.1111/tpj.14742

Guo, N., Zhang, S., Gu, M., and Xu, G. (2021). Function, transport, and regulation of amino acids: What is missing in rice? *Crop J.* 3, 530–542. doi: 10.1016/j.cj.2021.04.002

Jerez, M. P., Ortiz, J., Castro, C., Escobar, E., Sanhueza, C., Del-Saz, N. F., et al. (2023). Nitrogen sources differentially affect respiration, growth, and carbon allocation in Andean and Lowland ecotypes of *Chenopodium quinoa* Willd. *Front. Plant Sci.* 14. doi: 10.3389/fpls.2023.1070472

Kiers, E. T., Duhamel, M., Beesetty, Y., Mensah, J. A., Franken, O., and Verbruggen, E. (2011). Reciprocal rewards stabilize cooperation in the mycorrhizal symbiosis. *Science*. 333 (6044), 880–882. doi: 10.1126/science.1208473

Kumar, R. G., Shah, K., and Dubey, R. S. (2000). Salinity induced behavioural changes in malate dehydrogenase and glutamate dehydrogenase activities in rice seedlings of differing salt tolerance. *Plant Sci.* 156, 23–34. doi: 10.1016/S0168-9452(00)00224-7

Lea, P. J., Blackwell, R., Chen, F., and Hecht, U. (1990). "Enzymes of primary metabolism," in *Methods in Plant Biochemistry* (Academic Press, London San Diego).

Llebrés, M. T., Castro-Rodríguez, V., Pascual, M. B., Avila, C., and Cánovas, F. M. (2022). The amino acid permease PpAAP1 mediates arginine transport in maritime pines. *Tree Physiol.* 42 (1), 175–188. doi: 10.1093/treephys/tpab089

Lutz, M., and Bascuñán-Godoy, L. (2017). "The revival of quinoa: a crop for health," in *Superfood and Functional Food - An Overview Of Their Processing And Utilization* (InTech), 37–54.

Marquis, R. J., Newell, E. A., and Villegas, A. C. (1997). Non-structural carbohydrate accumulation and use in an understorey rain-forest shrub and relevance for the impact of leaf herbivory. *Funct. Ecol.* 11, 636–643. doi: 10.1046/j.1365-2435.1997.00139.x

Meyling, N. V. (2007). *Methods For Isolation Of Entomopathogenic Fungi From The Soil Environment - Laboratory Manual. January 2007* (Department of Ecology, Faculty of Life Sciences, University of Copenhagen). Available online at: https://www.orgprints.org/id/eprint/11200/ (Accessed 24 January).

Miflin, B. J., and Habash, D. Z. (2002). The role of glutamine synthetase and glutamate dehydrogenase in nitrogen assimilation and possibilities for improvement in the nitrogen utilization of crops. *J. Exp. Bot.* 53, 979–987. doi: 10.1093/jexbot/53.370.979

Miller, A. J., and Cramer, M. D. (2005). Root nitrogen acquisition and assimilation. *Plant Soil* 274, 1–36. doi: 10.1007/s11104-004-0965-1

Murashige, T., and Skoog, F. (1962). A revised medium for rapid growth and bioassays with tobacco tissue cultures. *Physiol. Plant* 15, 473–497. doi: 10.1111/j.1399-3054.1962.tb08052.x

Muratore, C., Espen, L., and Prinsi, B. (2021). Nitrogen uptake in plants: the plasma membrane root transport systems from a physiological and proteomic perspective. *Plants*. 10 (4), 681. doi: 10.3390/plants10040681

Pinto-Irish, K., Coba de la Peña, T., Ostria-Gallardo, E., Ibáñez, C., Briones, V., Vergara, A., et al. (2020). Seed characterization and early nitrogen metabolism performance of seedlings from Altiplano and coastal ecotypes of Quinoa. *BMC Plant Biol.* 20, 343. doi: 10.1186/s12870-020-02542-w

R Core Team (2024). *_R: A Language and Environment for Statistical Computing_* (Vienna, Austria: R Foundation for Statistical Computing). Available at: https://www.R-project.org.

Rizaludin, M. S., Stopnisek, N., Raaijmakers, J. M., and Garbeva, P. (2021). The chemistry of stress: understanding the 'Cry for Help' of plant roots. *Metabolites* 11, 357. doi: 10.3390/metabo11060357

Rosner, B. (1975). On the detection of many outliers. *Thechnometrics* 17 (2), 221–227. doi: 10.2307/1268354

Rui, W., Mao, Z., and Li, Z. (2022). The roles of phosphorus and nitrogen nutrient transporters in the arbuscular mycorrhizal symbiosis. *Inter. J. Mol. Sci.* 23, 11027. doi: 10.3390/ijms231911027

Smith, C. J., and Osborn, A. M. (2009). Advantages and limitations of quantitative PCR (Q-PCR)-based approaches in microbial ecology. *FEMS Microbiol. Ecol.* 67, 6–20. doi: 10.1111/j.1574-6941.2008.00629.x

Smith, S. E., and Read, D. J. (2008). *Mycorrhizal Symbiosis* (London: Academic Press), 815.

Song, J., Yang, J., and Jeong, B. R. (2022). Root GS and NADH-GDH play important roles in enhancing the ammonium tolerance in three bedding plants. *Inter. J. Mol. Sci.* 23, 1061. doi: 10.3390/ijms23031061

Stewart, W. M., Dibb, D. W., Johnston, A. E., and Smyth, T. J. (2005). The contribution of commercial fertilizer nutrients to food production. *Agron. J.* 97, 1–6. doi: 10.2134/agronj2005.0001

Sun, K., Zhang, W., Yuan, J., Song, S. L., Wu, H., Tang, M. J., et al. (2020). Nitrogen fertilizer-regulated plant-fungi interaction is related to root invertase-induced hexose generation. *FEMS Microbiol. Ecol.* 96, fiaa139. doi: 10.1093/femsec/fiaa139

Svennerstam, H., Ganeteg, U., and Näsholm, T. (2008). Root uptake of cationic amino acids by *Arabidopsis* depends on functional expression of amino acid permease 5. *New Phytol.* 180, 620–630. doi: 10.1111/j.1469-8137.2008.02589.x

Tall, S., and Meyling, N. V. (2018). Probiotics for Plants? Growth promotion by the entomopathogenic fungus *beauveria bassiana* depends on nutrient availability. *Microbial Ecol.* 76, 1002–1008. doi: 10.1007/s00248-018-1180-6

Udvardi, M. K., and Poole, P. (2013). Transport and metabolism in legume-rhizobia symbioses. *Ann. Rev. Plant Biol.* 64, 781–805. doi: 10.1146/annurev-arplant-050312-120235

Usuki, F., and Narisawa, K. (2007). A mutualistic symbiosis between a dark septate endophytic fungus, Heteroconium chaetospira, and a nonmycorrhizal plant, Chinese cabbage. *Mycologia* 99, 175–184. doi: 10.1080/15572536.2007.11832577

Wang, S., Chen, A., Xie, K., Yang, X., Luo, Z., Chen, J., et al. (2020b). Functional analysis of the OsNPF4.5 nitrate transporter reveals a conserved mycorrhizal pathway of nitrogen acquisition in plants. *Proc. Natl. Acad. Sci.* 117, 16649–16659. doi: 10.1073/pnas.2000926117

Wang, W., Shi, J., Xie, Q., Jiang, Y., Yu, N., and Wang, E. (2017). Nutrient exchange and regulation in arbuscular mycorrhizal symbiosis. *Mol. Plant* 10, 1147–1158. doi: 10.1016/j.molp.2017.07.012

Wang, Y., Tang, D. X., Duan, D. E., Wang, Y. B., and Yu, H. (2020a). Morphology, molecular characterization, and virulence of *Beauveria pseudobassiana* isolated from different hosts. *J. Invertebr. Pathol.* 172, 107333. doi: 10.1016/j.jip.2020.107333

Yang, T., Li, H., Tai, Y., Dong, C., Cheng, X., Xia, E., et al. (2020). Transcriptional regulation of amino acid metabolism in response to nitrogen deficiency and nitrogen forms in tea plant root (*Camellia sinensis* L.). *Sci. Rep.* 10, 6868. doi: 10.1038/s41598-020-63835-6

Zhou, J., Li, X., Huang, P. W., and Dai, C. C. (2018). Endophytism or saprophytism: decoding the lifestyle transition of the generalist fungus *Phomopsis liquidambari*. Microbiol. *Res.* 206, 99–112. doi: 10.1016/j.micres.2017.10.005

Frontiers in Plant Science

Cultivates the science of plant biology and its applications

The most cited plant science journal, which advances our understanding of plant biology for sustainable food security, functional ecosystems and human health.

Discover the latest Research Topics

See more →

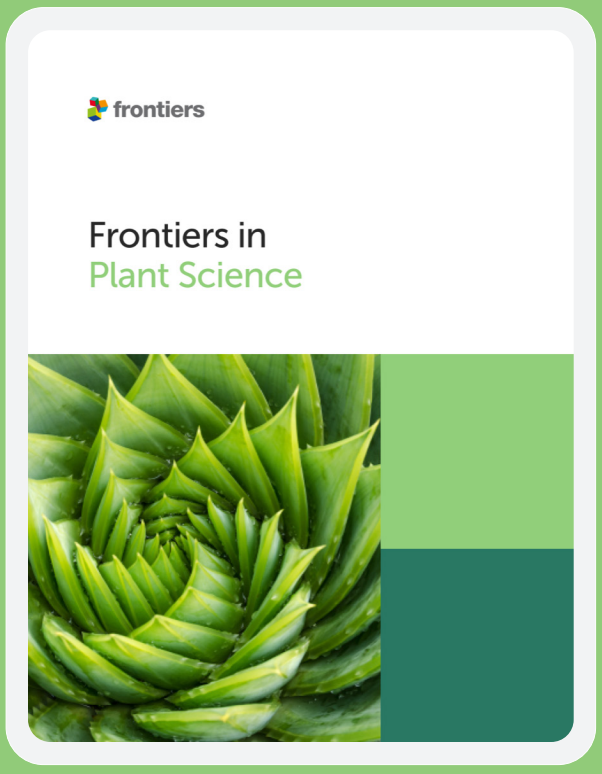

Frontiers

Avenue du Tribunal-Fédéral 34
1005 Lausanne, Switzerland
frontiersin.org

Contact us

+41 (0)21 510 17 00
frontiersin.org/about/contact